Numeric geochemical reaction modelling, incorporating systems theory and implications for sustainable development – Study on East Rand Basin acid mine drainage, Witwatersrand, South Africa

by
Robert Neill Hansen

Dissertation presented for the degree of *Doctor of Geology in the Faculty of Science at Stellenbosch University*

Supervisor: Prof Alakendra Roychoudhury

December 2014

Declaration

By submitting this thesis electronically, I declare that the entirety of the work contained therein is my own, original work, that I am the sole author thereof (save to the extent explicitly otherwise stated), that reproduction and publication thereof by Stellenbosch University will not infringe any third party rights and that I have not previously in its entirety or in part submitted it for obtaining any qualification.

December 2014

ABSTRACT

In recent years acid mine drainage (AMD) has become the focus on many mine sites throughout the world. The Witwatersrand gold mines have been the main focus of AMD in South Africa due to their extensive impact on especially groundwater resources. The Witwatersrand Basin is a regional geological feature containing the world-famous auriferous conglomerate horizons. It is divided into sub-basins and the East Rand Basin is one of them. Due to the regional scale of the East Rand Basin AMD issues, a systems approach is required to provide a useful tool to understand the pollution source term and fate and transport dynamics and to aid in environmental decision making and to evaluate the geochemical impact of mitigation measures and evaluate future scenarios.

The numeric geochemical models, using a systems perspective, show that the mine waste facilities, specifically the tailings dams are significant contamination point sources in the East Rand Basin, specifically for acidity (low pH), SO_4, Fe, Mn, U, Ni, Co, Al and Zn. When the AMD solution enters the soil beneath the tailings, ferrous and SO_4 concentrations remain elevated, while Mn, U, Ni and Co and perhaps other metals are adsorbed. After ~50 years the pollution plume starts to break through the base of the soil profile and the concentration of the adsorbed metals increase in the discharging solution as the adsorption capacity of the soil becomes saturated. The pollution pulse then starts to migrate to the shallow groundwater where contamination of this resource occurs.

Toe seepage from the tailings either first reacts with carbonate, where acidity is neutralised to a degree and some metals precipitated from solution, where after it reaches the surface water drainage, such as the Blesbokspruit, where it is diluted. Some evaporation can occur, but evaporation only leads to concentration of acidity and dissolved constituents, thereby effectively worsening the AMD solution quality. The mixing models have shown that the dilution factor is sufficient to mitigate much of the AMD, although seasonal variability in precipitation and evapotranspiration is expected to have some influence on the mixing ratio and some variability in the initial solution will also be reflected in variation in surface water quality.

From a sustainability perspective, a basic cost benefit analysis shows that the costs for the operating mine and society in general is lower when mitigation measures are employed during operation. For a theoretical mine in the ERB with an operating life of 100 years, the cost of operational mitigation measures is ~R 31 billion. This value is 4% of turnover and 19% of profits over the time period. Post closure remediation costs are ~R 67 billion. This value is 8% of turnover and 41% of profit over the time period. Although the initial capital investment in mitigation measures is substantial, although some measures will be implemented during operation, it is a smaller percentage of profits than eventual post-closure mitigation.

OPSOMMING

In die laaste paar jaar het suur mynwater loging (SML) die fokus geword by baie myn areas regoor die wêreld. Die Witwatersrand goud myne het die hoof fokus van SML in Suid Afrika geword as gevolg van die groot impak wat Witwatersrand SML op veral grondwater bronne het.

Die Witwatersrand Kom is ‘n regionale geologiese struktuur wat die wêreld beroemde goud-draende konglomeraat horisonne bevat. Die Witwatersrand Kom word onderverdeel in sub-komme, waarvan die Oos-Rand Kom een is. As gevolg van die regionale skaal van die Oos-Rand Kom SML probleem sal ‘n sistemiese benadering ‘n bruikbare middel wees om besoedelingsbron migrasie en eindpunt dinamika te verstaan asook om omgewingsbesluitneming en die geochemiese impakte en mitigerings metodieke asook toekoms senarios te evalueer.

Die numeriese geochemiese modelle, wat vanuit ‘n sitemiese oogpunt beskou is, wys dat die myn afval fasiliteite, veral die slikdamme in die Oos-Rand Kom, beduidende kontaminasie puntbronne is van veral suur inhoud, SO_4, Fe, Mn, U, Ni, Co, Al and Zn. Wanneer die SML oplossing die grond onder die slikdamme binnedring, bly Fe^{2+} en SO_4 konsentrasies hoog, terwyl Mn, U, Ni en Co asook ander metale geadsorbeer word. Na ~50 jaar begin die besoedelingsoplossingspluim deur die basis van die grond profile breek. Die konsentrasie van die geadsorbeerde metale neem dan toe in die oplossing wat deur die grondprofiel beweeg het soos wat die adsorpsie kapasiteit van die grond versadig word. Die besoedelingspuls begin dan stadig na die vlak grondwater akwifeer migreer waar dit dan besoedeling van die grondwater versoorsaak.

Water wat van die slikdam basis sypel reageer eers met karbonaat, waar suur tot so ‘n mate geneutraliseer word, dat sommige metale uit die oplossing neerslaan, waarna dit die oppervlak water lope, soos die Blesbokspruit, beryk en verdun word. Verdamping van die SML oplossing kan plaasvind, maar verdamping veroorsaak die konsentrasie van suur en opgeloste stowwe, wat die SML probleem dus kan vererger. Meng modelle het gewys dat die verdunning faktor genoegsaam is om baie van die SML te mitigeer, alhoewel seisoenale fluktuasies in reënval en verdampings syfers kan verwag word om ‘n mate van invoed op die meng verhouding tussen die SML oplossing en oppervlak water te hê wat dan in die oppervlak water kwaliteit gereflekteer sal word.

Vanuit ‘n volhoubaarheidsperspektief is ‘n basiese koste voordeels analise gedoen. Hierdie analise het gewys dat die koste van ‘n operasionele myn en die samelewening as geheel laer is wanneer mitigasie metodieke tydens operasie toegepas word. Vir ‘n teoretiese myn in die Oos-Rand Kom met ‘n operasionele lewe van 100 jaar, is die operasionele mitigeringsmetodieke koste ~R31 miljard. Hierdie waarde is 4% van die myn omset en 19% van winste oor die tyds periode. Na operasionele remdiasie kostes is ~R67 miljard. Hierdie syfer is 8% van omset en 41% van winste oor die tydperk. Alhoewel die inisiële kapitaal uitleg van mitigasie metodes groot is, alhoewel sekere metodes eers tydens operasie implimenteer sal word, is die uitleg ‘n kleiner persentasie van winste as wanneer remediasie na operasie implimenteer word.

ACKNOWLEDGEMENTS

I would firstly like to thank God for His inspiration and providing the strength to complete this work. Thank to my wife, Thea, for her patience and constant support throughout the study. I would also like to thank my mentor Dr. Koos Vivier for his support in terms of helping me to focus, but also granting me the time to complete my studies. Thank you to Exigo Sustainability for their financial support. Lastly, but not least, I would like to thank Council for Geoscience for providing me with the opportunities and guidance for the project.

Table of Contents

List of Figures

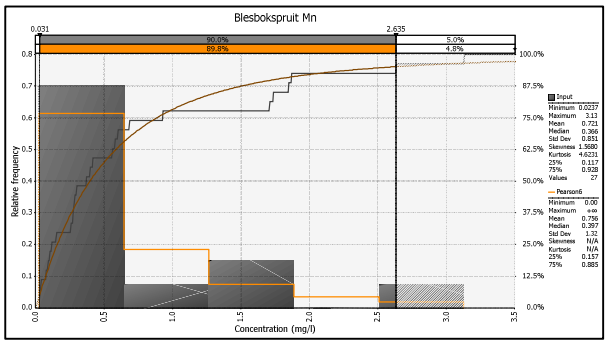

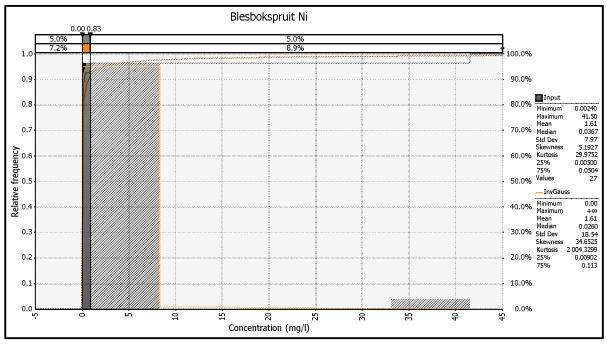

List of Tables

1 CHAPTER 1: INTRODUCTION

The acid mine drainage (AMD) issue related to the Witwatersrand gold mining activities could arguably be seen as the greatest environmental catastrophe to be faced by the people of the Republic of South Africa. This fact has been highlighted by the formation of an inter-ministerial committee inn 2010, consisting of ministers from various government departments, to tackle this issue. The committee appointed a panel of experts to assess the status quo and provide an options analysis on potential mitigation measures. The status quo report was published in 2010 (Expert team of the inter-ministerial committee).

The report highlighted three priority gold mining basins, which form part of the larger Witwatersrand Basin. One of these priority basins is the East Rand Basin (ERB). At the time of publication, only one mine was pumping polluted water from its underground operations. This water was pumped at a rate of between 75 and 108 Mℓ/day, treated with lime and discharged into the Blesbokspruit. The Blesbokspruit is a RAMSAR classified wetland flowing past many of the ERB mining operations. The inter-ministerial committee report does not contain any reference to dynamic geochemical modelling studies. Some studies have been conducted on specifically mine tailings facilities to improve impact prediction (Bezuidenhout and Rousseau, 2005; Tutu et al., 2008). None have used dynamic geochemical reaction modelling as a tool to assess AMD in the ERB.

The East Rand Basin has an aerial extent of 561 km^2 and consist if many geochemical environments. The challenge therefore is to develop a model that can incorporate detailed numeric geochemical reaction modelling on a regional level for a range of geochemical environments. Although these types of ecosystem models have been applied to regional water management concerns (Côte, 2010; Barthel, 2008), none have been applied to geochemical systems in the ERB. Therefore a systems approach thought to provide a context in which detailed reaction modelling can be placed in a regional context to better understand AMD geochemical dynamics in the ERB.

In addition to understanding AMD interactions in the regional ERB, questions could also be asked on the economic implications of AMD impacts for a mine in the ERB. International studies have shed light on negative economic aspects of AMD, such as depreciation in property value (McCluskey and Rausser, 2003). Estimates of the implementation of short to medium term remedial solutions to curb rising AMD in the three priority basins are placed at around R 1 billion. One of the questions that arise from the Witwatersrand AMD legacy is whether operational mitigation or post-closure remediation makes more economic sense. This question makes sense if the source is considered constant or whether the pollution source will dissipate with time.

This study is therefore not only an attempt to shed light on the geochemical reaction dynamics of AMD in the ERB in order to facilitate clean-up strategies and to aid in future impact prediction studies. It is also an attempt to provide a basic economic context to current legislative debates in terms of mining projects in the Republic of South Africa.

1.1 Objective

The objective of this study is to develop a numeric geochemical reaction model of the East Rand Basin, which incorporates systems theory, and to describe the implications of such models for sustainable development.

1.2 Research question

The main research question can be formulated as follows:

What components and processes drive the East Rand Basin AMD and contaminant fate and transport from a geochemical perspective?

2 CHAPTER 2 LITERATURE REVIEW

Acid mine drainage (AMD) is defined as a low pH solution containing large amounts of iron, sulphuric acid and dissolved metals and is caused by the oxidation of sulphide minerals (Peretyazhko et al., 2009; Rimstidt, 2003; United States Environmental Protection Agency, 1994).

AMD has long been recognised internationally as a contamination concern resulting from the mining of sulphidic orebodies (Peretyazhko et al., 2009; Tutu et al., 2008). Numerous international studies have been focussed on identifying the characteristics, causes and fate and transport of AMD. Entire publication volumes have been dedicated to this research, such as the Mineralogical Association of Canada Short Course Handbook, Volume 22 entitled: The Environmental Geochemistry of Sulphide Mine-Wastes, edited by Jambor and Blowes and published in 1994. In recent years, focus has been moving towards the use of isotopic studies (Fernandez and Borrok, 2009; Tichomirowa and Junghans, 2009) as well as integration, specifically related to hydrogeological and geochemical modelling (Papassiopi et al., 2014). Geochemical modelling have been used successfully for specific aspects of AMD research, such as characterisation (Balistrieri, et al., 2007; Equeenuddin et al., 2010, Coggon et al., 2012; Sracek et al., 2004), metal speciation, bioavailability and toxicity (Balistrieri et al., 2007; Sondergaard et al., 2008) and hydrogeochemistry (Equeenuddin et al., 2010; Jung et al., 2012). Stable isotopes have also been successfully used to study the geochemical and hydrogeochemical dynamics of components in AMD (Chapman et al., 2013; Cowie et al., 2009; Kimball et al., 2009; Gammons et al., 2010; Hubbard et al., 2009). The latest research has focussed on coupling geochemical and hydrogeological models to study contaminant transport from AMD sources (Papassiopi et al., 2014; Hipsey et al., 2014). Geochemical modelling to date has been focussed on specific aspects of AMD.

Geochemical studies on the AMD in the Witwatersrand are less common and those focussed on the East Rand Basin even more so. Studies in AMD in the Witwatersrand was triggered after it was realised in the early to mid-1990's that mine water is rising in defunct mines (Scott, 1995). The first studies were focussed on characterisation of AMD in terms of characteristics, impacts and assessment methods (Rösner et al., 2001; Naicker et al., 2003; Cukrowska et al., 2004). Rösner et al (2001) showed that soil beneath the reclaimed residue deposits in the ERB are polluted with Co, Cr, Cu, Ni and Zn. Thea also showed that groundwater beneath and in close proximity to these footprints show evidence of being impacted on by acidic solutions. They also show that adsorption to solid particles is strongly dependent on soil pH. Naicker et al. (2003) confirmed these results when they showed that the upper 20 cm of soil is heavily contaminated by heavy metals. They also showed that groundwater in close proximity to mine residue deposits is not only polluted, but discharges into surface water streams, lowering the pH. They showed that Fe and Mn oxy-hydroxides precipitate from these solutions and scavenge metals. Their study showed that the effect of AMD could be seen up to 10 km from existing mine residue deposits. Cukrowska et al. (2004) showed that column leaching tests could be used to assess the leachability of contaminants from mine residue material.

Individual studies focussed on appropriate treatment technologies, specifically for the Grootvlei mine in the East Rand Basin (ERB), which was pumping and treating dewatered groundwater from its underground

workings (Schoeman and Steyn, 2001). Schoeman and Steyn (2001) showed that metal precipitation and ion exchange (GYP-CIX) and electrodialysis technologies were the most cost effective in terms of operational costs in the treatment of polluted ERB deep groundwater.

Later studies focussed on impact prediction and assessment methods and on the specific impacts of AMD in the ERB and Witwatersrand (Coetzee et al., 2005; Coetzee et al., 2006; Roychoudhury and Starke, 2006; Durand, 2012). Coetzee et al. (2005) showed that wetlands downstream of mining areas are mitigating the effects of AMD pollution. They pointed out that this mitigating effect cannot continue *ad infinitum* and intervention will be required to curb pollution before saturation of mitigation potential is reached. They also showed that areas within the wetlands are enriched in gold and that finances generated by extraction of this gold could be used to rehabilitate the wetland systems. Coetzee et al. (2006) showed in a geochemical and isotope study on the water and sediments in the Wonderfontein spruit catchment that the stream water contains uranium in excess of background values and that the sediments are contaminated by U and Cd. They found that the majority of metals in the sediments are associated with the reduced fraction, with obvious deleterious effects should the redox regime change. Another conclusion from their study is that at least some of the Pb in the stream water and sediments is radiogenic in origin. In a study on the Blesbokspruit, a RAMSAR classified wetland in the ERB with many mine residue facilities on its banks, Roychoudhury and Starke (2006) showed that the stream water is pH buffered by bicarbonate ions, originating from the dolomites over which the stream flows. In addition, metals from mine residue material are precipitated due to the high pH due to the inherent bicarbonate as well as the liming process at Grootvlei mine, prior to discharge of the effluent. They showed that the metals are associated with carbonates and that the wetland is accumulating trace metals due to co-precipitation, rather than adsorption. The Blesbokspruit pollution level was shown to be low to moderate. Durand (2012) conducted a study on the karst regions and streams in areas within the Witwatersrand gold mining regions. He found that the river systems and karst groundwater is polluted by AMD.

Some studies incorporated geochemical data analysis (Nengovhela at al., 2007; Yibas et al., 2010) and analytical modelling (Bezuidenhout and Rousseau, 2005) to develop an understanding of the origins of AMD in the Witwatersrand gold mines and to more accurately predict long term effects. Nengovhela et al. (2007) conducted a study on the oxygen content of mine residue material and tried to determine the relationship between oxygen content and AMD. They found a strong correlation between AMD development in a mine residue facility and the availability of oxygen. They also showed that oxygen diffuses to about 4 m into the residue deposits. Yibas et al. (2010) studied the origin and development of oxidation zones in the Witwatersrand residue facilities. The aim was to better predict AMD impacts. They found a good correlation between depth of oxidation and oxygen content within the residue deposits. They showed that oxidation proceeds deeper into the mine residue deposits along preferential flow paths, such as cracks, but that this is not expected to be significant. Stabilisation is expected to occur around 4 m within a given residue facility. Bezuidenhout and Rousseau (2005) conducted a study in which an analytical geochemical model was developed to study the depth and rate of pyrite oxidation in the Witwatersrand residue deposits. The aim was

to develop a screening tool to evaluate the impact relating to AMD from residue deposits in the Witwatersrand. They found that oxygen is the driver of pyrite oxidation. They also found that the first 2 m oxidises rapidly in less than 10 years, after which the oxidation rate decreases. A surprising conclusion of their study is that acidification is only expected to occur after > 1 000 years.

The latest studies have been commissioned by the Department of Water Affairs (DWA) and focus on defining the status quo of AMD in the Western, Central and Eastern gold mining basins of the Witwatersrand in terms of treatment objectives (DWA, 2013). These three basins were prioritised and the short to medium term solution presented in a regional report on the Witwatersrand AMD to the inter-ministerial commission tasked to look into the AMD issue (Expert team of the inter-ministerial commission, 2010). The inter-ministerial commission report (2010) showed that AMD in the Witwatersrand and specifically the ERB is due to the oxidation of pyrite by mostly oxygen. However, the author is unaware of any studies conducted on the potential bacterial catalysis of pyrite oxidation specifically on ERB residue facilities. The study accentuated that polluted water in the deep mine voids (> 600 m depth) is rising to the surface in the East Rand and Central Rand basins and are expected to decant on surface. This caused a large hype in the media surrounding potential erosion of building foundations in the Johannesburg CBD, although much of this is unfounded, as the lowest elevation point at which water is expected to decant in the CRB is south of the Johannesburg CBD. The report highlighted that the AMD in the Witwatersrand has contributed to surface water, soil, shallow and deep groundwater pollution and that urgent remediation measures are required to curb further AMD contamination. A pump-and-treat option was selected as a short to medium term solution in the ERB and CRB (DWA, 2013).

None of the above mentioned studies on AMD in the ERB focussed on dynamic geochemical reaction modelling as a tool to characterise the long term behaviour of AMD, as it has been internationally. However, international studies have focussed on detailed geochemical modelling of specific aspects of AMD. It is also apparent from the regional nature of the ERB that no one geochemical reaction model can be developed to study all aspects of ERB AMD fate and transport. Therefore a modelling approach is required which can take into account all the geochemical environments in the ERB. Systems theory provides an avenue by which such a detailed modelling exercise can be used to provide a regional perspective on the AMD issue in the ERB from specifically a geochemical reaction perspective.

Systems theory is the idea that the world around us consists of various systems, all interrelated and interacting with each other. A system refers to a complex whole of related parts, whether it is biological, structural, organized ideas or any other assemblage of components constituting a whole as well as the networks of relationships among them (Cabrera et al., 2008; Werhane, 2007). The modern idea of systems theory is traced back to Von Bertalanffy (1950), although allusions to more ancient roots of systems thinking have been made (Guangqing, 2005). Von Bertallanffy (1950) proposed a systems model for biological systems and was one of the first modern scientists to suggest that systems theory can be applied to other disciplines.

Systems theory acknowledges that real-world problems do not adhere to the traditional disciplinary boundaries, but are multidimensional problems that must be addressed in an inter-disciplinary way, i.e. pluralism. Systems theory enshrines a commitment to holism, where any system is viewed in its entirety, including the interaction with factors outside the immediate system, i.e. its environment, and it is recognised that insights are gleaned from this holistic view (Jackson, 2001). The systemic world view stands in stark contrast to the traditional, modernistic reductionist scientific view, that all systems can be broken down into smaller components and that the components can be studied in isolation. This notion has been cited as naïve empiricism (Vivier, 2011). Jackson (2001) states that holism has provided a useful antidote to reductionism when tackling real-world problems.

A system boundary is the boundary that differentiates the system from its environment. A system's boundary is not a fixed, rigid structure, but it rather is osmotic, with feedback between the systems and the environment. These system boundaries should constantly be reviewed because of systems change over time. Because boundaries are chosen, boundary critique is extremely important in any systems definition as boundaries define what issues are to be included and who is to be consulted or involved (Midgley, 2008).

The systems perspective is therefore deemed to be useful to develop conceptual and dynamic geochemical reaction models for the East Rand Basin geochemical system. Although a systems perspective can conceptually provide an overview of geochemical processes active in the East Rand Basin with regards to AMD and contaminant fate and transport, the practical implications are not always clear. Therefore the geochemical modelling needs to be placed in some kind of practical context in terms of rehabilitation and remediation.

Although such ecosystem type models have been developed successfully in other disciplines, only a few have been focussed on natural systems (Côte et al., 2010; Barthel, R.; An, 2012; Ewel, 1999). To the author's knowledge, none to date have been done for geochemical systems in relation to AMD in the ERB.

It has been shown that there are financial (Chamber of Mines South Africa, 2007) and practical (World Wildlife Fund South Africa, 2012; International Council on Mining & Metals, 2008) benefits to concurrent rehabilitation versus post-closure remediation. Although guideline documents (Chamber of Mines South Africa, 2007) indicate that it is most probably not possible to conclude all remediation concurrently with mining, the liabilities are decreased due to greater certainties regarding successful remediation techniques and smaller financial provision is most probably required when concurrent rehabilitation is conducted.

Although no study could be sourced which places geochemical modelling in an environmental economic context, environmental economics has been found useful in determining the cost of environmental degradation in monetary terms using other methods, such as studying the impact of environmental depreciation on property value (McCluskey and Rausser, 2003). The results of the geochemical models could thus provide valuable input to the debate of whether, from a financial perspective, it is beneficial to either remediate concurrently or post-closure.

3 CHAPTER 3: STUDY AREA DESCRIPTION

3.1 Climate and topography

The East Rand Basin is located in the Gauteng Province and contains the towns of Germiston, Springs and Nigel (Figure 3-1). It covers an area of 56 091 ha. Gold mining started in September 1888 and continues till today, although current production is a fraction of what it was historically (Pretorius, 1974; Robb and Robb, 1998).

The topography is relatively flatlying with an average elevation of 1 602 m ranging from a maximum height of 1 710 m to a minimum of 1 492 m (σ = 23) as determined from a light detection and ranging (Lidar) survey. The lower lying areas are defined by stream and river channels, with the prominent channel of the Blesbokspruit, the main drainage channel in the area easily observed in Figure 3-2.

The mean annual precipitation (MAP) is 749.4 mm/a calculated from the Springs weather station (station 0476762A3) which has data from 1977 to 2004 (South African Weather Service data, 2004). The mean annual evaporation is 1 651 mm/a (Water Research Commission, 2005). The MAE is more than twice the MAP.

3.2 Geological context

The Witwatersrand Supergroup is dominated by repetitive layering of quartzite, conglomeratic quartzite, shale, diamictite and volcanic rocks. The Witwatersrand Supergroup in the East Rand Basin is represented by the Turfontein and Johannesburg subgroups, belonging to the Central Rand Group. Overlying the Witwatersrand Supergroup are the sandstone, shale and dolomitic rocks of the Transvaal Supergroup. In terms of geochemistry, the dolomite rocks of the Malmani Subgroup are important. Overlying the Transvaal Group rocks are the sandstone and shale layers of the Karoo Supergroup (Figure 3-3 and Figure 3-4). The Karoo Supergroup rocks dominate in terms of surface area (Robb and Robb, 1998; East Rand Basin 1:250 000 geological map).

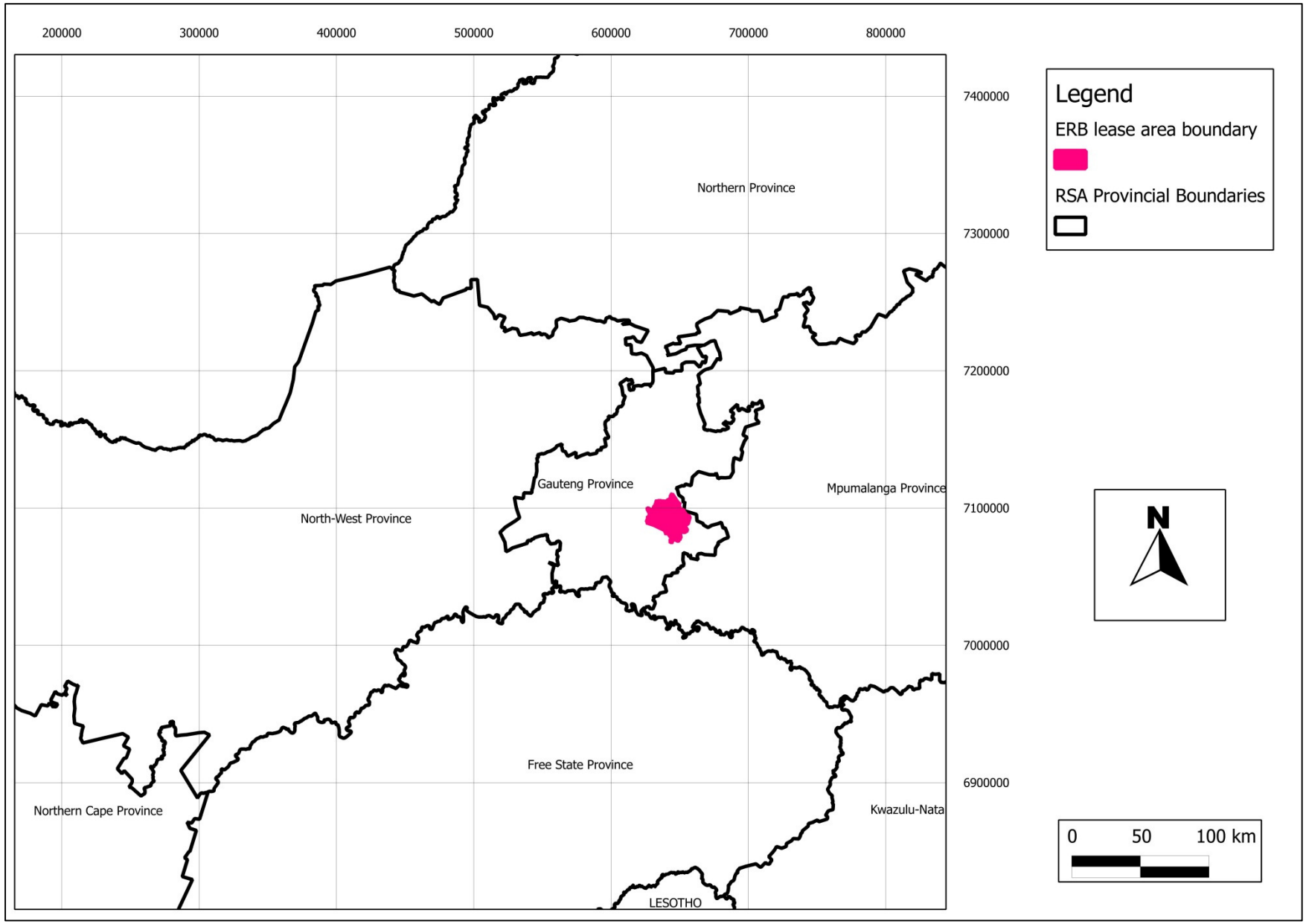

Figure 3-1 East Rand Basin regional locality map. The map uses a WGS 1984 datum and is projected in UTM Zone 35 S.

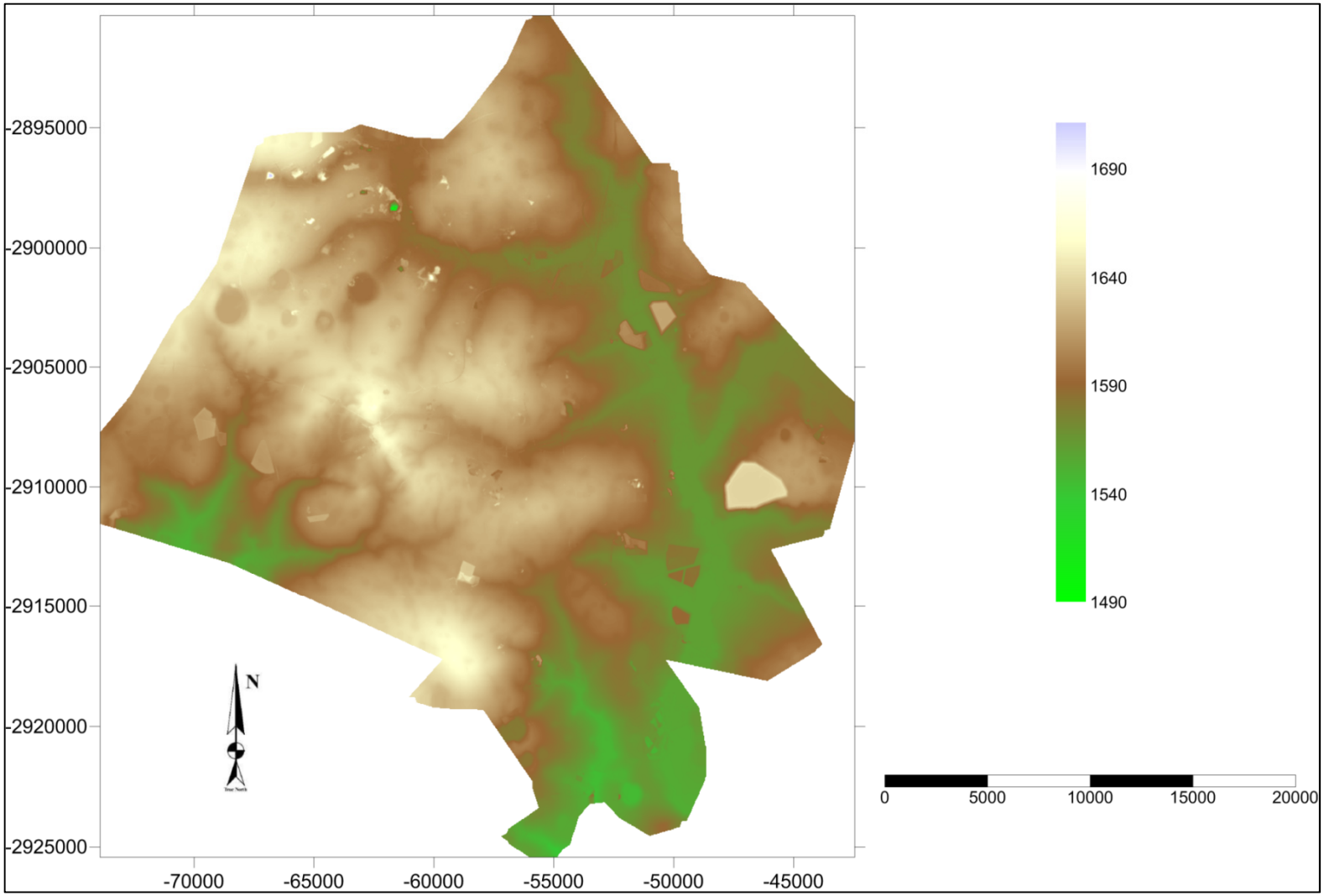

Figure 3-2 Coloured contour map showing the topography of the East Rand Basin mine lease and study area (contoured from existing LIDAR data, Council for Geoscience; Strategic mine water management project)

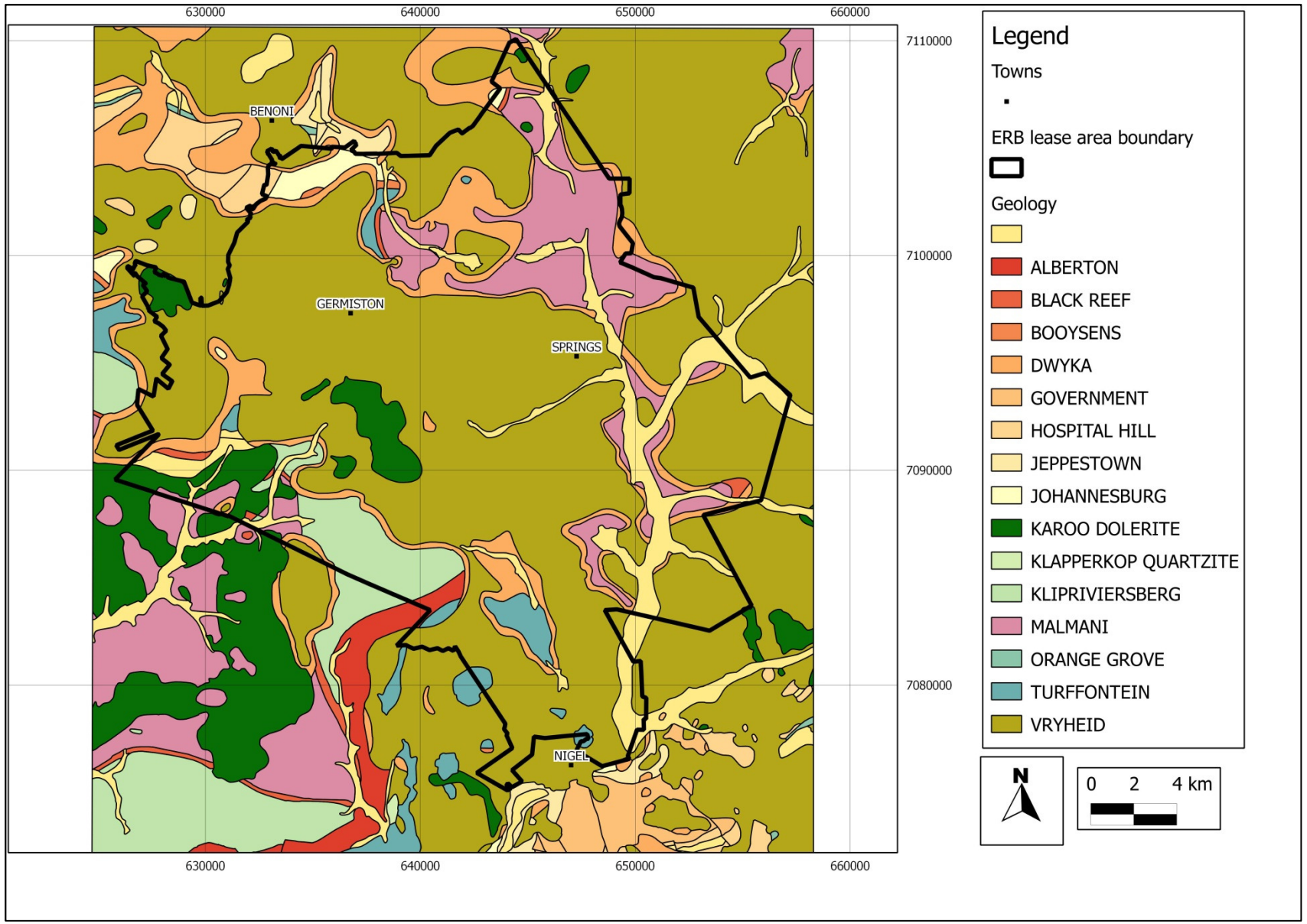

Figure 3-3 Simplified East Rand Basin geological map showing the various formations (simplified from the 1:250 000 geological map, Council for Geoscience).

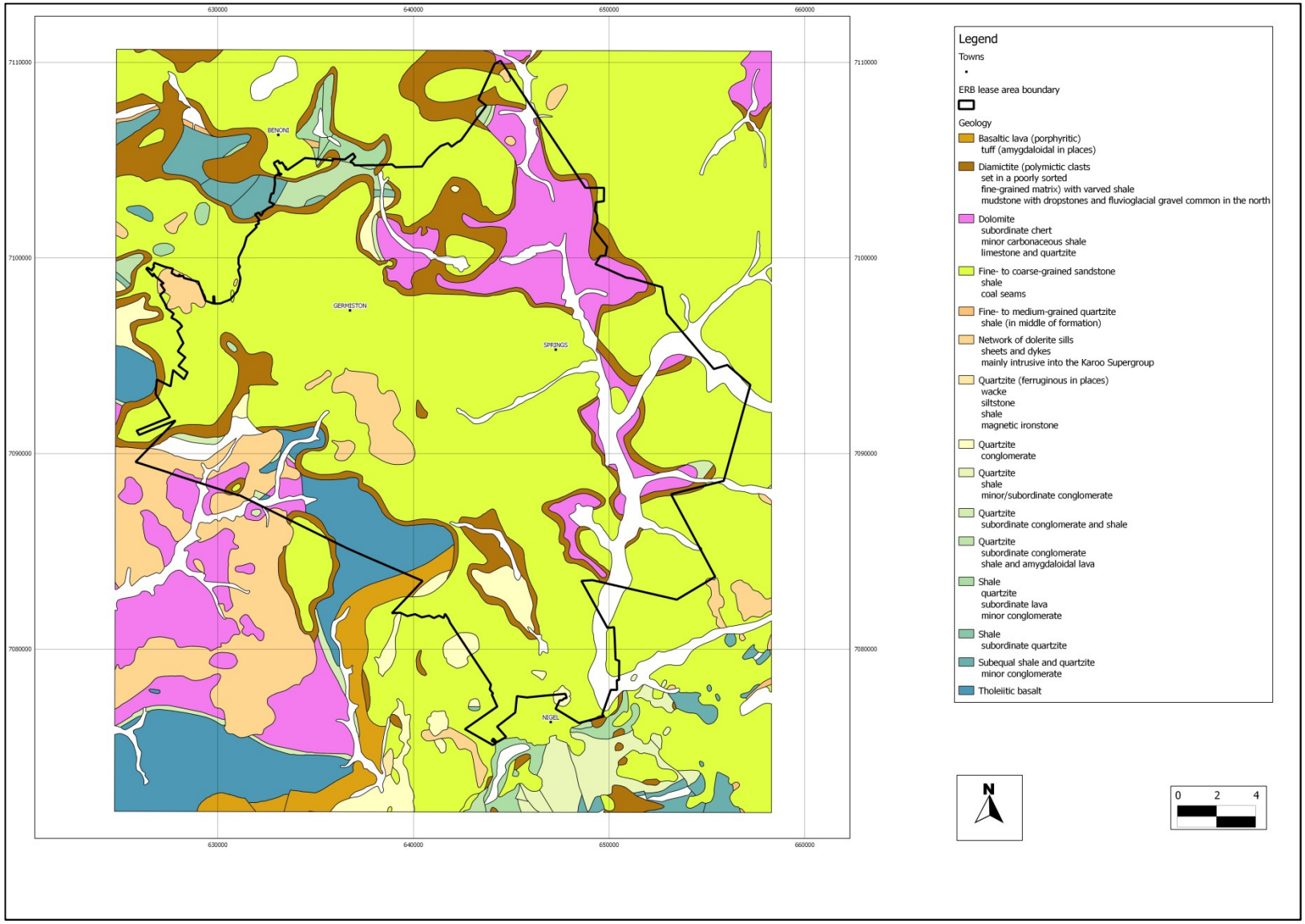

Figure 3-4 Simplified East Rand Basin geology showing geological descriptions simplified from the 1:250 000 geological map, Council for Geoscience).

4 CHAPTER 4: STUDY METHODOLOGY

The study consists of three main phases:

1. Data analysis and conceptual modelling
2. Dynamic geochemical reaction modelling
3. Basic cost benefit analysis

4.1 Data analysis and conceptual modelling

Geochemical data for specifically the ERB was sourced from the literature. Hydrogeochemical data for the ERB underground mine water as well as for the shallow groundwater was sourced from the Council for Geoscience.[1] Other data sources are referenced in the relevant sections (see specifically Chapters 5 and 6.

The ERB geochemical and hydro-geochemical data was statistically analysed with the aim of developing conceptual models of key geochemical system components. The data analysis is aided by data distribution analysis, including assessment of best fit distributions. The statistical program @Risk®[2] is used for the data distribution and probability analyses. One of 4 data boundary conditions can be set when assessing data distributions with @Risk. These are:

- *Fixed bound:* This is when specific minimum or maximum values are defined for the data distribution. This is usually appropriate for geochemical physio-chemical parameters, as it is generally impossible for them to be less than 0. There are exceptions, e.g. Eh, so care must be taken in choosing this option, although it will most likely be appropriate. Generally setting an upper bound will not be appropriate, as e.g. the concentration of a chemical specie will depend on other parameters, such as pH
- *Bounded but unknown:* This boundary condition is used when the values in the distribution have bounds, but they are not known. The software thus sets the boundaries automatically, depending on the distribution fit. This may be appropriate for the upper limit for most geochemical parameters, but may still be limited, as the upper boundary may vary to a larger extent as the value which is chosen by the software based on the data fit.
- *Open:* This automatically sets the bounds of the data between ± infinity. This may be appropriate for some geochemical parameters, e.g. Eh, but not for most, as geochemical parameters, especially specie concentrations are defined by the laws of thermodynamics and depend on system variables.
- *Unsure:* This option falls between the *bounded by unknown* and the *open* options. Not all data distributions can be bounded, e.g. the lognormal distribution, which varies to infinity as a

[1] The data itself is unpublished, but it can be requested from the Council for Geoscience. The contact person is Magda Roos (012) 841 1911 and the relevant project is "The strategic water management project." The data period is the years 2005 – 2006.

[2] www.palisades.com/risk/

maximum. This option is most probably best most geochemical parameters, as bounded and unbounded distribution fits are shown. Thus the most appropriate can be selected, based on the specific parameter being assessed and other tests, such as the probability-probability and quantile-quantile plots and percentile analysis.

In this study, for dissolved chemical species, the *fixed bound* option is used for the lower limit, set to 0, as a concentration of a dissolved specie cannot be lower than 0. The *unsure* option is used for the upper limit, as dissolved species have upper concentrations bounds although the upper bound is generally unknown. The upper solubility bounds are determined by the solubility dynamics of each species in relation to the available dissolved ions, gasses and minerals in the system. The best fit to the data is selected based on the parameter being assessed and other tests, e.g. probability-probability plots and percentile analysis.

@Risk distinguishes between 2 main data types: continuous and discreet. Discreet data consists of integers only, while continuous data can be any range of values. Since the data pertaining to the current study is of the latter, only statistical parameters pertaining to this data type are used. To fit a theoretical distribution to an actual distribution, three different fit parameters can be used, each with its own advantages and disadvantages. These are the Chi-Squared, Kolmogorov-Smirnov (K-S) and Anderson-Darling (A-D) parameters (Groebner and Shannon, 1993; Law and Kelton, 1991; Walpole and Myers, 1993).

The advantages of the Chi-Squared parameter are that it can be used for continuous and discreet data and is generally a good estimate of fit. The disadvantages are that the parameter depends on a rather arbitrary selection of bins for the x-axis. The K-S and A-D parameters are more robust in that binning is not required. However, the disadvantage of the K-S parameter is that it does not detect tail discrepancies very well. The A-D parameter highlights the differences between tails of fitted distributions. The Chi-Squared distribution is used in this study as a default, as it generally provides a good fit and handles skewed distributions well. However, when the Chi-Squared parameter showed week fit, the K-S and A-D parameters were compared and the parameter showing the best fit following percentile and parameter analysis was used, unless the tail of the distribution was of specific interest.

4.2 Dynamic geochemical reaction modelling

Following the definition of conceptual geochemical subsystems of the ERB, numeric reaction models are developed for these subsystems (components). The geochemical modelling software package The Geochemists' Workbench® is used to develop the models. The mineral rate constants and reaction orders were derived from the literature and are referenced in the appropriate sections. A modified version of the BRGM thermodynamic data base is used for the modelling (Blanc et al., 2007).

4.3 Cost benefit analysis

The results of the numeric geochemical reaction modelling were used to define the source terms of AMD impacts. These parameters were used to develop a mining scenario to evaluate two scenarios financially. These are implementation of mitigation measures in the operational phase of mining and the post-closure remediation of impacts, without operational mitigation.

Various mitigation and remediation costs were acquired from published reports, company brochures and journal and magazine articles (United States Environmental Protection Agency, 1997b, 1998, 2001, 2003, 2010b, Sorwebplus, 2006; Goldstein and Ritterling, 2001; Du Plessis et al., Swartz, 2006; Welcare, 2009; Sanders et al., 2009; Summersgill, 2005; English Partnerships, 2008). This data represents mitigation and remediation costs in various currencies ($, €, £ and R) published in various years. Consumer price index (CPI) inflation data from the United Kingdom (Office of national statistics, 2013), the USA (McMahon, 2013), Europe (Anon, 2013) and the RSA (Statistics South Africa, 2013) were used to correct prices for inflation. Exchange rate data of foreign currencies with the Rand (OANDA, 2013). The conversion from foreign currencies to Rand and corrected for inflation is conducted in two ways.

1. Method 1: The foreign currency price for a mitigation or remediation measure was converted to a Rand value directly and the Rand value corrected for inflation.
2. Method 2: The foreign currency price was first corrected for inflation and then to converted to Rand.

The difference between the values from these approaches was calculated. Differences in Rand converted values using these conversion methods varied from -31% to 14%. The minus sign indicates lower calculated Rand values using Method 2 relative to values calculated using Method 1. This analysis implies that a maximum error of 31% can be expected when converting foreign currency prices to Rand and adjusting for uncertainty. The values calculated using Method 2 are used in the basic cost benefit analysis assessment, as it is expected that this will minimise relative inflation discrepancies between Rand and foreign exchange currencies.

A theoretical mine site was conceptualised based on the East Rand Basin Grootvlei mine. This approach was followed due to lack of mine specific information and Grootvlei was the only mine to pump and treat during operation (Roychoudhury and Starke, 2006; Expert team of the inter-ministerial commission, 2010). The mitigation and remediation cost data was used to conduct the cost benefit analysis for the two proposed scenarios.

5 CHAPTER 5: SYSTEMS COMPONENT DEFINITION AND DATA ANALYSIS

5.1 Conceptual regional systems model

A conceptual systems model was developed prior to the development of the dynamic numerical models (Figure 5-1). The physical systems boundary was chosen as the mine lease area. This boundary represents the physical geographical boundary of the ERB study area. Another boundary is the focus on specifically geochemical processes. Water in the system is considered a mass transport medium. Basic numeric water dynamics is considered in some components out of necessity. However, the focus is not on the hydrogeological flow dynamics of the East Rand Basin, as this has been considered previously (Africa Geo-Environmental Services (Pty) Ltd., 2006), but on the geochemical reactions of each component, which has not been considered in its entirety for the ERB before. The approach is therefore a *reduction to dynamics* rather than a *reduction to components.*

The physical boundary is considered osmotic in that interaction with the system and its environment can occur through various physical and chemical processes. The system itself is considered open, as mass and energy is transferred to and from the environment. The individual subsystems, termed components for this study, of the ERB geochemical system are chosen to represent the macro physical water and mass flow components within the ERB. The geochemical interactions of these components will be considered in the dynamic geochemical reaction modelling. Consideration of anthropogenic influences on the system is limited in this study to mining. This is a data availability consideration. Although non-mining activities are not considered, the contribution of mining to pollutant loads is assessed in terms of ERB baseline conditions. Therefore exclusion of other anthropogenic influences, such as sewerage plants and other industry and agriculture are not considered limitations to the current study. The focus is therefore on the differential geochemical impacts from mining activities on the ERB baseline.

Biological aspects are not taken into account as separate components, although they are taken into account in the detail of the numerical modelling and geochemical data assessments, e.g. microbiological activity on tailings are taken into account in the rate constants used for the oxidation of the sulphides. This approach is heuristic in nature, taking into account a larger set of forces and events acting on and by the system (Laszlo and Krippner, 1998).

5.2 System component and process definition and data analysis

In this section the characteristics of each ERB systems component are defined, as opposed to defining the process acting on and within the components. The processes are described in the conceptual models of the components (Chapter 6). Data analysis of component specific data is conducted in this section.

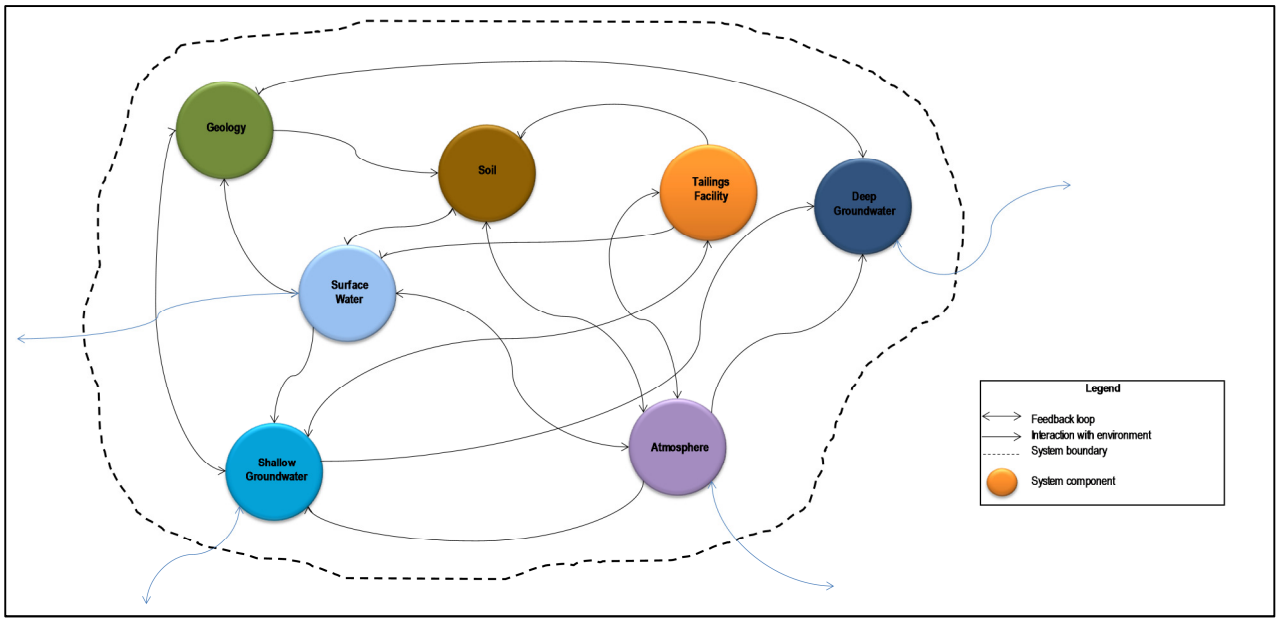

Figure 5-1 Conceptual geochemical systems model for the East Rand Basin. Each coloured bubble represents a component of the system with the lines between them representing conceptual mass and energy transfer processes. The black lines in the ERB conceptual systems model show the links between the components within the system. Single arrows depict unidirectional and double arrowed lines depict bi-directional interaction, i.e. feedback loops. The links are defined based on mass and fluid flow considerations and thus in essence represent fluxes and processes. The blue lines show processes in components which form links to the environment. The boundary is shown as a dashed line, indicating its osmotic character. The links between the atmosphere and the other components depict precipitation from the atmosphere and evaporation back to the atmosphere. Seepage can occur from the tailings facility though the underlying soil to the shallow groundwater. The geology interacts with atmospheric water, surface water and groundwater and weathers to form soil, thereby facilitating the transfer of mass and energy. Surface water and atmospheric water recharges shallow groundwater. Shallow groundwater can seep into streams through the process of base flow. Shallow groundwater seeps along faults and fissures to form deep groundwater. Deep groundwater can also be recharged though shallow groundwater by ingress zones, such as shallow coal mines. The geology influences deep groundwater through the process of weathering. The system boundary is depicted as a dashed line to show that the system should be considered thermodynamically open. The atmosphere, shallow groundwater, deep groundwater and surface water are all components through which mass and energy can be transported to and from the ERB geochemical system.

5.2.1 Component 1: Tailings

Studies have been conducted on the tailings dams in the ERB and on similar deposits in other parts of the world (Simon et al., 2005; Hayes et al., 2009; Body and Lomberg, 2008; Sidenko et al., 2007; Al and Blowes, 1999; Nenghovela et al., 2007; Dold and Fontbote, 2001; Gunsinger et al., 2006, Cukrowska et al., 2004, Hansen et al., 2008, Salmon and Malmström, 2004, 2006; Néel et al., 2003; Tutu et al., 2009; Gleisner and Herbert, 2002; Nicholsom et al., 1995; Acero et al., 2009; Bezuidenhout and Rousseau, 2005). Parameter

data for gold tailings from Bezuidenhout and Rousseau (2005), Rösner et al. (2001) and Hallbauer (1986) is shown in Table 5-1.

Table 5-1 Literature data for Witwatersrand tailings facility parameters.

	unit	Average	Maximum	Minimum
Moisture	wt%	18.75	8.5	20.5
Recharge	%	3.5	1	6
Pyrite content	%	3		
Grain size (D75)	µm	75		
Grain size (D10)	mm	0.03		
Porosity	%	32.25	31	34
Void ratio		0.49	0.46	0.51
Hydraulic conductivity	$m.s^{-1}$	5×10^{-7}	1×10^{-6}	1×10^{-8}
Hydraulic head recedence	$m.yr^{-1}$	0.5		
Density	$g.cm^{-3}$	1.42		

According to these studies, the tailings in the ERB contains a 5 – 10 cm leaching zone, followed by a hardpan layer, usually defined by various iron sulphates. These two layers form the oxidation zone, which has been shown to be up to 4 m in depth in tailings in the larger Witwatersrand (Bezuidenhout and Rousseau, 2005; Nengovhela et al., 2007; Yibas et al., 2010). Beneath this oxidation layer occurs unoxidised sulphides. This implies that the base of the hardpan layer is the oxidation front, as defined by Dold and Fontbote (2001).

The mineralogy of the tailings were derived from XRD analyses published in Rösner et al. (2001) (Table 5-2). According to their analyses, the tailings consist mostly of quartz, muscovite, pyrite, chlorite and pyrophyllite with jarosite and gypsum occurring in places as accessories. This correlates well with analyses of the quartzitic Witwatersrand gold ore (Pretorius, 1974). The high quartz content of the Witwatersrand gold ore is confirmed by XRF analyses, which shows an average the SiO_2 of 86.08 wt%, ranging from 62.08 to 93.14 wt%.

Table 5-2 Summary of tailings mineralogical analysis

	Jarosite	Gypsum	Quartz	Muscovite	Chlinochlor	Pyrophyllite
Average	***3***	***0***	***78***	***11***	***6***	***2***
Standard Deviation	2	1	7	4	5	3
Maximum	7	2	93	17	13	8
Minimum	1	0	70	4	0	0
95th Percentile	6	1	89	16	12	7
5th Percentile	1	0	71	5	0	0
n	16	16	16	16	16	16

Tailings in the ERB are defined by the oxidation of sulphides (Bezuidenhout and Rousseau, 2005; Naicker et al., 2003;, Nengovhela et al., 2007; Tutu et al., 2008). The primary sulphide mineral contained in the Wiwatersrand gold ore, including the gold ore of the ERB, is pyrite (Hallbauer, 1986). The amount of pyrite in the Witwatersrand ore ranges from ~3 to ~7 wt% with an average of ~3 wt% (Hallbauer, 1986; Rösner et al., 2001).

It has been shown that the soil on reclaimed tailings footprints are contaminated by Co, Cr, Cu, Ni and Zn (Rösner et al., 2001). It was also shown that shallow groundwater under this soil and in close proximity to it shows evidence of being impacted on by an acidic solution. These elements are therefore likely to leach from the tailings by the acidic mine drainage effluent during its operation and post-operational phases. This is confirmed by studies of AMD in the Witwatersrand which showed that surface water, soil and shallow groundwater is contaminated by heavy metals and acidity from mine drainage emanating from tailings facilities (Naicker et al., 2003; Tutu et al., 2008). It is also confirmed by studies on column leach tests of tailings material (Cukrowska et al., 2004).

Studies on the oxygen content of tailings dams (Nengovhela et al., 2007; Yibas et al., 2010) showed that oxygen depleting is 97% up to a depth of 5 m in selected tailings facilities. This implies a definite dynamic oxygen concentration gradient with depth to about 5 m.

5.2.2 Component 2: Wetlands and surface water

The ERB contains a few wetland systems, locally termed *spruite*. One of these systems, the Blesbokspruit, is a RAMSAR classified riparian wetland system. These systems are defined by slow moving water through patches of *Typha* and *Phragmite* reed species. Many tailings facilities line the banks of the stream channels of these wetlands and mines and other industries discharge water into the wetlands (Roychoudhury and Starke, 2006). In addition to seepage from the tailings and addition of contaminated groundwater to the wetland systems, particulate matter is also washed into the wetlands from the tailings. This has the effect of clogging the water course, especially the culverts during high rain and flood events, as well as providing particles with large reactive surface areas to the system. These particles can quickly participate in geochemical processes, such as dissolution and precipitation. Some studies have been conducted on these wetland systems, with most studies being focussed on the Blesbokspruit (Roychoudhury and Starke, 2006; Coetzee et al., 2006; Schoeman and Steyn, 2001). The sediments in the stream channels are characterised by clayey silt with abundant organic material. The clay and silt provide potential adsorption capacity for heavy metals, although a study by Roychoudhury and Starke (2006) suggests that adsorption may not be the principal process of heavy metal removal in the Blesbokspruit. Sequential extraction results from the same study shows that metal concentration may rather be controlled by precipitation and co-precipitation with iron oxides and carbonates. The bedrock to specifically the Blesbokspruit belongs to the Malmani dolomites, which, in addition to carbonate produced by the decay of organic material, provides a carbonate buffer to acid leaching from the tailings. The wetland systems in the ERB are currently acting as natural remediation systems, by removing heavy metals from solution via various processes and by neutralisation of any acid reaching the wetland system (Coetzee et al., 2005). Roychoudhury and Starke (2006) show that specifically the Blesbokspruit is accumulating contaminants, but can presently be regarded as low to moderately polluted and that at constant physio-chemical conditions, will remain so for the foreseeable future.

5.2.2.1 Surface water characterisation

The Blesbokspruit is the most prominent surface water drainage in the ERB. Published surface water data from the Blesbokspruit was used in the surface water characterisation of the main drainages in the ERB (Roychoudhury and Starke, 2006; Coetzee et al., 2006) (Figure 5-2). Geochemical data for the Blesbokspruit water and sediment from Roychoudhury and Starke (2006) is shown in Table 5-3 and Table 5-4. The Roychoudhury and Starke (2006) data did not contain carbonate alkalinity values. Alkalinity in the form of bicarbonate concentration was calculated using the charge imbalances. The results were compared with the Coetzee et al. (2005) data, which did contain alkalinity values. The calculated values are in good agreement with the existing data.

The most important anions are SO_4, HCO_3, Cl and NO_3 (

). The most important cations in the Blesbokspruit water are Na, Ca, Mg, K and Ni (Figure 5-3 **Pie chart showing the relative abundance of anions in the Blesbokspruit water**

Figure 5-4). The fact that Ca, Mg and HCO_3 are dominant is a reflection of the influence of the dolomitic rocks forming the base of the Blesbokspruit drainage channel. The dominance of Na, SO_4 and NO_3 are indicative of possible pollution sources.

Various graphical methods exist which can be used to characterise groundwater (Hem, 1985). Of these, the most useful are the Piper and Stiff diagrams. The Piper diagram is a trilinnear plot of the major cations and anions in groundwater as milli-equivilents per litre (meq/ℓ) and is used to characterise water samples. It is also useful to determine whether a particular water sample may represent a mixture of other samples for which analyses are available and to show trends in stream or groundwater flow.

The advantage of the Piper diagram is that it can be used for multiple samples, whereas the Stiff diagram can only be plotted for single samples. A Piper diagram is thus well suited to get a first impression of a large data set. Stiff diagrams are useful in showing differences or similarities in waters and changes in water composition with depth, or along a profile. It is also generally used for water classification purposes.

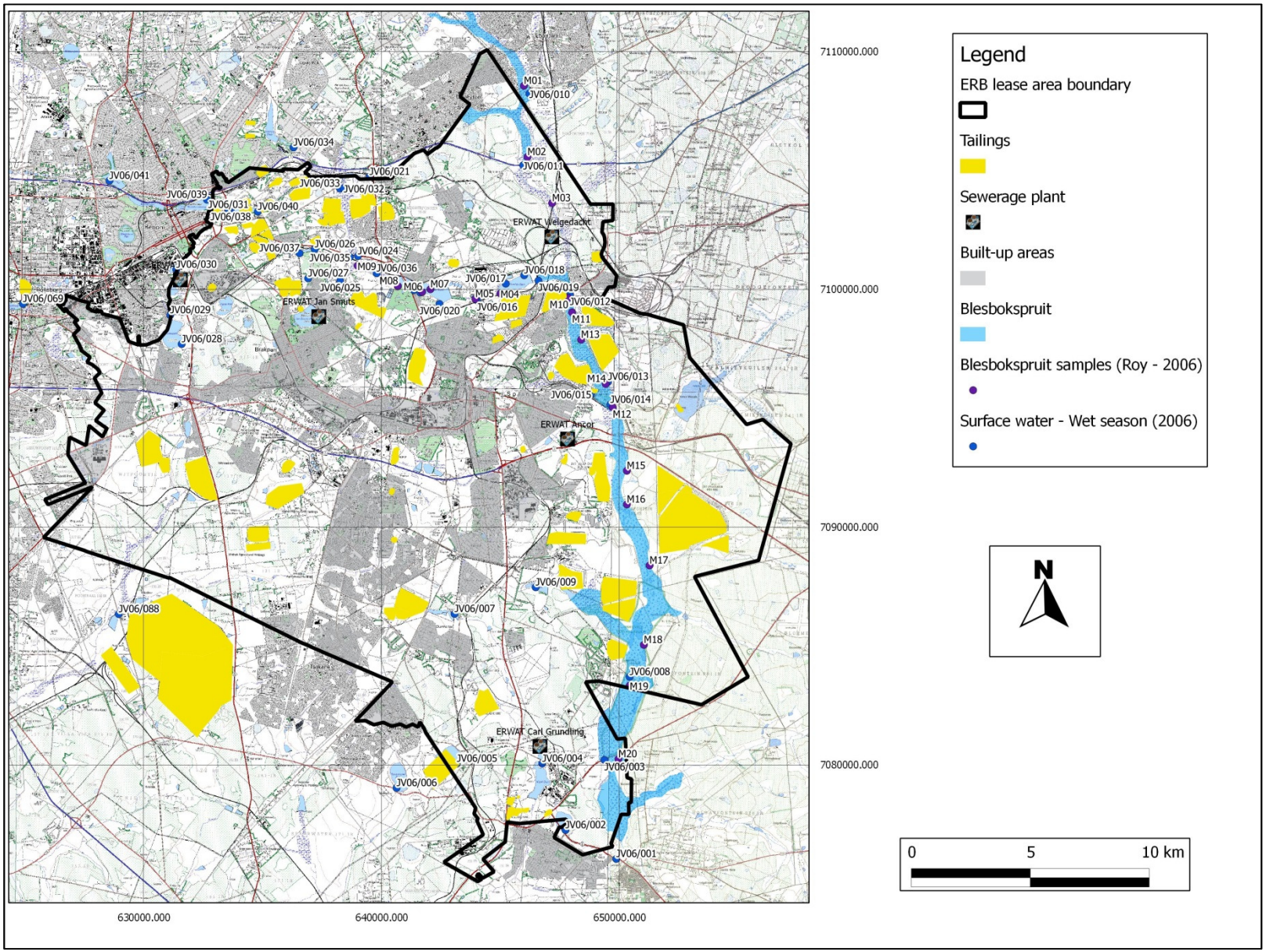

Figure 5-2 ERB surface water samples points

Table 5-3 Summary of surface water ICP-MS data of the Blesbokspruit (after Roychoudhury & Starke (2006))

	Units	Average	Standard Deviation	Maximum	Minimum	95th Percentile	5th Percentile	n
pH		7.9	0.9	9.2	5.6	9.2	6.8	20
DO	*mg/l*	7.7	2.3	10.8	2.5	10.3	3.6	20
Eh	*mV*	242.1	139.5	538.0	54.0	476.8	102.6	19
EC	*mS/cm*	1 862.9	1 974.9	9 660.0	521.0	2 763.0	582.8	20
T	*℃*	14.1	4.0	24.2	5.7	18.8	9.0	20
F	*mg/l*	0.1						1
Cl	*mg/l*	118.5	37.7	161.0	28.0	155.3	65.1	20
NO_2	*mg/l*	8.8	12.8	28.0	2.0	24.3	2.0	4
Br	*mg/l*	4.0	3.5	8.0	2.0	7.4	2.0	3
NO_3	*mg/l*	31.6	41.8	188.0	1.0	78.8	3.9	20
SO_4	*mg/l*	521.4	904.0	4 194.0	73.0	876.6	81.6	20
Na	*mg/l*	220.3	171.4	855.0	69.0	313.5	74.7	20
K	*mg/l*	16.8	4.4	32.0	9.0	21.6	12.8	20
Ca	*mg/l*	100.5	73.8	195.0	21.0	193.1	22.9	20
Mg	*mg/l*	29.8	19.9	56.0	9.0	56.0	10.0	20
Be	*ug/l*	0.1	0.1	0.2	0.0	0.2	0.0	4
Ti	*ug/l*	109.5	87.7	324.3	26.5	206.4	28.6	20
V	*ug/l*	3.1	2.1	7.2	0.6	6.5	0.6	20
Cr	*ug/l*	4.3	2.5	11.3	0.7	7.2	1.2	20
Mn	*ug/l*	653.0	857.7	3 128.5	23.7	2 659.3	30.7	20
Fe	*ug/l*	318.4	185.7	559.6	56.8	508.3	72.7	20
Co	*ug/l*	226.7	947.3	4 250.0	2.6	329.4	2.9	20
Ni	*ug/l*	2 121.9	9 267.7	41 495.0	2.4	2 354.2	3.6	20
Cu	*ug/l*	16.4	60.7	267.0	0.1	31.6	0.1	19
Zn	*ug/l*	109.7	246.3	1 119.0	8.3	315.0	10.0	20
As	*ug/l*	5.2	2.8	9.9	0.0	9.4	0.2	20
Se	*ug/l*	5.0	8.8	41.3	0.2	8.2	0.2	20
Sr	*ug/l*	234.6	118.6	485.0	81.7	372.0	88.4	20
Zr	*ug/l*	0.3	0.1	0.5	0.1	0.4	0.1	20
Mo	*ug/l*	6.9	4.4	16.8	0.1	15.7	0.1	20
Ag	*ug/l*	1.4	0.3	2.0	0.9	1.8	1.0	20
Cd	*ug/l*	0.3	0.3	1.5	0.0	0.4	0.1	20
Ba	*ug/l*	28.1	17.0	79.0	13.0	65.5	14.3	20
Au	*ug/l*	0.3	0.2	0.8	0.0	0.5	0.0	20
Hg	*ug/l*	0.7	0.6	2.5	0.1	2.1	0.1	20
Pb	*ug/l*	1.1	1.7	7.6	0.1	2.6	0.3	20
Th	*ug/l*	0.0	0.0	0.1	0.0	0.1	0.0	8
U	*ug/l*	24.3	11.5	39.9	2.0	38.4	2.7	18

Table 5-4 Summary of properties of sediments from the Blesbokspruit (after Roychoudhury & Starke (2006)

	Units	Average	Standard Deviation	Maximum	Minimum	95th Percentile	5th Percentile	n
Gravel	%	5.7	11.1	44.0	0.0	27.9	0.0	20
Sand	%	40.0	21.5	85.0	11.0	67.9	15.8	20
Silt	%	39.9	20.6	73.0	8.0	73.0	9.0	20
Clay	%	14.6	12.4	43.0	4.0	38.3	4.0	20
Organic Carbon	%	2.3	2.1	9.0	0.5	6.0	0.6	20
Ti	mg/kg	3 462.0	1 318.2	5 359.0	1 289.0	5 267.8	1 312.8	20
V	mg/kg	93.7	44.7	238.0	33.0	157.3	38.7	20
Cr	mg/kg	191.4	105.0	532.0	62.0	348.7	78.2	20
Mn	mg/kg	828.0	876.4	3 488.0	68.0	2 597.9	77.5	20
Fe	mg/kg	33 888.8	14 862.9	58 347.0	10 462.0	57 006.6	11 669.5	20
Co	mg/kg	35.7	34.1	123.6	3.6	102.9	7.4	20
Ni	mg/kg	119.0	112.3	438.2	16.2	348.1	28.3	20
Cu	mg/kg	66.5	80.2	361.6	12.9	207.5	14.3	20
Zn	mg/kg	155.6	95.7	423.5	35.8	334.7	42.8	20
As	mg/kg	27.3	38.8	130.7	2.5	127.0	3.6	20
Se	mg/kg	2.7	2.5	8.2	0.1	7.7	0.4	20
Sr	mg/kg	34.9	21.4	96.7	9.1	69.2	12.8	20
Zr	mg/kg	95.2	36.4	175.7	26.5	137.5	41.3	20
Mo	mg/kg	1.3	0.6	2.7	0.5	2.1	0.5	20
Ag	mg/kg	1.2	2.2	10.2	0.3	1.9	0.3	20
Cd	mg/kg	0.2	0.1	0.4	0.0	0.3	0.1	20
Ba	mg/kg	274.4	276.0	1 160.5	59.8	754.3	108.2	20
Au	mg/kg	0.4	0.4	1.7	0.1	1.0	0.1	20
Hg	mg/kg	0.8	1.3	5.8	0.0	2.3	0.0	20
Pb	mg/kg	19.6	8.9	38.7	7.4	36.2	8.2	20
Th	mg/kg	7.9	3.0	12.2	2.3	11.5	3.7	20
U	mg/kg	12.0	16.9	62.4	1.4	45.8	1.7	20

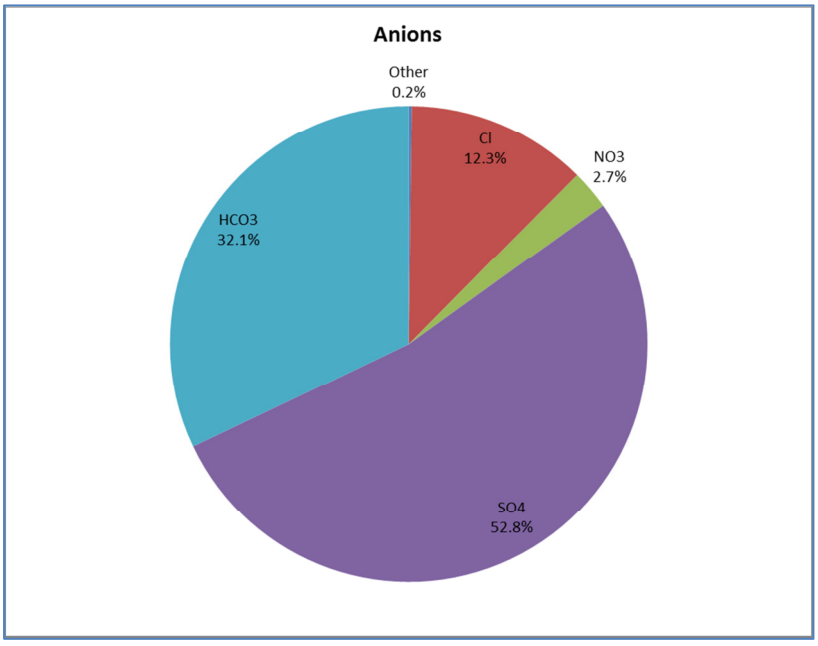

Figure 5-3 Pie chart showing the relative abundance of anions in the Blesbokspruit water

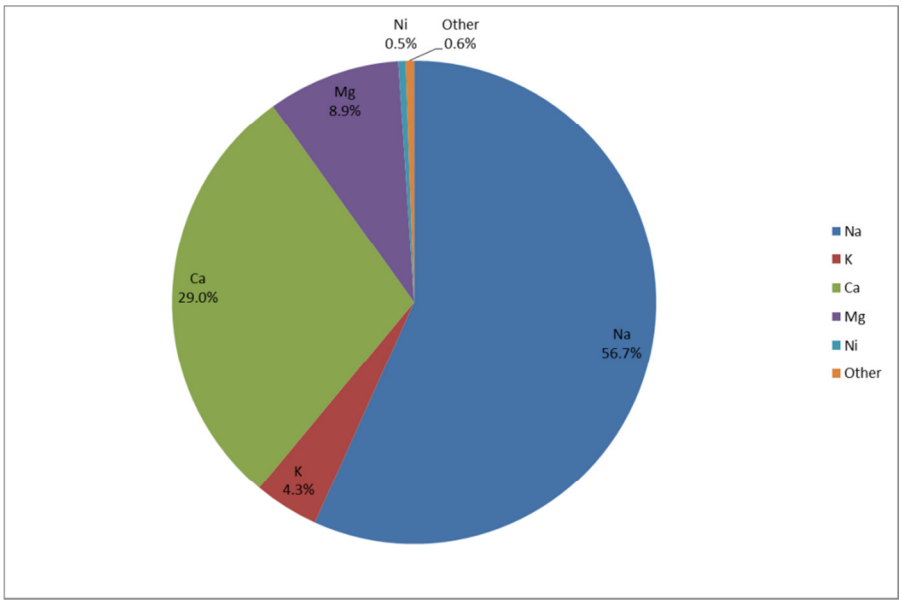

Figure 5-4 Pie chart showing the relative abundance of cations in the Blesbokspruit water

A Piper diagram was constructed for the Blesbokspruit surface water data (Table 5-4).

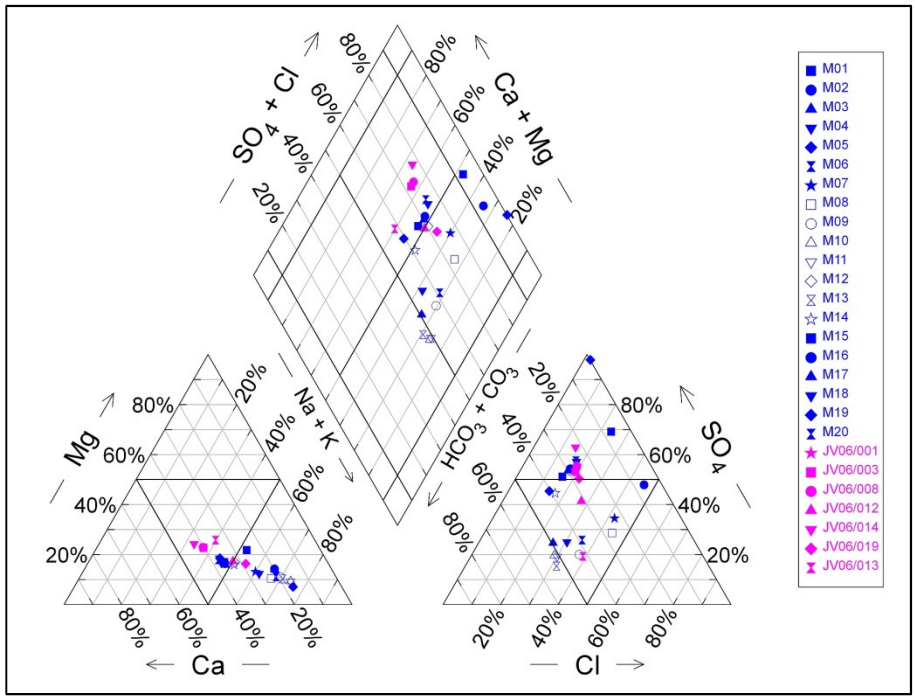

Figure 5-5 Piper diagram of the Blesbokspruit surface water. The Roychoudhury and Starke (2006) data is indicated by the blue markers, while the Coetzee et al. (2005) data is indicated by the pink markers. It can be seem that the data sets correlate. The data sets also show < 60% equivalent HCO_3 than would be expected in a pristine setting of a stream flowing over dolomitic rocks. The data shows a strong trend towards enrichment in SO_4.

The diagram shows that the Roychoudhury and Starke (2006) and Coetzee et al. (2005) data correlates in terms of the major cations and anions. The Coetzee et al. (2005) data is slightly elevated in terms of Ca content and shows a stronger trend towards increasing SO_4 than the Roychoudhury and Starke (2006) data. The Blesbokspruit data in general shows at least 3 different types of water and mixing of water between the different types.

A Durov diagram is an extension of the Piper diagram, showing pH and TDS in addition to major cations and anions. A Durov diagram of the Blesbokspruit surface water samples (Figure 5-6) shows that based on the anions, TDS and pH values, between 3 and 5 different water types occur in the Blesbokspruit channel. Since the Stiff diagrams show that all the samples are from essentially the same water, the variations in the Piper and Durov diagrams indicate 3 to 5 different processes acting on the Blesbokspruit surface water. There are a number of industries situated along the banks of the Blesbokspruit drainage channel (Roychoudhury and Starke, 2006) (Figure 5-9).

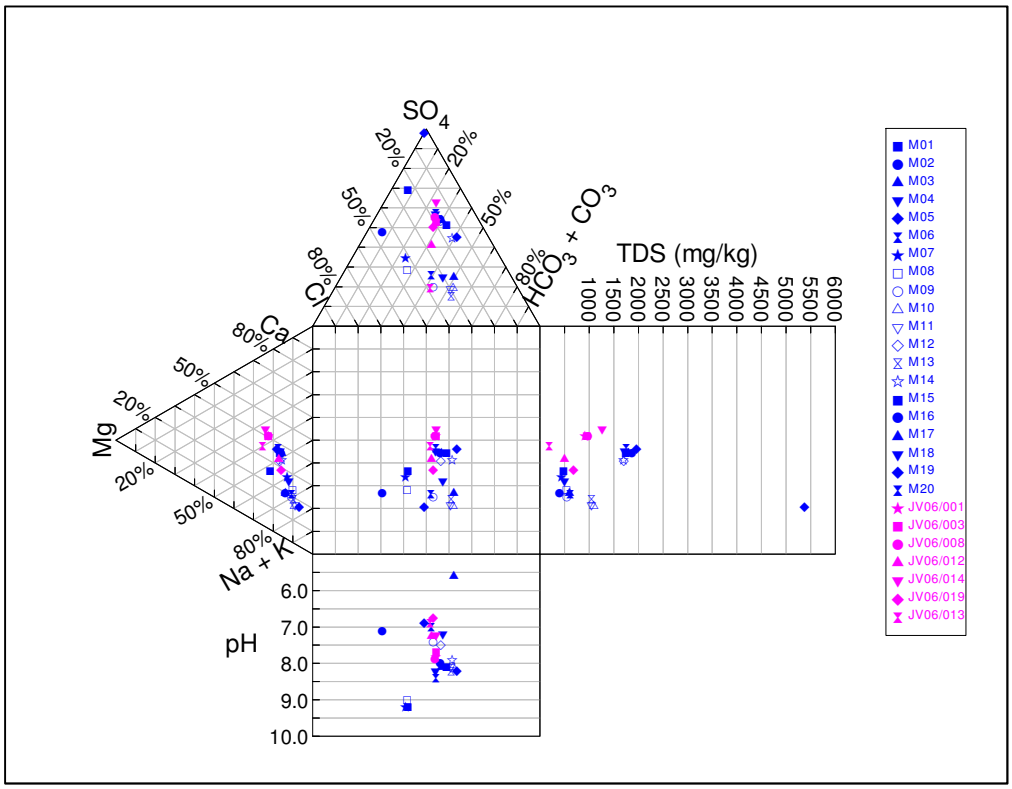

Figure 5-6 Durov plot of the Blesbokspruit surface water. The Roychoudhury and Stark (2006) data is indicated with blue markers, while the Coetzee et al. (2005) data is indicated with pink markers. The data shows only one acidic sample (pH 5.6, Roychoudhury and Starke (2006) sample M03). The rest are circum-neural to alkaline. The TDS ranges from moderate (~500 mg/ℓ) to high (5 364 mg/ℓ, Roychoudhury and Starke (2006) sample M05).

Stiff diagrams were constructed for three Blesbokspruit water samples upstream from the ERB (M01, M02 and M03) and three water samples close to the point of outflow from the ERB (M14, M15 and M18) using the

Roychoudhury and Starke (2006) data. These diagrams show that even though samples M01, M02 and M03 are located upstream from the ERB, they show strong SO_4, Na and K signatures in the water. This implies that although the water is upstream from the main mining areas, there may be impacts on the surface water upstream from these sample points. The downstream Blesbokspruit samples show that SO_4 concentrations in meq/ℓ have doubled with respect to the other ions. The Na and K signature remains strong, while Ca and HCO_3 has been added to the surface water. This indicates potential dissolution of Ca and HCO_3 as water flows past the mine sites. The data indicates that the Blesbokspruit is being influenced by externalities, such as sewerage plants and other industries, in addition to mining activities.

A correlation matrix, using the Pearson's product moment correlation coefficient, was constructed for the Blesbokspruit surface water data and the correlations evaluated using scatterplots (Table 5-5). These correlations were evaluated using scatterplots and it was found that the correlations are more complex than is shown by the correlation matrix. For example, Ca and Mg have a correlation coefficient (r) value of 0.98 Figure 5-7.

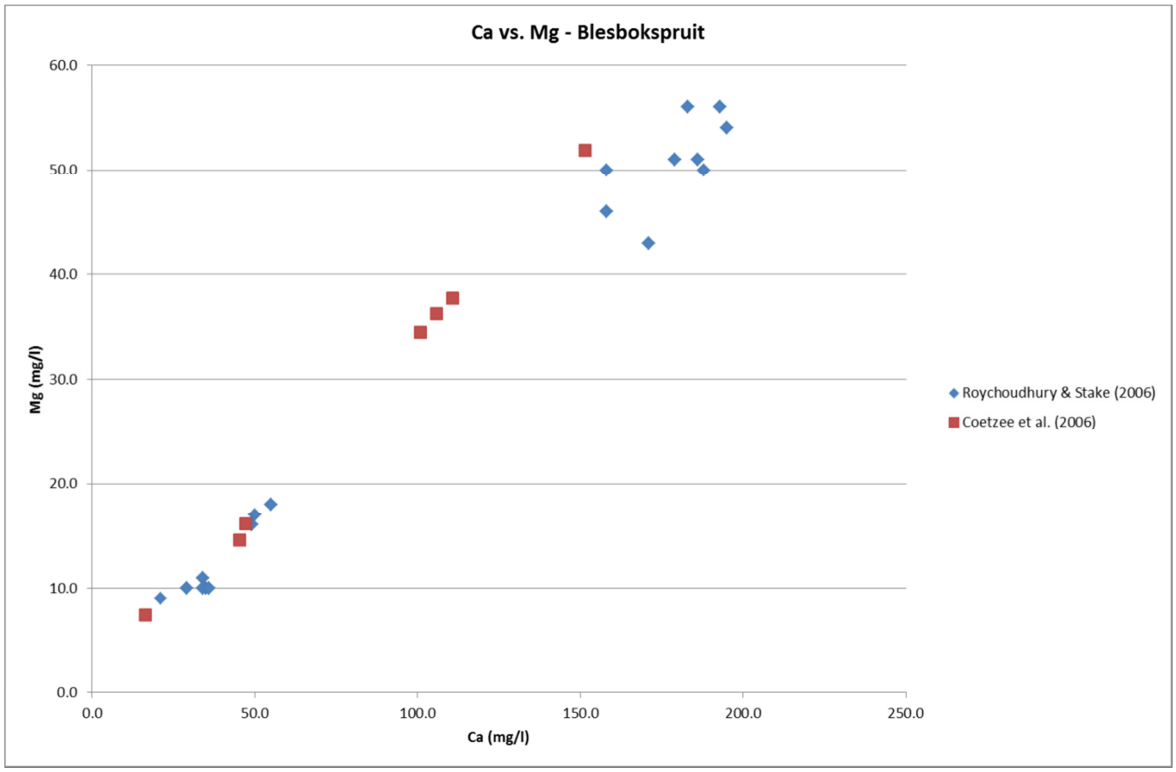

Figure 5-7 Ca vs. Mg scatterplot of the Blesbokspruit surface water data.

The scatterplot shows that although the correlation is 0.98, the data plots in distinct groups. One group has high Ca and Mg and the other relatively lower Ca and Mg. The Coetzee et al. (2005) data shows 3 samples plotting between the Roychoudhury and Starke (2006) data groups. The Coetzee et al. (2005) data was collected in the wet season of 2006, while the Roychoudhury and Starke (2006) data could have been sampled at a drier time of the year. If this is the case, then the difference in samples are simply due to seasonal variation and are a result of better mixing for the water sampled by Coetzee et al. (2005).

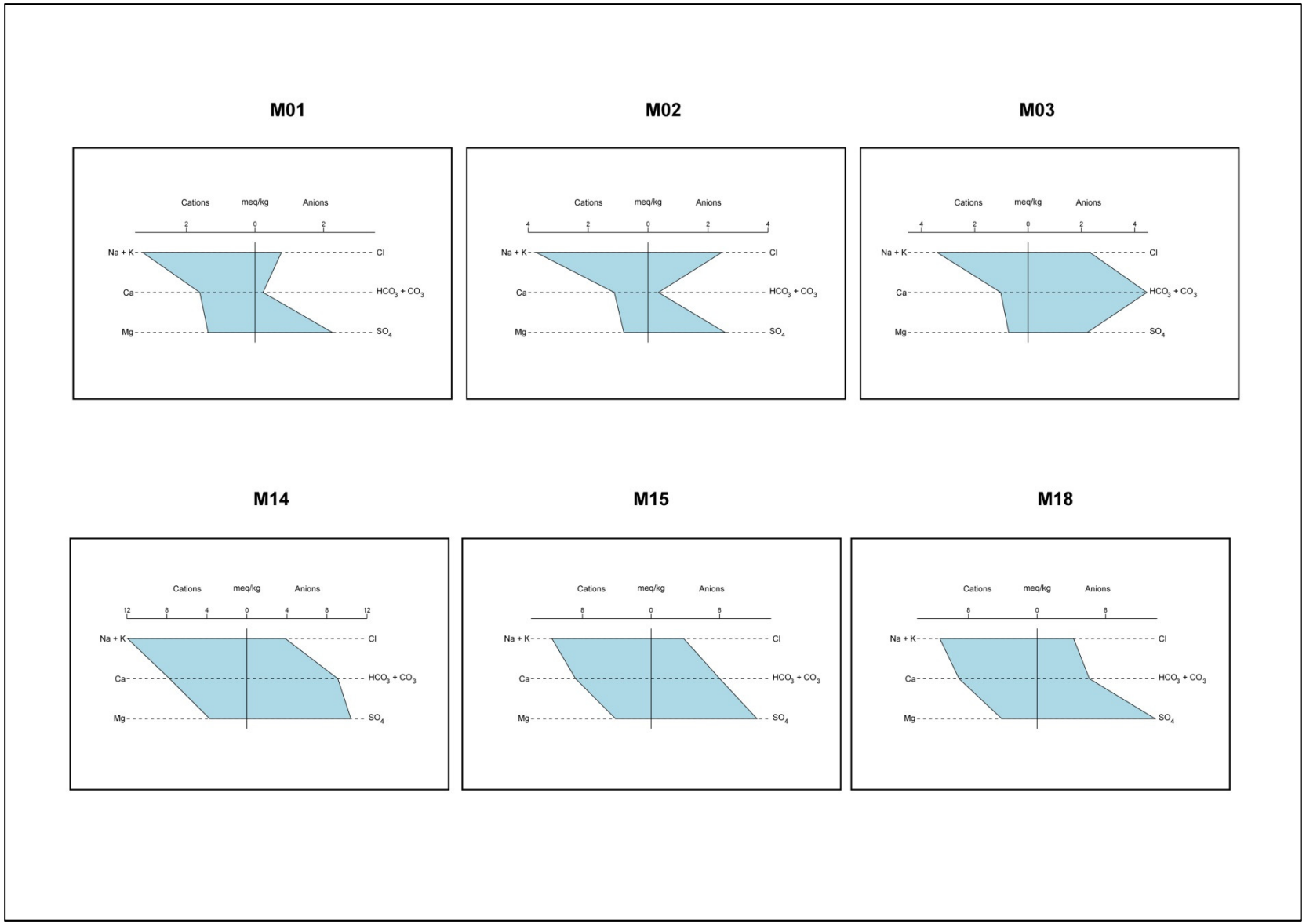

Figure 5-8 Stiff diagrams of Blesbokspruit surface water data

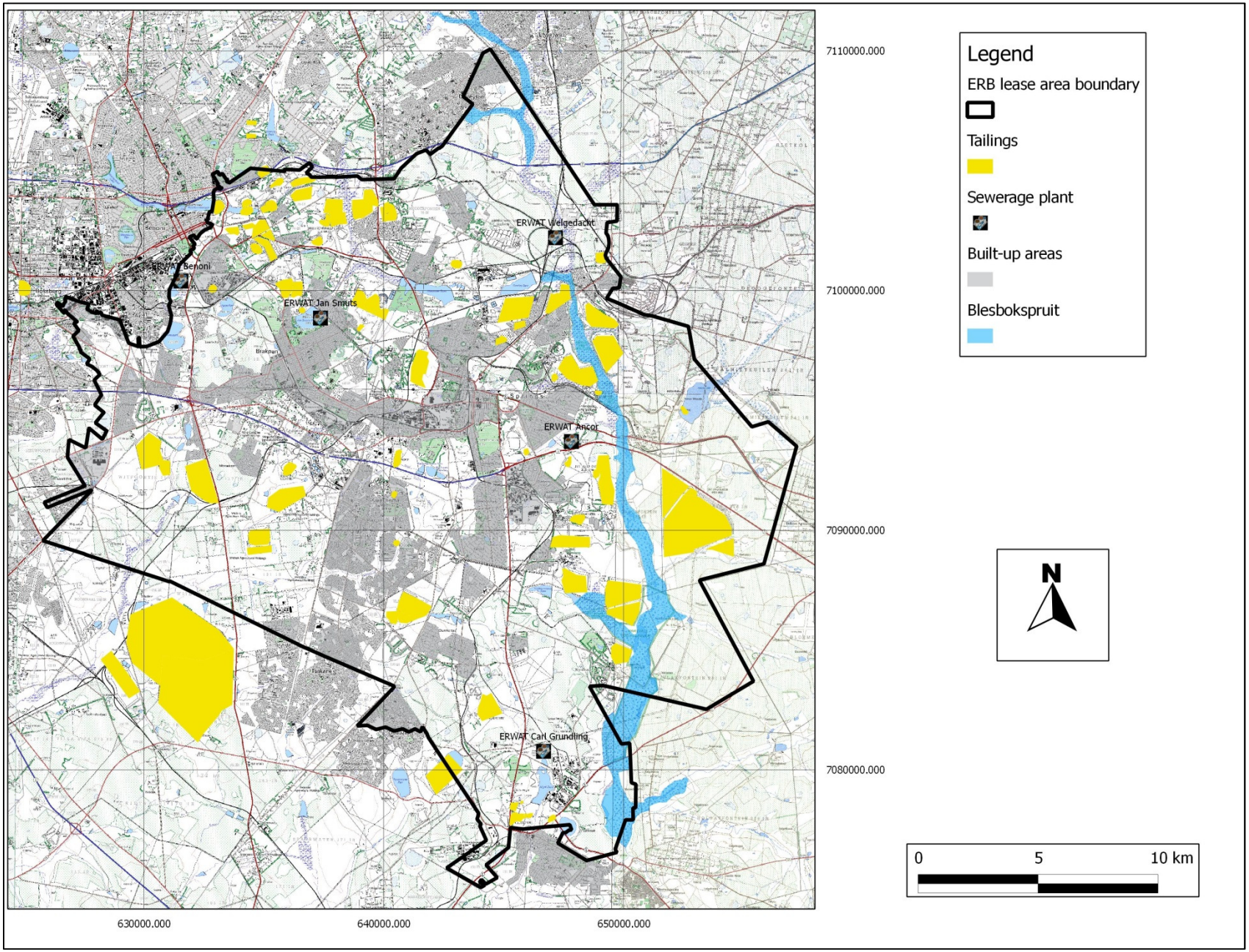

Figure 5-9 Tailings dams and sewerage treatment plants in the ERB

Table 5-5 Correlation matric for the Blesbokspruit surface water chemistry

	pH	DO	Eh	NO_2	Br	Cl	NO_3	SO_4	HCO_3	Na	K	Ca	Mg	Ni	Cr	Mn	Fe	Co	Cu	Zn	As	Se	Sr	Mo	Ag	Cd	Ba	Au	Hg	Pb
pH																														
DO	0.47																													
Eh	0.09	-0.05																												
NO_2	-0.2	-0.11	-0.15																											
Br	0.08	0.25	0.04	-0.04																										
Cl	0.24	0.31	0.11	-0.22	0.22																									
NO_3	0.4	-0.14	0.12	0.28	-0.13	-0.4																								
SO_4	-0.17	-0.06	-0.13	0.95	0.02	-0.07	0.17																							
HCO_3	0.14	0.21	0.16	-0.26	0.46	0.84	-0.31	-0.13																						
Na	-0.05	-0.01	-0.08	0.87	0.13	0.24	0.16	0.92	0.16																					
K	0.14	-0.03	0.09	0.67	0.1	0.27	0.29	0.68	0.1	0.81																				
Ca	0.16	0.19	0.04	0.24	0.29	0.56	-0.18	0.5	0.58	0.57	0.38																			
Mg	0.16	0.16	0.03	0.16	0.29	0.52	-0.18	0.43	0.59	0.48	0.26	0.98																		
Ni	-0.23	-0.12	-0.16	0.99	-0.06	-0.26	0.25	0.95	-0.33	0.85	0.65	0.22	0.14																	
Cr	-0.07	0.16	-0.36	-0.12	0.01	0.1	-0.41	0.01	0.12	-0.07	-0.38	0.32	0.38	-0.1																
Mn	-0.71	-0.15	-0.14	0.47	-0.1	-0.3	0	0.41	-0.25	0.31	0.06	-0.11	-0.15	0.48	-0.13															
Fe	-0.14	0.01	0.36	0.12	0.28	0.45	-0.01	0.28	0.48	0.39	0.39	0.61	0.57	0.09	-0.26	0.32														
Co	-0.24	-0.12	-0.18	0.99	-0.06	-0.26	0.26	0.95	-0.33	0.85	0.64	0.21	0.13	1	-0.09	0.5	0.08													
Cu	-0.23	-0.12	-0.17	0.99	-0.06	-0.27	0.25	0.95	-0.33	0.85	0.64	0.21	0.14	1	-0.09	0.48	0.08	1												
Zn	-0.44	-0.19	-0.23	0.87	-0.12	-0.45	0.23	0.82	-0.45	0.65	0.36	0.05	0	0.9	-0.02	0.7	0.05	0.91	0.9											
As	0.4	0.06	0.12	0.04	0.13	0.47	0.11	-0.04	0.39	0.25	0.42	-0.01	-0.07	-0.01	-0.27	-0.39	-0.07	-0.01	-0.02	-0.28										
Se	-0.25	-0.08	-0.29	0.9	-0.02	-0.18	0.11	0.89	-0.21	0.8	0.44	0.28	0.23	0.91	0.19	0.44	-0.03	0.92	0.91	0.88	-0.06									
Sr	0.1	0.11	-0.01	0.5	0.24	0.44	-0.09	0.72	0.43	0.77	0.59	0.94	0.9	0.49	0.24	-0.02	0.54	0.48	0.48	0.27	0.09	0.5								
Mo	0.29	0.03	-0.23	0.05	-0.05	0.22	0.18	-0.09	0.11	0.11	0.21	-0.27	-0.28	0.02	0	-0.36	-0.49	0.03	0.02	-0.14	0.66	0.1	-0.15							
Ag	0.2	-0.04	-0.24	0.39	-0.16	-0.03	0.23	0.22	-0.24	0.28	0.46	-0.3	-0.37	0.37	-0.33	0.02	-0.32	0.37	0.36	0.22	0.38	0.26	-0.13	0.46						
Cd	-0.32	-0.11	-0.46	0.3	-0.18	-0.45	-0.22	0.32	-0.37	0.07	-0.37	0.05	0.11	0.33	0.66	0.26	-0.43	0.35	0.35	0.5	-0.57	0.56	0.08	-0.16	-0.13					
Ba	-0.38	-0.22	0.16	0.02	-0.16	-0.5	0.42	-0.01	-0.28	-0.16	-0.36	-0.21	-0.17	0.04	-0.44	0.61	0.37	0.03	0.04	0.28	-0.68	-0.07	-0.26	-0.5	-0.35	0.04				
Au	0.17	-0.11	-0.17	0.49	-0.17	-0.29	0.64	0.43	-0.27	0.4	0.38	0.08	0.09	0.46	0.32	0.19	-0.05	0.47	0.46	0.48	-0.02	0.47	0.2	0.19	0.22	0.46	0.21			
Hg	0.06	-0.07	-0.16	-0.15	0.08	0.23	0.06	-0.15	0.2	-0.05	-0.2	0.04	0.11	-0.19	0.45	0.06	0.2	-0.18	-0.19	-0.13	0.04	-0.11	-0.05	0.06	-0.12	-0.19	0.16	0.54		
Pb	0.5	0.21	-0.34	-0.15	-0.08	-0.2	0.24	-0.25	-0.24	-0.26	-0.21	-0.38	-0.38	-0.14	-0.21	-0.3	-0.52	-0.14	-0.14	-0.19	0.44	-0.14	-0.34	0.24	0.46	-0.14	-0.24	-0.03	-0.08	
U	0.38	0.26	0.21	0.01	0.25	0.7	-0.11	0.16	0.66	0.37	0.48	0.69	0.63	-0.04	0.04	-0.29	0.47	-0.05	-0.06	-0.25	0.47	-0.06	0.64	-0.01	0.06	-0.43	-0.53	-0.04	0	-0.09

Naicker et al. (2003) showed that seasonal variations do have an influence on the mass loads of the shallow groundwater and surface water in the larger Witwatersrand.

Sodium and SO_4 has a linear correlation coefficient value of 0.92 (Figure 5-10). The plot shows the same trend as the Ca vs. Mg plot. The Roychoudhury and Starke (2006) data shows at least 3 distinctive groups, while the Coetzee et al. (2005) data shows 2 groups, with a more linear distribution of sample water data.

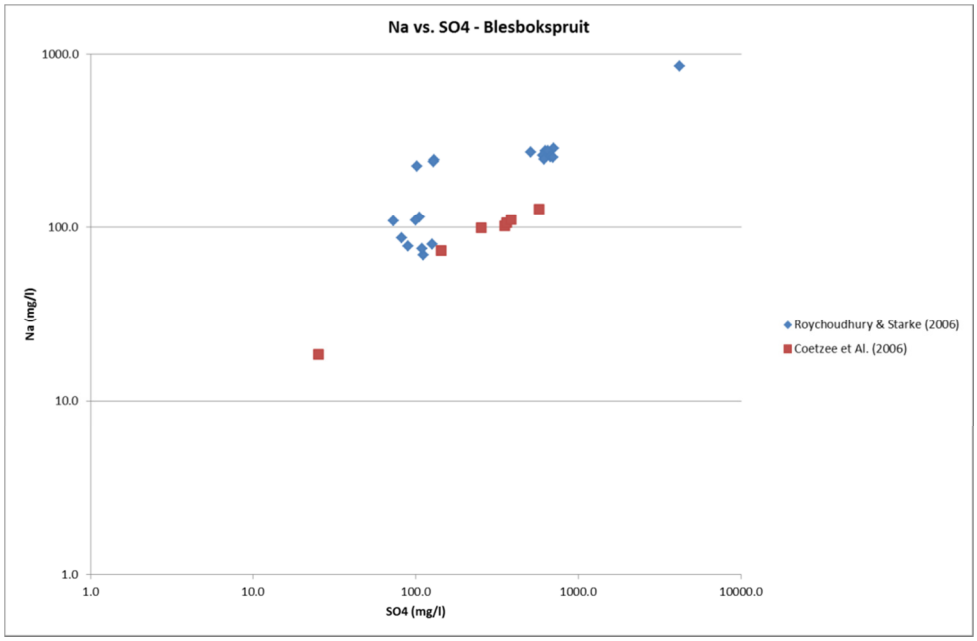

Figure 5-10 Scatterplot of Na vs. SO4 of the Blesbokspruit surface water data.

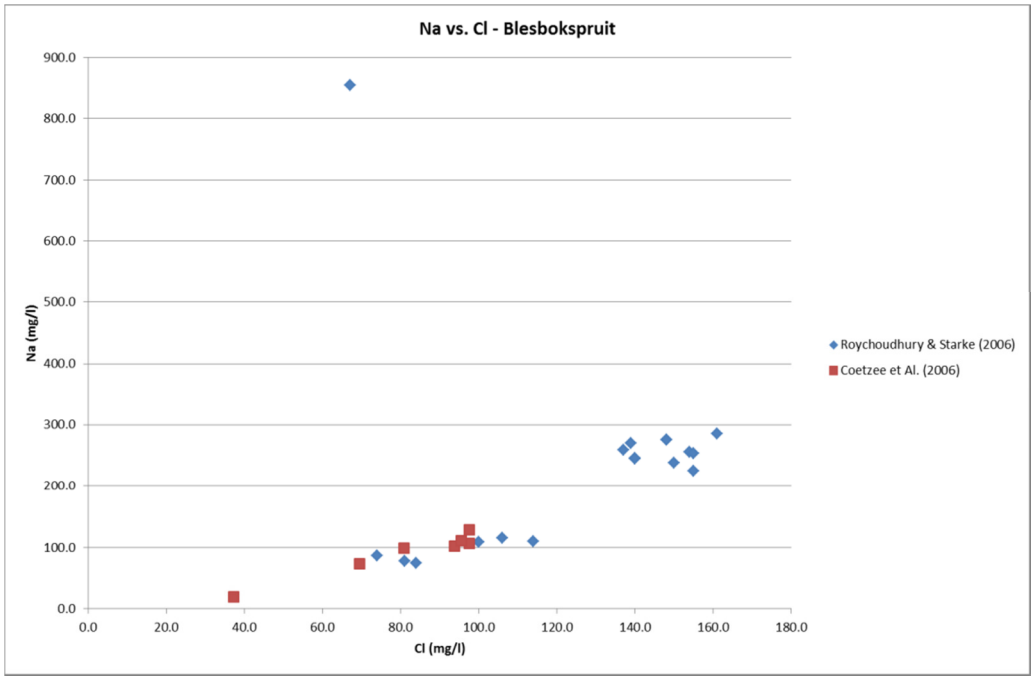

Figure 5-11 Na vs. Cl scatterplot of the Blesbokspruit surface water data.

The correlation coefficient between Na and Cl is 0.24 (Figure 5-11). The plot shows that one outlier sample of the Roychoudhury and Starke (2006) dataset is causing the low r value. In actual fact Na and Cl do correlate and shows a trend on increasing Na vs. Cl.

These plots confirm the notion that although the Blesbokspruit consists of one water type, shown by the Stiff diagrams, there is definitely impacting water sources on the Blesbokspruit, containing especially SO_4 and Na. These impacting activities have low volumes, as the Stiff diagrams would show significantly different water types of high volumes relative to the volume of flow in the Blesbokspruit were being discharged. Mining impacts, specifically seepage of polluted groundwater (Naicker et al., 2006) and seepage from tailings facilities form part of these activities. The plots also show that the linear correlation coefficient is too simplistic to provide understanding of the non-linear dynamics of mass transport in the ERB.

5.2.2.2 Statistical analysis of Blesbokspruit surface water

5.2.2.2.1 pH

The average pH of the Blesbokspruit groundwater is 7.74 (σ = 0.79) with a maximum of 9.20 and a minimum of 5.60. The histogram of Blesbokspruit pH data (Figure 5-12) shows a fairly uniform distribution, slightly skewed to the right with a skewness of -0.33.

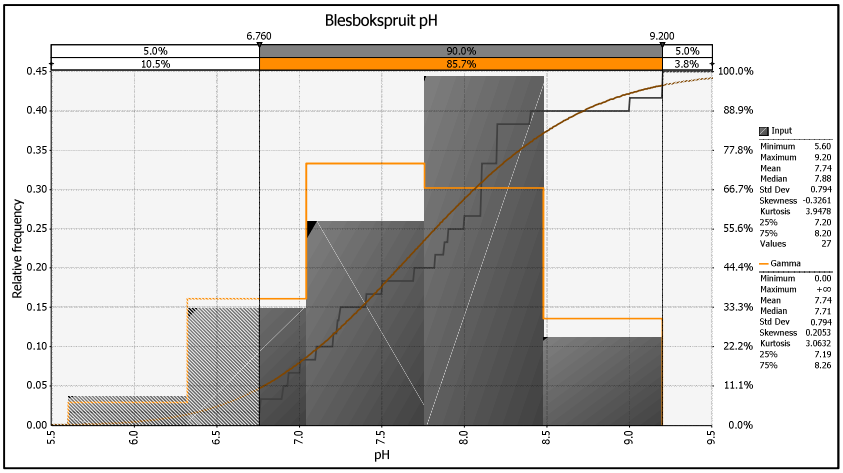

Figure 5-12 Histogram plot of the Blesboskpruit surface water pH data. The plot shows relative frequency (probability of a value in the range of a bin occurring) on the y-axis on the left-hand side and cumulative frequency on the y-axis on the right-hand side. The dark grey line is the cumulative distribution plot for the actual data. The dark brown curve is the cumulative curve for the best fit distribution. The x-axis is the histogram bin ranges for the pH data. The graph shows e.g. that a pH value of between 7.8 and 8.5 has a probability of 0.44 of occurring. The cumulative probability of the same range is 89%, implying that the chance that a value will be lower than 8.5 has a probability of 89%. The orange curve is the best fit distribution for the data. In this case a Gamma distribution. The summary statistics of both the actuial data and best fit curve are in the legend on the right-hand side of the plot. Areas falling outside the 95% confidence levels are shaded.

A study of the extreme values shows that the values above 9.55 and those below 5.81 can be considered outliers[3]. Only one sample falls outside this range. Sample M03 (Roychoudhury and Starke, 206) has a pH of 5.6. The Blesbokspriut surface water is circum-neutral to alkaline with pH values in the 95% conficence levels between 6.80 and 9.14. This is most probably due to the influence from the Malmani dolomites, which form the base of the stream in many places. The acidic waters are most probably derived from tailings dams on the banks of the Blesbokspruit drainage channel. The alkaline waters are either also effluent from industry or a response of the dolomites to the introduction of acidic waters from tailings dams.

5.2.2.2.2 SO_4

The SO_4 data distribution or the Blesbokspruit surface water shows a very strong bimodal character (Figure 5-13). The average SO_4 concentration for the Blesbokspruit surface water is 464 (σ = 183) with a maximum of 4 195 and a minimum of 25. The distribution is positively skewed (skewness = 4.43). An analysis of the extreme values show that values outside the range 0 to 1 358 can be considered outliers. The 95% confidence levels are 78 and 701. The bimodal distribution indicates that the Blesbokspruit surface water is being impacted upon by a solution containing elevated concentrations of SO_4. This solution is impacting on the Blesbokrptuit surface water baseline concentration, most probably causing it to increase with time. This will however depend on the solubilities of sulphate minerals such as gypsum, which may precipitate from solution and buffer sulphate concentrations. These aspects will be explored in the numeric geochemical reaction modelling in Section **Error! Reference source not found.**.

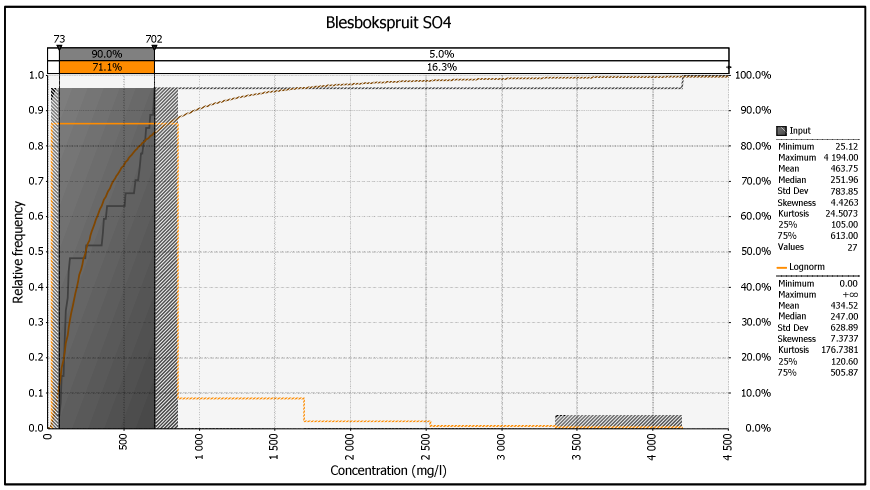

Figure 5-13 Data distribution of Blesbokspruit surface water SO_4. The data distribution is bimodal. Almost all the data occurs between 0 and 700 mg/ℓ, as evidenced by the high probability for this bin range to occur (0.95). A second distribution has values between 3 400 to 4 300.

[3] The outliers were determined by using the standard Box plot equations. The upper limit of the data range was calculated by multiplying the inter quantile range with 1.5 and adding it to the 3rd quantile. The lower limit of the data range was calculated by multiplying the inter quantile range by 1.5 and subtracting the result from the 1st quantile.

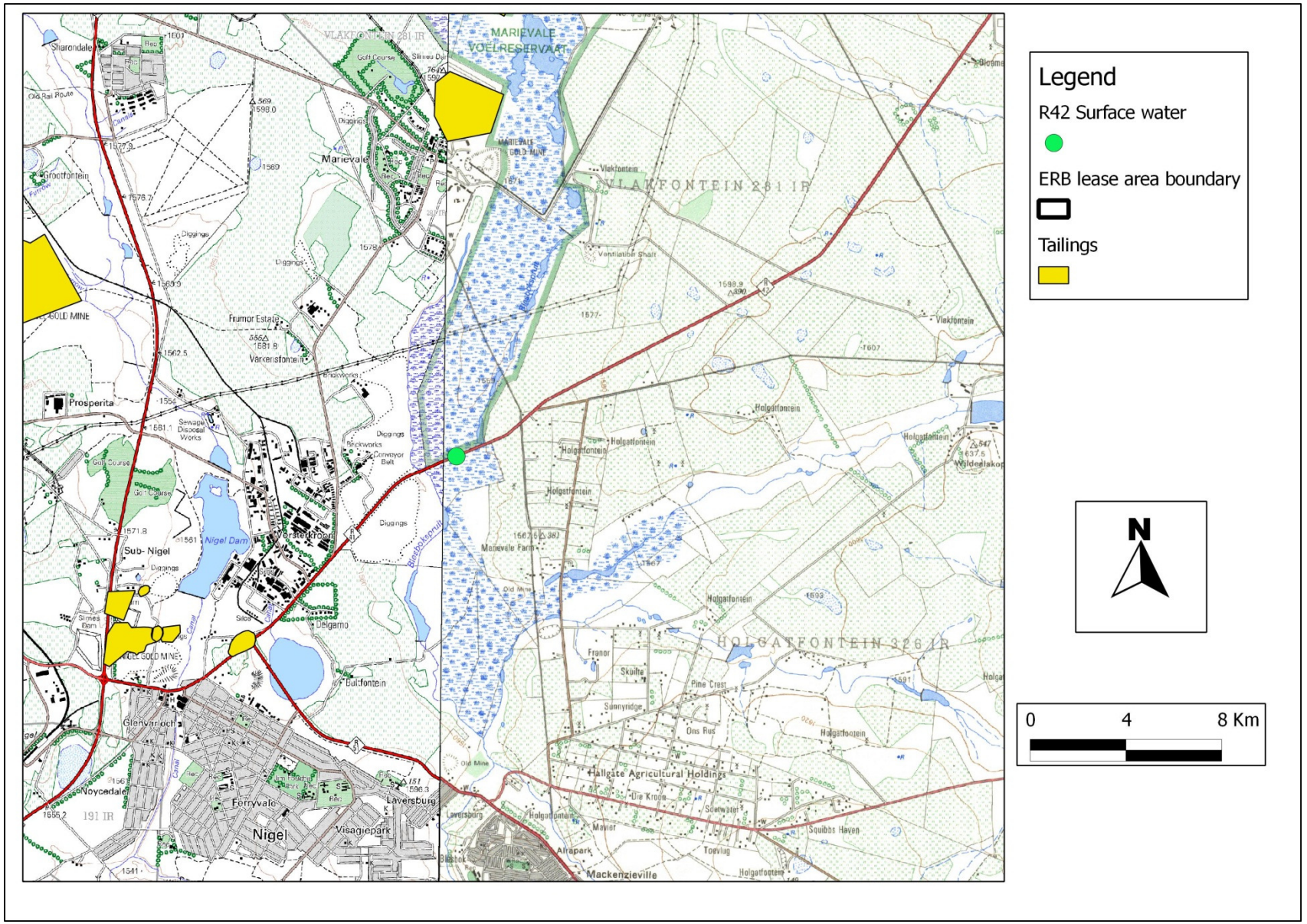

Figure 5-14 R42 Blesbokspruit R42 surface water monitoring point

Analysis of time series surface water monitoring data for two time periods from the same point in the Blesbokspruit was conducted (Figure 5-14, Figure 5-15 and **Error! Not a valid bookmark self-reference.**)[4].The plots show that there is a general inverse relationship between rainfall and sulphate concentrations. The charts show that there is an average 1 to 2 month delay between peak rainfall events and minimum sulphate values. This implies that rainfall and evaporation cycles play a significant role in

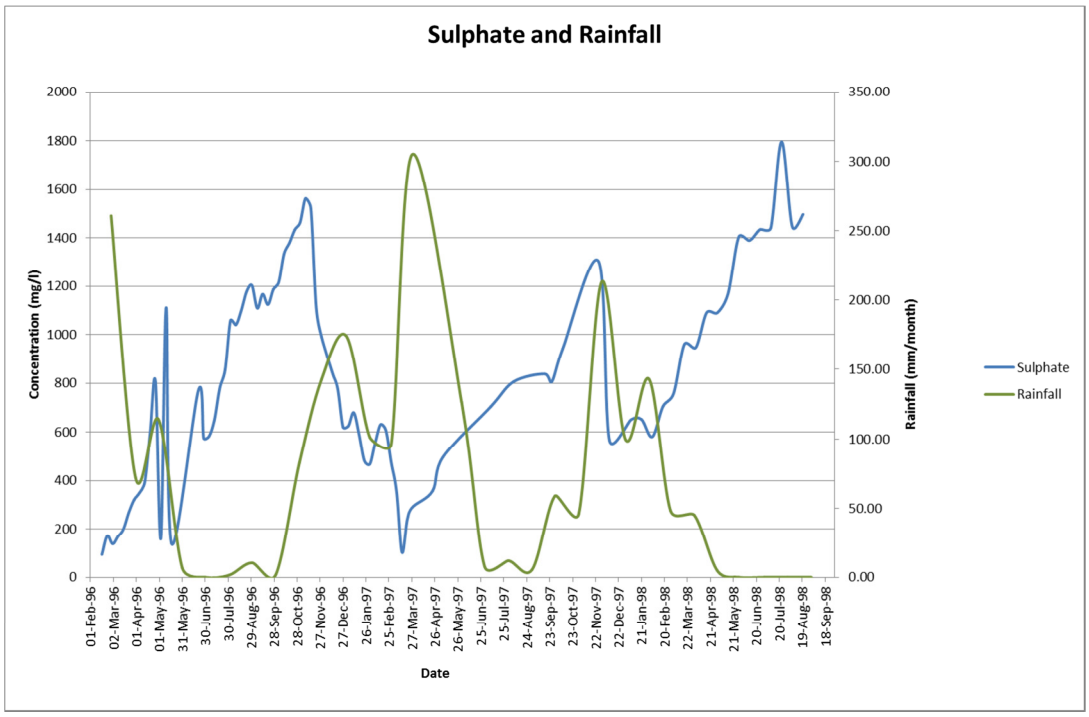

influencing contaminant loads in the Blesbokspruit.

Figure 5-15 Time series Blesbokspruit monitoring point from February 1996 to August 1998. The data shows an approximate lag time of a month or 2 between increasing monthly rainfall and decreasing SO_4 concentrations.

This trend seems to change in the time period from January 2000 to December 2004, where increasing rainfall is followed by increasing sulphate concentrations. This trend was also observed by Naicker et al. (2003). They attributed it to increased seepage of polluted groundwater following rainfall events. This phenomenon has been termed “first flush” by other researches (Norsdstrom, 2009, Winde, 2010).

[4] The data was sourced from Grootvlei Proprieties mine in the ERB and can be accessed via the Council for Geoscience. The contact person is Magda Roos and the data was sourced for the Strategic Water Management Project (2005).

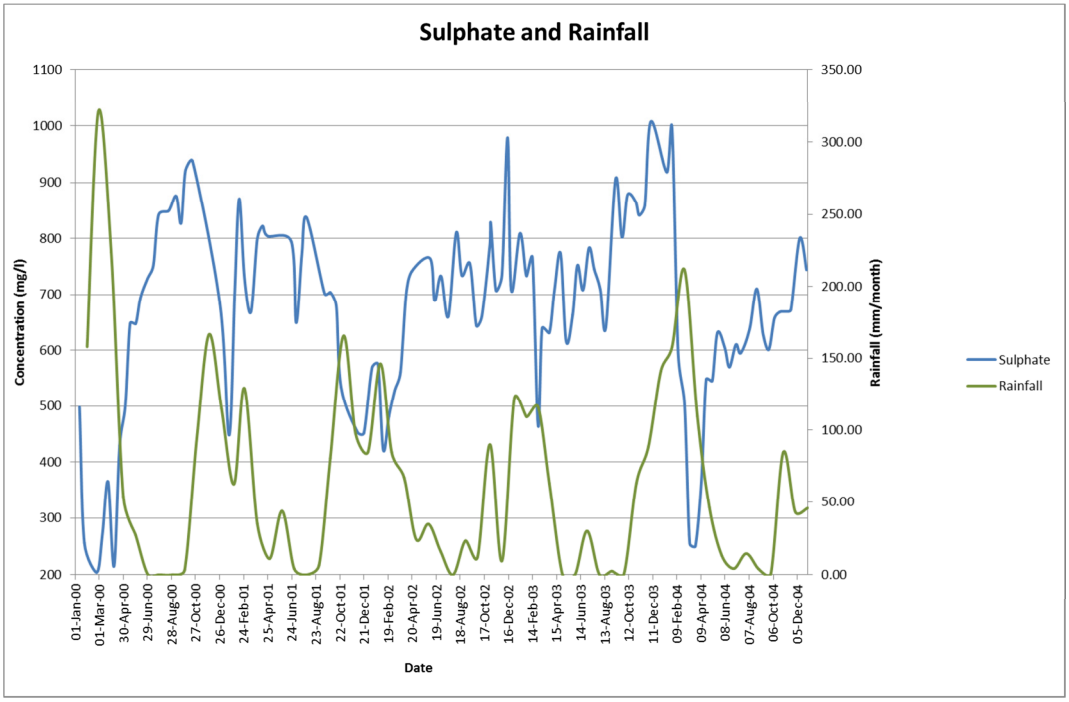

Figure 5-16 Time series plot of the monitoring data of the Blesbospruit from January 2000 to December 2004. This data indicates that after rainfall starts to increase, so do SO_4 concentrations.

5.2.2.2.3 Ca and Mg

The Pearson's correlation for Ca and HCO_3 is low (0.33) and is therefore not statistically significant. The dolomites are expected to be the main sources for both these elements. Therefore the low correlation may be related to process, e.g. precipitation of gypsum, while HCO_3 remains in solution. Calcium and Mg display a high linear correlation (Figure 5-7) showing that these two cations vary together.

The dolomites are expected to be the main source for these 2 cations. The high correlation between them lends credence to this notion. Many of the HCO_3 concentrations needed to be calculated based on the principle of electroneutrality in solutions. This principle states that any charge, whether dissolve ion or electrically charged surface, must have an equal and opposite quantity of charges in its vicinity (Dickinson et al., 2011). This principle can only be applied to calculate the concentration of a cation or anion if the analysis is complete with respect to the analysed cations and anions. The assumption is that this is the case. Comparison between calculated and actual alkalinity values of the Coetzee et al. (2006) data shows an average difference of 19%. The differences range from a maximum of 34% and a minimum of 1%. The uncertainty in alkalinity analysis, from which the HCO_3 is calculated, may also play a role in the discrepancy between calculated and actual values.

Both the Ca and Mg data distributions show strong bimodal distributions (Figure 5-17 and Figure 5-18). Comparison of the data distributions of Ca and Mg reflect the high Pearson's correlation coefficient between the two constituents. The bimodal data distributions can be interpreted as 2 subsets, within the larger dataset.

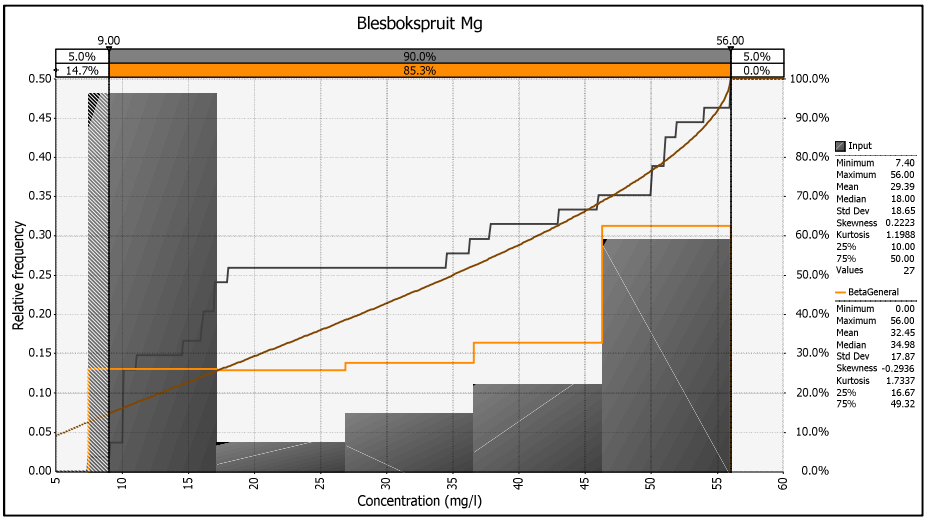

Figure 5-17 Data distribution of the Blesbokspruit surface water Ca concentrations. The data distribution is bimodal with the bulk of the value falling between 15 and 50 and 160 and 190 mg/ℓ.

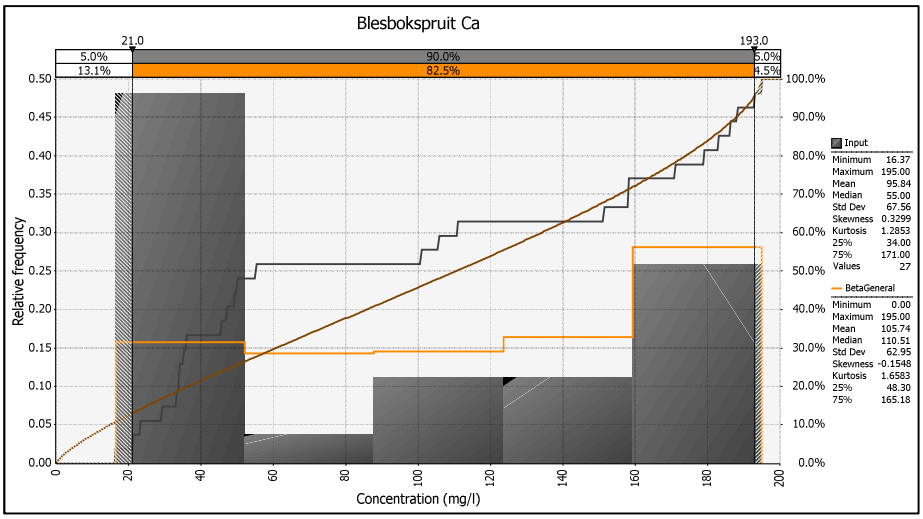

Figure 5-18 Data distribution of the Blesbokspruit surface water Mg concentrations. The data distribution is bimodal and is similar to the data distribution for Ca. The bulk of the Mg concentrations fall between 7 and 17 and 46 and 56 mg/ℓ

The lower Ca and Mg values may represent the natural Blesbokspruit surface water concentrations. The higher values are either as a result of a solution with elevated Ca and Mg being introduced to the Blesbokspruit or due to the dissolution of dolomite due to the introduction of acidic solutions, or a combination of the two.

Neither Ca nor Mg show significant correlation with pH. The same processes responsible for the lack of Ca and Mg correlation with pH may be responsible for the lack of Ca and Mg correlation with HCO_3. The pH in

the Blesbokspruit surface water is buffered by HCO_3. Therefore even though Ca, Mg and HCO_3 may have the same source, i.e. the Malmani dolomites, their trends diverge. This is most probably because of HCO_3 being involved in acid-base reactions and Ca and Mg becoming involved in precipitation and dissolution reactions, most probably due to precipitation of secondary carbonate and sulphate minerals.

5.2.2.2.4 Na

The Na concentrations in the Blesbokspruit surface water are elevated. The average Na concentration is 187 mg/ℓ (σ = 158) with the maximum value 855 and the minimum 18 mg/ℓ. The Na data distribution shows a strong bimodal trend (Figure 5-19). The bimodal distributions indicates that a baseline distribution is being impacted on by a solution with high Na concentrations.

5.2.2.2.5 Iron

The average Fe concentration in the Blesbokspruit surface water is 0.29 mg/ℓ (σ = 0.23) with a maximum of 0.99 and a minimum of 0.06 mg/ℓ. The Fe data distribution (Figure 5-20) shows a trimodal data distribution. This is indicative of a complex geochemistry and is most likely influenced by a leachate solution from mine tailings and/or other sources with elevated Fe concentrations and most probably reflects dissolution and precipitation cycles and redox dynamics as well.

Iron shows statistically significant correlation with Ca (0.61) and Mg (0.57). This indicates that Fe may be associated with the dissolution of dolomite and the precipitation of secondary carbonates. The origin, transport and fate of Fe will be further explored during the numeric modelling.

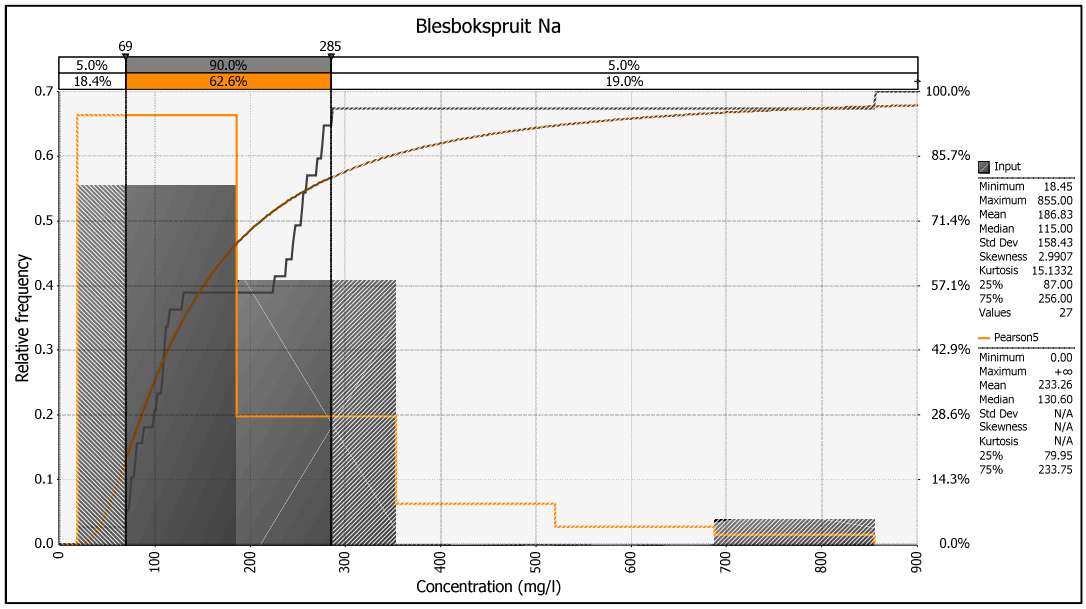

Figure 5-19 Data distribution of Na concentrations of the Blesbokspruit surface water

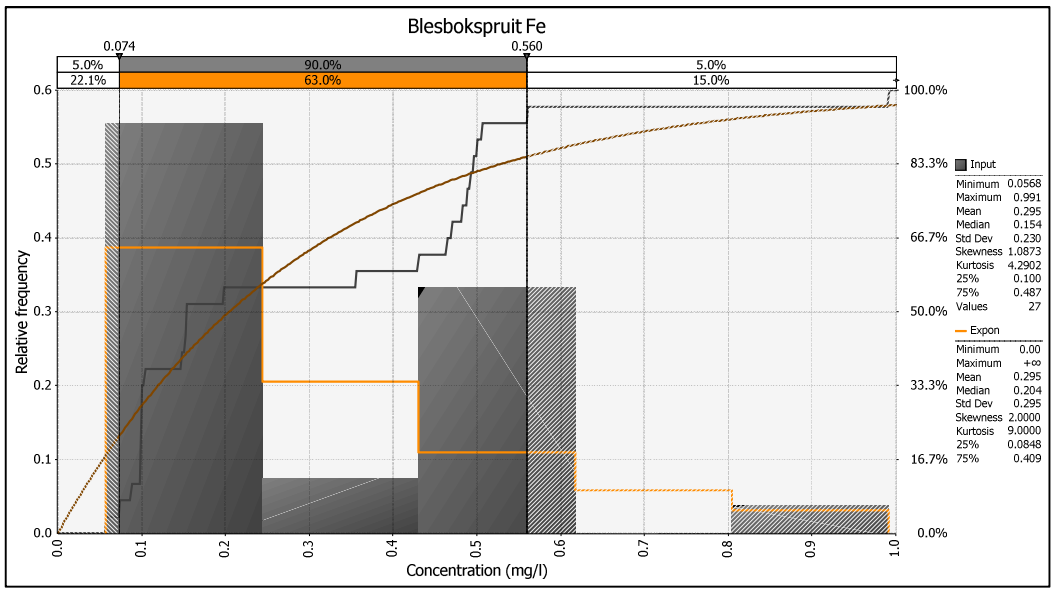

Figure 5-20 Data distribution of Fe concentrations in the Blesbokspruit surface water

5.2.2.2.6 Heavy metals (Mn, Co, Ni, Cu and Zn)

The heavy metals Mn, Co, Ni, Cu and Zn were assessed due to their presence in Witwatersrand pyrite grains (Hallbauer, 1986), their presence in the Blesbokspruit (Roychoudhury and Starke, 2006), their leachability from Witwatersrand tailings dams (Cukrowska et al., 2004) and their presence in the footprints of reclaimed tailings dams (Rösner et al., 2001). Another motivation for discussing these specific metals is their co-correlation with each other and with SO_4, indicating that these metals may be closely related to the pyrite oxidation process and may also be controlled by similar geochemical processes in the Blesbokspruit. Roychoudhury and Starke (2006) have shown that Cu, Co and Ni are predominantly associated with the organic and Fe-Mn oxide phases, with a significant portion also associated with the carbonate phase. Zinc is associated predominantly with the carbonate and Fe-Mn oxide phases, implying that the Fe-Mn oxides and hydroxides and carbonate phases are important controls in the transport and fate of all these heavy metals.

A summary table of some statistical parameters are shown in Table 5-6. The table shows that Ni concentrations are elevated. It also shows that the heavy metals show large variations in their concentrations in the Blesbokspruit surface water. The heavy metals in Table 5-6 all have positively skewed bimodal data distributions (Figure 5-21 to Figure 5-25) with inflections in their probability-probability and quantile-quantile plots. This implies the superposition of one dataset, generally with higher values, upon another. This is consistent with a surface water drainage channel being impacted on by mining and industrial activity.

5.2.2.2.7 U

Uranium is discussed separately from the other heavy metals due to its close association with the gold deposits, its lack of correlation with any of the heavy metals and its different data distribution pattern. The average U concentration in the Blesbokspruit surface water is 0.018 mg/ℓ (σ = 0.01).

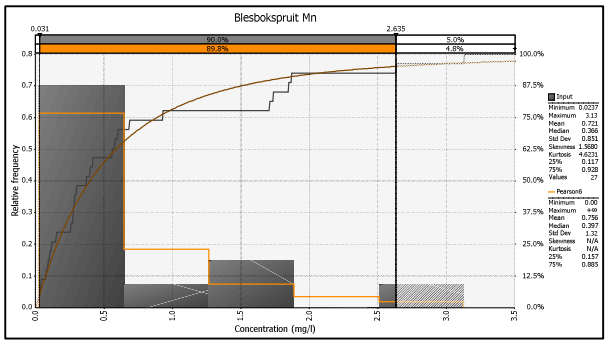

Figure 5-21 Data distribution of Blesbokspruit surface water Mn concentrations

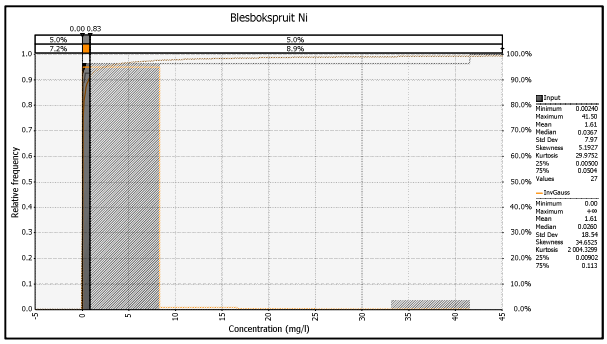

Figure 5-24 Data distribution of Blesbokspruit surface water Ni concentrations

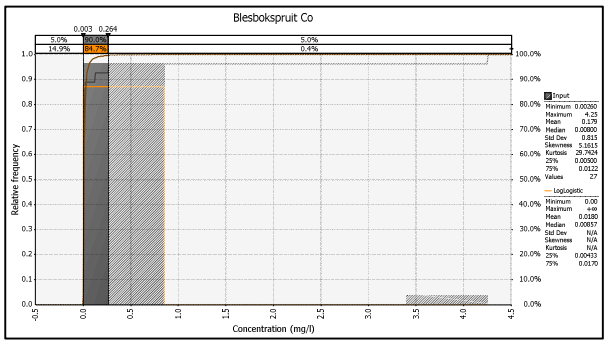

Figure 5-22 Data distribution of Blesbokspruit surface water Co concentrations

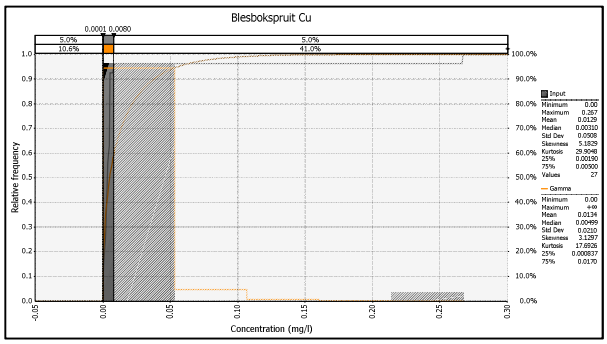

Figure 5-25 Data distribution of Blesbokspruit surface water Cu concentrations

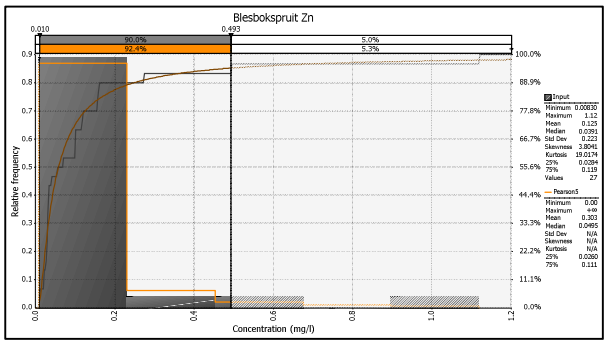

Figure 5-23 Data distribution of Blesbokspruit surface water Zn concentrations

The average lies between a maximum of 0.040 and a minimum of 0.000 mg/ℓ. Uranium is statistically significantly correlated with HCO_3 (0.66), Ca (0.69) and Mg (0.63). Roychoudhury and Starke (2006) showed that U is associated with the carbonate and the Fe-Mn oxide phases. The positive correlation with HCO_3 in this study confirms their results.

Table 5-6 Summary statistics of Blesbokspruit heavy metal data

Metal	Average	Standard deviation	COV[5]	Maximum	Minimum	n[6]
Units	*mg/l*		*%*			
Mn	0.72	0.85	118	3.13	0.02	27
Ni	1.61	7.97	497	41.50	0.00	27
Co	0.18	0.82	456	4.25	0.00	27
Cu	0.01	0.05	393	0.27	0.00	27
Zn	0.13	0.22	178	1.12	0.01	27

The U histogram shows that the U data () is bimodally distributed, centred around higher and lower values

This is consistent with most parameters for the Blesbokspruit surface water data, implying an impacting solution with elevated U concentrations on a baseline variation with lower values.

In general all the studied parameters showed at least a bimodal data distribution, confirmed by the probability-probability plots. This is indicative of a lower pH solution with elevated metal and sulphate concentrations impacting the Blesbokspruit surface water. There are many industries along the banks of the Blesbokspruit, including sewerage plants, a paper mill and mining activities. Of these only the mining activities are related to pyrite oxidation and acid mine

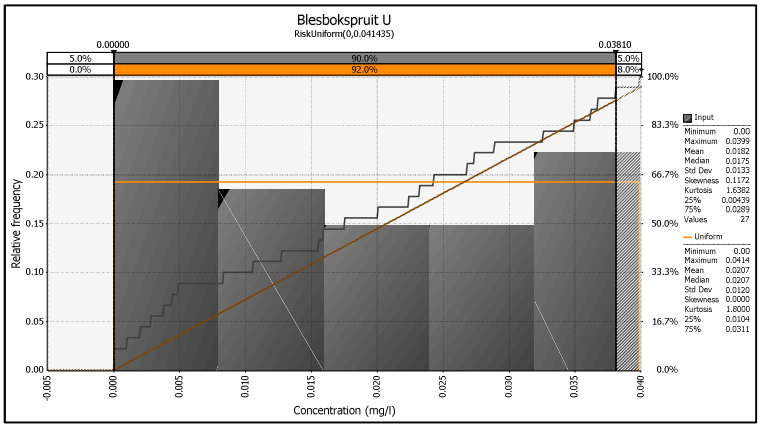

Figure 5-26 Data distribution of Blesbokspruit surface water U data drainage.

This will be explored further in the detailed geochemical models.

[5] Coefficient of variation

[6] Number of observations

5.2.3 Component 3: Shallow groundwater

The groundwater in the East Rand Basin is dominated by the dolomites in the region. The water is prevented from seeping below an impermeable layer termed the greensill. This results in a shallow perched aquifer with a water depth of about 16 m throughout the ERB (Africa Geo-Environmental Services (Pty) Ltd., 2006). A perched aquifer of shallower depth exists in places where it is developed in the weathered zone atop unweathered rocks of the Vryheid formation, belonging to the Karoo Supergroup. There is a deep water aquifer below 600 mbg*ℓ*, which is being replenished by ingress of water in zones such as e.g. sinkholes or subsidence areas from areas of shallow mining and shafts sunk through the greensill.

The shallow groundwater will thus be a mixture of rain water recharge, water from the dolomites and tailings seepage. A summary of the available shallow groundwater data is shown in Table 5-7.

Table 5-7 Summary of shallow groundwater geochemical data[7].

	Units	Average	Std Dev	Maximum	Minimum	95th Percentile	5th Percentile	n
pH		7.21	1.09	11.00	4.33	8.98	5.63	65
Total Dissolved Solids	*mg/ℓ*	1 230.56	1 480.84	8 610.00	46.80	3 653.00	67.98	55
Dissolved Oxygen	*mg/ℓ*	3.49	2.45	10.40	0.56	9.15	1.11	36
HCO_3	*mg/ℓ*	398.23	760.77	4 700.00	12.00	938.50	24.60	40
Na	*mg/ℓ*	255.60	564.28	3 393.77	1.07	1 182.87	2.50	70
Mg	*mg/ℓ*	58.67	66.72	283.17	0.89	205.19	6.44	70
Al	*mg/ℓ*	3.84	17.76	103.02	0.01	2.08	0.01	59
K	*mg/ℓ*	6.19	7.08	43.26	0.46	19.41	1.54	70
Ca	*mg/ℓ*	106.68	122.06	424.61	1.21	369.18	8.02	70
Fe	*mg/ℓ*	16.66	55.33	323.83	0.00	62.14	0.02	70
Mn	*mg/ℓ*	4.93	19.16	119.43	0.01	18.78	0.01	70
Co	*mg/ℓ*	0.45	2.16	12.01	0.00	0.67	0.00	59
Ni	*mg/ℓ*	0.71	3.16	18.43	0.00	1.32	0.00	59
Cu	*mg/ℓ*	0.03	0.02	0.11	0.00	0.07	0.00	59
Zn	*mg/ℓ*	1.21	1.97	11.84	0.00	3.92	0.00	70
Ba	*mg/ℓ*	0.34	0.46	1.61	0.01	1.42	0.02	59
Pb	*mg/ℓ*	0.05	0.05	0.22	0.00	0.14	0.01	59
U	*mg/ℓ*	0.04	0.18	1.04	0.00	0.21	0.00	59
F	*mg/ℓ*	0.46	2.29	17.81	0.00	0.90	0.00	69
Cl	*mg/ℓ*	167.70	211.80	928.00	1.50	587.59	3.29	69
NO_3	*mg/ℓ*	20.18	45.71	332.00	0.00	67.41	0.00	68
PO_4	*mg/ℓ*	4.79	6.94	34.93	0.00	16.02	0.00	69
SO_4	*mg/ℓ*	520.26	784.73	3 818.00	0.79	1 779.63	3.02	69

The shallow groundwater is perched on top of the greensil layer the water table between 58.95 and 0.81 m and has an average depth of 11.23 m (σ = 13.91) with a standard error of 2.58 m (Africa Geo-Environmental Services (Pty) Ltd., 2006; Bosch, 2012). The soil layer is on average 2 m thick, implying that the major part of

[7] This data was collected for the Council for Geoscience Strategic Water Management Project.

the shallow groundwater is located in the fractured Karoo aquifer and in the Transvaal Supergroup dolomites. A database of 67 boreholes was available for analysis (Figure 5-28).

Of the 67 boreholes, 29 have water level data and 63 have associated geochemical data containing sufficient data for geochemical modelling. The average shallow groundwater cation and anion compositions are shown in Figure 5-29 and Figure 5-30. Figure 5-29 shows that the most important cations in the shallow groundwater are Na, Ca and Mg with lesser amounts of Fe, Mn, K and Al. Cobalt, Ni, Zn, Ba, Pb, U and NH_4 are present in varying concentrations in trace amounts. Figure 5-30 shows that the most important anions are HCO_3, SO_4 and Cl. Nitrite, NO_3 and PO_4 are present in trace amounts of varying concentrations.

It is unusual for groundwater to exhibit concentrations of Fe, Mn and Al in percentage levels. This, together with the generally high concentrations of sulphate is indications of contamination of the shallow groundwater, potentially from pyrite oxidation in tailings dams. This was found in studies in other areas of the Witwatersrand (Naicker et al., 2003; Rösner et al., 2001; Tutu et al., 2008).

A Piper diagram was constructed for the shallow groundwater chemistry and is shown in Figure 5-27.

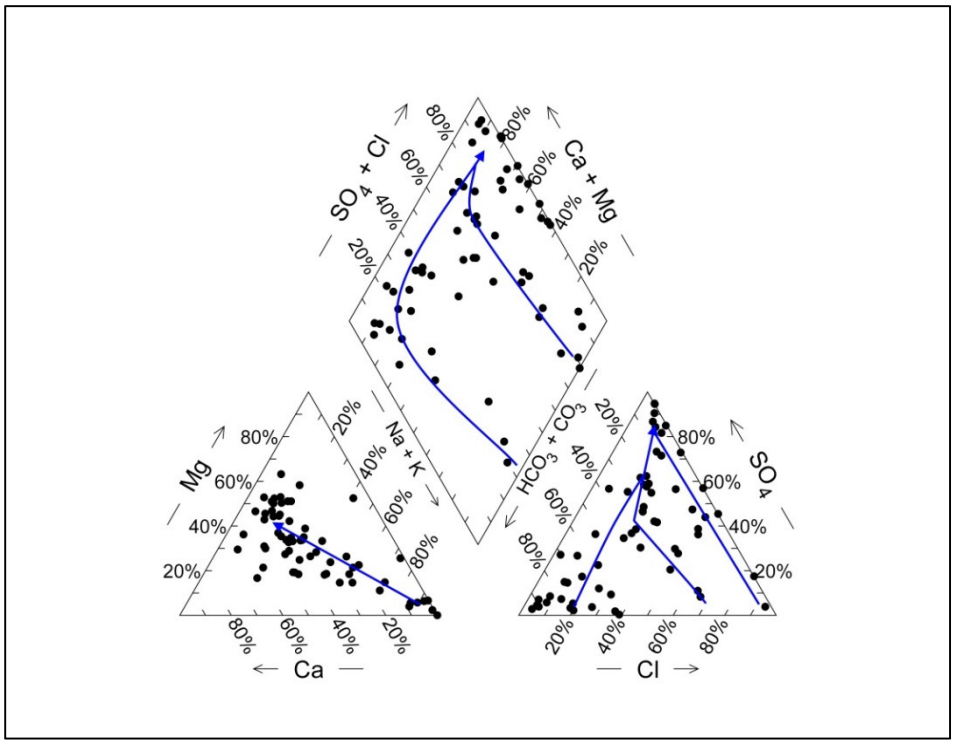

Figure 5-27 Piper diagram of the shallow groundwater major element chemistry. The discernable trends are shown in blue. Overall the trends are towards higher Ca and Mg and higher SO_4 concentrations. This is shown more clearly in the cation (bottom left) and anion (bottom right) parts of the plot.

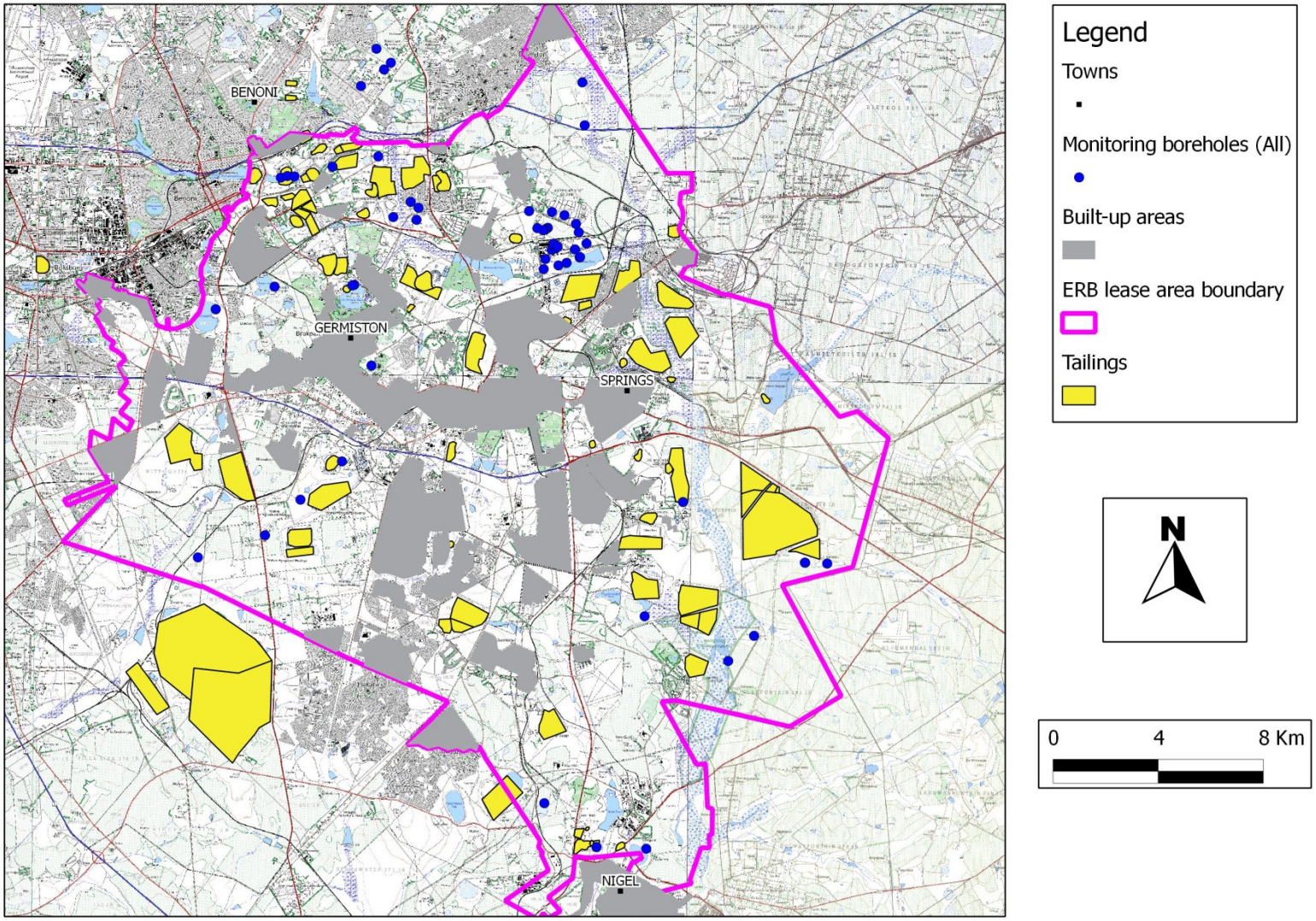

Figure 5-28 Map showing the shallow groundwater borehole positions

Figure 5-27 shows that the shallow groundwater does not display any specific water type. A few general trends are shown in blue on the diagram. The diagram shows a relative increase in Ca and Mg concomitant with a relative decrease in Na and K. The left-most blue line on the anion plot shows a trend of constant Cl concentrations with increase in SO_4 relative to HCO_3 and CO_3.The middle line shows a trend of increasing SO_4 concentration relative to a decrease in Cl concentration, while HCO_3 and CO_3 remain relatively constant. The right-hand line on the anion plot shows the same trend as the aforementioned, but at higher Cl concentration. These trends are reflected in the summary diamond plot, where two general trends can be observed. The bottom line shows an increase in Ca and Mg concentrations with relatively constant SO_4. The top line shows an increase in SO_4 and in Ca and Mg.

This would point to at least two types of water from two different aquifers or sources. Due to the large amount of shallow groundwater borehole (n = 62), Stiff diagrams could not be constructed for all samples.

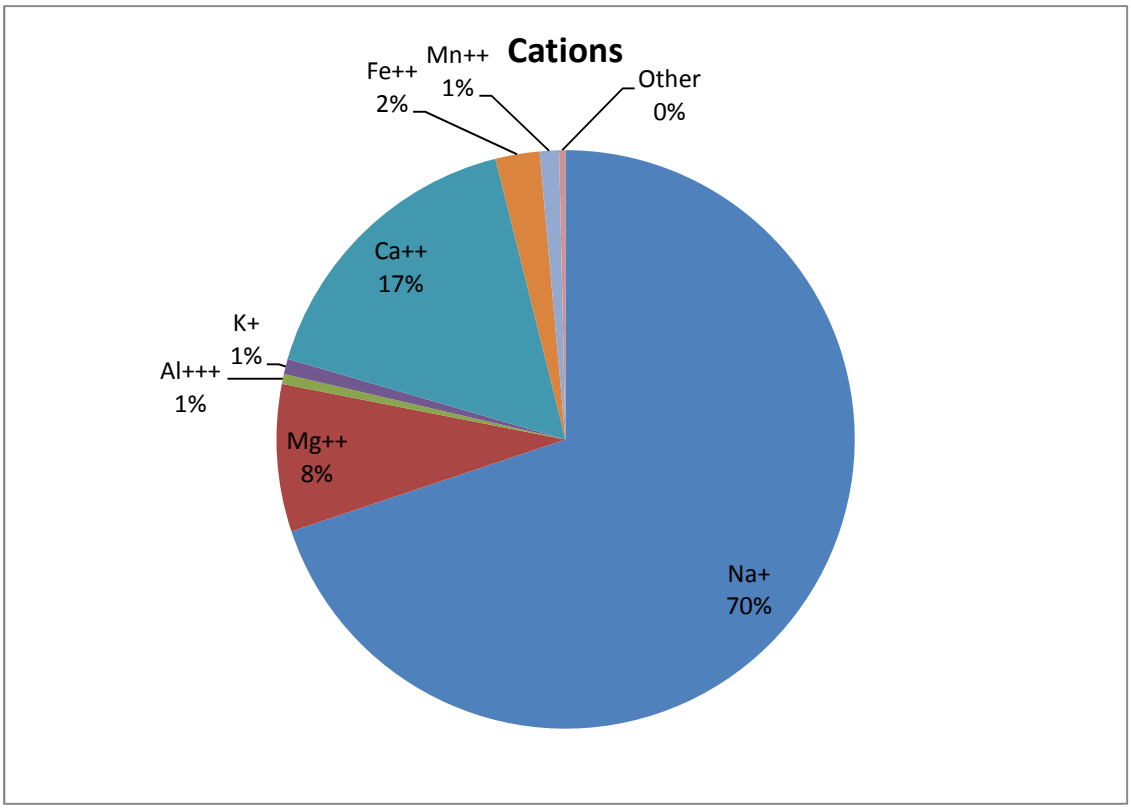

Figure 5-29 Average major cation composition of the shallow groundwater

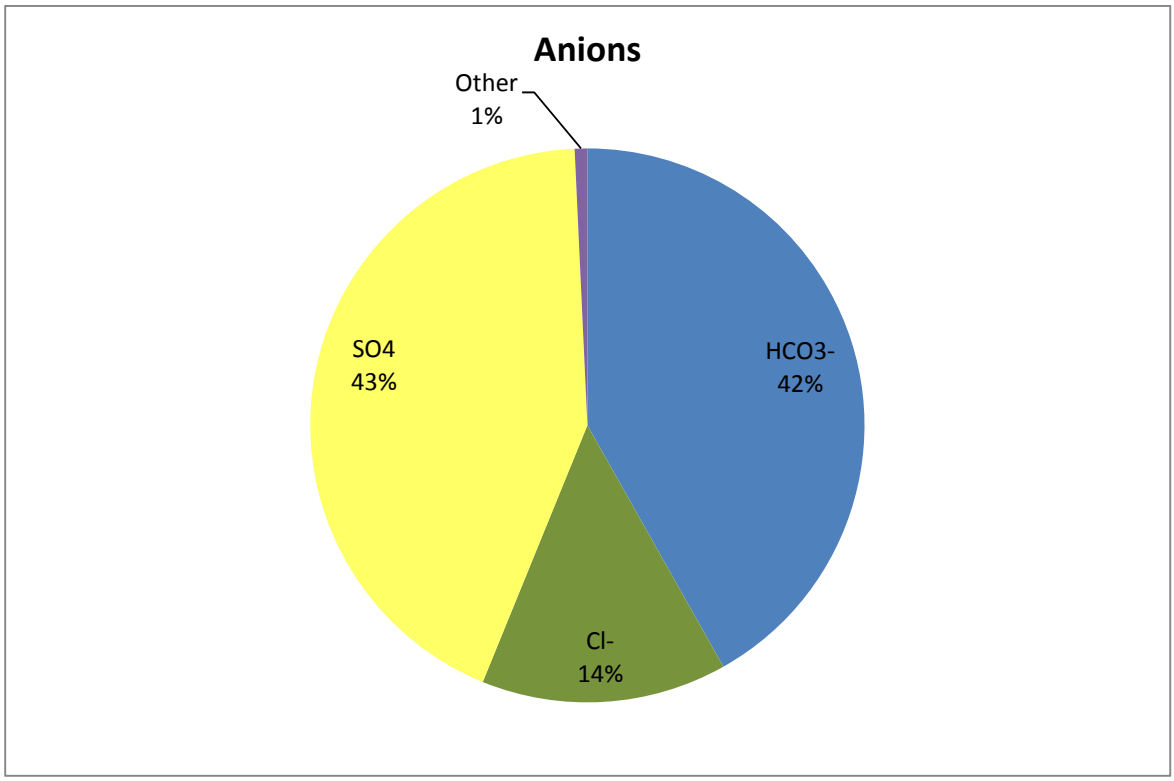

Figure 5-30 Average major anion composition of the shallow groundwater

Therefore representative samples were selected from each of the groundwater facies and plotted (Figure 5-31). The shallow groundwater samples from GP 152 to GP 147, following a zigzag pattern from left to right, indicate a trend of increasing SO_4. The samples Cen 444 to SRK LP1/Leeu 1 indicate a trend in increasing Na, K and Cl. The importance of Ca, Mg, HCO_3 and CO_3 in the shallow groundwater of the ERB is shown in samples GP 152, Cen 466, Cen 444, implying the generally strong influence of the dolomites in the study area. The samples not indicating the strong HCO_3 signature are most probably being impacted on by solutions from other sources. These impacting solutions have a strong sulphate signature and a strong Na, K and Cl signature. The Stiff diagrams indicate that these are two distinct solutions impacting on the baseline shallow groundwater.

5.2.3.1 Statistical analysis of shallow groundwater geochemical data

5.2.3.1.1 pH

The average pH of the shallow groundwater is 7.16 (σ = 1.15) with a maximum of 11.00 and a minimum of 4.33). The data distribution of the pH data (Figure 5-32) shows a polymodal distribution. The 95% confidence levels are 5.57 and 9.24. Some values fall outside these values on both sides. This implies a solution that is being impacted on by two others, one acidic and one alkaline.

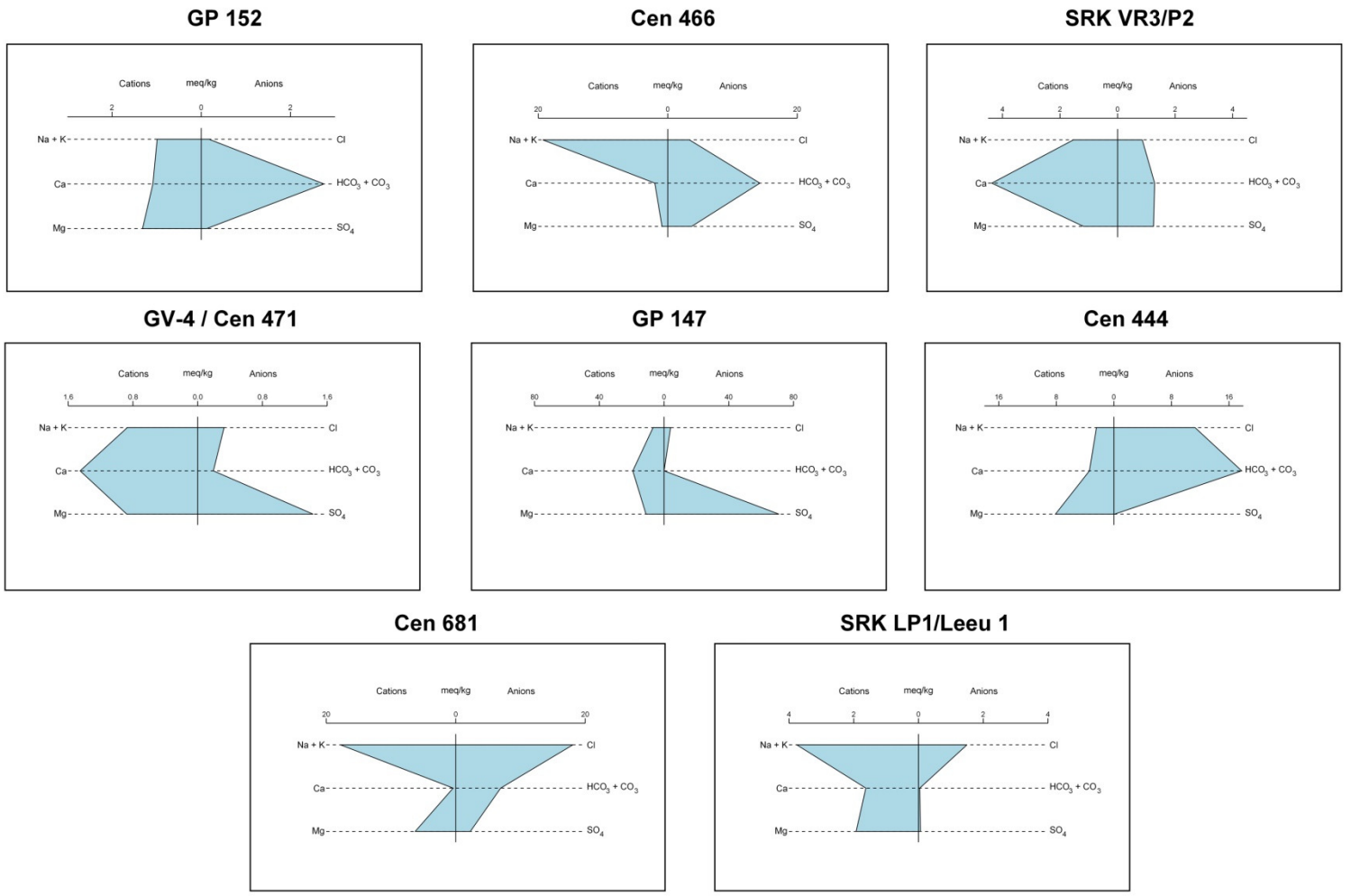

Figure 5-31 Stiff diagram of representative shallow groundwater samples

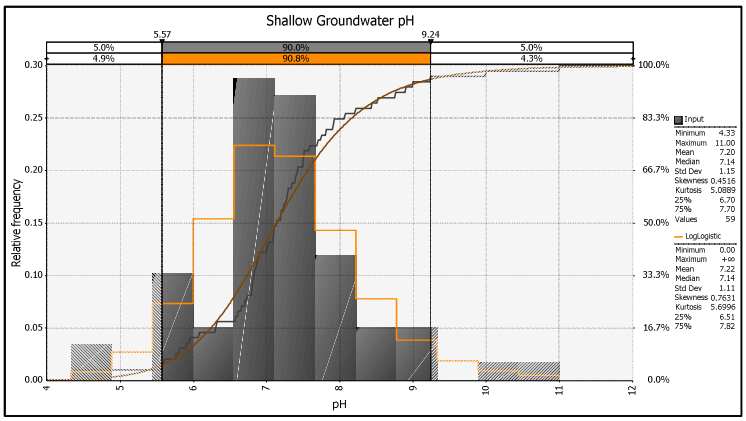

Figure 5-32 Data distribution of shallow groundwater pH data.

The lower value of the 95% confidence level is 5.57, which is slightly lower than would be expected for natural groundwater being influenced by dolomites. This implies that the data at the lower and upper end of that falling between 5.57 and 9.24 are representative of groundwater that has already been mixed with the alkaline and acidic solutions.The circum neutral pH values are indicative of buffering capacity of the groundwater. This is due to the relatively high HCO_3 concentrations (μ = 523 mg/ℓ) in the groundwater. This is significantly higher than the deep groundwater, which has an average concentration of 212 mg/ℓ.

5.2.3.1.2 SO_4

The average SO_4 concentration of the shallow groundwater is 803.46 mg/l (σ = 1 005.85). The data ranges from a maximum of 3 818 to a minimum of 0.79 mg/l. The data distribution is shown in Figure 5-33. The best fit for the distribution is a BetaGeneral distribution using the Anderson-Darling statistic, as the tail of the distribution is important.

The SO4 data shows a polymodal distribution with a large range. It is not clear on Figure 5-33, but there are values between 3 400 and 3 800 mg/l. There are only 2 values, so they are not clear, due to the depression of the data from the fitted distribution. The distribution therefore implies at least 2 data subsets within the larger dataset. This is confirmed by the probability-probability plot, which indicates at least 2 data subsets. This is interpreted as the influence of a high SO_4 solution impacting on the natural groundwater, especially in the light of the large concentrations range and the skewed distribution (the higher the sulphate values, the lower the frequency of number of samples with higher values, implying less samples with higher values, implying lower volumes of high SO_4 solution, which is consistent with a polluting effluent).

5.2.3.1.3 Ca and Mg

Like the surface water, the shallow groundwater shows a significant Pearson's correlation between Ca and Mg (0.91). This implies covariance and is, as the surface water, most probably due to the influence of the dolomites.

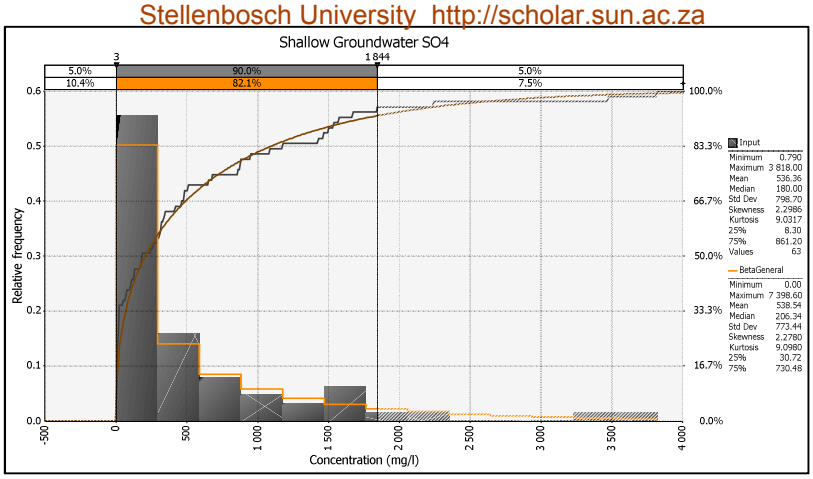

Figure 5-33 Data distribution of the shallow groundwater SO_4 concentrations.

The data distribution of Ca (Figure 5-34) and Mg (Figure 5-35) show polymodal distributions with at least 2 data subsets in each dataset. The Ca distribution shows 2 peaks in the tail end of the dataset, one at around 300 and one around 400 mg/ℓ. These higher Ca and Mg values could be either due to a solution of higher Ca and Mg content impacting the shallow groundwater, or it could be due to greater dissolution of the dolomites due to impacting acidic solutions from the surface. A statistically significant correlation between SO_4 and Ca (0.75) and Mg (0.81) indicates the latter.

Calcium and Mg show no significant correlation with HCO_3. This may be due to CO_2 degassing in areas of high acidity, or the removal of Ca and Mg as precipitates of secondary salts. The degassing reaction is shown below:

$$HCO_3^- + H^+ = CO_{2(g)} + H_2O \qquad \textbf{Equation 1}$$

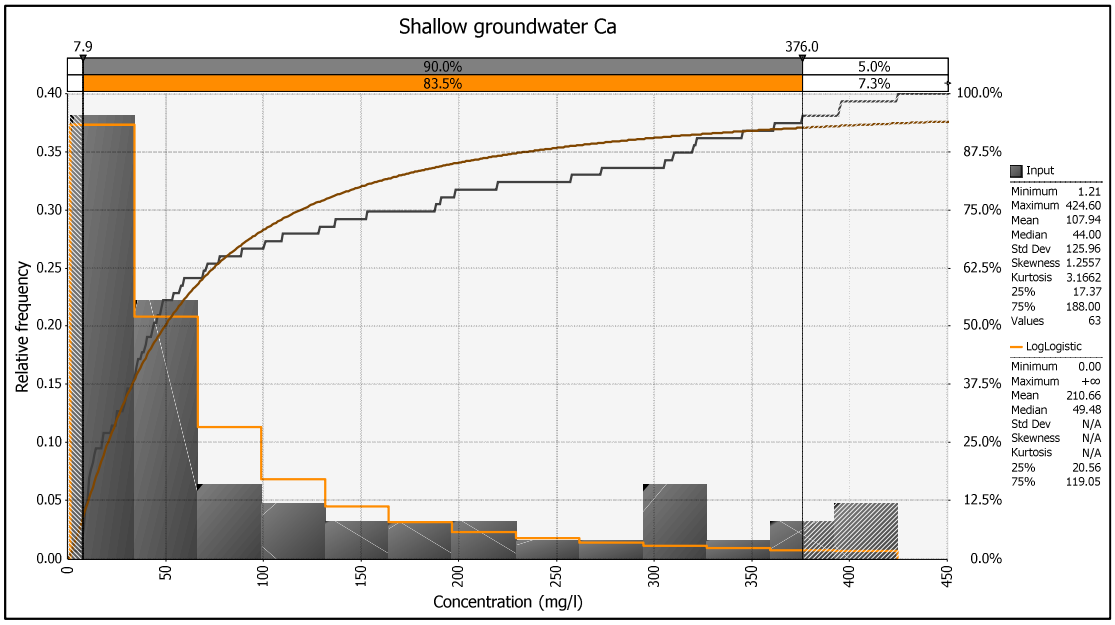

Figure 5-34 Data distribution of shallow groundwater Ca concentrations.

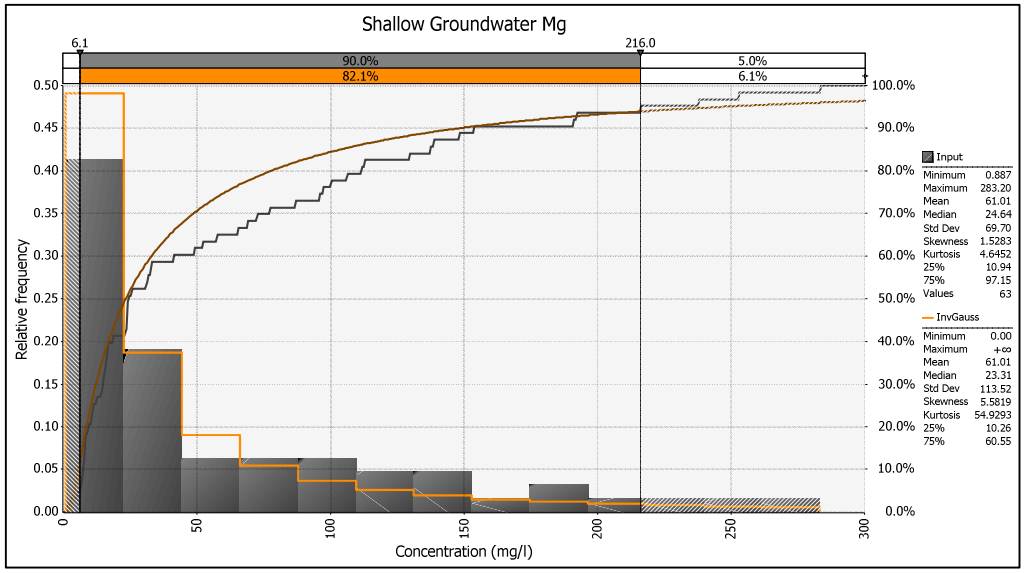

Figure 5-35 Data distribution of shallow groundwater Mg concentrations.

5.2.3.1.4 Na

The average Na content of the shallow groundwater is 278 mg/ℓ (σ = 591) and ranges between a minimum of 1.07 mg/ℓ and a maximum of 3 394 mg/ℓ. The Na data distribution is polymodal with at least 2, possibly as many as 5 subsets in the Na dataset (Figure 5-36).

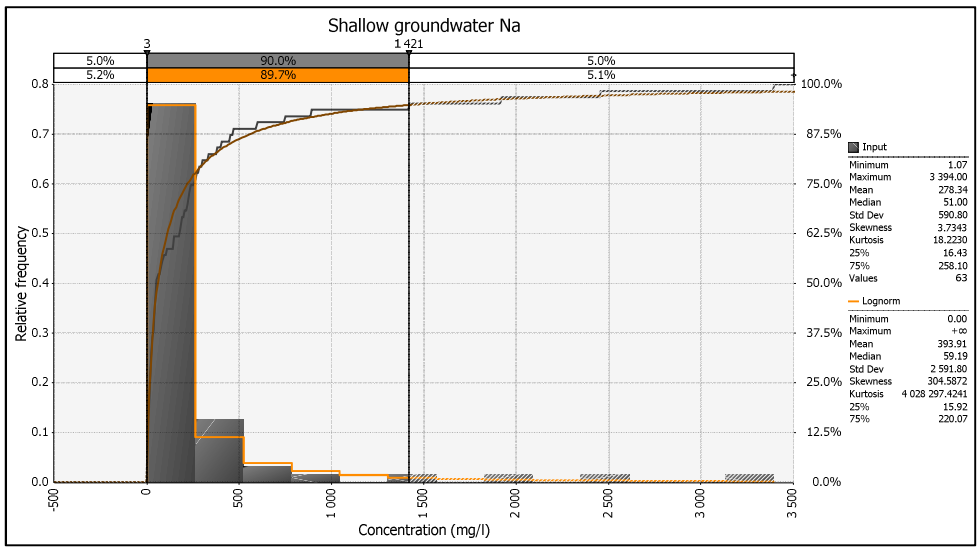

Figure 5-36 Data distribution of shallow groundwater Na concentrations.

This is indicative of a solution with elevated Na concentrations impacting on the background distribution of the shallow groundwater.

5.2.3.1.5 Fe

The average Fe content of the shallow groundwater is 18.30 mg/ℓ (σ = 58.11) ranging between a minimum of 0.00 and a maximum of 323 mg/ℓ.

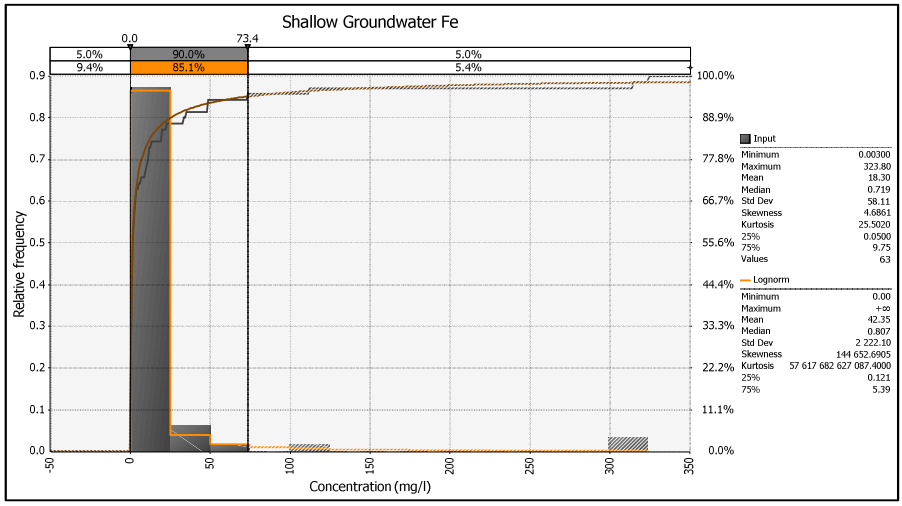

Figure 5-37 Data distribution of the shallow groundwater Fe concentrations.

The Fe data distribution shows a polymodal character. The elevated Fe concentrations in the shallow groundwater are an indication that the shallow groundwater is impacted upon by a solution with high Fe concentrations. The oxidation of pyrite produces Fe^{2+}, which can occur in elevated concentrations at circum neutral pH values.

5.2.3.1.6 Heavy metals (Mn, Co, Ni, Zn and Al)

In contrast to the heavy metals in the surface water, the heavy metals Mn, Co, Ni, Zn and Al in the shallow groundwater do not show significant Pearson's correlation coefficients with each other. Manganese, nickel and cobalt correlate and Zn and Al. Copper is not included in the shallow groundwater system, as very limited Cu data was available for the shallow groundwater. Potassium shows significant correlation with Mn, Co and Ni as well as SO_4, showing that secondary mineral precipitation may be a significant process controlling metal mobility in the shallow groundwater. A summary of the most important statistical parameters for the heavy metal concentration data of the shallow groundwater is shown in Table 5-8.

The table shows that all the heavy metals show significant coefficients of variations, indicating a large variability in the datasets.

Table 5-8 Summary statistics of the shallow groundwater heavy metal concentrations. The high COV shows high variability in the dissolved metal concentrations in the shallow groundwater.

Metal	Average	Standard deviation	COV[8]	Maximum	Minimum	n[9]
Units	*mg/ℓ*		*%*			
Mn	4.69	19.31	412	119.40	0.01	63
Ni	0.73	3.34	460	18.43	0.00	52
Co	0.48	2.29	473	12.00	0.00	52
Zn	1.16	2.05	177	11.84	0.00	63
Al	4.18	18.91	452	103.00	0.01	52

The data distributions of the heavy metals show significantly positively skewed, bimodal to polymodal data distributions (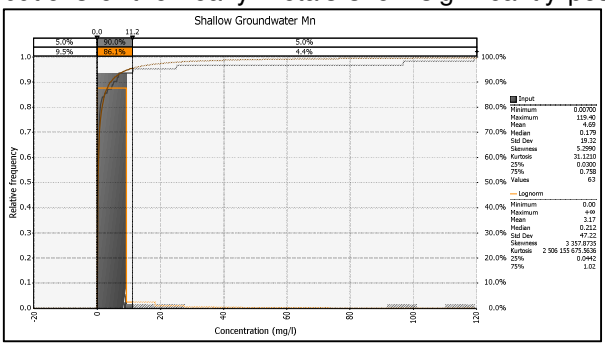

Figure **5-38** to Figure 5-42). The data distributions show that although the heavy metals do not all correlate with each other, their data distributions are similar. They all show a scatter of data in the lower concentration regions of the dataset and single values with very high concentrations.

This is indicative of baseline concentrations being impacted on by solutions containing elevated concentrations of these metals. Particular distributions of specific heavy metals most probably reflect precipitation and adsorption dynamics, as much as impact by a solution containing elevated concentrations of these metals.

5.2.3.1.7 U

The Average U concentration in the shallow groundwater is 0.05 mg/l (σ = 0.19) and varies between a maximum of 1.04 and a minimum of 0.00 mg/l. The data distribution is shown in Figure 5-43.

The data shows a polymodal distribution with at least 2 subsets in the U data. Concentrations are centred on lower values and single values are in higher ranges, removed from the central dataset. This suggests a solution with elevated U concentrations impacting on a solution with lower U concentrations.

[8] Coefficient of variation

[9] Number of observations

Uranium correlates with Na, F and NO_2, which may imply that U behaves like a conservative ion, remaining in solution in the shallow groundwater in stable complexes. Simple speciation models show that the U can form stable complexes with phosphate, carbonate and sulphate, depending on whether the uranium redox pairs are coupled in the model or not. Uranium does not show significant correlation with either PO_4 or SO_4 species.

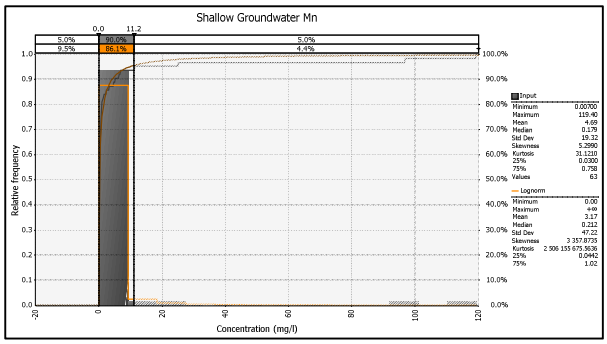

Figure 5-38 Data distribution of the shallow groundwater Mn concentrations.

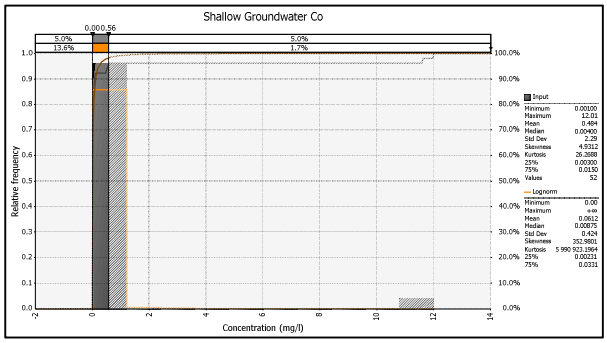

Figure 5-39 Data distribution of the shallow groundwater Co concentrations.

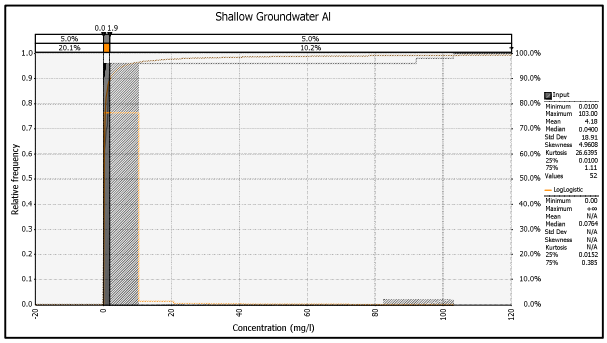

Figure 5-40 Data distribution of the shallow groundwater Al concentrations.

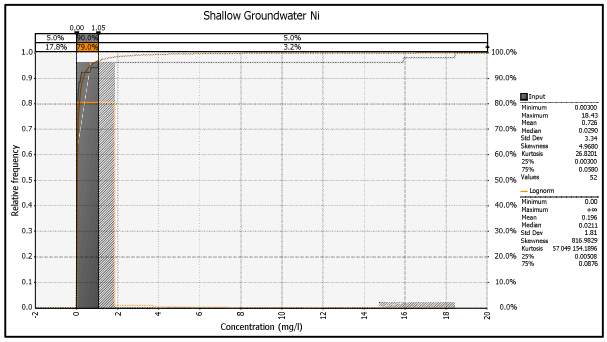

Figure 5-41 Data distribution of the shallow groundwater Ni concentrations.

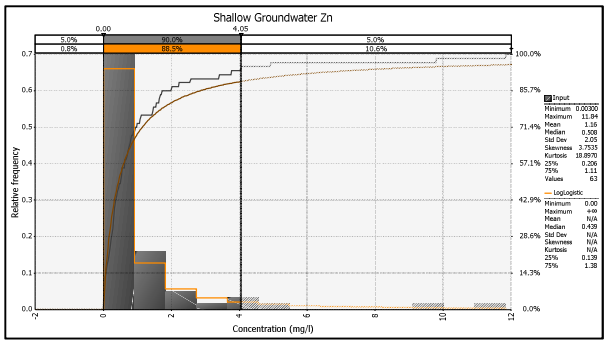

Figure 5-42 Data distribution of the shallow groundwater Zn Concentrations.

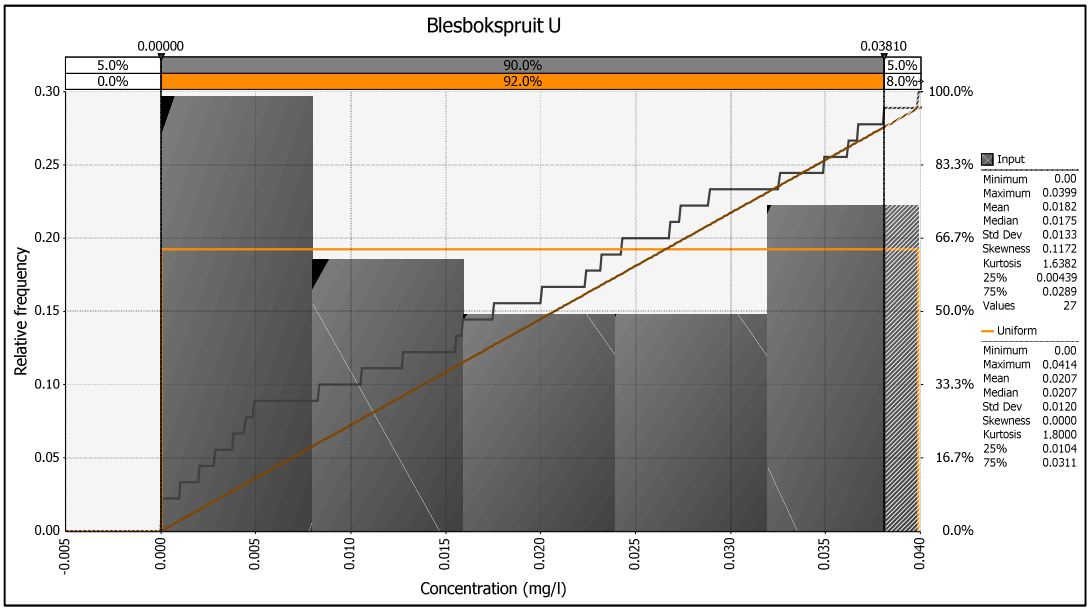

Figure 5-43 Data distribution of the shallow groundwater U concentrations.

The lack of correlation between U and the anions shown in the speciation model to form U complexes is indicative that the behaviour of U in the shallow groundwater is complex. Adsorption dynamics is not taken into account in the speciation modelling.

5.2.4 Component 4: Deep groundwater

Deep groundwater in the ERB is defined as water occurring below the upper dolomite, i.e. below 340 mbgℓ[10] (1 150 mamsℓ[11]). This depth is considered the environmental critical level for the East Rand Basin (Lenong and Hansen, 2009). The environmental critical level is defined as the depth at which the deep groundwater should not be allowed to rise as not to contaminate the clean groundwater in the dolomite aquifer. At the time of sampling (2005) the Grootvlei mine was still dewatering the mine and the water level was below 550 mbgℓ (Roychoudhury and Starke, 2006; Expert team of the inter-ministerial committee, 2010).

The only existing data for the ERB deep groundwater is from samples collected from mine shafts and stopes during a 2005 survey of deep mine water and water quality by the Council for Geoscience[12] (Figure 5-44). During this survey, water quality and quantity data was acquired from Grootvlei mine. The shaft and Grootvlei mine data are used to characterise the deep mine water as the Grootvlei mine data did not contain data for all relevant parameters and chemical constituents.

[10] Meters below ground level

[11] Meters above mean sea level

[12] Council for Geoscience Strategic Water Management Project (2005)

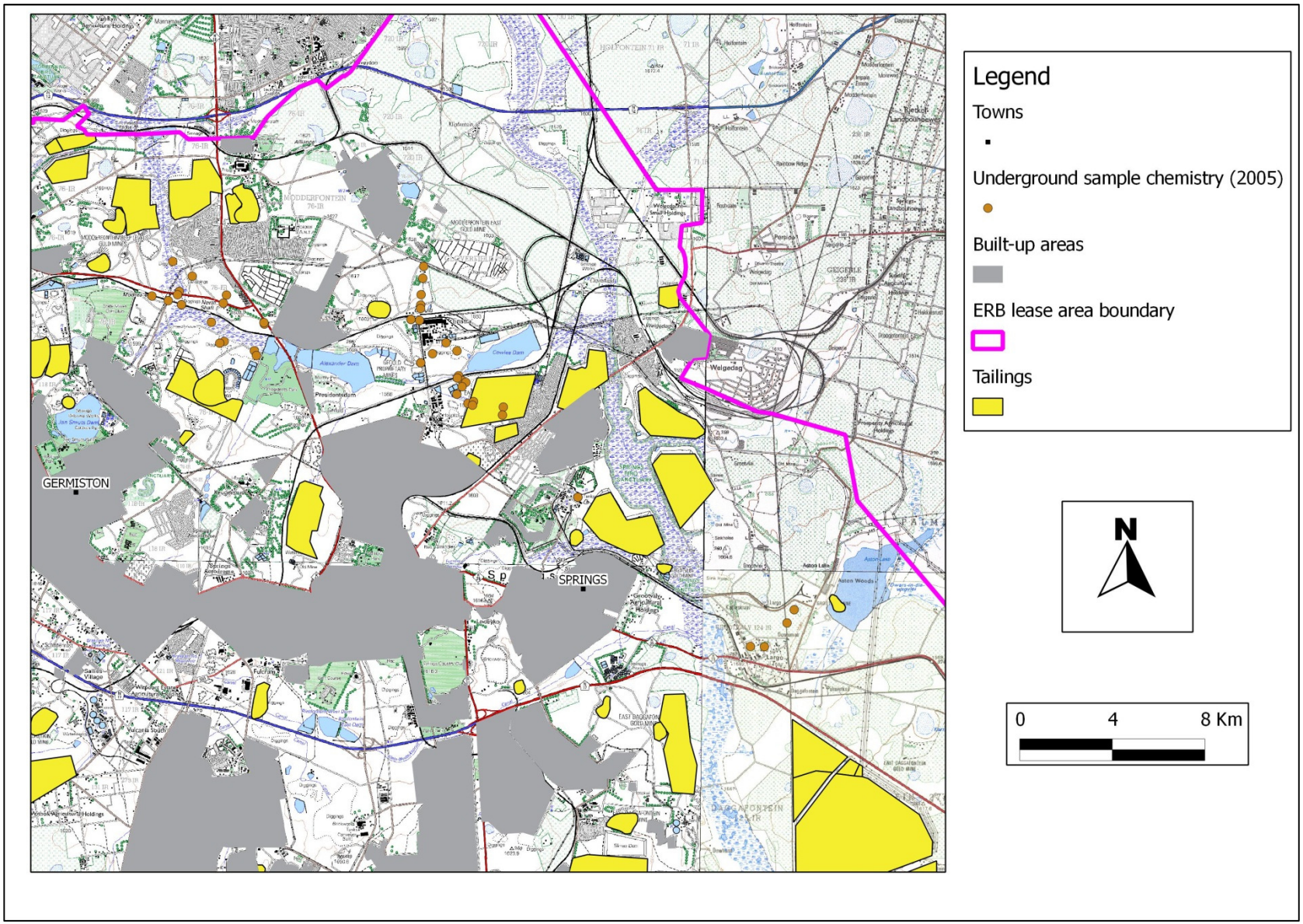

Figure 5-44 Sample positions of samples collected from deep mine water

A summary of the deep aquifer geochemical data is shown in Table 5-9.

Table 5-9 Summary of deep aquifer geochemical data

Site name	Units	Average	Standard Deviation	Maximum	Minimum	95th Percentile	5th Percentile	n
Electrical Conductivity	*uS/cm*	1 743.00	509.92	2 780.00	900.00	2 565.50	1 056.20	12
pH		7.60	1.06	10.78	6.66	9.20	6.74	12
Total Dissolved Solids	*mg/L*	883.09	263.80	1 390.00	450.00	1 293.00	521.00	11
Eh	*mV*	-45.15	62.65	14.50	-230.60	8.45	-138.42	12
Temperature	*℃*	20.16	1.39	22.40	17.00	22.02	18.27	12
M-Alkalinity	*mg CaCO3/l*	554.50	1 277.15	4 600.00	110.00	2 290.00	110.00	12
P-Alkalinity	*mg CaCO3/l*	187.18	565.16	1 890.00	7.00	985.00	7.50	11
Li	*ug/l*	8.00	4.56	17.88	1.75	14.42	2.13	12
B	*ug/l*	233.50	219.03	923.99	124.37	533.74	125.34	12
Na	*ug/l*	479 546.45	1 211 778.16	4 319 006.17	47 426.42	2 130 044.27	56 423.38	12
Mg	*ug/l*	79 450.98	38 901.01	150 241.08	233.55	136 692.93	27 665.36	12
Al	*ug/l*	247.06	48.64	358.58	200.84	342.70	204.76	12
K	*ug/l*	5 592.37	3 124.74	14 579.50	3 235.47	11 322.77	3 602.20	12
Ca	*ug/l*	145 255.64	40 945.97	218 644.30	74 836.99	200 730.31	82 050.66	11
V	*ug/l*	62.53	198.80	693.36	1.00	325.89	1.00	12
Cr	*ug/l*	24.08	16.75	69.73	5.00	48.93	5.00	12
Fe	*ug/l*	245.50	362.04	1 352.68	50.00	779.24	50.00	12
Mn	*ug/l*	168.13	178.80	460.23	7.72	448.46	9.02	12
Co	*ug/l*	19.99	33.34	120.94	2.50	74.12	2.50	12
Ni	*ug/l*	536.79	983.66	2 517.71	2.50	2 413.63	2.50	12
Cu	*ug/l*	10.16	25.61	91.45	2.50	44.16	2.50	12
Zn	*ug/l*	159.74	243.44	716.93	50.00	674.57	50.00	12
Ga	*ug/l*	5.38	1.93	10.30	2.50	7.72	2.50	12
As	*ug/l*	21.94	74.28	257.80	0.50	116.29	0.50	12
Se	*ug/l*	16.75	21.93	62.22	2.50	61.33	2.50	12
Rb	*ug/l*	10.56	5.44	18.98	4.47	18.78	4.75	12
Sr	*ug/l*	339.61	135.36	571.87	21.52	499.81	144.94	12
Mo	*ug/l*	8.82	15.73	58.18	2.50	30.47	2.50	12
Cd	*ug/l*	1.36	1.24	5.31	1.00	2.94	1.00	12
Ba	*ug/l*	195.07	32.24	295.04	175.08	242.01	175.73	12
Pb	*ug/l*	14.69	4.06	27.46	12.91	20.31	12.92	12
U	*ug/l*	3.94	2.97	11.78	0.50	9.20	1.09	12
F	*mg/l*	1.06	2.55	7.72	0.00	6.24	0.00	12
Cl	*mg/l*	180.29	90.92	411.67	101.51	320.16	102.42	12
NO_3	*mg/l*	5.55	7.04	20.15	0.00	17.18	0.00	12
SO_4	*mg/l*	500.21	198.56	833.84	174.67	806.95	256.69	12

The deep groundwater data is plotted on a Piper diagram (Figure 5-45). The diagram shows that the anions have a definite trend towards SO_4 enrichment with a concomitant decrease in HCO_3 relative to the other anions. The cations show a trend of Ca enrichment with concomitant decrease in Na and K relative to HCO_3.

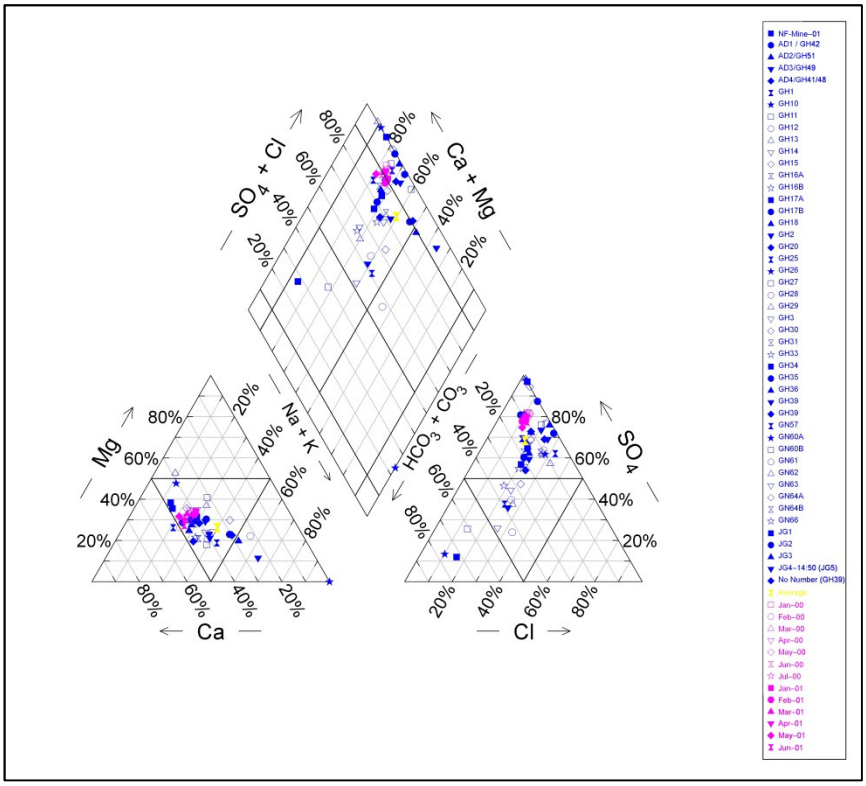

Figure 5-45 Piper diagram showing the deep groundwater data. The blue represents samples collected from various mine shafts and stopes in the East Rand Basin. The purple represents the Grootvlei data. The yellow and turquoise represent the average of the East Rand Basin mine data and Grootvlei data respectively.

These same trends are shown in a Durov diagram, which is a diagram showing the physical parameters, pH and TDS in addition to the major cations and anions (Figure 5-46). The Durov plot in Figure 5-46 shows the same trends as the Piper diagram (Figure 5-45), except that the Grootvlei samples show generally higher TDS values than those of deep mine water samples of other mines in the East Rand Basin. Grootvlei was the only mine dewatering in the East Rand Basin and hence was the only mine treating and discharging (Roychoudhury and Starke, 2006). The effluent from underground, representing deep groundwater was treated using lime and sewerage sludge to precipitate iron hydroxides, which adsorb heavy metals (Schoeman and Steyn, 2001; Expert team of the inter-ministerial committee, 2010). The water was discharged into the Blesbospruit. Studies on the mine have shown that the Blesbokspruit has ingress zones in its flow channel and that water ingresses from the Blesbokspruit to the Grootvlei mine, which is pumped and treated, creating a loop of groundwater flow, with a potential to increase salt load (Africa Geo-Environmental Services (Pty) Ltd, 2005). Due to the fact that although the groundwater is treated, it is never treated to background levels and hence presents an opportunity for salt build-up in mine reticulation through the pump, treat and discharge activities.

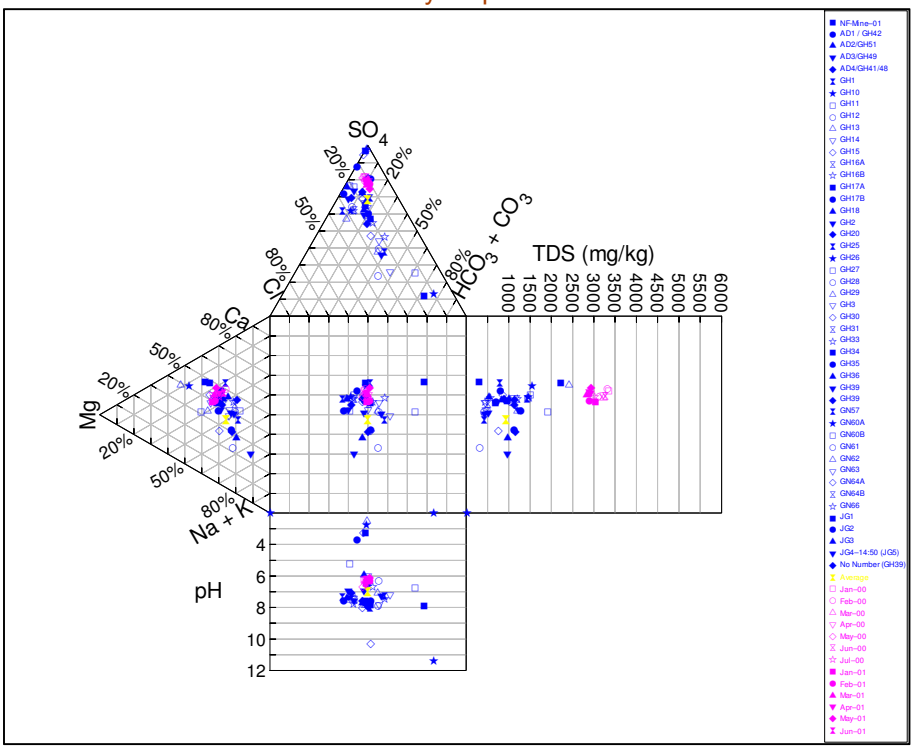

Figure 5-46 Durov diagram showing the deep groundwater data of the East Rand Basin. The blue represents samples collected from various mine shafts and stopes in the East Rand Basin. The purple represents the Grootvlei data. The yellow and turquoise represent the average of the East Rand Basin mine data and Grootvlei data respectively.

The deep groundwater is dominated by the cations Ca, Na, Mg, Fe, K and Al with smaller amounts of Co, Ni, Cu, Zn, Ba, Pb and U. The most important anions are SO_4, HCO_3 and Cl, with smaller amounts of F and HPO_4.

Due to the large amount of samples (n = 62) of deep groundwater, specific representative samples were selected from the various water facies and used to construct Stiff diagrams (Figure 5-47). The samples show an increasing SO_4 trend from left to right in a zigzag pattern. The importance of Na, K, Cl and HCO_3 varies from sample to sample. Sample GH15 indicates that it is being influenced by a Na-K-Cl solution as well as a SO_4 solution, although in general, there seems to be an inverse relationship with regards to Na-Cl and SO_4. There also appears to be an inverse relationship between Ca-HCO_3 content and SO_4 content in the deep groundwater.

5.2.4.1 Statistical analysis of deep groundwater geochemical data

5.2.4.1.1 pH

The average pH of the deep groundwater in the East Rand Basin is 6.96. Individual samples exist with low pH values (minimum of 2.49) and high values (maximum of 11.38). The average is 6.96 with a standard deviation (σ) of 1.49 and a standard error of the mean (95% confidence levels) of 0.38 (Figure 5-50).

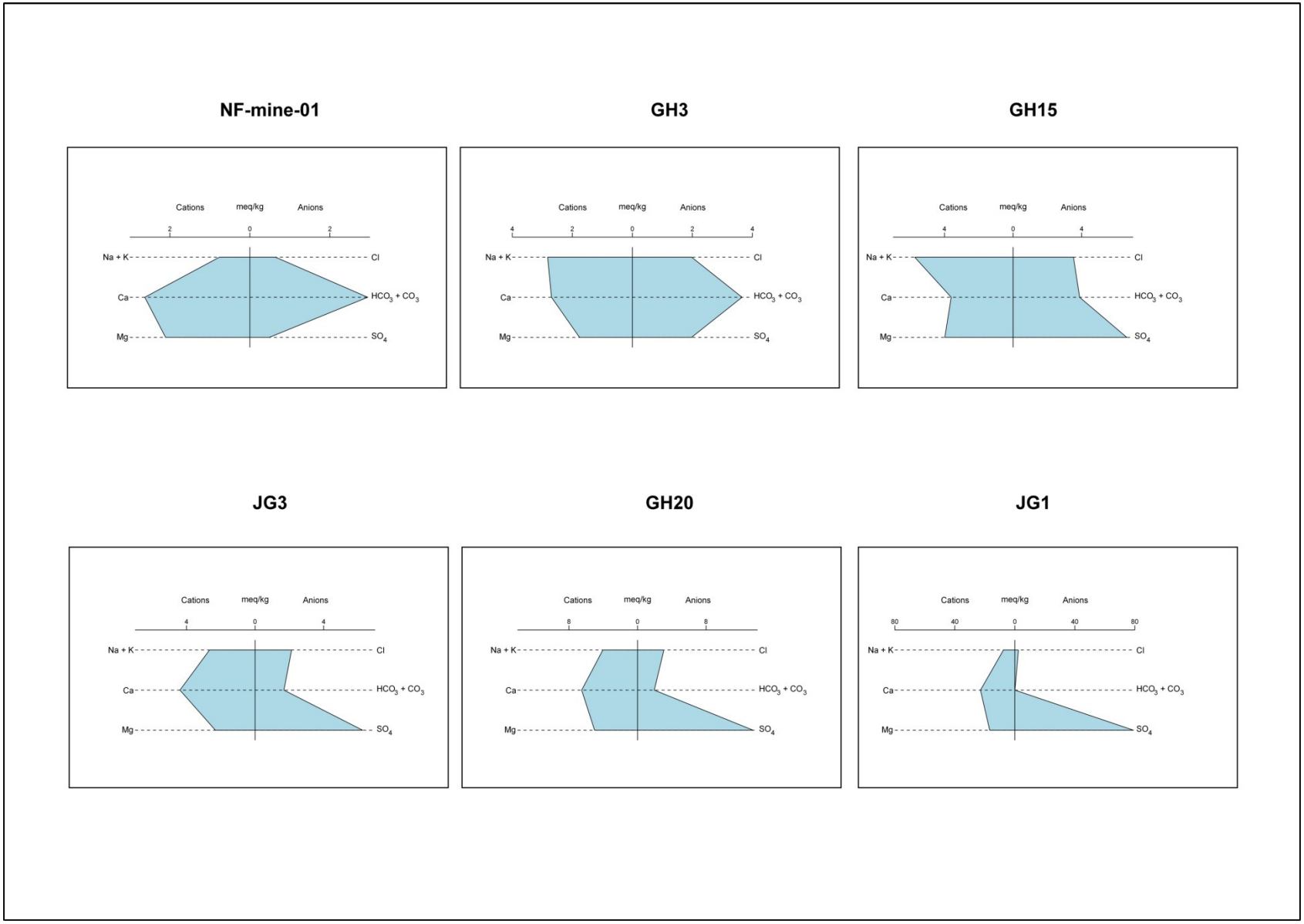

Figure 5-47 Stiff diagrams of selected deep groundwater

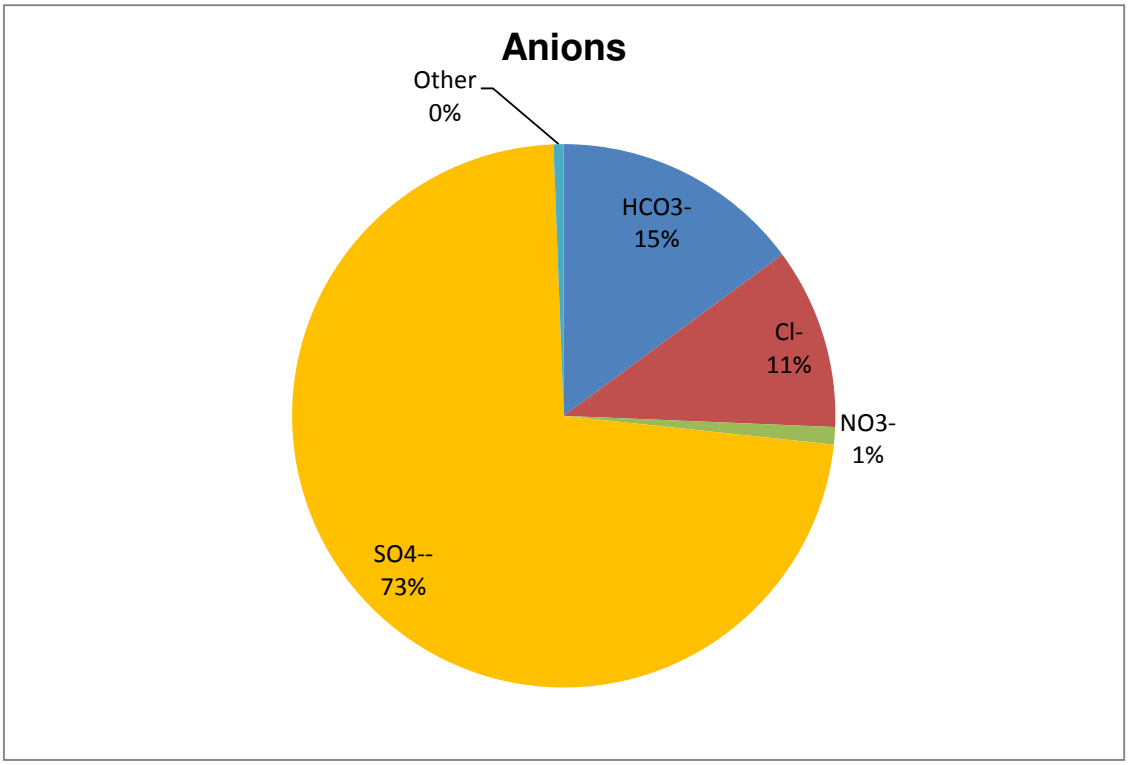

Figure 5-48 Average anion content of the deep groundwater

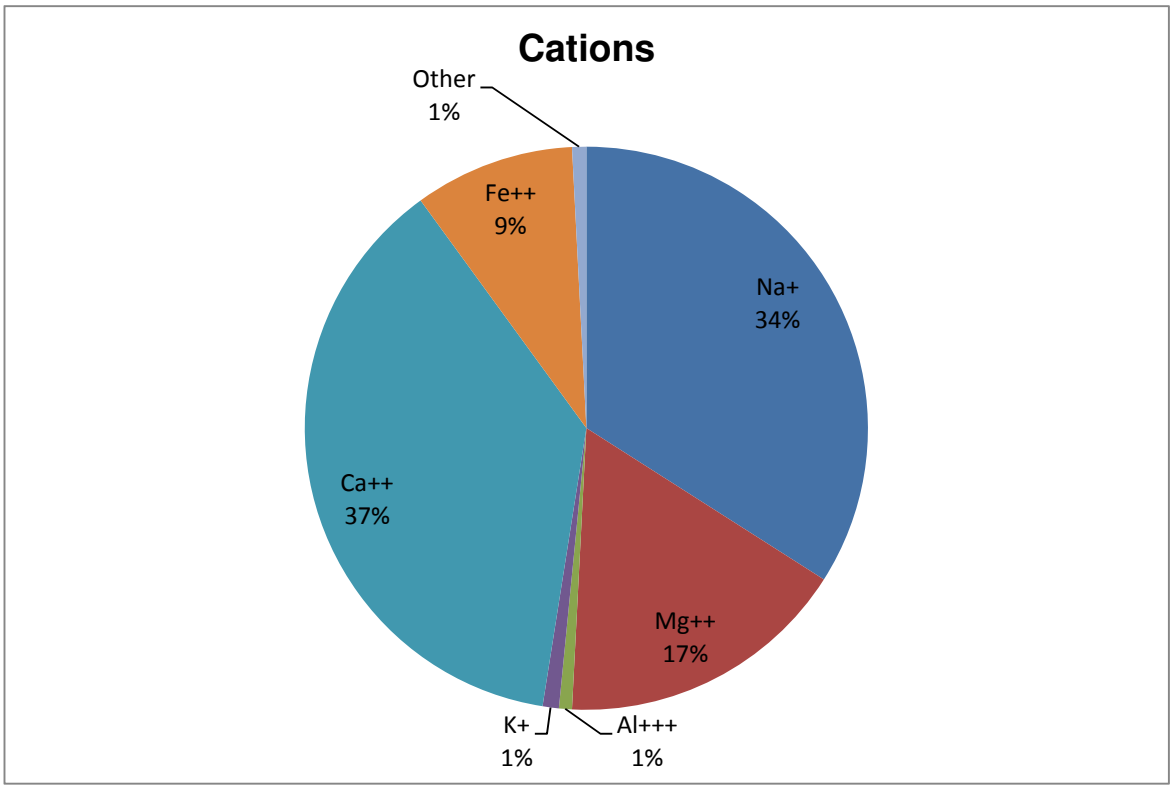

Figure 5-49 Average cation content of the deep groundwater

The histogram in Figure 5-50 shows a polymodal data distribution with at least 3 data sets. The following scenarios can be advocated to explain this phenomenon:

a) The groundwater data represents data from different mines, which are of different ages and thus represent different onset times for pyrite oxidation and the resultant formation of AMD.
b) The deep groundwater pH data represents mixed water from different sources and different ratios of mixing from water from different sources. Examples are mixing of AMD effluent from tailings with surface water ingress to the shallow groundwater and surface water ingress through mine shafts, sink holes, old shallow mine workings, such as the old Largo colliery close to Grootvlei mine and ingress through rock fissures and fractures.
c) The groundwater represents heterogeneities due to varying geology and ore body characteristics.

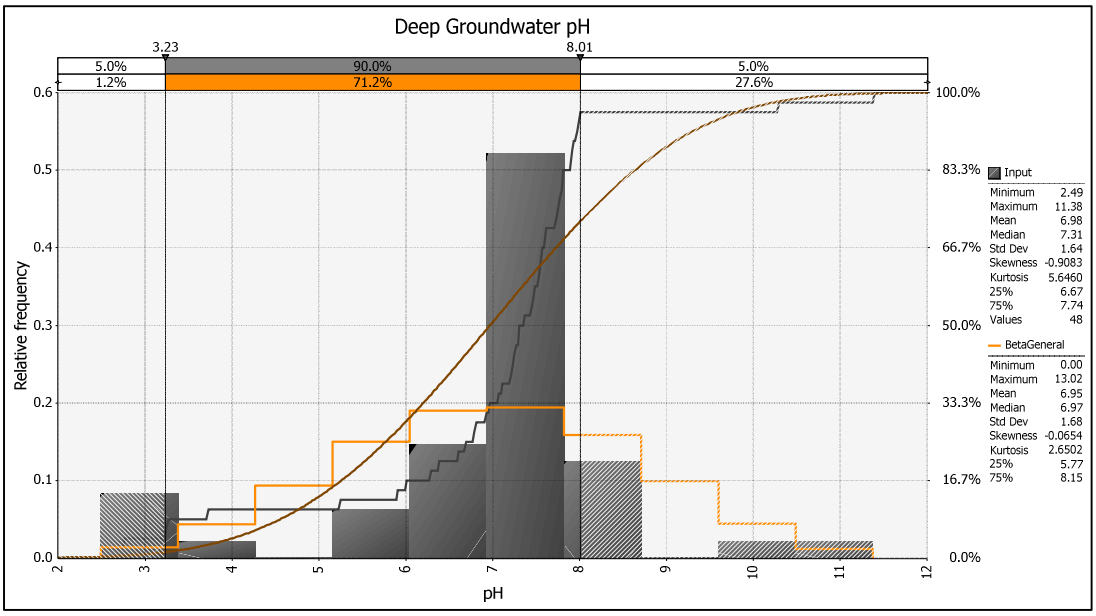

Figure 5-50 Histogram of deep groundwater pH values. The graph also shows the fitted data distribution in red.

Pearson's correlation analysis shows that pH is negatively correlated with, amongst others, Al, Cr, Fe, Mn, Co, Cu and Zn. This is an indication that the higher the pH, the lower the concentrations of these elements. This trend has been observed in other studies, where lower pH promotes dissolving of heavy metals and more alkaline pH values lead to precipitation and adsorption (Smith, 1999; Smith and Huyck, 1999). These correlations may also be indicative of a lower HCO_3 buffer capacity in the deep groundwater, as only Mn was negatively correlated with pH in the surface water.

5.2.4.1.2 SO_4

The average SO_4 concentration in the deep groundwater is 803 mg/ℓ (σ = 1 006) with a maximum of 5 610 and a minimum of 23.66 mg/ℓ. The SO_4 data distribution is a positively skewed (3.30). It also has a trimodal

distribution (Figure 5-51). This indicates that 3 data distributions, representing 3 processes or SO_4 sources are present in the larger dataset.

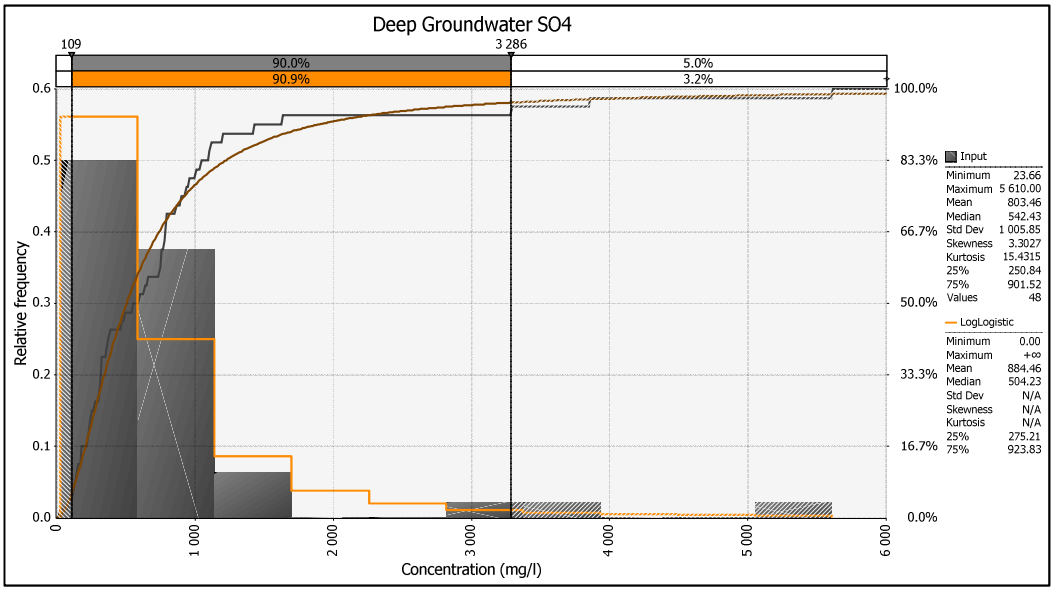

Figure 5-51 Data distribution of the Underground water SO_4 concentrations. The data shows that a sample collected of the deep groundwater has a probability of 0.5 to have a SO_4 concentration between 0 and 500 mg/ℓ. The cumulative distribution function shows that > 60% of the data points is below 500 mg/ℓ. SO_4 concentration > 500 mg/ℓ have a lower probability of occurring and are therefore sparser. This indicates a smaller volume solution containing higher concentrations of SO_4. This is indicative of a smaller volume of a solution containing higher concentrations of SO_4 impacting on a larger volume of a solution with lower SO_4 concentrations.

The cumulative distribution function overlay shows that 90% of the data is below 1 650 mg/l. A total of 77% of the data is below 950 mg/l. Using the Box Plot approach to calculate data range, any value exceeding 1 868 mg/l can be considered as an outlier. This range is defined by the data cluster on the left-hand side of Figure 5-51. Therefore the data clusters with values exceeding 1 868 mg/ℓ can be considered superimposed and therefore most probably represents secondary impacts on the main deep groundwater baseline.

At the time of sampling, Grootvlei mine was pumping water from undergournd, treating it in a treatment plant on site and clean water was pumped back to the Blesbokspruit. The initial concept that the underground mine water was a groundwater problem was challenged in a study (Africa Geo-Environmental Services (Pty) Ltd., 2006), which showed that the deep groundwater had a surface water component representing `75% of the water volume. This is due to ingress of surface water into underground mine voids, thereby recharging the deep aquifer (SRK Consulting, 2005). The Grootvlei mine was conducting mining underneath the Blesbokspruit at the time of sampling, which may explain the volumes of water reporting to the underground mine voids. The source of at least some of the SO_4 may be due to treated effluent pumped into the Blesbokspruit, especially at treatment plant down times. The average SO_4 concentrations in treated water from January 1996 to December 2008 is 833 mg/l (σ = 648) and varies between a maximum of 2 790 and a

minimum of 78 mg/l. This shows that, based on elevated sulphate concentrations of the deep groundwater, that the treated effluent discharged into the Blesbokspruit could be at least partly responsible for an increase in underground mine water volumes. The Blesbokspruit has been shown to recharge deep groundwater in certain sections of its channel (Africa Geo-Environmental Services (Pty) Ltd., 2005).

Daily mine dewatering pumping volumes, rainfall, underground water levels and raw and treatment effluent monitoring data exist for the Grootvlei mine from 1996 to 2009[13]. The daily mine dewatering pumping volumes and mine water level (meters above datum) are shown in Figure 5-52. A data gap occurs in the water level data for the whole of 2005. Figure 5-52 shows that higher pumping rates generally coincide with higher water levels.

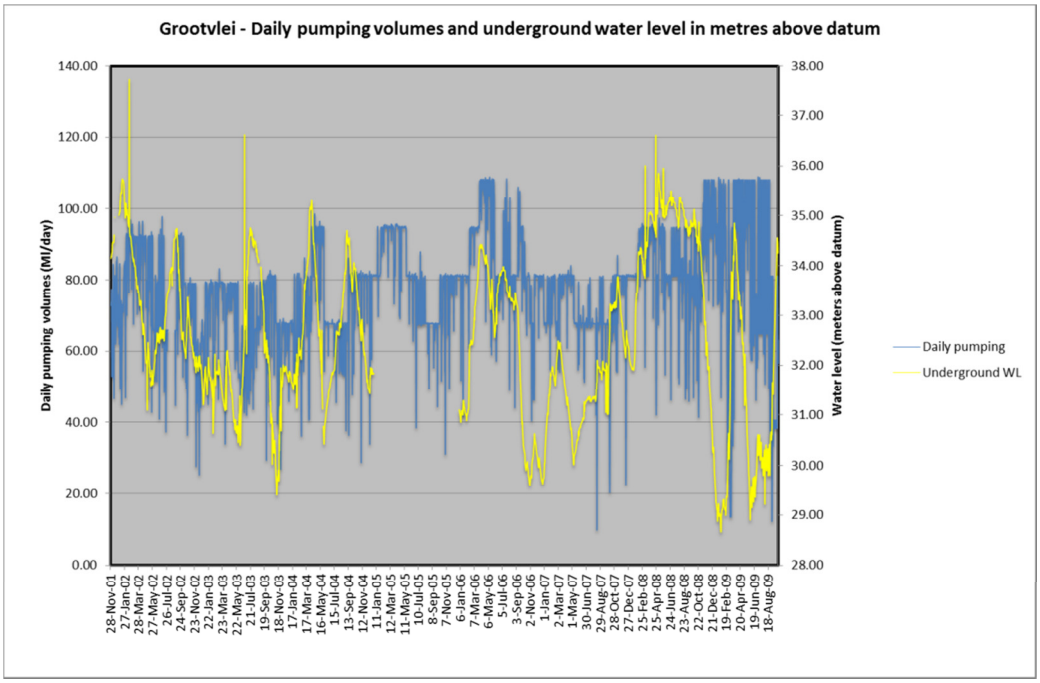

Figure 5-52 Grootvlei daily pumping volumes and underground water levels. Higher pumping rates generally correspond to higher water levels, implying a reactive response between rising water levels and pumping volumes.

This implies that the mine was attempting to balance the pumping volumes with water ingress into the mine voids. The figure also shows a trend of a slow rise in water levels from the onset of pumping to August 2009. For most of the time period, the pumping volumes were around 85 Mℓ/day. At the end of the time period, pumping volumes were around 108 Mℓ/day.

[13] Council for Geoscience Strategic Water Management Project data.

A chart showing underground water levels and rainfall is shown in Figure 5-28.

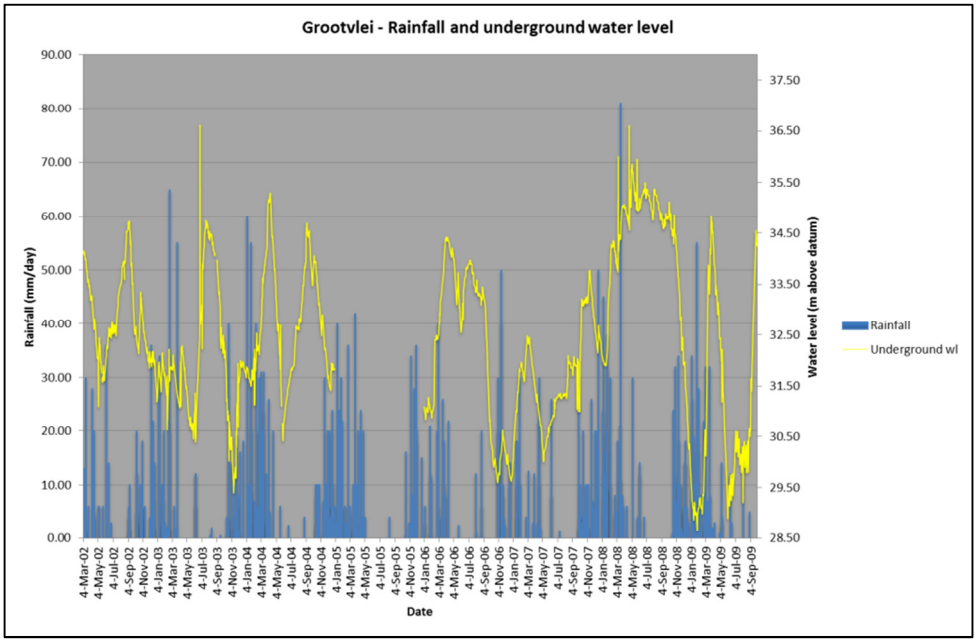

Figure 5-53 Grootvlei rainfall and underground water level

The chart shows that generally high rainfall events are followed by high water levels. This implies that in addition to the mine dewatering, rainfall is a major influence in the underground mine voids. The rapid response between rainfall and underground water levels point to a surface water influence on the underground mine water levels.

Due to the information gap in underground water levels and the correlation between water levels and mine dewatering rates, the raw effluent SO_4 concentrations were plotted against mine dewatering rates (Figure 5-55). The Chart shows that the mine dewatering rates slowly increase with time, which implies that water ingress into the mine also increases with time. Concomitantly the SO_4 concentrations in the underground water show a general decrease, implying that dilution plays a role in the underground mine voids. This also implies that the deep groundwater aquifer in the ERB is being affected by surface water ingress.

Mine surface water monitoring data of the Blesbokspruit shows that from January 1996 to June 2009 the upstream monitoring point (R555) had an average SO4 concentration of 119 mg/ℓ (σ = 49) (Figure 5-54). This value was between a maximum of 601 and a minimum of 1.35 mg/ℓ. The downstream monitoring point (N17) had an average of 647 mg/ℓ (σ = 332) and varied between a maximum of 2 344 and a minimum of 90 mg/ℓ for the same time period. This implies that the mine was impacting the Blesbokspruit surface water in terms of SO_4 loads.

The Grootvlei SO_4 concentrations of the raw effluent, i.e. mine water, has a positively skewed (skewness = 0.93) trimodal data distribution (Figure 5-52). This data distribution shows a strong correlation to the data distribution of Figure 5-51, which is the SO_4 concentrations of underground mine water data in mines throughout the ERB.

Figure 5-54 Map of the Grootvlei mine upstream (R555) and downstream (N17) Blesbokspruit surface monitoring points

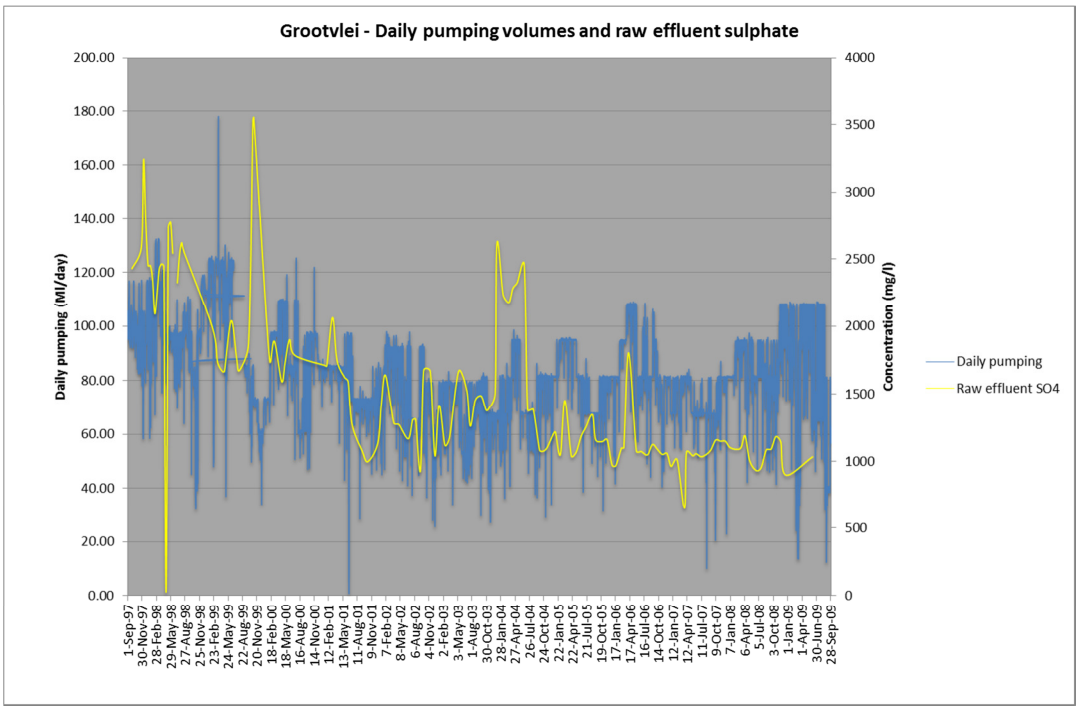

Figure 5-55 Mine dewatering rates and raw effluent SO_4 concentrations

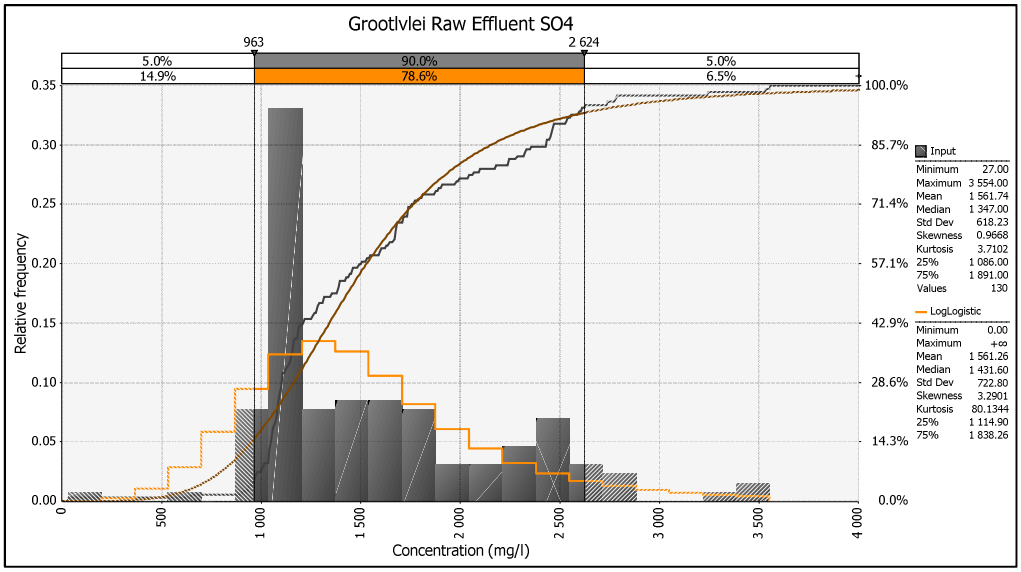

Figure 5-56 Data distribution of Grootvlei mine raw effluent SO4 concentrations

5.2.4.1.3 Ca and Mg

As with the shallow groundwater and Blesbokspruit surface water, Ca and Mg show a strong correlation (0.90) and no correlation with alkalinity. The average concentration of Ca in the deep groundwater is 135 mg/ℓ (σ = 79) and varies between a maximum of 465 and a minimum of 0.5 mg/ℓ. The average Mg concentration is 62 mg/ℓ (σ = 43) and varies between a maximum of 206 and a minimum of 0.3 mg/ℓ. These values are lower than the shallow groundwater and higher than the surface water values.

The Ca (Figure 5-57) and Mg (Figure 5-58) data distributions indicate that the distributions are positively skewed and are trimodal in the case of Ca and bimodal in the case for Mg. The trimodal character of the Ca data corresponds to the trimodal character of the pH and SO_4 data. This is indicative of process and may imply impact on the deep groundwater by a leachate with lower pH and dissolved solids concentrations. The higher Ca and Mg concentrations in the deep groundwater may be either due to an impacting solution with higher Ca and Mg concentrations, or be as a result of dolomite dissolution due to low pH leachate solutions entering the deep groundwater system, most likely through shafts, sink holes and other ingress areas (SRK Consulting, 2005).

As with the shallow groundwater and surface water, the deep groundwater Ca and Mg do not show any correlation with pH. This is most probably due to the pH buffering effect of HCO_3 and the dolomites.

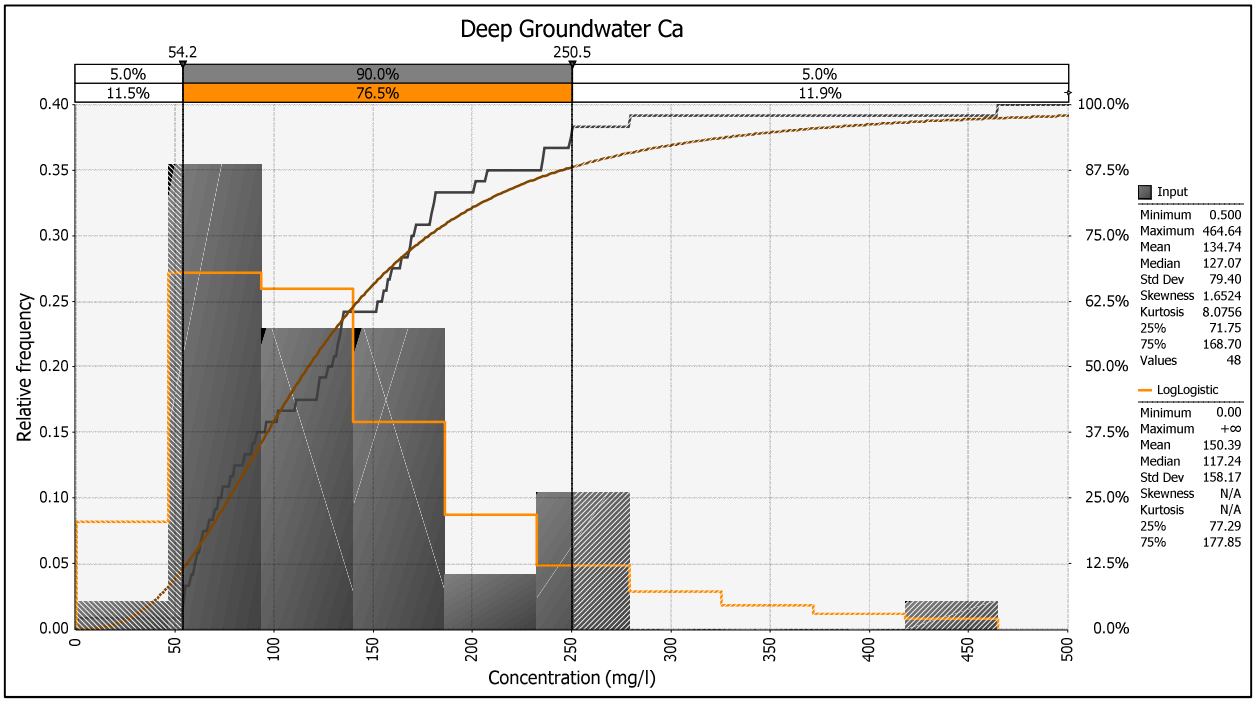

Figure 5-57 Data distribution of the Ca concentrations of the deep groundwater. Values above 314 mg/ℓ can be considered outliers.[14] Therefore the distribution with values exceeding 314 mg/ℓ can be considered as a solution with high Ca values impacting on the baseline deep groundwater.

[14] As defined by the standard Boxplot equation of the upper data limit: *Third Quartile + 1.5 x Inter-Quartile Range*

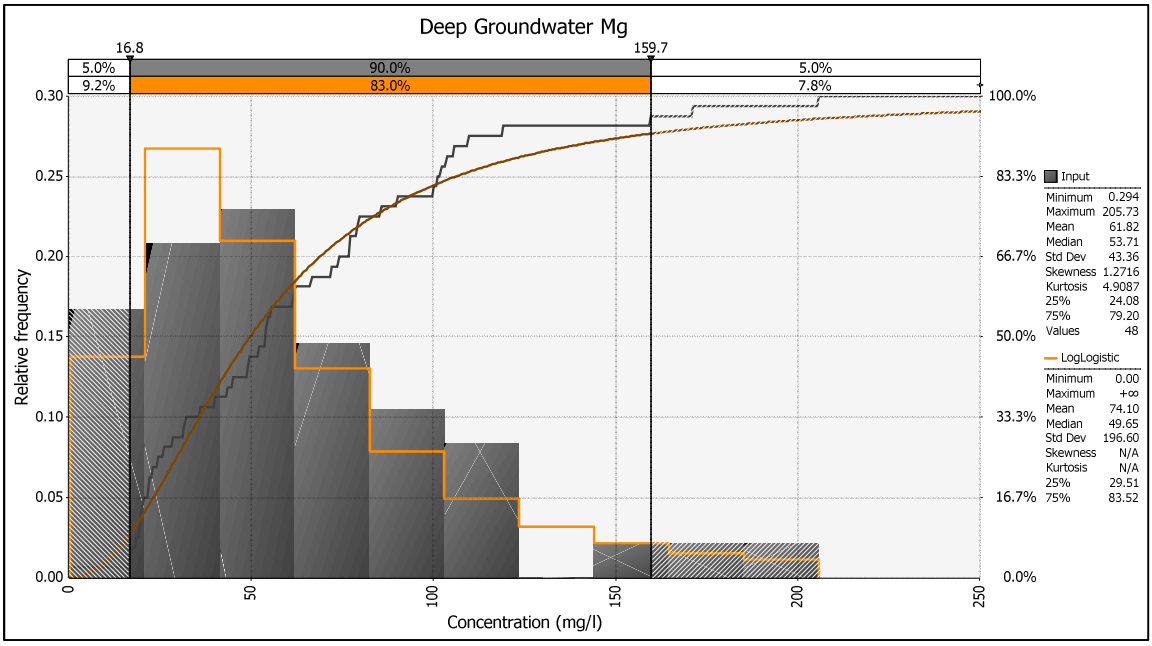

Figure 5-58 Data distribution of the Mg concentrations of the deep groundwater. Values above 164 mg/ℓ are outliers as defined by the standard Boxplot equation[15]. Therefore the data cluster containing values in excess of 164 mg/ℓ can be viewed as a solution with elevated Mg concentrations impacting on the deep groundwater baseline.

5.2.4.1.4 Na

The average Na concentration of the deep groundwater is 174 mg/ℓ (σ = 381) and varies between a maximum of 2 706 and 10 mg/ℓ. The Na data distribution is bimodal (Figure 5-59).

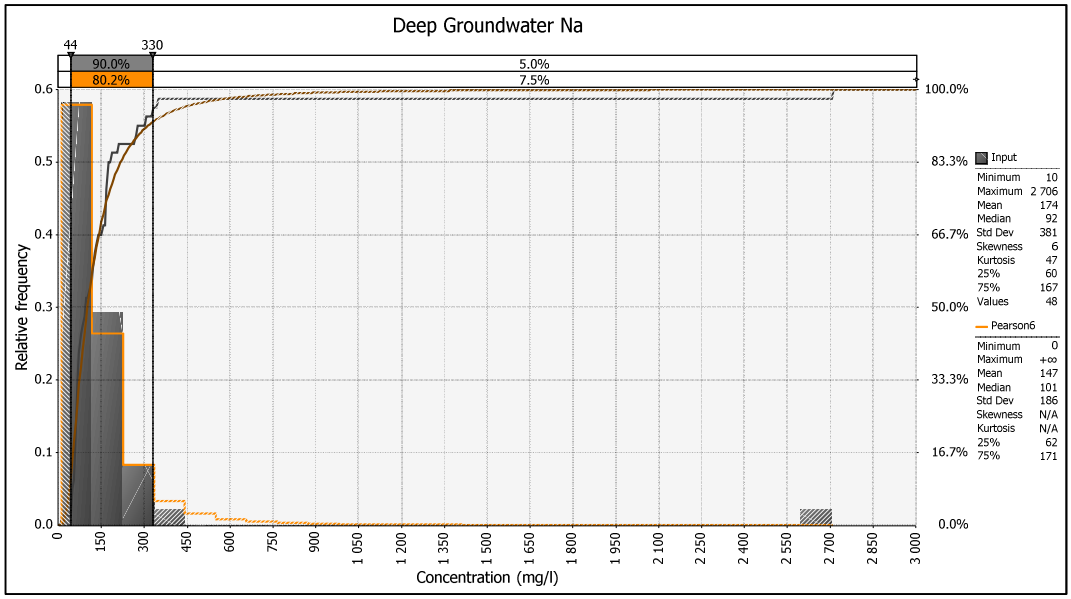

Figure 5-59 Data distribution of deep groundwater Na concentrations.

[15] As defined by the standard Boxplot equation of the upper data limit: *Third Quartile + 1.5 x Inter-Quartile Range*

The bimodal character of the Na data implies the impact of a Na rich solution on the deep groundwater. Sodium concentrations greater than 326 mg/ℓ can be considered outliers[16]. This implies that the data cluster containing Na concentrations in excess of 326 mg/ℓ can be considered a fluid with elevated sodium concentrations impacting on the deep groundwater baseline.

5.2.4.1.5 Fe

The average Fe concentration in the deep groundwater is 10.66 mg/ℓ (σ = 45) varying between a maximum of 292 and a minimum of 0.05 mg/ℓ. The deep groundwater Fe concentrations are 3 orders of magnitude higher than the surface water and 1 order of magnitude higher than the shallow groundwater. The relatively low Fe surface water average (0.29 mg/ℓ) implies either that solution Fe removal processes are in place or dilution is more effective in the surface water system.

The data shows a trimodal distribution, which is positively skewed (skewness = 5.6). Most values (81%) are below 1 mg/ℓ and any value above 4.11 mg/ℓ is in the top 5% of the dataset. Any value exceeding 1.6 mg/ℓ can be considered an outlier. The data clusters containing values in excess of 1.6 mg/ℓ are thus caused by external processes, most likely a solution with elevated Fe concentrations impacting on the deep groundwater baseline. The Pearson's correlation coefficient between Fe concentrations and pH is 0.6. This is a statistically significant correlation and is most likely related to Fe solubility. Ferric Fe is soluble at pH values < 3 (Byrne and Luo, 2000).

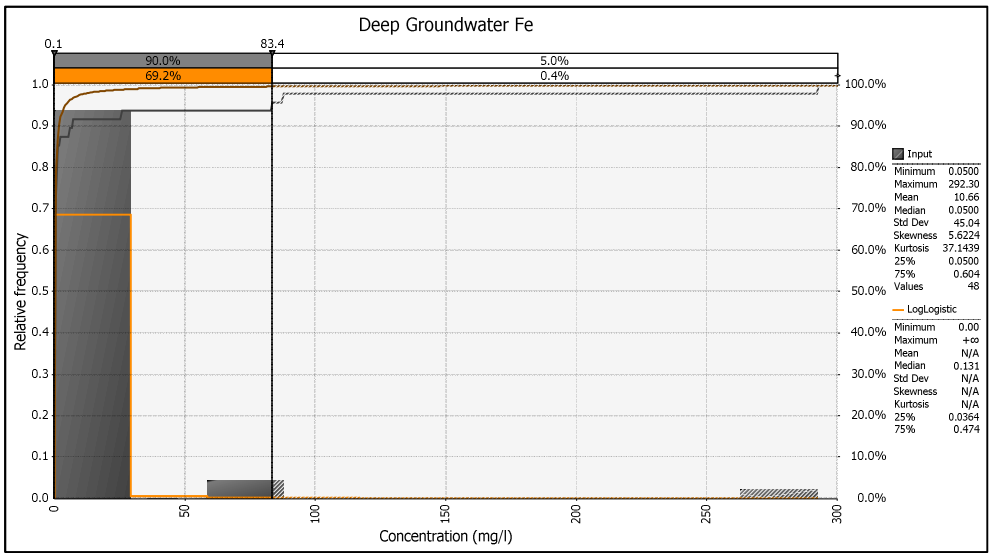

Figure 5-60 Data distribution of deep groundwater Fe concentrations. The distribution shows a trimodal dataset.

[16] As defined by the standard Boxplot equation of the upper data limit: *Third Quartile + 1.5 x Inter-Quartile Range*

5.2.4.1.6 Heavy metals (Mn, Co, Ni, Cu, Zn and Al)

In contrast to the shallow groundwater and as with the surface water, the heavy metals show significant correlation with each other. One potential reason for the correlations is that suspended solids, such as plant material and clay minerals, are probably less in the deep groundwater. This implies less adsorption potential. Precipitation could also be controlling metal solubility with metals forming precipitates with similar ligands, such as HCO_3 and/or SO_4. Viewed from this perspective, the groundwater geochemical system may be a simpler system than the shallow groundwater and surface water systems. A summary of statistical parameters for the underground water is shown in Table 5-10.

Table 5-10 Summary statistics of heavy metal concentrations in the deep groundwater

Metal	Average (mg/ℓ)	Standard Deviation	Coefficient of Variation (%)	Maximum	Minimum	Number of samples (n)
Mn	0.70	1.78	254	11.24	0.01	48
Ni	0.71	1.10	155	1.07	0.00	48
Co	0.18	0.43	232	2.61	0.00	48
Cu	0.07	0.20	303	1.07	0.00	48
Zn	1.21	1.39	114	7.39	0.24	48
Al	3.68	13.97	380	88.76	0.11	48

As in the shallow groundwater and surface water data, the heavy metals in the deep groundwater all show skewed data distributions (Figure 5-61 to Figure 5-66). The distributions are also all polymodal. This implies that more than one subset of data occurs within the larger datasets. This is indicative of varying sources of these elements and varying processes impacting upon them.

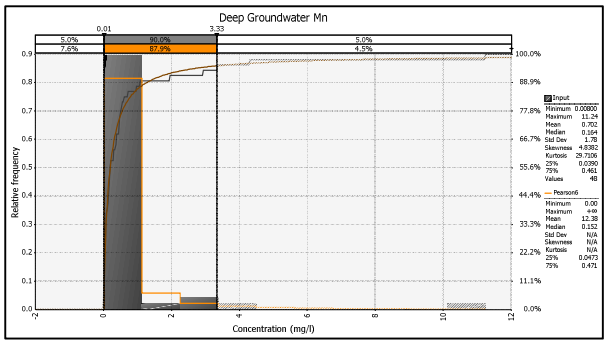

Figure 5-61 Data distribution of the deep groundwater Mn concentrations

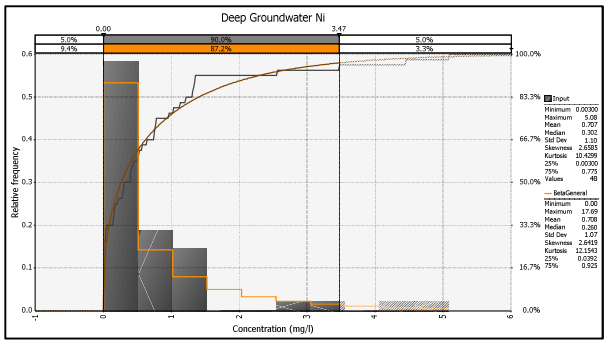

Figure 5-64 Data distribution of the deep groundwater Ni concentrations

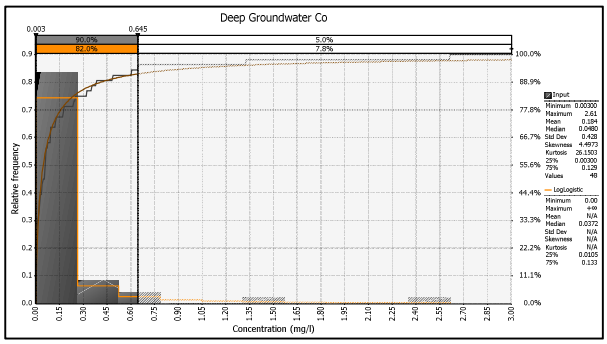

Figure 5-62 Data distribution of the deep groundwater Co concentrations

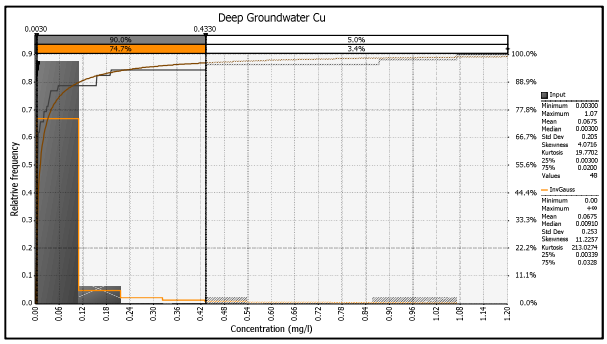

Figure 5-65 Data distribution of the deep groundwater Cu concentrations

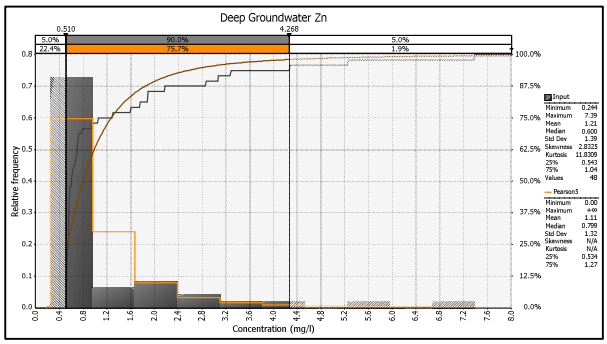

Figure 5-63 Data distribution of the deep groundwater Zn concentrations

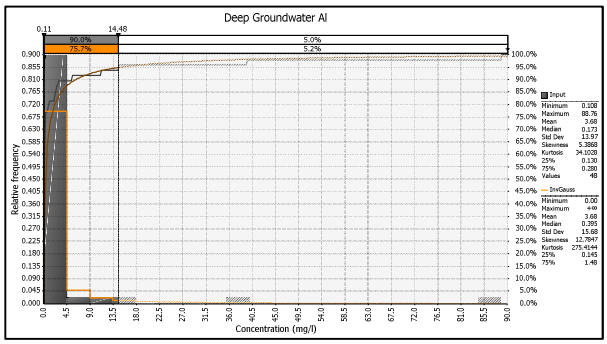

Figure 5-66 Data distribution of the deep groundwater Al concentrations

5.2.4.1.7 U

Uranium correlated with the heavy metals discussed above in the deep groundwater. This is different than the shallow groundwater and the surface water, where U does not correlate with any of the other heavy metals. This reflects the complexity of U geochemistry in the ERB. The surface water contains organic matter, which has an affinity for U. The shallow groundwater is in contact with clay-rich geologic formations, which can also adsorb U. U is sensitive to redox dynamics and the redox conditions of the deep groundwater could be significantly different compared to the shallow groundwater and surface water conditions. These aspects may explain at least some of the variations in U behaviour in the deep groundwater compared to the shallow groundwater and surface water. The average HCO_3 content of the deep groundwater (211.56) is comparable to the average concentration in the surface water (283.69 mg/l). Sulphate is also high for both the deep groundwater and surface water. The only real difference between the deep groundwater and surface water is the absence of organic matter in the deep groundwater.

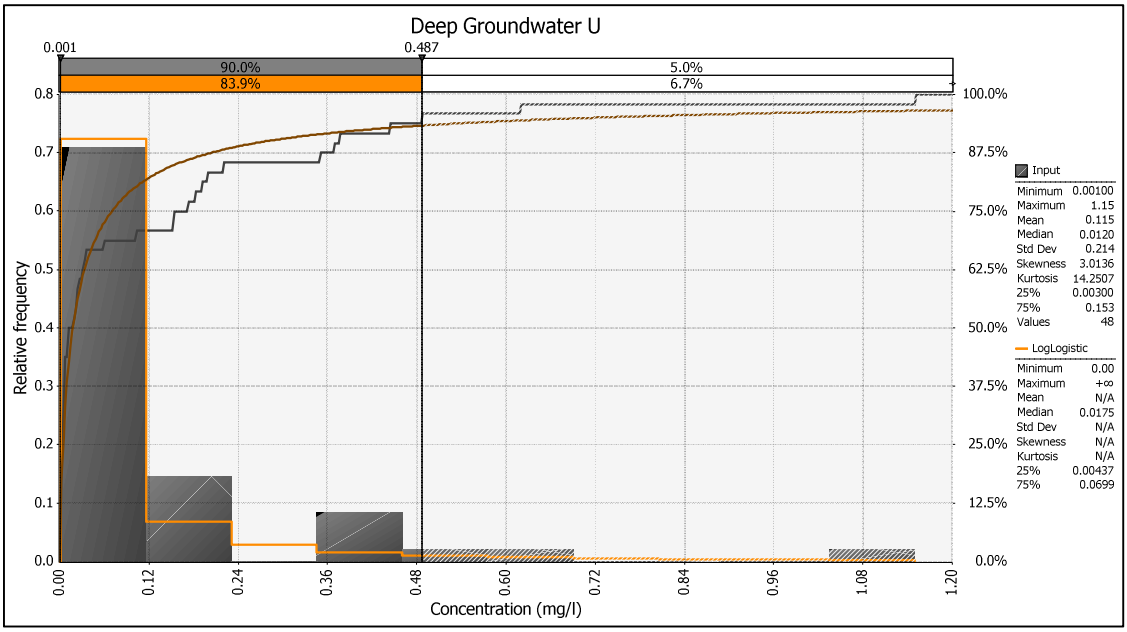

Figure 5-67 Data distribution of the deep groundwater U data. The data has a polymodal distribution. Any concentration above 0.4 mg/ℓ can be considered as an outlier. The data therefore indicates that a solution containing higher U concentrations may be impacting on the deep groundwater baseline.

Uranium, together with the other heavy metals, shows a significant correlation with SO_4. This shows either that U is closely linked to sulphide oxidation, perhaps by acidic leaching, or that U forms SO_4 complexes.

Simple speciation modelling shows that U predominantly forms a complex with phosphoric acid at low pH values. This is in contradiction of the correlation coefficients, which show no correlation between U and PO_4. When redox couples are decoupled, the predominant U complex is $U(SO_4)_2^{2+}$, showing firstly that U^{6+} is in equilibrium in the deep groundwater system, but it also shows a predominant correlation of U with SO_4,

which affirms the statistical correlation. This is in contrast to U in the shallow groundwater, which seems to be acting more conservatively.

5.2.5 Component 5: Soil

The soils in the East Rand Basin, according to the unified soil classification system (USCS), are of the Avalon, Glencoe, Shortlands, Willowbrook, Katspruit and Rensburg soil forms. The study of Rösner et al. (2001) shows that the soils underlying reclaimed tailings are contaminated. They showed that Co, Cr, Cu, Ni and Zn are the main trace metal contaminants. This indicates that tailings facilities are causing pollution plumes below their footprints.

Various elements interact with the soils. These include shallow groundwater, rainfall and leachate from the tailings facilities. The soils in the ERB are dense soils. The volume of dense soils is vulnerable to increase under loading as the particles dilate. This, in conjunction with low permeability implies high surface runoff in rain events (Rösner at al., 2001).

The following processes are important within the soils:

- Adsorption/Surface complexation
- Oxidation/reduction
- Precipitation/co-precipitation
- Dissolution
- Acid neutralisation'
- Leaching of sorbed metals (changing Eh/pH)
- Groundwater movement and advective transport of metals
- Mixing of various water sources:
    - Rain water
    - Effluent
    - Groundwater

5.2.5.1 Soil characterisation

Published data was used for the characterisation of the soil in the project are (Rösner et al., 2001). The East Rand Basin soil profile is relatively shallow, with an average soil depth of 2 m. A summary of the physical parameters is shown in Table 5-11.

Table 5-11 Physical data for East Rand Basin soil

Parameter	Average	unit
Clay	30.1	%
Silt	25.77	%
Sand	40.19	%
Gravel	4.08	%
pH	5.48	
Dry density	1 670	$kg.m^{-3}$
SG	2.65	$g.cm^{-3}$
Void ratio	0.59	
Porosity	37	%
Hydraulic conductivity	5.81×10^{-7}	$cm.s^{-1}$

The East Rand Basin soil is consists of the following soil types:

- Avalon
- Glencoe
- Shortlands
- Willowbrook
- Katspruit
- Rensburg

No mineralogical data on the soil could be sourced and needed to be determined from the local geology (Rösner et al., 2001; Johnson et al., 2006; Erickson et al., 2006; Bühmann, 1992). The geology of the East Rand Basin consists of the Karoo supergroup sandstones and mudstones, belonging predominantly to the Vryheid formation, Karoo age intrusive dolerites, the Transvaal supergroup dolomites belonging to the Malmani subgroup and Recent alluvium along river channels (Figure 5-68). The rocks of the Vryheid formation consist mostly of quartz, K-feldspar, plagioclase, apatite, pyrite, mica, chlorite, illite/smectite and kaolinite. Illite is the dominant clay mineral (Bühman, 1992). The dolerites consist mostly of labradorite and clinopyroxene with accessory amounts of olivine, magnetite, ilmenite, amphibole and biotite (Johnson et al., 2006). The Malmani dolomites consist mostly of the minerals dolomite and calcite. It is therefore expected that the soils will consist mostly of these minerals.

Table 5-12 Summary statistics of uncontaminated soil overlying the Vryheid formation

Sample	n	Average	Standard Deviation	Standard Error	Maximum	Minimum
TiO_2	21	0.96	0.06	0.03	1.08	0.84
MnO	21	0.08	0.03	0.01	0.14	0.04
Fe_2O_3 Total	21	4.40	1.07	0.47	6.44	2.51
Sc	21	12.86	2.37	1.04	18.00	8.00
V	21	65.43	20.11	8.78	106.00	34.00
Cr	21	129.86	31.89	13.92	223.00	80.00
Co	21	14.19	3.08	1.34	21.00	10.00
Ni	21	45.57	9.99	4.36	61.00	26.00
Cu	21	34.57	7.09	3.09	46.00	21.00
Zn	21	103.33	54.74	23.89	230.00	41.00
As	21	22.14	4.41	1.92	31.00	14.00
Rb	21	77.81	9.63	4.20	97.00	50.00
Sr	21	33.43	16.72	7.30	102.00	22.00
Y	21	26.14	3.02	1.32	31.00	21.00
Zr	21	567.57	72.56	31.67	793.00	443.00
Nb	21	19.14	4.21	1.84	24.00	2.00
Mo	21	22.19	6.48	2.83	39.00	3.00
Sn	21	1.05	1.96	0.86	7.00	0.00
Sb	21	0.76	3.49	1.52	16.00	0.00
Ba	21	213.05	60.72	26.50	341.00	85.00
W	21	7.90	1.73	0.75	14.00	6.00
Pb	21	14.48	8.04	3.51	33.00	3.00
Th	21	13.33	2.69	1.17	18.00	8.00
U	21	0.00	0.00	0.00	0.00	0.00

The surface geology is dominated by the Vryheid formation of the Karoo Supergroup and the soil is therefore expected to mostly represent minerals and weathering products of primary minerals of this formation. The background geochemistry of uncontaminated soil overlying the Vryheid formation is shown in Table 5-12 (Rösner et al., 2001). Extraction data for the background soil samples are presented in Table 5-13 (Rösner et al., 2001).

Table 5-13 Extractable threshold values for soils using NH_4NO_3

	As	Co	Cr	Cu	Mo	Ni	Pb	U	V	Zn
Units	*mg/kg*	*mg/kg*	*mg/kg*	*mg/kg*	*mg/kg*	*mg/kg*	*mg/kg*	*mg/kg*	*mg/kg*	*mg/kg*
	0.1	0.5	0.1	2	1	1	2	0.04	1	10

The data in Table 5-12 and Table 5-13 will be used for comparison to determine potential contaminants from tailings.

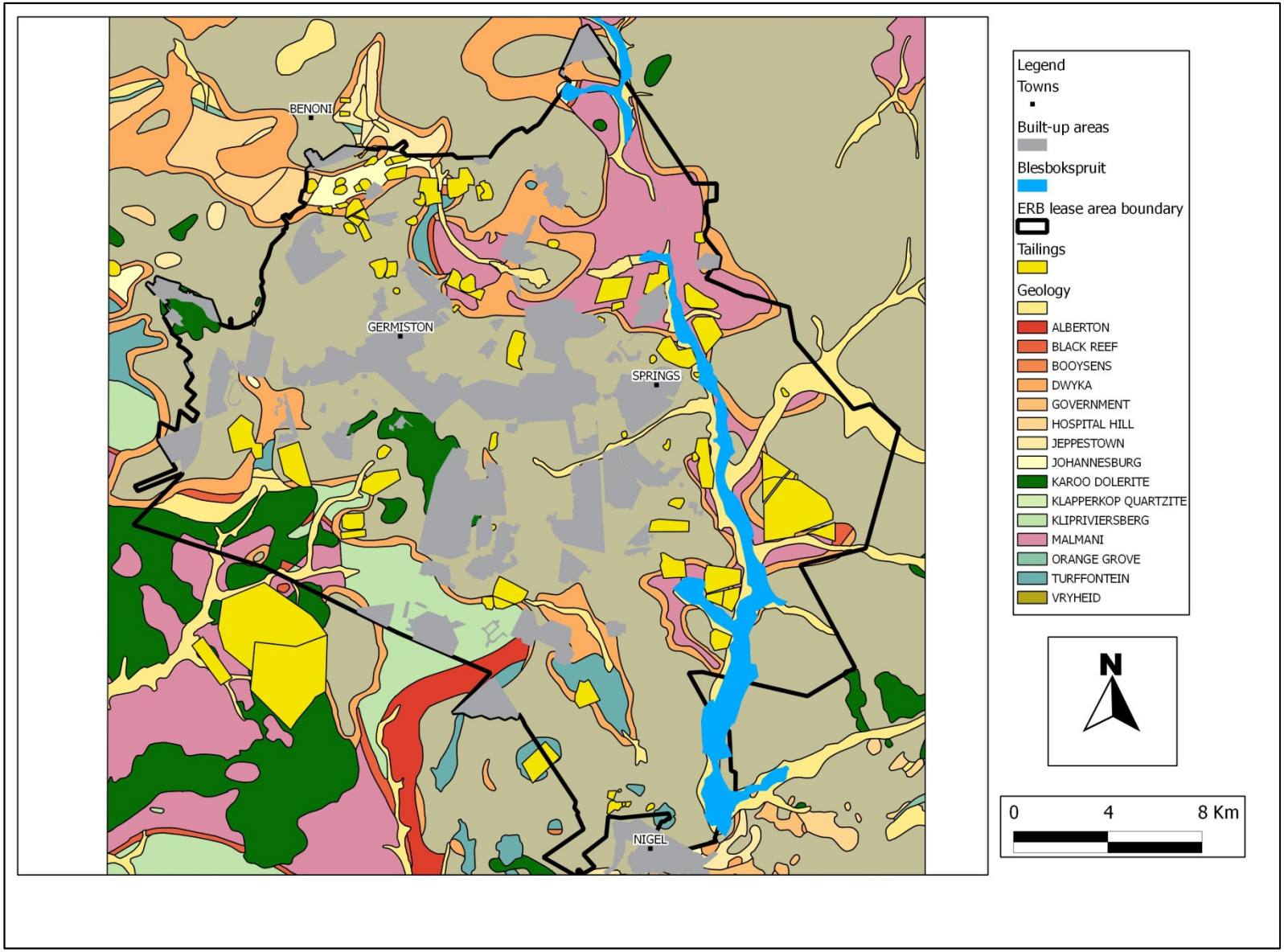

Figure 5-68 Simplified geological map of the East Rand Basin study area.

6 CHAPTER 6: COMPONENT CONCEPTUAL MODELS

Before any meaningful numeric geochemical models can be developed, conceptual models need to be developed. The data analyses of the preceding section as well as reviewed literature of international studies are used to develop conceptual models for each ERB geochemical system component.

6.1 Conceptual model – Tailings facilities

A review of the literature shows that the effluent from sulphide mineral containing tailings are acidic in nature and contain elevated concentrations of metals and SO_4 (Simón et al., 2005; Nengovhela et al., 2007; Dold and Fontbote, 2001; Gunsinger et al., 2006; Gleisner and Herbert, 2002). This leachate is referred to as acid mine drainage (AMD). The Witwatersrand Au-U deposits contain pyite [FeS_2] (Hallbauer, 1986). Pyrite is unstable in the presence of oxygen, whether dissolved in water or contained in the atmosphere. In contact with oxygen, pyrite oxidises to form ferrous Fe (Fe^{2+}), SO_4 and H^+ (Equation 2) (Williamson and Rimstidt, 1994). These chemical species, together with the SO_4 forms sulphuric acid (Table 6-2, Equation 2). Equation 2 shows that for every mole of pyrite that oxidised 2 moles of H^+ is formed or 1 mole of sulphuric acid. The Fe^{2+} resulting from the reaction in Equation 2, can be oxidised to ferric Fe (Fe^{3+}) (Equation 4). At pH values < 3 Fe^{3+} is soluble (Byrne and Lou, 2000) and can in turn also act as an oxidant for pyrite (Equation 3) (Williamson and Rimstidt, 1994). Equation 4 shows that for every mole of pyrite that is oxidised by ferric iron, 16 moles of H^+ is formed or 8 moles of acid. The rate of oxidation by Fe^{3+} is higher than when pyrite is oxidised by O_2 (Singer and Stumm, 1970; Williamson and Rimstidt, 1994). The oxidation of ferrous to ferric iron is usually slow, but can be catalysed by bacteria, such as *Acidothiobacillus Ferrooxidans* (Schrenk et al., 1998; Liu et al., 2009; Boon et al., 1999; Gleisner et al., 2006).

The mineralogy of the Witwatersrand Au-U ore consists mostly of quartz, pyrite, muscovite and chlorite with accessory amounts of chromite, pyrophyllite, titanite, zircon and trace amounts of uraninite (Table 6-1).

Table 6-1 Mineralogy of the Vaal and Ventersdorp Contact Reef (VCR) (after Rösner et al. (2001))

Mineral	Ideal mineral formula	Vaal reef	VCR
Quartz	SiO_2	88.3	88.9
Pyrite	FeS_2	6.6	3.2
Muscovite	$KAl_2(AlSi_3O_{10})(OH)_2$	4.4	3
Chlorite	$(Mg,Fe)_3(Si,Al)_4O_{10}(OH)_2.(Mg,Fe)_3(OH)_6$	0.8	4.9
Chromite	$FeCr_2O_4$	0.2	0.2
Pyrophyllite	$Al_2Si_4O_{10}(OH)_2$	0.1	0.2
Titanite	$CaTiO(SiO_4)$	0.1	0.1
Zircon	$ZrSiO_4$	0.1	0.2
Uraninite	UO_2	0.0050	0.0044

Rösner et al. (2001) has shown that the tailings generally consist of quartz, muscovite, chlorite, pyrophyllite, jarosite and gypsum.

Table 6-2 Tailings geochemical reactions

Oxidation Reactions

$$FeS_2 + H_2O + \frac{7}{2}O_{2(aq)} = Fe^{2+} + 2SO_4^{2-} + 2H^+$$ **Equation 2**

$$FeS_2 + 8H_2O + 14Fe^{3+} = 15Fe^{2+} + 2SO_4^{2-} + 16H^+$$ **Equation 3**

$$Fe^{2+} + \frac{1}{4}O_{2(aq)} + H^+ = Fe^{3+} + \frac{1}{2}H_2O$$ **Equation 4**

$$U^{4+} + H_2O + \frac{1}{2}O_{2(aq)} = UO_2^{2+} + 2H^+$$ **Equation 5**

$$UO_2^{2+} + 3HCO_3^- = UO_2(CO_3)_3^{4-} + 3H^+$$ **Equation 6**

$$3UO_2^{2+} + 4H_2O = (UO_2)_3(OH)_4^{2+} + 4H^+$$ **Equation 7**

$$Mn^{2+} + \frac{3}{2}H_2O + \frac{5}{4}O_{2(aq)} = MnO_4^- + 3H^+$$ **Equation 8**

Secondary mineral formation reactions

$$K^+ + 3Fe^{3+} + 2SO_4^{2-} + 6H_2O = KFe_3(SO_4)_2(OH)_6 + 6H^+$$ **Equation 9**

$$Ca^{2+} + SO_4^{2-} + 2H_2O = CaSO_4.2H_2O$$ **Equation 10**

$$Fe^{3+} + 3H_2O = Fe(OH)_{3(s)} + 3H^+$$ **Equation 11**

$$Fe^{2+} + \frac{3}{2}H_2O + \frac{1}{4}O_{2(aq)} = FeOOH_{(s)} + 2H^+$$ **Equation 12**

Mineral weathering reactions

$$CaCO_3 + H^+ = Ca^{2+} + HCO_3^-$$ **Equation 13**

$$UO_2 + 4H^+ = U^{4+} + 2H_2O$$ **Equation 14**

$$KAl_2(Si_3Al)O_{10}(OH)_{2(s)} + 10H^+ = K^+ + 3Al^{3+} + 3SiO_{2(aq)} + 6H_2O$$ **Equation 15**

$$Al_2Si_4O_{10}(OH)_{2(s)} + 6H^+ = 2Al^{3+} + 4SiO_{2(aq)} + 4H_2O$$ **Equation 16**

$$K(Mg,Fe)_3(AlSi_3)O_{10}(OH)_{2(s)} + 10H^+ = K^+ + \frac{7}{2}Mg^{2+} + \frac{3}{2}Fe^{2+} + Al^{3+} + 3SiO_{2(aq)} + 6H_2O$$ **Equation 17**

$$NaAl_2(Si_3Al)O_{10}(OH)_{2(s)} + 10H^+ = Na^+ + 3Al^{3+} + 3SiO_{2(aq)} + 6H_2O$$ **Equation 18**

$$(Mg,Fe)_3(Si,Al)_4O_{10}(OH)_4.(Mg,Fe)_3(OH)_6 + 10H^+ = 3Fe^{2+} + 3Mg^{2+} + SiO_{2(aq)} + 7H_2O$$ **Equation 19**

$$CaMg(CO_3)_{2(s)} + 2H^+ = Ca^{2+} + Mg^{2+} + 2HCO_3^-$$ **Equation 20**

$$SiO_{2(s)} = SiO_{2(aq)}$$

Adsorption reactions

$$> X: + Me^{2+} => X{:}Me^{2+}$$ **Equation 21**

Jarosite and gypsum are secondary minerals that are known to form in AMD environments (Moncur et al., 2009; Gunsinger et al., 2006; Alpers et al., 1994; Hammastrom et al., 2005). Jarosite is stable below pH values of 3 (Welch et al., 2008; Liu et al., 2009; Drouet et al., 2004; Baron and Palmer, 1996; Smith et al., 2006). The presence of jarosite in the ERB tailings is an indication of prevailing acidic conditions. Jarosite may be important in the ERB tailings system in controlling the mobility of Fe^{3+} and Al.

A sulphide oxidation model, the shrinking core model, was published by Hansen et al. (2008). According to this model, the O_2 flux into the tailings remains constant over the operational life of the tailings. Upon decommissioning, the O_2 flux increases, due to the subsidence of the piezometric head. The pyrite oxidation rate is proportional to the O_2 flux into the system and increases upon decommissioning. However, due to the depletion of pyrite and/or armouring of pyrite grains by secondary products, inhibiting O_2 to reach fresh pyrite surface to oxidise it, the oxidation rate gradually decreases with time, till either the pyrite has been completed or there is no fresh pyrite surface to oxidise.

Acidity in the form of protons is produced in each of the above reactions. This acid is the source of the AMD seeping from tailings deposits in the East Rand Basin (Bezuidenhout and Rosseau, 2005; Tutu et al., 2008; Yibas et al., 2010). Hallbauer (1986) has shown that the Witwatersrand pyrite contains trace concentrations of other metals. The most important of these in terms of concentration and in decreasing order of abundance are Ni (μ[17] = 1 930 mg/kg), As (μ = 1 394 mg/kg), Co, (μ = 1 006 mg/kg). Pb (μ = 844 mg/kg), Cu (μ = 346 mg/kg), Zn (μ = 90 mg/kg), Cr (μ = 33 mg/kg) and Mn (μ = 16 mg/kg).These metals are released upon oxidation. In addition, the dissolution of various silicate minerals as well as the uraninite associated with the Witwatersrand gold ore (Hallbauer, 1986) releases metals into the acidic solutions. The specific composition of an AMD solution mostly depends on the original composition of the pyrite being oxidised and the pyrite host rock composition. It has been shown that Cu, Ni, Cr, Co and Zn occur in the extractable concentrations in the tailings (Rösner et al., 2001). The concentration of extractable metals is dependent on the position in the tailings from where they were collected, as the top few cm are generally oxidised leached (Bezuidenhout and Rosseau, 2005; Nengovhela et al., 2007). The oxidation zone has been shown in previous studies on Witwatersrand tailings dams to extend to a depth of ~4 m (Bezuidenhout and Rosseau, 2005; Nengovhela et al., 2007). The extractable metal concentrations indicate that the tailings are a source of trace metals and that the most important metals in the leachate are Cu, Ni, Cr, Co and Zn. Naicker et al (2006) have also shown in their study that white gypsum crust that develops in winter on the banks of streams draining Witwatersrand mining areas contains Co, Ni and Zn, thus correlating with the data of Rösner et al. (2001).

Leaching of metals occurs when the acid solution exits the tailings, either into the groundwater through the soil or as toe seepage. Leaching of metals and acid from tailings facilities occur in three main processes:

- Leaching by water and dissolved oxygen moving vertically through the tailings.

[17] μ is the symbol for average.

- Erosion of particulate matter from the side slopes of the tailings into surface water systems and onto surrounding soil.
- Wind-blown erosion of tailings material.

The leaching by water occurs by vertical percolation through the tailings facility. Layers containing clayey material in the tailings, formed due to the sedimentation processes active during operation, may provide hydraulic barriers to flow and cause water to flow from the sides of the tailings due to lower hydraulic conductivities. This process is apparent specifically in older tailings observable as the deep ravines or cracks on the sidewalls of the facillities. Where tailings were constructed on impermeable layers, such as bedrock or a clay layer, toe seepage occurs. This toe seepage seeps into surrounding river and wetland systems and the shallow groundwater. In addition, water moving vertically through the tailings forms a pollution plume in the soil below the tailings, as evidenced by a study on the footprints of reclaimed tailings facilities (Rösner et al., 2001). The pollution plume will have vertical and horizontal flow vectors, depending on the media through which the groundwater flows. When groundwater encounters an impermeable zone it will flow laterally over this zone.

It has been shown in general that tailings have a general internal structure, which depends on whether the tailings is operational or not. Post-operational tailings contain a 5 to 50 cm oxidised layer, although Witwatersrand gold tailings dams have been found to have oxidation layers of up to 4 m deep (Bezuidenhout and Rousseau, 2005; Nengovhela et al., 2007; Yibas et al., 2010;). Below this depth is a zone in which the acid neutralising minerals, mostly carbonates (if present), have been depleted (Dold and Fontbote, 2001; Gunsinger et al., 2006). The boundary separating the oxidised and the neutralisation depletion zone is defined by the oxidation front. The oxidation front migrates inwards from the tailings dam extremities and vertically through the tailings towards the tailings base at a rate which is dependent on the O_2 diffusion rate (Ritchie, 1994; Bezuidenhout and Rousseau, 2005). The oxygen flux remains relatively constant during the operation phase as the tailings facility remains relatively saturated hydraulically due to the continuous deposition of wet tailings onto the surface. Oxygen dissolved in rainwater is considered a negligible process in introducing O_2 into tailings and waste rock environments (Ritchie, 1994). The post-operational drop in hydraulic head causes an influx of oxygen into the tailings facility and oxidation progresses rapidly (Bezuidenhout and Rosseau, 2005; Nengovhela et al., 2007). The O_2 flux in dissolved or in gaseous form decreases through the tailings as time progresses. This is due to the difficulty of O_2 diffusion with depth (Ritchie, 1994) and due to the formation of secondary oxidation products, which coat pyrite grains limiting further reaction and causing a reduction in oxidation rates (Hansen et al., 2005).

The layer below the oxidation front is the unoxidised zone. The boundary between the unoxidised and neutralisation depletion zone is defined by the acid front. This front also migrates inwards and vertically through the tailings towards its base, but at a much faster rate than the oxidation front, as oxidation reactions are much slower than the vertical velocity of the downward percolating acidic solution (Dold and Fontbote, 2001). The Witwatersrand Au-U ore does not contain carbonate minerals (Pretorius, 1974; Rösner et al., 2001). Therefore buffer capacity in the tailings facilities is limited. Acidic solutions can be buffered by Al- and

Fe-hydroxides at pH values between 5.7 and 3.5. Aluminosilicate minerals buffer pH values to ≥ 1.3 (Gunsinger et al., 2006). The pH values of ERB tailings pore waters are therefore expected to be in the rather large pH range of 5.7 and 1.3. Rösner et al. (2001) showed that soil, paste pH values in reclaimed tailings footprints are as low as 3.1. This indicates that the pH of ERB tailings pore waters can be expected to be in the lower range of 3.5 to 1.3.

The oxidation products of pyrite together with products liberated from the dissolution of acid neutralising reactions and the weathering of gangue minerals can combine to produce secondary minerals. These are usually a range of metal salts and the specific minerals to form depend on the prevailing conditions in the area of the tailings that they form in (Jönsson et al., 2006; Dold and Fontbote, 2001; Petrunic et al., 2009; Hammarstrom et al., 2005). In more arid conditions where MAE exceeds MAP, these secondary minerals form hardpan layers (Meima et al., 2012; Gunsinger et al., 2006; Bezuidenhout and Rousseau, 2005; Rösner et al., 2001). These hardpan layers form a few cm below the tailings surface and consist of a variety of secondary minerals, mostly sulphates of Fe and Al. Hardpan layers have been shown to form in the Witwatersrand and thus also the ERB tailings dams (Bezuidenhout and Rousseau, 2001; Nengovhela et al., 2007).

In terms of the ERB tailings underground water was pumped from the largest operating mine in the ERB, Grootvlei, at the time for when this study is conducted. The effluent was limed in a treatment plant and the sludge deposited on the tailings, with the treated water discharging into the Blesbokspruit (Roychoudhury and Starke, 2006; Expert team of the inter-ministerial commission, 2010).

In summary, the most important mass fluxes and processes active in the tailings component are shown below.

1. Influxes of matter into the tailings component system from other components in the ERB system and environment:
    - Water (rainfall and groundwater rise due to capillary action)
    - O_2 (diffusion from the atmosphere and dissolved in rainwater)
    - Dissolved mass in groundwater introduced into the base of tailings
    - New water and mass deposited on the tailings during the operational phase of the mine
2. Fluxes of material from the tailings component system to other components within the ERB system and environment are:
    - Water (toe seepage and infiltration of leachate into soil and shallow groundwater; evaporation)
    - Dissolved constituents in tailings leachate and in return water to the mine (only during operation)
    - Dust particles from wind action

Processes active within the tailings system:

- Sulphide oxidation (abiotic and microbially catalysed)

- Mineral dissolution and precipitation
- Leaching of dissolved mass
- O_2 diffusion
- Adsorption

The conceptual model is summarised in Figure 6-1. A list of the most important geochemical reactions is shown in Table 6-2. This is not an exhaustive list and does not attempt to show all possible reactions. The most important reactions are shown, which imply important processes, rather than attempting to show every possible reaction for all geochemical components in the tailings system.

6.2 Conceptual model – Wetlands and surface water

Studies on natural and artificial wetland systems have shown that wetlands have the capacity to significantly reduce, even remediate, the polluted effluent flowing through them (Lizama et al., 2011; Coetzee et al., 2006; Sheoran and Sheoran, 2006; Tooth and McCarthy, 2007). The wetlands in the ERB are no exception (Roychoudhury and Starke, 2006; McCarthy and Venter, 2006; Coetzee et al., 2006).

Studies in the ERB wetlands have shown that metals are mostly associated with exchangeable fractions as opposed to residual phases and are associated with the Fe-Mn oxides and hydroxides and carbonate phases (Roychoudhury and Starke, 2006). This implies that the metal mobility is controlled by dissolution-precipitation and adsorption reactions. The association with Fe and Mn in the Roychoudhury and Starke (2006) study shows that adsorption to Fe-Mn phases are more important than adsorption to organic matter. Copper, Ni, Co and Th were associated with organic matter in some samples. This may be due either to adsorption to organic matter or chelation with organic ligands, showing that the interaction of metals in the wetlands with the clay, silt and organic matter of the wetland drainage channel is complex.

Microbial activity is a possibility in the wetlands and can assist in reduction and oxidation. Oxidation and reduction reactions will depend on the on the vertical position of the ion in the wetland drainage channel strata. The top few cm are generally considered to be oxidative, while the lower layers are considered to be reducing (Coetzee et al., 2006).

The presence of red Fe-hydroxide precipitates have been reported in studies on ERB wetland systems (McCarthy and Venter, 2006; Coetzee et al., 2006; Naicker et al., 2003). This implies that Fe is being introduced into the wetland systems and is, at least in part, precipitating as Fe-oxyhydroxides. This correlates with the association of metals in the wetland sediments with Fe-Mn phases of a previous study (Roychoudhury and Starke, 2006). This implies that the precipitating Fe-Mn oxyhydroxides are introducing additional adsorption capacity to the wetland system.

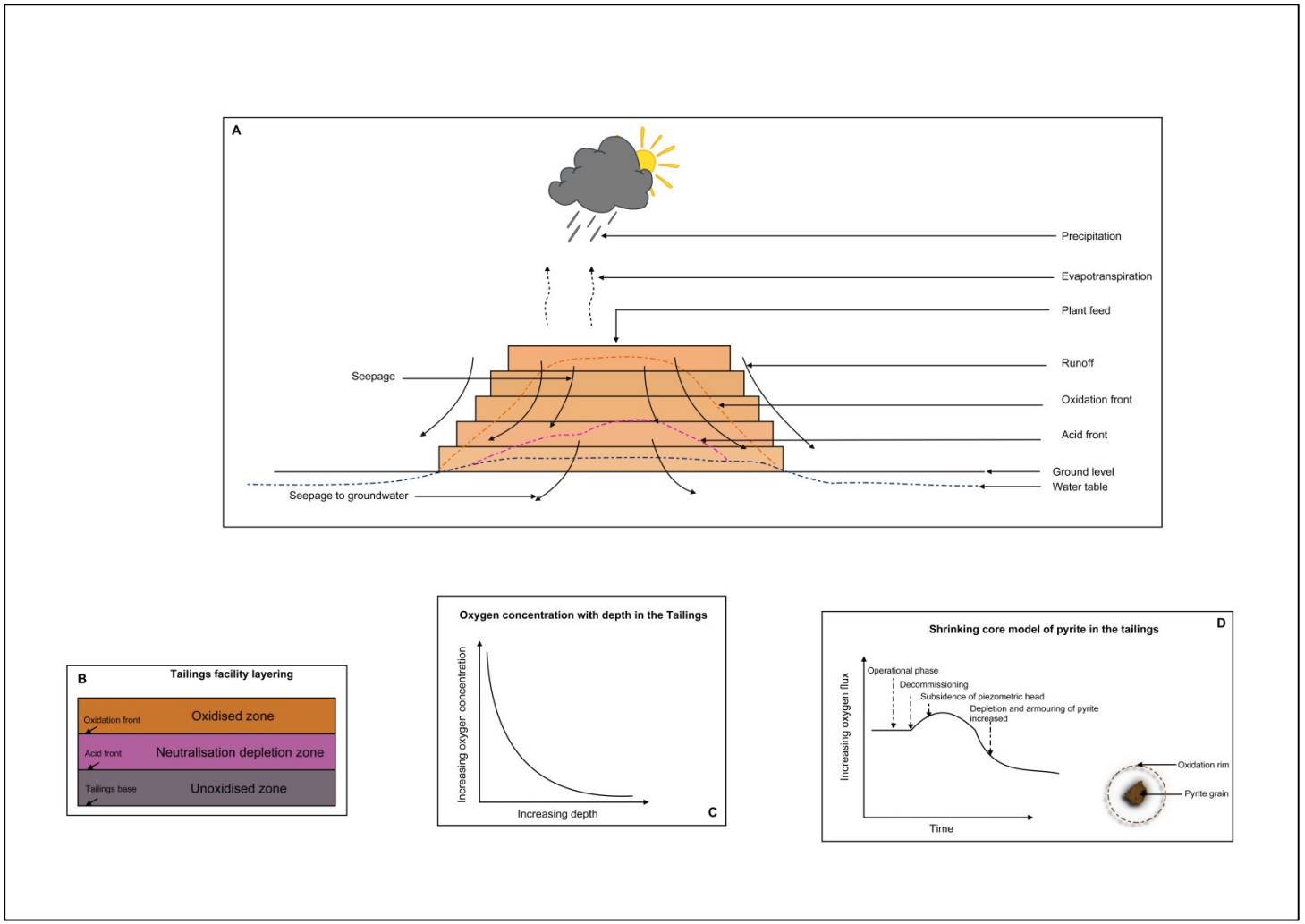

Figure 6-1 Conceptual model of the tailings component. The generic macro geochemical structure of the tailings facilities in the ERB is shown in box A. The most important aspect is that the acid front migrates more rapidly through the tailings facility than the oxidation front. This layering is shown in box B. The oxygen depletion model through the tailings is shown in box C on a plot of oxygen concentration with depth. The sulphide oxidation core shrinkage model is depicted in box D on a plot of oxygen flux and time.

The processes that are important in the wetland systems are:

- Dilution (by rain, groundwater influx and water from tributaries)
- Microbial reduction of sulphides and oxidation of iron
- Precipitation and co-precipitation
- Adsorption by plant roots as well as on organic matter and Fe-Mn-oxyhydroxides
- Chelation

One important process is the reaction of organic material with sulphate to produce metal sulphides and bicarbonate. The reaction is as follows:

$$\mathbf{2}CH_2O_{(s)} + SO_4^{2-} = H_2S_{(aq)} + \mathbf{2}HCO_3^- \qquad \textbf{Equation 22}$$

In this reaction CH_2O represents organic matter. This reaction is subject to an anoxic environment and will most probably only be important deeper in the soil profile of the river bed.

A summary of the aforementioned is shown in Figure 6-2 and a list of the most important geochemical reactions are shown in Table 6-3.

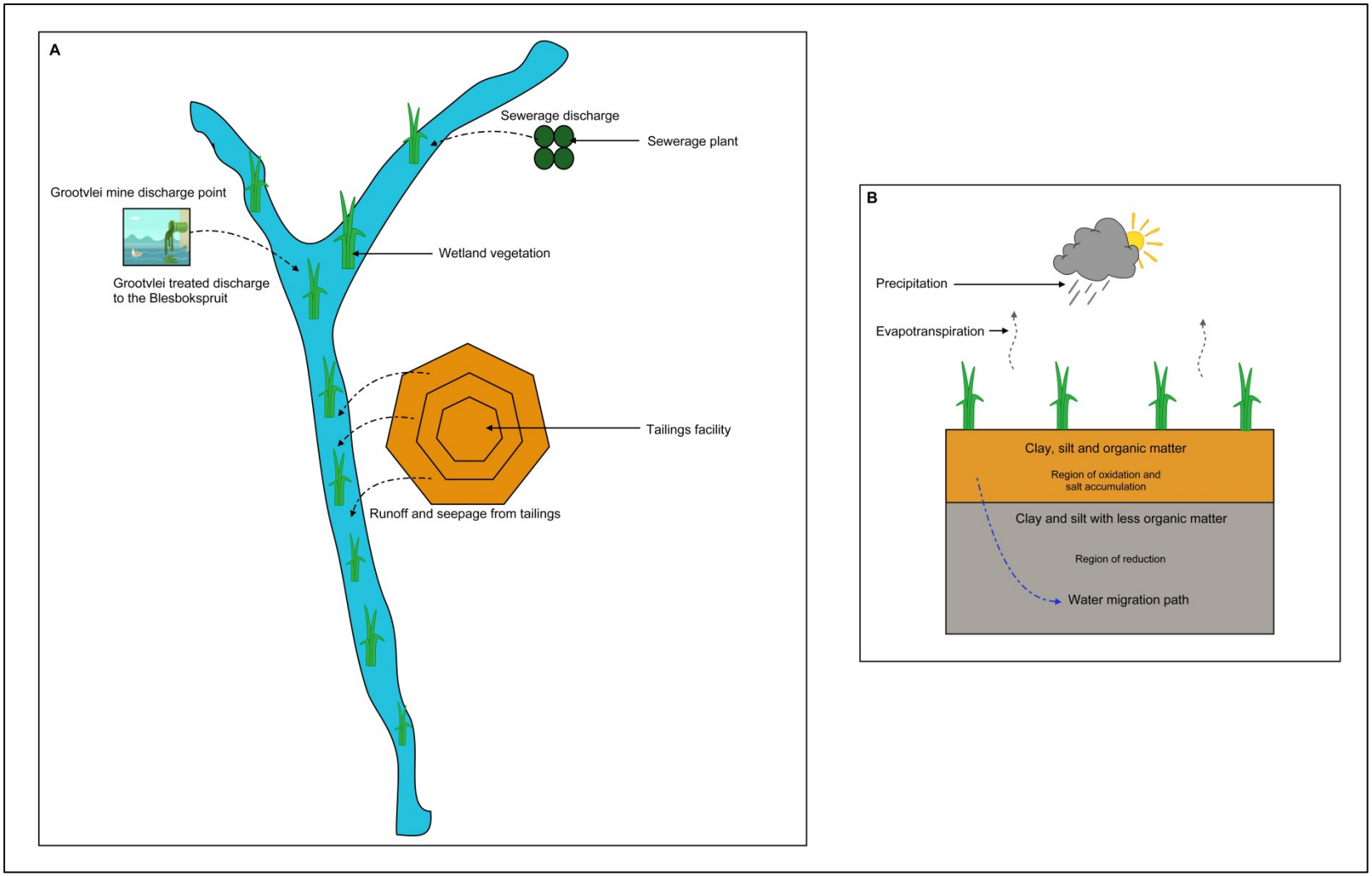

Figure 6-2 Wetland conceptual model. Box A shows the regional impacts on the Blesbospruit. Box B shows the channel base layering and the prevailing redox conditions.

Table 6-3 Most important geochemical reactions of the wetland and surface water system

Oxidation reactions

$$Fe^{2+} + \frac{1}{4}O_{2(aq)} + H^+ = Fe^{3+} + \frac{1}{2}H_2O$$ **Equation 23**

$$U^{4+} + H_2O + \frac{1}{2}O_{2(aq)} = UO_2^{2+} + 2H^+$$ **Equation 24**

$$Ca^{2+} + SO_4^{2-} + 2H_2O = CaSO_4.2H_2O$$ **Equation 25**

$$Fe^{3+} + 3H_2O = Fe(OH)_{3(s)} + 3H^+$$ **Equation 26**

$$Fe^{2+} + \frac{3}{2}H_2O + \frac{1}{4}O_{2(aq)} = FeOOH_{(s)} + 2H^+$$ **Equation 27**

$$UO_2 + 4H^+ = U^{4+} + 2H_2O$$ **Equation 28**

$$2CH_2O_{(s)} + SO_4^{2-} = H_2S_{(g)} + 2HCO_3^-$$ **Equation 29**

$$Me^{2+} + H_2S_{(g)} + 2HCO_3^- = MeS_{2(s)} + 2H_2O + 2CO_{2(g)}$$ **Equation 30**

$$UO_2^{2+} + 3HCO_3^- = UO_2(CO_3)_3^{4-} + 3H^+$$ **Equation 31**

$$3UO_2^{2+} + 4H_2O = (UO_2)_3(OH)_4^{2+} + 4H^+$$ **Equation 32**

$$Mn^{2+} + \frac{3}{2}H_2O + \frac{5}{4}O_{2(aq)} = MnO_4^- + 3H^+$$ **Equation 33**

$$CH_3COO^- + 4U^{6+} + 4H_2O = 4U^{4+} + 2HCO_3^- + 9H^+$$ **Equation 34**

$$UO_2^{2+} + \frac{7}{4}H^+ + \frac{1}{4}CH_{4(aq)} = U^{4+} + \frac{5}{4}H_2O + \frac{1}{4}HCO_3^-$$ **Equation 35**

$$HCO_3^- + H_2O + H^+ = CH_{4(aq)} + 2O_{2(aq)}$$ **Equation 36**

Mineral weathering reactions

$$CaCO_3 + H^+ = Ca^{2+} + HCO_3^-$$ **Equation 37**

$$KAl_2(Si_3Al)O_{10}(OH)_{2(s)} + 10H^+ = K^+ + 3Al^{3+} + 3SiO_{2(aq)} + 6H_2O$$ **Equation 38**

$$Al_2Si_4O_{10}(OH)_{2(s)} + 6H^+ = 2Al^{3+} + 4SiO_{2(aq)} + 4H_2O$$ **Equation 39**

$$K(Mg,Fe)_3(AlSi_3)O_{10}(OH)_{2(s)} + 10H^+ = K^+ + \frac{7}{2}Mg^{2+} + \frac{3}{2}Fe^{2+} + Al^{3+} + 3SiO_{2(aq)} + 6H_2O$$ **Equation 40**

$$NaAl_2(Si_3Al)O_{10}(OH)_{2(s)} + 10H^+ = Na^+ + 3Al^{3+} + 3SiO_{2(aq)} + 6H_2O$$ **Equation 41**

$$(Mg,Fe)_3(Si,Al)_4O_{10}(OH)_4.(Mg,Fe)_3(OH)_6 + 10H^+ = 3Fe^{2+} + 3Mg^{2+} + SiO_{2(aq)} + 7H_2O$$ **Equation 42**

$$CaMg(CO_3)_{2(s)} + 2H^+ = Ca^{2+} + Mg^{2+} + 2HCO_3^-$$ **Equation 43**

$$SiO_{2(s)} = SiO_{2(aq)}$$ **Equation 44**

$$Me^{2+} + CH_2O_{(s)} = MeCH_2O^{2+}$$ **Equation 45**

Adsorption reactions

$$> X: + Me^{2+} => X{:}Me^{2+}$$ **Equation 46**

6.3 Conceptual model – Shallow and deep groundwater components

The shallow and deep groundwater components are described together in one conceptual model, due to their close interaction. The shallow groundwater is considered to extend from ground level to a depth of 60 mbgℓ (1 540 mamsℓ). This is based on the shallow borehole data for the ERB[18]. The deep groundwater is considered to be from a depth of 470 mbgℓ (1 280 mamsℓ), which is the environmental critical level[19] for the ERB (DWA, 2012). Studies on the deep and shallow groundwater systems (Africa Geo-Environmental Services (Pty) Ltd., 2006; Lippman et al., 2003; Duane et al., 1997; Expert team of the inter-ministerial committee, 2010) show that the most important groundwater aquifer for the shallow groundwater are the fractured Karoo rocks and the Malmani dolomites. The shallow groundwater is perched on an impermeable, weathered dolorite sill. In places the dolorite sill is perforated by mine shafts, which cause interaction between the shallow and deep groundwater aquifers. The Blesbokspruit and perhaps other wetlands in the ERB are fed by the shallow groundwater and in turn recharge the shallow aquifer by seepage.

At the time of data collection the deep groundwater aquifer was being dewatered to allow for deep mining at ~750 mbgℓ (850 mamsℓ) (DWA, 2012). This water was being treated and discharged into the Blesbokspruit.

A number of tailings facilities are located throughout the ERB. Most of these are not lined and are thereby freely seeping AMD into the groundwater system. The shallow groundwater system and surface water systems are also being impacted by runoff from the tailings in the rainy season, whereby eroded silt from the tailings enters the surface water system. AMD contaminated water also seeps from the tailings facilities through the soil to the shallow groundwater system.

At the time for which data is available, the deep groundwater table was kept below the environmental critical level (DWA, 2012). Therefore the shallow groundwater could percolate downwards, but deep groundwater could only interact with the shallow groundwater and surface water due to the pump, treat and discharge at Grootvlei mine (Roychoudhury and Starke, 2006; Expert team of the inter-ministerial committee, 2010).

The ERB is truncated in the west by the Boksburg gap, which is represented by a zone through which no mining has occurred and essentially separates the ERB and the Central Rand Basin (CRB) to the west (Bosch, 2010).

A summary of the shallow and deep groundwater conceptual models are shown in Figure 6-3 and a list of the most important geochemical reactions are shown in Table 6-4.

[18] Council for Geoscience, Strategic water management project.

[19] The environmental critical level is defined as the highest point to which the deep groundwater can be allowed to rise and still not impact on the clean shallow groundwater in the Malmani dolomites.

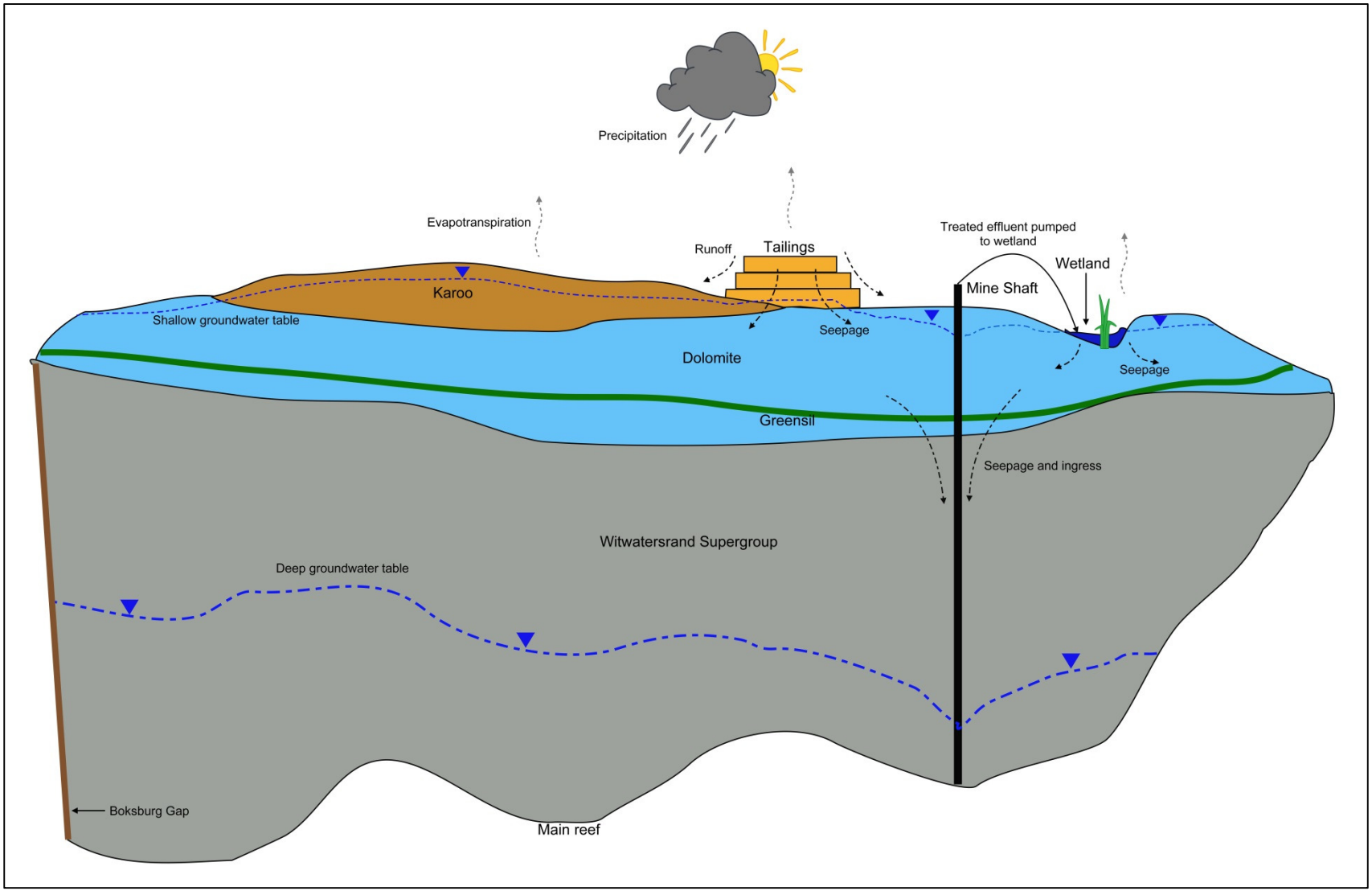

Figure 6-3 Shallow and deep groundwater conceptual model (modified from Africa Geo-Environmental Services (Pty) Ltd. (2006). The diagram shows the impacts on the deep and shallow groundwater as well as the interaction pathways.

Table 6-4 Most important geochemical reactions for the shallow and deep groundwater systems

Oxidation Reactions

$$FeS_2 + H_2O + \frac{7}{2}O_{2(aq)} = Fe^{2+} + 2SO_4^{2-} + 2H^+$$ **Equation 47**

$$FeS_2 + 8H_2O + 14Fe^{3+} = 15Fe^{2+} + 2SO_4^{2-} + 16H^+$$ **Equation 48**

$$Fe^{2+} + \frac{1}{4}O_{2(aq)} + H^+ = Fe^{3+} + \frac{1}{2}H_2O$$ **Equation 49**

$$U^{4+} + H_2O + \frac{1}{2}O_{2(aq)} = UO_2^{2+} + 2H^+$$ **Equation 50**

$$UO_2^{2+} + 3HCO_3^- = UO_2(CO_3)_3^{4-} + 3H^+$$ **Equation 51**

$$3UO_2^{2+} + 4H_2O = (UO_2)_3(OH)_4^{2+} + 4H^+$$ **Equation 52**

$$Mn^{2+} + \frac{3}{2}H_2O + \frac{5}{4}O_{2(aq)} = MnO_4^- + 3H^+$$ **Equation 53**

Secondary mineral formation reactions

$$K^+ + 3Fe^{3+} + 2SO_4^{2-} + 6H_2O = KFe_3(SO_4)_2(OH)_6 + 6H^+$$ **Equation 54**

$$Ca^{2+} + SO_4^{2-} + 2H_2O = CaSO_4.2H_2O$$ **Equation 55**

$$Fe^{3+} + 3H_2O = Fe(OH)_{3(s)} + 3H^+$$ **Equation 56**

$$Fe^{2+} + \frac{3}{2}H_2O + \frac{1}{4}O_{2(aq)} = FeOOH_{(s)} + 2H^+$$ **Equation 57**

Mineral weathering reactions

$$CaCO_3 + H^+ = Ca^{2+} + HCO_3^-$$ **Equation 58**

$$UO_2 + 4H^+ = U^{4+} + 2H_2O$$ **Equation 59**

$$KAl_2(Si_3Al)O_{10}(OH)_{2(s)} + 10H^+ = K^+ + 3Al^{3+} + 3SiO_{2(aq)} + 6H_2O$$ **Equation 60**

$$Al_2Si_4O_{10}(OH)_{2(s)} + 6H^+ = 2Al^{3+} + 4SiO_{2(aq)} + 4H_2O$$ **Equation 61**

$$K(Mg,Fe)_3(AlSi_3)O_{10}(OH)_{2(s)} + 10H^+ = K^+ + \frac{7}{2}Mg^{2+} + \frac{3}{2}Fe^{2+} + Al^{3+} + 3SiO_{2(aq)} + 6H_2O$$ **Equation 62**

$$NaAl_2(Si_3Al)O_{10}(OH)_{2(s)} + 10H^+ = Na^+ + 3Al^{3+} + 3SiO_{2(aq)} + 6H_2O$$ **Equation 63**

$$(Mg,Fe)_3(Si,Al)_4O_{10}(OH)_4.(Mg,Fe)_3(OH)_6 + 10H^+ = 3Fe^{2+} + 3Mg^{2+} + SiO_{2(aq)} + 7H_2O$$ **Equation 64**

$$CaMg(CO_3)_{2(s)} + 2H^+ = Ca^{2+} + Mg^{2+} + 2HCO_3^-$$ **Equation 65**

$$SiO_{2(s)} = SiO_{2(aq)}$$ **Equation 66**

Adsorption reactions

$$> X: + Me^{2+} => X{:}Me^{2+}$$ **Equation 67**

6.4 Conceptual model - Soil

A study on the ERB soil underlying reclaimed tailings in the ERB (Rösner et al., 2001) show that soils are contaminated, implying that leaching from the tailings to the soils occur. The general soil profiles, derived from test pits dug to an average of 2 – 3 m, show a distinct layering. The study distinguishes between 2 *colluvium* and 2 *nodular ferruginous colluvium* layers in some of the studied profiles. These are grouped together in this study for simplicity, as the simplification has no consequence for the geochemical models.

Table 6-5 Generalised soil profile from reclaimed tailings sites (modified from Rösner et al. (2001))

	Tailings: Slightly moist, light grey banded pale yellow-brown, very soft, layered sandy silt
	Colluvium: Slightly moist, dark red-brown, dense, open structured, sandy silt or silty sand with gypsum crystals
	Nodular ferruginous colluvium: Moist, red-brown, firm, intact, sandy clay with numerous coarse-, medium- and fine-grained subrounded ferricrete nodules.

Enrichment of Fe, Mn, Zn, Ni, Co, Pb, As, V and U occur at most sites. This shows that the soil has adsorption capacity for these metals, with Fe and Mn most probably precipitating and adding to the adsorption capacity of the soil. It has been shown that the probability that the shallow groundwater is contaminated is high (Section 5.2.3.1). This may be an indication of the fact that the adsorption capacity of the soil to remove metals from tailings effluent leaching through the soils is either depleted or is close to depletion, at least locally beneath tailings.

A summary of the soil conceptual model is shown in Figure 6-4 and the list of the most important possible reactions is shown in Table 6-6.

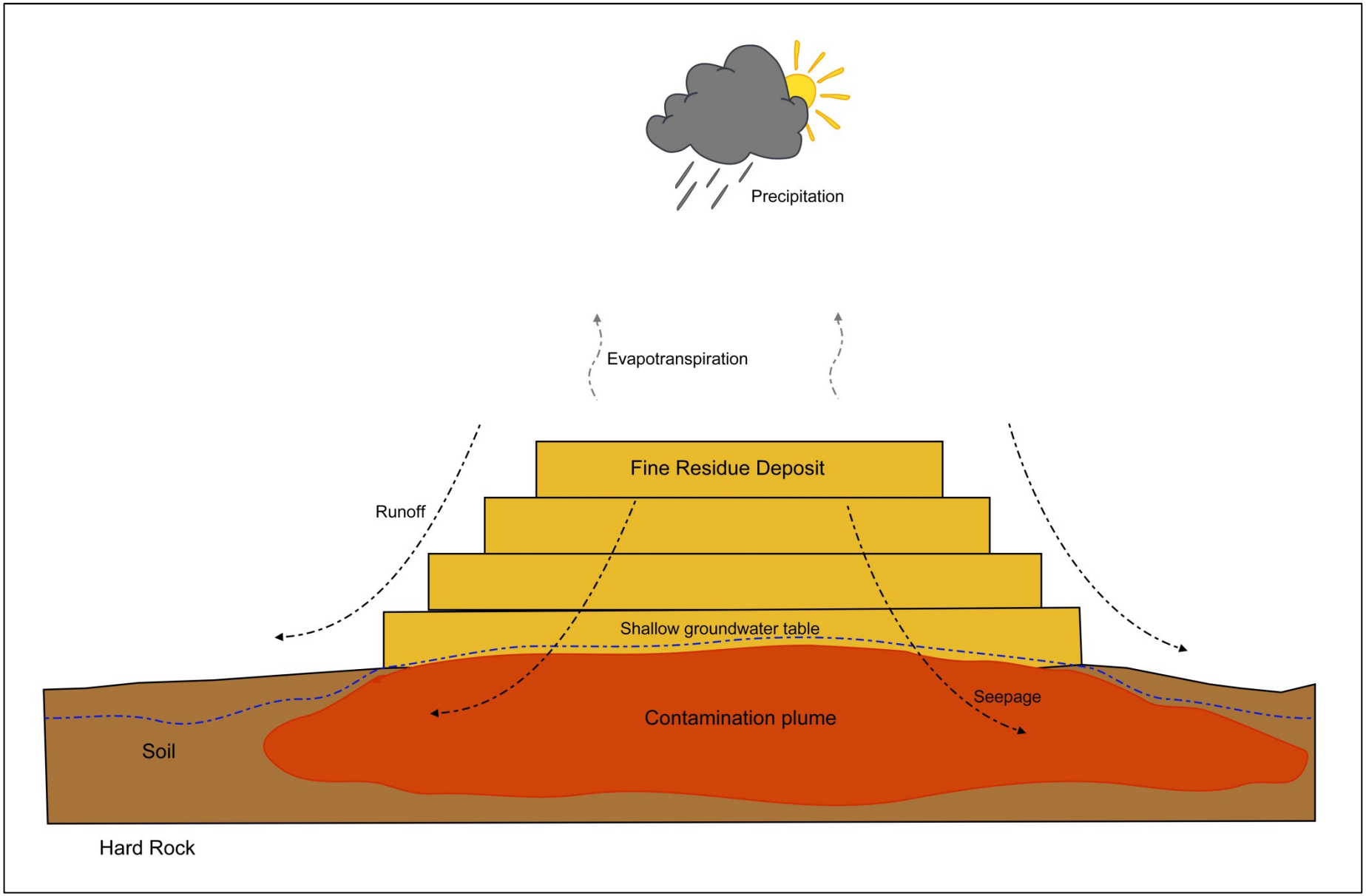

Figure 6-4 Conceptual model of the soil system. The diagram shows the contamination plume resulting from seepage from the tailings facility.

Table 6-6 Most important reactions of the soil system

Oxidation Reactions

$$FeS_2 + H_2O + \frac{7}{2}O_{2(aq)} = Fe^{2+} + 2SO_4^{2-} + 2H^+$$ **Equation 68**

$$FeS_2 + 8H_2O + 14Fe^{3+} = 15Fe^{2+} + 2SO_4^{2-} + 16H^+$$ **Equation 69**

$$Fe^{2+} + \frac{1}{4}O_{2(aq)} + H^+ = Fe^{3+} + \frac{1}{2}H_2O$$ **Equation 70**

$$U^{4+} + H_2O + \frac{1}{2}O_{2(aq)} = UO_2^{2+} + 2H^+$$ **Equation 71**

$$UO_2^{2+} + 3HCO_3^- = UO_2(CO_3)_3^{4-} + 3H^+$$ **Equation 72**

$$3UO_2^{2+} + 4H_2O = (UO_2)_3(OH)_4^{2+} + 4H^+$$ **Equation 73**

$$Mn^{2+} + \frac{3}{2}H_2O + \frac{5}{4}O_{2(aq)} = MnO_4^- + 3H^+$$ **Equation 74**

Secondary mineral formation reactions

$$K^+ + 3Fe^{3+} + 2SO_4^{2-} + 6H_2O = KFe_3(SO_4)_2(OH)_6 + 6H^+$$ **Equation 75**

$$Ca^{2+} + SO_4^{2-} + 2H_2O = CaSO_4.2H_2O$$ **Equation 76**

$$Fe^{3+} + 3H_2O = Fe(OH)_{3(s)} + 3H^+$$ **Equation 77**

$$Fe^{2+} + \frac{3}{2}H_2O + \frac{1}{4}O_{2(aq)} = FeOOH_{(s)} + 2H^+$$ **Equation 78**

Mineral weathering reactions

$$CaCO_3 + H^+ = Ca^{2+} + HCO_3^-$$ **Equation 79**

$$UO_2 + 4H^+ = U^{4+} + 2H_2O$$ **Equation 80**

$$KAl_2(Si_3Al)O_{10}(OH)_{2(s)} + 10H^+ = K^+ + 3Al^{3+} + 3SiO_{2(aq)} + 6H_2O$$ **Equation 81**

$$Al_2Si_4O_{10}(OH)_{2(s)} + 6H^+ = 2Al^{3+} + 4SiO_{2(aq)} + 4H_2O$$ **Equation 82**

$$K(Mg,Fe)_3(AlSi_3)O_{10}(OH)_{2(s)} + 10H^+ = K^+ + \frac{7}{2}Mg^{2+} + \frac{3}{2}Fe^{2+} + Al^{3+} + 3SiO_{2(aq)} + 6H_2O$$ **Equation 83**

$$NaAl_2(Si_3Al)O_{10}(OH)_{2(s)} + 10H^+ = Na^+ + 3Al^{3+} + 3SiO_{2(aq)} + 6H_2O$$ **Equation 84**

$$(Mg,Fe)_3(Si,Al)_4O_{10}(OH)_4.(Mg,Fe)_3(OH)_6 + 10H^+ = 3Fe^{2+} + 3Mg^{2+} + SiO_{2(aq)} + 7H_2O$$ **Equation 85**

$$CaMg(CO_3)_{2(s)} + 2H^+ = Ca^{2+} + Mg^{2+} + 2HCO_3^-$$ **Equation 86**

$$SiO_{2(s)} = SiO_{2(aq)}$$ **Equation 87**

Adsorption reactions

$$> X: + Me^{2+} => X{:}Me^{2+}$$ **Equation 88**

7 NUMERIC GEOCHEMICAL MODELLING

7.1 Numeric geochemical modelling approach

From the preceding discussions it can be deduced that the tailings facilities may have a major environmental geochemical impact on other components in the ERB geochemical system. Previous studies have shown that the tailings facilities in the ERB do have a major geochemical impact on other components in the ERB geochemical system (Rösner et al., 2001; Cukrowska et al., 2004; Bezuidenhout and Rousseau, 2005; Roychoudhury and Starke, 2006; Naicker at al., 2007; Nengovhela et al., 2007; Tutu et al, 2008; Yibas et al., 2010; Expert team of the inter-ministerial committee, 2010). This has been shown to be the case in other areas of the world as well (Moreno and Neretnieks, 2006; Dold and Fontbote, 2001).It may be that the tailings facilities may be the dominant geochemical environmental impact in the ERB. For this reason the numerical geochemical modelling will be centred around the tailings facilities and its impact on the ERB environmental system as defined in Section 5.

Due to the detailed nature of geochemical reaction modelling, no one geochemical model can reflect the complexity of the individual component systems and the myriad of processes involved in linking the various component systems in the entire ERB geochemical system. The numeric geochemical should therefore be approach from as much a topological as a thermodynamic perspective. Therefore a number of geochemical models were developed to identify, characterise and understand the most important geochemical processes active in the ERB system (Table 7-1).

Due to the limitations of computing time and the complexity of the individual component systems, the models necessarily represent a simplified version of reality. George Box coined the phrase: “All models are wrong, some are useful.” The usefulness of the ERB models is assessed by outlining the assumptions and uncertainties in the various models and testing these by sensitivity analyses. The models are constantly evaluated using existing data and information from the ERB and similar systems worldwide.

7.2 Model set-up

The model set-up is discussed on a generic level in this section. Each individual model will be discussed with regards to its specific quantities of interest (QOI), assumptions and uncertainties in the section pertaining to that specific model. The quantities of interest, assumptions and uncertainties are discussed in this section are generic to the ERB component models. Specifics are discussed in the section pertaining to the specific component model.

Table 7-1 ERB geochemical processes identified and geochemical models developed to study them. The processes identified are derived from the data analysis (Section 5) and conceptual models (Section 6) in preceding sections.

	Geochemical models	Process	Components in which process is dominant
1	Pyrite oxidation model	Pyrite oxidation	Tailings
2	Soil adsorption model	Adsorption (soil)	Soil (clays); Surface water (wetlands - Fe-Hydroxides and organic material)
3	Toe seepage models with carbonate added; Blesbokspruit dilution and neutralisation model	Neutralisation	Surface water (HCO3); Geology (dolomites)
4	Dilution model with Blesbokspruit surface water; shallow groundwater and deep groundwater; Contaminated shallow groundwater and pristine deep groundwater mixing model	Dilution of contamination (principally from tailings leachate)	Surface water; Shallow groundwater; Deep groundwater
5	Evaporation model of toe seepage and Blesbokspruit - tailings leachate dilution solution	Natural concentration of dissolved constituents	Surface water and Tailings principally through seasonal variations in rainfall and evaporation
6	Weathering model	Natural mineral weathering	Geology; Soil; Shallow Groundwater; Deep Groundwater; Tailings; Surface water

7.2.1 Quantities of interest

It is important to identify the quantities of interest (QOI)[20] in any scientific model. The QOI of the current study are defined based on the data analysis in Section 5. These are the parameter pH, the major element components SO_4, HCO_3, Ca, Mg, K and Na, and the metals Fe, U, Al, Mn, Co, Ni and Zn.

Uraninite [UO_2] is the most abundant uranium mineral in the Witwatersrand (Pretorius 1974). Therefore uraninite is used in the numerical model to account for the potential partitioning of U in the mine waste leachate. The average rate constant from a number of studies on uraninite dissolution (Ulrich et al. 2009) is 8.76×10^{-14} mol.cm^{-2}.s^{-1} varying between a maximum of 8.58×10^{-16} and a minimum of 1.5×10^{-12} mol.cm^{-2}.s^{-1}. This rate is used in the models and evaluated by sensitivity analysis for each model.

Nickel has been shown to be associated with the Witwatersrand pyrite (Hallbauer, 1986). Therefore, if the assumption is made that all Ni is associated with the pyrite, then the same rate constant for the NiO reaction can be used as that of pyrite, thereby constraining the amount of Ni able to enter the mine waste system.

The precipitation of specific minerals, such as jarosite, which have been observed in tailings samples of tailings facilities in the East Rand Basin (Rösner et al., 2001) and Fe-oxyhydroxides, which has been observed in streams affected by AMD in the ERB (Naicker et al., 2003; Coetzee et al., 2006) are also

[20] The QOI are those quantities for which the output is important and is related to the purpose of the model.

considered QOI. The presence of these minerals can, together with existing water quality data of the ERB, be used as a calibration tool to evaluate the model results.

7.2.2 Assumptions

7.2.2.1 Use of literature rate constants

The assumption is made that the literature rate constants used are applicable to the ERB system. Although this assumption may not be valid, the assumption is considered conservative. This is due to the fact that laboratory rates are generally faster than actual rates and can be up to 3 orders of magnitude fatser (White and Brantley, 2003; Wilson, 2004; Brantey, 2008). The rate constants serve to allow some minerals to react faster or slower than others, thereby introducing a measure of disequilibrium into the system, as exists for the real-life system. Carbonate would react faster than quartz, for example. A sensitivity analysis on the rate constants used is conducted to test the validity of this assumption.

7.2.2.2 Use of default software rate equation

The default rate equation of the software is applicable to the minerals in the ERB system and is applicable to all minerals in the system. The rate equation used by the software is:

$$r_{\vec{k}} = A_s k_+ \left(1 - \frac{Q}{K}\right) \qquad \text{Equation 89}$$

In Equation 89, $r_{\vec{k}}$ is the forward direction rate of the reaction in mol.s^{-1}, A_s is the mineral surface area (cm^2), k_+ is the rate constant in mol.cm^{-2}.s^{-1}, Q is the activity product and K is the equilibrium constant (Bethke, 2008).

This assumption is not necessarily valid. However, the purpose of the rate equation and rate constants used are to instil a relative scale of reaction rates to various minerals in the system. The scale of the model is the tailings facilities. The model is therefore not designed to evaluate the minutiae of individual mineral systems in the ERB component, but to give an overview of the most important minerals and processes active in the component. The validity of this assumption is evaluated in the sensitivity analysis.

7.2.2.3 The forward direction and backwards direction reaction rates are equal

This assumption is not necessarily valid, as the rate of reaction in a given direction is, amongst other things, also dependent on the composition of the fluid from which the precipitation and dissolution occurs. However, the error is expected to be small relative to the high concentrations of contaminants in the tailings facility leachate.

7.2.3 Calculated mineral surface areas are applicable to the models

Although this assumption may not be valid, the error is expected to be small. The mineral surface areas used in the model are calculated specifically for the ERB system and is comparable to values used in other studies. The calculation was done by using the tailings particle size distribution of 75% < 75 µm and

assuming for pyrite that 50% of the particles are spherical and 50% are cubic. This assumption is based on the various modes of pyrite occurring in the Witwatersrand Au-U deposits (Hallbauer, 1986). A crystal volume could be calculated for each grain. This was divided by the total volume of a tailings facility with a surface area of 1 km^2 and 60 m thick to calculate the amount of grains. Idealised crystal dimensions were used to calculate the surface area of other minerals (Table 7-2).

Table 7-2 Calculated mineral surface areas

Mineral	Surface area (cm^2/g)	Surface area (m^2/g)
Quartz	326	0.0326
Muscovite	562	0.0562
Pyrite	247	0.0247
Chlorite	473	0.0473
Pyrophillite	356	0.0356

The validity of this assumption is evaluated in the sensitivity analysis.

7.2.3.1 Initial oxygen fugacity

The initial fugacity of oxygen is unknown for the ERB component systems. However, the value cannot exceed the atmospheric oxygen fugacity of 0.21. Therefore this value is used as the initial oxygen fugacity of the component systems. Nengovhela et al. (2007) used the same assumption their study. The effect of changing initial oxygen fugacity values is evaluated in a sensitivity analysis.

7.2.3.2 Redox equilibrium

Redox equilibrium is rarely achieved in natural systems. This is due to the relatively slow rate of redox reactions under the physio-chemical conditions of the Earth's surface (Bethke, 2008). However, some redox systems do achieve a measure of equilibrium and can therefore be assumed to reach equilibrium in the simulation. The challenge is to determine which redox pairs would reach equilibrium, or at least a measure of local equilibrium, in the system being modelled and which need to be decoupled to simulate redox disequilibrium conditions for a specific redox pair. The ferrous-ferric redox pair is assumed to be in equilibrium. It has been shown that this redox pair can achieve a measure of equilibrium in natural systems, due to the catalytic effect of iron oxidising bacteria, such as Acidithiobacillus Ferrooxidans (Gleisner et al., 2006). This assumption is evaluated in a sensitivity analysis.

7.2.3.3 Rate constant of Uraninite

The rate constant of uraninite by biotic and abiotic processes has been shown to range between $8.58x10^{-16}$ $mol.cm^{-2}.s^{-1}$ and $1.5x10^{-13}$ $mol.cm^{-2}.s^{-1}$ ($\sigma = 1.35x10^{-9}$) respectively (Ulricj et al., 2009). The high standard deviation of the rate constant data shows that the variation is significant. The average of the data range provided by (Ulrich et al., 2009) is $7.35x10^{-10}$ $mol.cm^{-2}.s^{-1}$. The uraninite rate constant is evaluated in the sensitivity analysis.

7.2.4 Analysis of Uncertainty

7.2.4.1 General sources of uncertainty in numeric geochemical models

There are mainly 6 main types of uncertainty in scientific models (Zhu and Anderson, 2002; Bethke, 2008; United States Environmental Protection Agency, 2009; Taleb, 2001). These are:

1. *Uncertainty due to completely random events*. This type of uncertainty cannot be quantified. Although the impacts of some extreme events can be simulated, no one can foresee all potential random events. Simulating extreme events is however useful for planning and disaster mitigation purposes.
2. *Uncertainty due to errors in the conceptual model.* This type of uncertainty cannot be quantified initially and if the numerical model results do not allude to errors in the concept, then it may be some time before conceptual errors are detected, in some cases perhaps never. There is no acceptable method of quantifying this type uncertainty. Only peer review can provide a qualitative guard against conceptual model errors.
3. *Uncertainty due to spatial and temporal data variation.* This type of uncertainty can be quantified and be incorporated into the model, not into the modelling software itself, but through sensitivity analyses. There are various ways in quantifying these types of uncertainty, the most common method being Monte Carlo probability analysis using the Latin Hypercube Sampling method (United States Environmental Protection Agency, 1997). Whether spatial and temporal variations in the data need to be taken into account will depend on which of these two types of variation introduce the greatest uncertainty for the model. If e.g. the spatial variation has a much larger data range than the temporal variability, then local data must be considered. If the whole area is under consideration, the spatial data variation will be a guide to the uncertainty introduced into the model, as the spatial data variation usually introduces the greatest data variation in the data.
4. *Uncertainty due to assumptions.* This type of uncertainty cannot be quantified, but it can be evaluated and qualified by sensitivity analysis. The sensitivity analysis will show which parameters cause the greatest variation in the model results. These parameters can be focused on and appropriate data collected for re-iteration of the model. Depending on the decisions that need to be made upon the model results, the upper or lower values of the data may need to be used as input to the model. Alternatively average values can be used and scenarios run to determine the effect of using upper or lower values as part of the sensitivity analysis.
5. *Uncertainty due to errors in the thermodynamic database.* Errors in the thermodynamic database have been decreasing with time as better thermodynamic databases become available. Although errors are still introduced, due to the fact that pure material is generally used to establish the values of the thermodynamic parameters, they are generally small compared to the model output values. Using commercial software decreases the risk of

large errors, as the database has been reviewed.

6. *Uncertainty due to incorrect solving of the mathematical equations by the software.* This type of uncertainty is limited by the use of commercial, peer reviewed software and is not taken into account in this model.
7. *Uncertainty due to analytical errors.* These errors can result from incorrect laboratory measurements or from parameters, such as pH, dissolved O_2 and total dissolved solids (TDS) that should be measured in the field, rather than in the laboratory. This is due to changes that occur in the samples in the time it takes to transport the samples to the laboratory and due to the amount of time that passes before the samples are analysed. Generally acceptable laboratory error is 2 – 10%, depending on the instrument, analyst and the sample preparation (Bethke, 2008). The ion balance can be used as an assessment of laboratory accuracy. Other analytical errors can be introduced by e.g. incorrect sample filtering methods. Water samples are commonly filtered through 0.45 µm filters to remove suspended material. Iron and Mn colloid particles are < 0.45 µm implying that the resultant Fe and Mn analysis will reflect more dissolved species that are actually present in the sample.

The evaluation of the types of uncertainty listed above indicates that the most important sources of uncertainty in the tailings models are:

- Uncertainty due to errors in the conceptual model;
- Uncertainty due to spatial and temporal data evaluation.

Uncertainty due to errors in the conceptual model will become apparent when the numeric model shows results inconsistent with observation and can also be determined via peer review. Uncertainty due to spatial and temporal data variation can be incorporated in the model by running multiple scenarios or by choosing an approach to follow, which will depend on the decisions that need to be made, e.g. conservative or “best case”.

7.2.4.2 Uncertainty in ERB geochemical models

A qualitative assessment of the uncertainty due to spatial and temporal data variation in some of the ERB component systems was conducted on existing data to get an idea of the amount of uncertainty introduced by these types of variation. The results are shown in Table 7-3 and Table 7-4.

The results show that a significant amount of uncertainty surrounds the spatial and temporal separation of data points in the East Rand Basin, for surface and ground water sources. The uncertainty surrounding Fe and some of the heavy metals, e.g. Mn and Ni, are particularly high.

The results of the uncertainty assessment beg the question whether model calibration is possible, as the field data is used for comparison with model results? The International Atomic Energy Association (IAEA) does not deem it possible (Nordstrom, 2012). The term “model evaluation” is preferred (Nordstrom, 2012;

United States Environmental Protection Agency, 2009) and is used in this study.

Spatial and temporal data variability is considered to be non-reducible uncertainty (Nordstrom, 2012). However, the uncertainty in especially spatial data points for data from samples of the same medium (e.g. shallow groundwater), is most probably due, at least in part, to process. Samples e.g. of groundwater and surface water in close proximity to a tailings facility can be expected to contain higher pollutant concentrations due to a pollution plume than samples from the same medium farther away. Therefore one way in which to handle spatial uncertainty, at least in the East Rand Basin models, is to evaluate leachate models using the upper values form the dissolved contaminant concentrations and the lower values when considering pH.

The data evaluation process is divorcing the various data subsets within a larger dataset by analysis of data distribution patterns. Using this method, the uncertainty due to spatial data variability can be reduced.

As with spatial variability, data variability due to temporal fluctuations is most probably also, at least in part due to process. Climatic factors such as seasonal rainfall and evaporation cycles have been shown to cause fluctuations in contaminant concentrations in water sources (Dold and Fontbote, 2001). Therefore the upper values of these variations can be considered in model evaluation in the East Rand Basin models. The focus in the geochemical models of the tailings facilities are the contaminants released into the pore water, which becomes the tailings AMD leachate and the concentrations of these contaminants.

Table 7-3 Maximum uncertainty due to spatial variation. All values in %.

	Shallow Groundwater	Deep Groundwater	Surface water (BBS)
pH	70	64	28
Dissolved oxygen	185	n.a.	67
HCO_3	1 355	845	136
Na	1 119	1 454	360
Mg	364	233	78
Al	2 363	2 312	n.a.
K	559	187	123
Ca	293	245	330
Fe	1 669	2 642	592
Mn	2 448	1 500	350
Ni	2 439	618	2 485
Zn	924	509	825
U	2 034	897	124
Cl	418	175	44
SO_4	612	598	837

Table 7-4 Maximum uncertainty due to spatial variation. The timespan of the monitoring data is from 1996 to 2008, although not all parameters were monitored all the time. All values are in %.

	Surface water - R555 (BBS)	Surface water - Largo (BBS)	Surface water - N17 (BBS)	Surface water - R42 (BBS)	Surface water - R51 (BBS)	Shaft - underground
pH	27	91	26	26	26	24
Dissolved oxygen	139	137	193	64	50	93
Alkalinity	273	97	251	250	232	362
Na	132	187	195	110	103	111
Mg	179	699	686	261	78	16
Al	451	455	313	423	372	714
Ca	109	377	84	98	99	37
Fe	1 185	4 230	5 530	2 030	768	230
Mn	1 574	742	2 836	2 982	687	263
Ni	201	n.a.	106	115	133	82
Cl	70	78	549	650	68	50
SO_4	406	217	262	182	106	128

7.3 Tailings pyrite oxidation model

In considering the tailings facilities, 2 scenarios are likely. These are the tailings facility when it is still in operation and post-closure. These systems are expected to be very different in terms of O_2 flux into the system, which is directly proportional to O_2 flux into the system (Section 5.2.1). Reaction models are therefore developed for each of these 2 scenarios.

The initial fluid composition is assumed to be rain water. In the operational phase rainwater will influence the hydrology of the tailings facility, as rain falling on the tailings embankments will runoff and erode the tailings sides and some rainfall will infiltrate into the tailings itself. The impact of rainfall in the post-closure phase is expected to become more important due to the cessation of new wet slurry deposition onto the facility, even though the total component is expected to contain less water. The trace metal content of rainfall is generally low, especially in terms of the ion concentrations expected for the tailings pore water, which in the ERB is high (Nenghovela, 2007). Therefore the rain composition is assumed to be essentially deionised water in equilibrium with atmospheric O_2. The atmospheric O_2 fugacity is 0.21 (Bethke, 2008).

The minerals added to the system are those that were shown to be contained in the tailings system and described in Section 5.2.1. Chlorite is a mineral group and can therefore not be added to the model as such. To account for chlorite in the system, the amount of chlorite in the system was divided equally between the Fe (chamosite) and Mg (clinochlore) end-members (Klein and Hurlbut, 1993). Reaction kinetics is added to the models to evaluate changes in the system as a function of time. The default rate equation of the software was used for the silicate minerals (Equation 89). The silicate reaction rates range from an order of magnitude of 10^{-12} to 10^{-15} $mol.cm^{-2}.s^{-1}$. Although these reaction rates are slow, the silicate minerals are entered into the

system as their weathering provide cations and anions which can contribute to the precipitation of secondary minerals. These are important as the precipitation of secondary minerals control the mobility of specific ions.

Equation 89 takes the mineral surface area into account, as the reaction rate is proportional to the reactive mineral surface area. Generally the higher the reactive mineral surface area, i.e. smaller mineral grains, the faster the rate (Bethke, 2008; Salmon and Malmström, 2006). The calculated mineral surface areas were used in the models (Section 7.2.3). The reaction rate of pyrite was treated differently than the silicates. Due to the fact that pyrite oxidation essentially drives changes in the tailings system, more detailed reaction kinetics were added to model pyrite oxidation.

Studies in pyrite oxidation kinetics (Williamson and Rimstidt, 1994; Jerz and Rimstidt, 2004; Blanchard et al., 2009; Caldeira et al., 2010; Molson et al., 2005; Chandra amd Gerson, 2010; Gleisner et al., 2006; Espana et al., 2007; Lefticariu et al., 2010; Holmes and Crundwell, 2000; Rimstidt and Vaughan, 2003; Heidel and Tichomirowa, 2010) show that pyrite oxidation mainly occurs via 2 possible mechanisms, oxidation by O_2 and by Fe^{3+}. The oxidation of pyrite by Fe^{3+} is orders of magnitude more rapid than oxidation by O_2 (Williamson and Rimstidt, 1994). Pyrite oxidation produces Fe^{2+}, which needs to be oxidised to Fe^{3+} for the pyrite to be oxidised by ferric iron. This process, however, is slow, but can be catalysed by certain bacteria, such as *Acidithiobacillus Ferrooxidans* (Gleisner et al., 2006). The catalysed reaction occurs rapidly and therefore renders the oxidation of pyrite by ferric iron in tailings system a viable reaction path.

Williamson and Rimstidt (1994) studied the oxidation of pyrite by O_2, ferric Fe in the presence of O_2 and the oxidation of pyrite by ferric Fe in a N_2 purged atmosphere, i.e. in the absence of O_2. They determined three rate equations for the three oxidation scenarios. The rate equation for the oxidation of pyrite by O_2 is:

$$r = 10^{-8.19(\pm 0.10)} \frac{m_{DO}^{0.5(\pm 0.04)}}{m_{H^+}^{0.11(\pm 0.01)}} \qquad \textbf{Equation 90}$$

The rate equation for the oxidation of pyrite by ferric Fe in the presence of O_2 is:

$$r = 10^{-6.07(\pm 0.57)} \frac{m_{Fe^{3+}}^{0.93(\pm 0.07)}}{m_{Fe^{2+}}^{0.93(\pm 0.07)}} \qquad \textbf{Equation 91}$$

The rate equation for the oxidation of pyrite by ferric Fe in the absence of O_2 is:

$$r = 10^{-8.58(\pm 0.15)} \frac{m_{Fe^{3+}}^{0.30(\pm 0.02)}}{m_{Fe^{2+}}^{0.47(\pm 0.03)} m_{H^+}^{0.32(\pm 0.04)}} \qquad \textbf{Equation 92}$$

In the above equations, r is the rate of pyrite destruction in $mol.m^{-2}.s^{-1}$, m is the molality of chemical species and DO is dissolved oxygen. Equations 90 and 91 were used to model the tailings facilities, as the facilities are all able to interact with the atmosphere. Each of Equation 90 and 91 were used to model the operational and post-operational phases. The results were evaluated to aid in identifying the most important reaction mechanism and thus cause of AMD in the tailings facilities. The oxidation of Fe^{2+} to Fe^{3+} was modelled using Equation 4 and a reaction rate of $1x10^{-12}$ $kg.mol^{-1}.s^{-1}$ (Stumm and Lee, 1961).

Previous studies on the Witwatersrand tailings facilities indicated that O_2 is most likely the dominant oxidant in these facilities (Bezuidenhout and Rousseau, 2005; Nengovhela et al., 2007). To evaluate this hypothesis,

models were developed for the operational and post-operational scenarios using first Equation 90 and then Equation 91. These equations imply O_2 and Fe^{3+} as the dominant oxidants respectively.

The metals Ni, Mn, Al, Fe and U, which were shown to be important in the leachate from ERB tailings facilities could not be entered into the system as separate mineral entities, as they all occur as trace elements in pyrite and in the silicate minerals. They were therefore added to the model as simple reactants as metal and metalloid oxides. Whole rock XRF data was used to constrain the concentrations of these metals in the tailing system. The model results were compared to known concentrations of ERB tailings leachate.

To take the depleting oxygen fugacity (f_{O_2}) with depth in the tailings into account, the f_{O_2} was slid from 0.21 (in equilibrium with the atmosphere) to the arbitrary value of $1x10^{-50}$, which simply represents a value close to 0, as the model cannot accommodate 0 values.

Water-rock ratios of the ERB tailings dams are unknown. In the Operational Phase, water is in over supply, and most surplus water is returned via the penstock to the return water dam (RWD). In the Post-Operational phase, i.e. after decommissioning, the water-rock changes due to the fact that new water-laden tailings material has ceased to be deposited onto the facility. The hydraulic head decreases, showing that the water balance becomes negative and O_2 influx increases in the system (Robertson, 1994; Ritchie, 1994). On the other hand the rate of reactions of pyrite and the silicate minerals is not dependent on the amount of water in the system due to fact that the reaction rates are slow. The most important impacts of a change in water-rock ratios is the influx of O_2 into the system due to the depression of the piezometric head and the decrease of leachate emanating from the tailings facility. The decrease of water-rock ratio and increase of O_2 flux can therefore be expected to increase tailings pore water concentrations of dissolved constituents and lead to increased secondary mineral formation (Dold and Fontbote, 2001). In reality, even though there is surplus water in the tailings system during the Operational Phase, the water-rock ratio is not expected to be higher than 1, due to the fact that water surplus water is return to the mine reticulation system. Therefore the water-rock ratio is set to an order of magnitude higher than for the Post-Operational model, but still less than the amount of rock in the system. The ratios used are evaluated in the sensitivity analysis.

The Operational Phase model was run over 25 years, the average life of mine for gold mines in the ERB, while the Post-Operational Phase model is run over 75 years, the time between the average life of mine and the ~100 years of gold production history in the ERB.

7.3.1 Quantities of interest

The QOI of the tailings component model are pH, SO_4, Ca, Mg, Na, K, Fe, U, Mn, Ni and Al. The presence of jarosite precipitation in the model is also a QOI, as this mineral has been detected in ERB tailings component systems.

7.3.2 Assumptions

The assumptions specific to the tailings component model are discussed in this section. The validity of assumptions made in the modelling can be evaluated by various means, such as sensitivity analyses.

7.3.2.1 Oxygen fugacity sliding – Accounting for oxygen depletion through the tailings component system

Dissolved oxygen concentrations for the tailings facilities at depths greater than ~4 m were not available at the time of this study. Research has shown that oxygen concentration generally decreases with depth in tailings and waste-rock facilities (Ritchie, 1994). This is incorporated into the conceptual model of the tailings component (Section 5.2.1). To account for this, the oxygen fugacity is slid from equilibrium with the atmosphere at the surface of the facilities to negligible concentrations. Although oxygen depletion generally displays a logarithmic concentration curve, the fugacity is linearly slid. This renders the model conservative, although not worst-case. The validity of this assumption and the evaluation of the dependence of the pyrite oxidation on oxygen fugacity are evaluated in a sensitivity analysis.

7.3.2.2 Water-rock ratio

The water-rock ratio was assumed to be 1:1 for the Operational Phase scenario and 1:5 for the Post-Closure scenario. A constant hydraulic head is maintained close to the tailings surface in the operational facility, due to the constant deposition of water laden tailings onto the facility. The hydraulic head in the post-closure tailings decreases rapidly shortly after decommissioning, due to the cessation of the addition of water saturated slurry onto the facility. The decrease in hydraulic head has the added effect of increasing the influx of oxygen into the tailings component system (Ritchie, 1994).

The effect of the water-rock ratio assumptions are evaluated in the sensitivity analyses.

7.3.2.3 Initial solution entering the system

The main source of water in the tailings facility is rainwater. The slurry water may be contaminated water from the mine reticulation system. The quality of slurry water is unknown.

As a first approach, rainwater was used as input. The composition of rain water is not known for the area. However the concentrations of dissolved constituents in rainwater are expected to be negligible compared to the eventual concentration of contaminants in the leachate solution. Therefore rainwater was assumed to be essentially distilled water in equilibrium with atmospheric oxygen. In terms of the purpose of the model, this assumption is deemed reasonable.

7.3.2.4 Redox equilibrium

In addition to the discussion in Section 7.2.3.2, the mineral jarosite is used as an additional QOI. It has been detected in the tailings material and jarosite only precipitates in the model if the ferrous-ferric redox pair is assumed to be in equilibrium (Norlund et al., 2010; Liu et al., 2009; Welch et al., 2008; Drouet et al., 2004;

Smith et al., 2006). The assumption is therefore deemed reasonable and is evaluated in the sensitivity analysis.

7.3.2.5 All Ni occurs as an accessory in pyrite

Nickel, together with V, Cr, Mn, Fe and Zn are associated with mafic rocks. The Witwatersrand is composed of sedimentary rocks with very high quartz content. Therefore it is conceivable that the majority of Ni in the Witwatersrand gold ore would be associated with pyrite, rather than with any of the silicates. This assumption is thus deemed as reasonable.

7.3.2.6 Porosity and permeability remain constant throughout the simulation

This assumption is most probably not valid. As the tailings AMD plume mixes with groundwater, secondary salts precipitate, which have a larger volume than the soil minerals. The precipitation of these minerals will most likely decrease the porosity with time, especially in the first few meters of soil. The precipitation of secondary minerals will most likely have the secondary effect of decreasing the hydraulic conductivity of the soil.

This introduces additional uncertainty into the model as there is no existing data regarding the porosity and permeability changes with time. The total effect on the model results is expected to be small, as the hydraulic conductivity of the ERB soils are small to begin with, but in soils with higher proportions of sand and/or gravel, this effect may be more pronounced.

7.3.3 Uncertainties

Spatial data for the ERB tailings facilities is lacking, therefore uncertainty in tailings data, e.g. mineralogical data, could not be quantitatively assessed. As pyrite is the most important mineral in the system in terms of AMD generation, the effect of varying pyrite concentrations on model output is evaluated in a sensitivity analysis.

Additional uncertainty is introduced by the assumptions mentioned in the preceding section. This uncertainty is evaluated in the sensitivity analysis.

Another source of uncertainty in the tailings component systems model stems from one important difference between thermodynamic models and reality, i.e. thermodynamic models are built on continuous equations, whereas reality may not be continuous. An example is that water, especially in the Post-Closure phase, most probably migrates through the tailings in pules. These pulses arise due to daily and seasonal rainfall variation. These pulses will be able to re-dissolve minerals, at least to a degree, that have formed by precipitation from a previous pulse. Over a longer period of time, it may be that the importance of the seasonal water pulses are negated, due to the decrease in resolution and the longer the time period under consideration, the lesser the importance of the pulses and the closer the thermodynamic model will resemble reality. This is analogous to nuclear decay of a specified mass of uranium. The escape of a radio nuclide from a U atom is random, but the escape of millions of nuclides from a mass of U is predictable and is

described formally by the U decay equation. The uncertainty in the tailings model is introduced by the lack of knowledge on the exact relationship between time and water pulse and the degree to which reality is resembled by the thermodynamic model. This type of uncertainty cannot be evaluated by sensitivity analysis and can only be qualitatively evaluated upon model evaluation using existing field data.

An additional source of uncertainty is the potential change in porosity and hydraulic conductivity due to the precipitation of secondary minerals. This source of uncertainty is not expected to exert a significant influence on the model results, due to the low hydraulic conductivity of the ERB soils.

7.3.4 Sensitivity analysis

A sensitivity analysis is different from an uncertainty analysis in that an uncertainty analysis seeks to determine what is not known of a QOI or its deviance from "exactness". A sensitivity analysis seeks to determine the magnitude of effect on output values of all or key QOI when an input parameter is changed by a specific amount, i.e. to determine how sensitive a numerical model is to changes in specific input values.

Sensitivity analyses are performed on some parameters that are expected to provide the most uncertainty.

7.3.4.1 Analysis of the effect of varying rate constants

A sensitivity analysis was conducted on the input rate constants by varying the rate constants by and order of magnitude higher and lower than the original input values. The results for the Operational phase are shown in Table 7-5.

Table 7-5 Sensitivity analysis results on the operational phase rate constants

	Units	Base Case	Order of magnitude lower	Order of magnitude higher
pH		1.71	5.06	1.15
TDS	*mg/kg*	8 735.00	832.00	48 935.00
Eh	*V*	0.98	0.78	1.01
Ca	*mg/kg*	0.98	0.99	0.94
Mg	*mg/kg*	76.05	137.50	73.10
K	*mg/kg*	249.10	60.67	179.50
Na	*mg/kg*	0.00	0.00	0.00
Mn	*mg/kg*	3.57	0.03	5.03
Ni	*mg/kg*	5.06	0.55	24.87
U	*mg/kg*	9.29	0.49	9.82
Fe	*mg/kg*	552.40	0.00	9 452.00
Al	*mg/kg*	584.90	0.02	598.50
SO4	*mg/kg*	7 199.08	621.90	38 347.00
HCO3	*mg/kg*	0.00	0.20	0.00

The results show that the model is sensitive to changes in reaction rates and that changes to higher rate constants have a larger influence on the QOI than changes to lower values. This indicates that even if the

rate constants used are wrong, the reactions will rather be faster than slower. This implies that contaminant concentrations in the AMD leachate will either be higher, than lower.

7.3.4.2 Analysis of the effect of varying mineral surface areas

A sensitivity analysis was conducted on the mineral surface areas by decreasing and increasing the mineral surface area input values by 2. The results for the Operational Phase are shown in Table 7-6.

Table 7-6 Results of a sensitivity analysis on the mineral surface areas on the operational Phase scenario

	Units	*Base Case*	Twice higher	Twice lower
pH		1.71	1.42	2.71
TDS	*mg/kg*	8 735.00	19 294.00	2 904.00
Eh	*V*	0.98	1.00	0.92
Ca	*mg/kg*	0.98	0.97	0.95
Mg	*mg/kg*	76.05	75.25	87.25
K	*mg/kg*	249.10	185.60	220.40
Na	*mg/kg*	0.00	0.00	0.00
Mn	*mg/kg*	3.57	4.50	1.67
Ni	*mg/kg*	5.06	9.20	2.66
U	*mg/kg*	9.29	10.10	8.35
Fe	*mg/kg*	552.40	2 763.00	2.20
Al	*mg/kg*	584.90	616.00	279.20
SO4	*mg/kg*	7 199.08	15 521.61	2 305.28
HCO3	*mg/kg*	0.00	0.00	0.00

The results show that only Fe and SO_4 show significant differences when surface areas are varied. This implies that the model is sensitive to changes in mineral surface areas of only pyrite, which is the only mineral to have a direct influence on Fe and SO_4 concentrations in the leachate solution.

7.3.4.3 Analysis of the effect of varying initial oxygen fugacity

Iron speciation data was not available for the ERB. Dissolved oxygen and pH data was available. In addition, when models were run using the ferric Fe rate equation, the model results were shown to be incompatible with results from previous studies on Witwatersrand tailings facilities and with existing data. This is an indication that even though oxidation of pyrite by ferric iron may be occurring in the Witwatersrand tailings facilities, it is most probably not the dominant oxidation mechanism. Thus the rate equation for the oxidation of pyrite by O_2 was used (Equation 90).

The results of the sensitivity analysis are shown in Table 7-7.

Table 7-7 Results of a sensitivity analysis on the initial oxygen fugacity of the Operational Phase scenario

	Units	Base Case	Fugacity 0.01	Sliding
pH		1.67	1.68	1.68
TDS	*mg/kg*	2 124.00	2 068.00	2 066.00
Eh		1.06	1.10	0.87
SO4		1 959.00	1 917.96	1 917.06
Fe		120.80	115.00	114.90

The results show that the model is insensitive, both to changes in initial oxygen fugacity as well as whether the fugacity is slid to negligible values or fixed at the atmospheric value, even though the rate equation used forces a dependence on oxygen. These results are important, as it shows that the pyrite oxidation in the ERB tailings component system is more sensitive to the presence of oxygen than its actual concentrations. This has implications for potential mitigation measures, such as capping, as a capping will not isolate the system from oxygen.

7.3.4.4 Analysis of varying water-rock ratios

A sensitivity analysis was conducted by varying the water-rock ratio by an order of magnitude higher and lower. Varying the water-rock ratio lower in the operational Phase caused the model not to converge, indicating that the water-rock ratio is unlikely to be as low as 1:10 in the Operational Phase. The results are shown in Table 7-8.

Table 7-8 Sensitivity analysis results on the water-rock ratio for the Operational Phase

	Units	*Base Case*	10:1
pH		1.71	2.29
TDS	*mg/kg*	8 735.00	955.00
Eh	*V*	0.98	0.95
Ca	*mg/kg*	0.98	0.99
Mg	*mg/kg*	76.05	5.25
K	*mg/kg*	249.10	42.41
Na	*mg/kg*	0.00	0.00
Mn	*mg/kg*	3.57	0.34
Ni	*mg/kg*	5.06	0.51
U	*mg/kg*	9.29	8.91
Fe	*mg/kg*	552.40	39.48
Al	*mg/kg*	584.90	49.34
SO_4	*mg/kg*	7 199.08	793.91
HCO_3	*mg/kg*	0.00	0.00

The results show that the model is sensitive to water-rock ratios and that the water-rock ratio will need to be constrained in detailed studies of tailings component systems.

7.3.4.5 Analysis of iron redox equilibrium-disequilibrium

A sensitivity analysis was done by running a scenario where the ferric-ferrous redox pair is decoupled. The results of the study are shown in Table 7-9 and contain jarosite as a QOI, as jarosite is known to form in ERB tailings component systems (Rösner et al., 2001).

Table 7-9 Sensitivity analysis results on ferrous-ferric redox disequilibrium for the Operational Phase

	Units	*Base Case*	Disequilibrium
pH		1.71	3.73
TDS	*mg/kg*	8 735.00	10 135.00
Eh	*V*	0.98	0.86
Ca	*mg/kg*	0.98	0.98
Mg	*mg/kg*	76.05	151.50
K	*mg/kg*	249.10	21.37
Na	*mg/kg*	0.00	0.00
Mn	*mg/kg*	3.57	0.18
Ni	*mg/kg*	5.06	5.05
U	*mg/kg*	9.29	10.80
Fe	*mg/kg*	552.40	3 369.00
Al	*mg/kg*	584.90	15.88
SO4	*mg/kg*	7 199.08	6 542.98
HCO3	*mg/kg*	0.00	0.01
Jarosite	*g*	14.14	0.00

The results show that the model is sensitive to the measure to which the system is en equilibrium with regards to the ferrous-ferric Fe redox system. Jarosite is shown to form in the Base Case scenario, where it does not precipitate in the Disequilibrium scenario. This indicates that the Base Case is closer to field observations and is therefore closer to the real system than a system in which the Fe redox pair is in disequilibrium.

7.3.4.6 Analysis of uraninite rate constants

A sensitivity analysis is conducted on the rate constant of uraninite by developing a separate model, in which uraninite is allowed to dissolve together with pyrite oxidation. The results are shown in Table 7-10.

Table 7-10 Sensitivity analysis on the uraninite rate constant for the Operational Phase

	Units	Base Case	Three orders of magnitude higher	Three orders of magnitude lower
pH		1.92	1.80	1.80
TDS	*mg/kg*	893.00	1 241.00	1 238.00
Eh	*V*	1.11	1.11	1.11
Fe	*mg/kg*	4.92	13.33	13.37
SO_4	*mg/kg*	848.43	1 185.77	1 185.77
U	*mg/kg*	8.76	4.87	2.04

The results show that the model is not significantly sensitive to changes in the uraninite rate constant. This is because minerals such as uranophane and various hydrous U-sulphates are stable and precipitate from solution, controlling uranium concentrations in solution. The model does show that even though there are minerals in the system which buffers the U concentration in the tailings component leachate, the U concentrations are still in excess of South African and international water standards.

7.3.4.7 Analysis of varying pyrite content

To test the model sensitivity to the initial mass of pyrite in the system, the pyrite content was varied lower and higher by an order of magnitude. The results are shown in Table 7-11.

Table 7-11 Results of a sensitivity analysis on the tailings component system initial pyrite mass for the Operational Phase Scenario.

	Units	*Base Case*	*Order of magnitude lower*	*Order of magnitude higher*	*50% lower*	*50% higher*
pH		1.71	5.07	0.93	2.67	1.53
TDS	*mg/kg*	8 735.00	365.00	128 786.00	1 692.00	15 904.00
Eh	*V*	0.98	0.78	1.03	0.92	0.99
Ca	*mg/kg*	0.98	0.86	0.87	0.88	0.97
Mg	*mg/kg*	76.05	11.57	189.30	32.39	111.10
K	*mg/kg*	249.10	126.60	301.30	170.20	257.50
Na	*mg/kg*	0.00	0.00	0.00	0.00	0.00
Mn	*mg/kg*	3.57	0.05	4.67	1.08	4.45
Ni	*mg/kg*	5.06	4.75	4.46	4.96	5.02
U	*mg/kg*	9.29	35.74	18.98	8.81	10.34
Fe	*mg/kg*	552.40	0.00	25 380.00	0.49	1 545.00
Al	*mg/kg*	584.90	0.02	2 240.00	151.10	946.20
SO4	*mg/kg*	7 199.08	211.64	100 149.88	1321.492	13028.77
HCO3	*mg/kg*	0.00	0.17	0.00	0.00	0.00

The results show that the model is sensitive to the initial mass of pyrite in the system. When the mass of pyrite is set to an order of magnitude lower, i.e. to 10% of the original value, the resulting solution is slightly

acidic with sulphate and other contaminant concentrations below drinking water standards. This implies that a management decision can be focussed to decreasing pyrite content to below 10% of the original value and that 100% of pyrite does not have to be removed to mitigate the AMD contamination issue. This has cost implications for remedial action.

When initial mass of pyrite in the system is reduced and increased by 50% of the Base Case, the results show that although the QOI output values indicate that the model is still sensitive to changes in pyrite mass, the changes are smaller and AMD occurs with elevated contaminant concentrations. This shows that although large changes (order of magnitude) to initial pyrite mass can produce significantly different results, variation of 50% does not cause significant changes, indicating that the system is not significantly sensitive to changes of pyrite content within 50% of the Base Case value of 3 wt% pyrite.

In all cases so far, sensitivity analyses on the Operational Phase and Post-Closure Phase scenarios have produced similar results. However, the sensitivity analysis on the Post-Closure scenario shows that the order of magnitude lower pyrite content scenario still produces AMD with significant concentrations of contaminants. This shows that the Post-Closure scenario is not significantly sensitive to changes in initial pyrite content. The reason for this is most probably due to the longer simulation time. Therefore time and pyrite content are important driving factors in the formation of AMD in tailings component systems as well as the severity of the AMD formed, in terms of acidity and pollutant loads.

Table 7-12 Results of a sensitivity analysis on the tailings component system initial pyrite mass for the Post-Closure Phase Scenario.

	Units	*Base Case*	*Order of magnitude lower*	*Order of magnitude higher*	*50% lower*	*50% higher*
pH		0.63	1.33	0.08	0.83	0.52
TDS	*mg/kg*	258 048.00	21 013.00	802 612.00	141 936.00	347 210.00
Eh	*V*	0.95	0.91	0.98	0.94	0.95
Ca	*mg/kg*	0.00	0.00	0.00	0.00	0.00
Mg	*mg/kg*	997.20	220.00	678.60	674.70	1 159.00
K	*mg/kg*	736.80	507.60	244.60	720.80	667.70
Na	*mg/kg*	0.75	0.97	0.22	0.86	0.66
Mn	*mg/kg*	56.81	49.75	17.44	63.00	50.78
Ni	*mg/kg*	97.32	124.30	29.21	111.10	86.36
U	*mg/kg*	11.04	10.90	3.31	12.70	9.77
Fe	*mg/kg*	52 800.00	3 135.00	177 000.00	28 240.00	72 170.00
Al	*mg/kg*	1 919.00	185.00	1 852.00	1 096.00	2 341.00
SO4	*mg/kg*	200 363.84	16 656.70	619 533.23	36 850.00	89 990.00
HCO3	*mg/kg*	0.00	0.00	0.00	0.00	0.00

7.3.5 Model results

7.3.5.1 Operational Phase Scenario

The results how significant differences between Scenario a and Scenario b. Scenario a shows an acidic leachate solution containing elevated concentrations of all the heavy metals (Mn, Ni, U, Fe and Al). Scenario b shows an alkaline leachate containing low dissolved solids and low metal contents, with the exception of U. The results of Scenario a and b confirms previous studies, which indicated that O_2 is the dominant oxidant in the Witwatersrand and specifically ERB, tailings facilities. Scenario c represents the reslts of a model which uses the output from Scenario 2 as input to the Fe^{3+} model. The pH further decreases from 1.37 in Scenario a to 0.31 in Scenario c. This pH is most probably too low, implying that further detail work will be required to pinpoint the exact reaction mechanism.

Table 7-13 Solution composition results of the pyrite oxidation model for the Operational Phase. An additional scenario, in which the output of the O_2 model is used as input to the Fe^{3+} model indicates significant differences. Although O_2 seems to be the dominant oxidant based on pH, the 3rd scenario indicates that these two mechanisms are most probably co-operational.

	Units	Scenario a – O_2 mechanism	Scenario b – Fe^{3+} mechanism	Scenario c – Fe^{3+} mechanism using output from O_2 model as input
pH	*pH units*	1.37	8.65	0.31
Eh	*V*	1.14	0.53	1.01
TDS	*mg/kg*	38 036	25	887 969
SO_4	*mg/kg*	278 816	0	61 833
HCO_3	*mg/kg*	0	0	0
Ca	*mg/kg*	0.0	0.0	0.0
Mg	*mg/kg*	190	0.3	192
K	*mg/kg*	356	0.2	6.4
Na	*mg/kg*	1.0	0.0	1.0
Mn	*mg/kg*	74.58	0.00	83.81
Ni	*mg/kg*	49.06	0.00	55.14
U	*mg/kg*	4.70	14.60	8.75
Fe	*mg/kg*	8 283	0.00	296 900
Al	*mg/kg*	964	0.05	977

The results do indicate that although Fe^{3+} may not be the dominant reaction mechanism in the tailings facilities, oxidation by this mechanism can contribute to the AMD problem, but only after the onset of oxidation by O_2. The results also challenge the conclusion of a previous study in which it was indicated that

tailings facilities may only produce acid solutions in a timespan > 1 000 years (Bezuidenhout and Rousseau, 2005).

Among the minerals isolated from the system throughout the simulation are secondary sulphates, hydroxides and clay minerals. Some of these have been shown to occur in other AMD environments in other part of the world (Moncur et al., 2009; Alpers et al., 1994). Rösner et al. (2001) reported some of these minerals in their study. It is interesting that gypsum [$CaSO_4.2H_2O$] did not form in the models. Rösner et al. (2001) reported gypsum in only one of 16 samples from various gold mine tailings facilities in the Witwatersrand. The absence of gypsum is most probably due to the low Ca content of the tailings facilities, due to its mineralogy. A secondary salt containing uranium [$UO_2SO_4.3H_2O$] precipitated from solution in Scenario c. This shows that although the U concentrations in the solution are elevated significantly, the concentrations are buffered by the U minerals and would be much higher if it were not for this buffering effect.

Table 7-14 Mineralogical results of the pyrite oxidation model for the Operational Phase in wt%[21]. Scenario a and scenario c contain minerals that have been observed in a previous study (Rösner et al., 2001)

	Scenario a – O_2 mechanism	Scenario b –Fe^{3+} mechanism	Scenario c – Fe^{3+} mechanism using output from O_2 model as input
Goethite	42	0	12
Jarosite	0	0	46
Pyrolusite	58	12	0
Daphnite	0	14	0
Kaolinite	0	26	0
NiSiO4	0	23	0
Mg Saponite	0	30	0
Mg Nontronite	0	0	1
$UO_2SO_4.3H_2O$	0	0	41

Jarosite precipitated from the AMD solution in Scenario c. This secondary sulpho-salt has been shown to be present in the soil from reclaimed tailings footprints (Rosner et al., 2001).

The smectite clay minerals shown to form will most probably form very slowly and may form via intermediate products, as these minerals generally crystallise very slowly, much slower than the timespan of operation of the tailings facility. When these minerals are suppressed, ferric hydroxide precipitates, supporting the notion.

[21] Weight percent

The concentrations of specifically Fe, Al and SO_4 are elevated, but these values represent the smaller volumes of pore water in equilibrium with the tailings facility minerals. When the solution is discharged from the tailings, by toe seepage or seepage top groundwater and surface water processes such as dilution, precipitation and neutralisation cause the concentrations to decrease. These scenarios are investigated in separate geochemical models, discussed in subsequent sections.

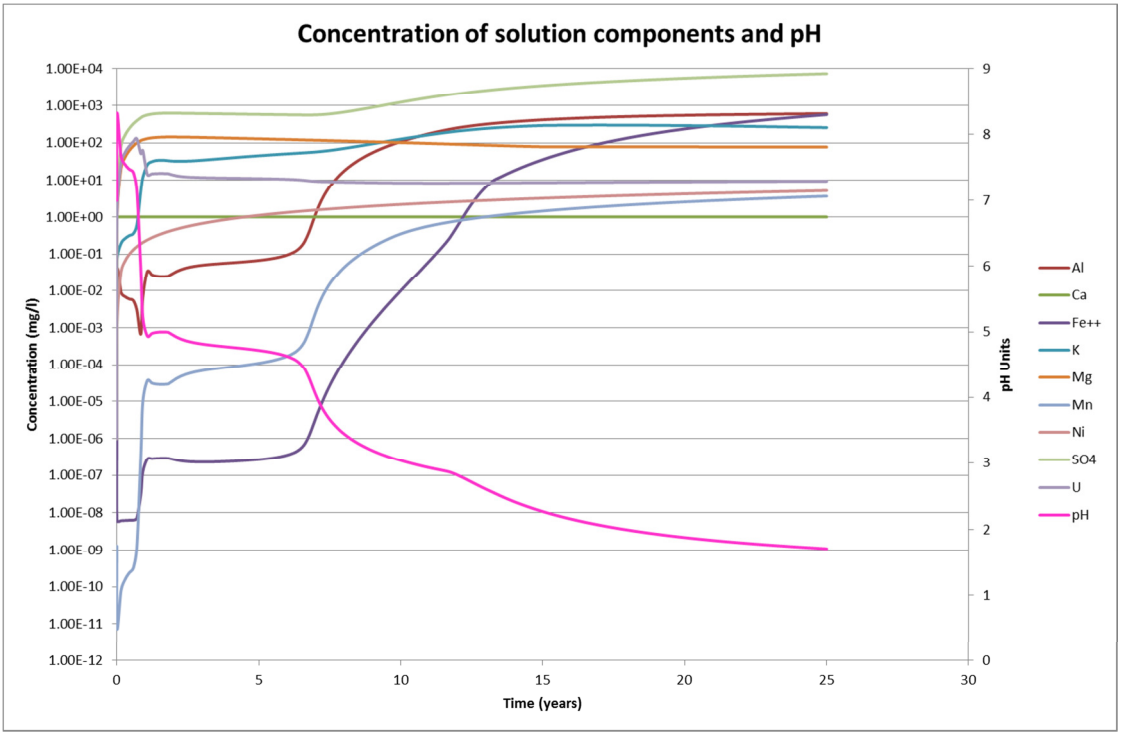

Figure 7-1 Model time series curves of pH and dissolved component concentrations for Scenario a. The graph shows a decrease in H values and concomitant increase in dissolved solids loads.

Time series curves of solution concentrations show a distinct inverse relationship between pH and dissolved component concentration. This relationship has been demonstrated in other studies on AMD (Molson et al., 2005; Tutu et al., 2008).

Time series curves of the decrease and increase of minerals in the tailings component system shows the distinct relationship between the decrease of pyrite and silicate mineral mass in the system and the increase of secondary minerals.

7.3.5.2 Post-Closure Scenario

The effluent solution results for the Post Operational model are similar to those of the Operational model (Table 7-15). One exception is that the pH of scenario c for the Post Operational model is higher than that of the Operational model scenario c. It also falls in the predicted range of 1.3 to 3.5 (Section 6.1).

Table 7-15 Solution composition results of the pyrite oxidation model for the Post-Closure Phase. The results are similar to those of the Operational scenario.

	Units	Scenario a – O_2 mechanism	Scenario b – Fe^{3+} mechanism	Scenario c – Fe^{3+} mechanism using output from O_2 model as input
pH	*pH units*	1.37	8.65	2.56
Eh	*V*	1.15	0.54	0.90
TDS	*mg/kg*	72 926	25	74 120
SO_4	*mg/kg*	46 878	0	50 719
HCO_3	*mg/kg*	0	0	0
Ca	*mg/kg*	0.0	0.0	0.0
Mg	*mg/kg*	518	0.3	683
K	*mg/kg*	906	0.2	775
Na	*mg/kg*	0.9	0.0	0.0
Mn	*mg/kg*	71.85	0.00	34.00
Ni	*mg/kg*	120	0.00	267
U	*mg/kg*	13.58	14.64	27.00
Fe	*mg/kg*	15 820	0.00	19 150
Al	*mg/kg*	2 504	0.05	2 426

The Post Operational effluent model results indicate that the same coupling between an O_2 and Fe^{3+} oxidation mechanism is operational in this phase. The results also show that oxidation by Fe^{3+} may become more pronounced in the Operational phase, as the modelled pH for scenario c is closer to expected values, based on other studies on AMD (Gunsinger et al., 2006).

A chart showing dissolved component concentration change with time is shown in Figure 7-2. The chart shows the same inverse correlation between pH and dissolved components observed for the Operational Phase model results. The implication is that pH the key variable in controlling contaminant concentration.

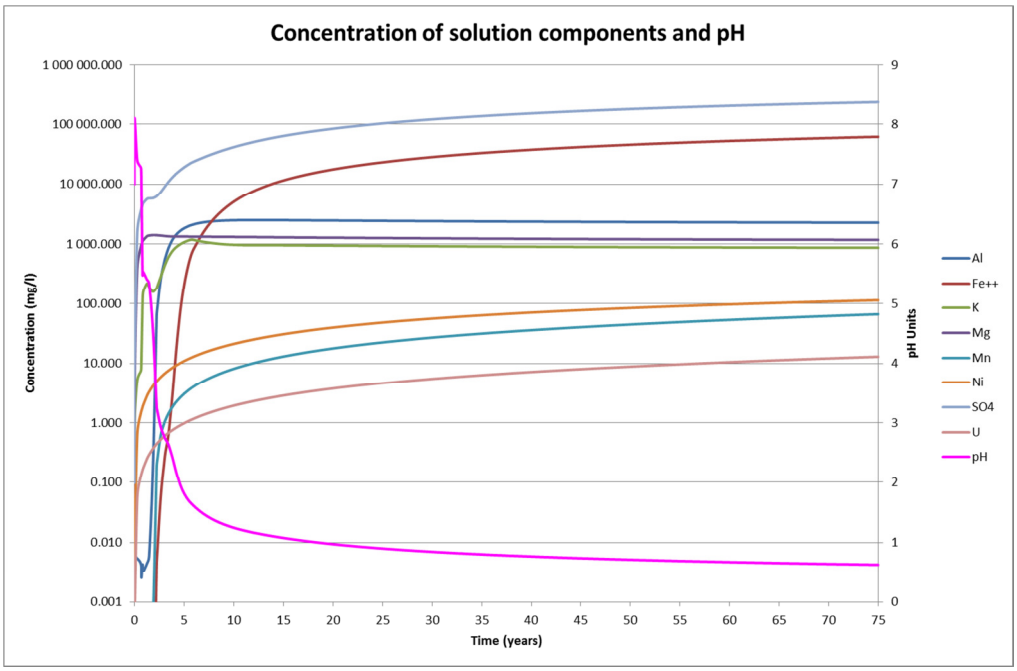

Figure 7-2 Model time series curves of pH and dissolved component concentrations. The same inverse relationship between pH and dissolved solids as for the Operational Phase model results can be observed for the Post-Operational Phase model.

The mineral results show of the Operational and Post Operational models are similar (Table 7-16). A range of hydroxide and sulpho-salts are shown to form as well as clay minerals and the same uranium sulphate phase as in the Operational model. It is interesting that instead of jarosite forming, as in the Operational Phase, the mineral alunite forms in the Post-Operational Phase. Jarosite and alunite are end members in a solid solution (Drouet et al., 2004). This implies that more Al may be available to form secondary salts than Fe^{3+} in the Post Operational phase.

Table 7-16 Mineralogical results of the pyrite oxidation model for the Post-Closure Phase in wt%. The results are similar to those of the Operational Phase model.

	Scenario a – O_2 mechanism	Scenario b –Fe^{3+} mechanism	Scenario c – Fe^{3+} mechanism using output from O_2 model as input
Goethite	42	0	0
Alunite	0	0	4
Pyrolusite	58	12	0
Daphnite	0	13	0
Kaolinite	0	24	0
$NiSiO_4$	0	22	0
Mg Saponite	0	29	0
Mg Nontronite	0	0	0
$UO_2SO_4.3H_2O$	0	0	96

Flowing from the ERB systems model (Figure 5-1) the pyrite oxidation model is the foundation from which all other models flow. The tailings component is the most important source of contaminants in the ERB as the oxidation of pyrite is the primary cause of AMD in the ERB system and hence dominates the contaminant transport into the various component systems.

7.4 Soil adsorption model

A model is developed to understand the interaction between the tailings and soil component though the interaction with the tailings leachate on the soil and shallow groundwater. This model incorporates solution transport and adsorption.

The soil of the ERB is derived predominantly from the Karoo Supergroup rocks, principally the Vryheid formation with some influence from the Malmani dolomites (Rösner et al., 2001). The Vryheid formation consists mostly of sandstone and mudstone containing. The soil formed from this formation consists predominantly of illite and quartz with lesser mica, kaolinite and chlorite. Due to the presence of clays, predominantly illite (Buhmann, 1992), the soil is expected to contain adsorption capacity, which needs to be taken account of in the model.

Sorption can be modelled in predominantly two ways; the distribution coefficient (K_d) models or using the surface complexation models (Bethke, 2008). The K_d model, although much used in hydrogeochemistry, hs been shown to provide unreliable results, usually overstating plume migration and overstating the effect of passive remediation methods, such as flushing the system with clean water, either artificially, or by recharge (Bethke and Brady, 2000; Zhu, 2003). Therefore the surface complexation model (Bethke, 2008; Dzombak and Morel, 1990) is used to model soil sorption in the ERB.

The software used to model the soil adsorption below the tailings is X1t (Bethke, 2008), which forms part of the , Geochemist's Workbench® programs. The program uses the Fe-hydroxide surface complexation model of Dzombak and Morel (1990) and therefore Fe-hydroxide is added to the system. The exact amount of Fe-hydroxide needed to balance the adsorption potential of the ERB soil is uncertain. However, published surface charge densities of illite (Srodon et al., 2006) are compared to that of the specific amount of Fe-hydroxide added to the ERB soil adsorption model to constrain the amount of Fe-hydroxide needed in the system.

The Post-Closure results of the O_2 oxidation mechanism model are used to develop the soil adsorption model. The conceptual model of the tailings component system (Figure 6-1) shows that the groundwater table reaches the base of the tailings due to pressure and capillary rise. Therefore the downwards migrating AMD will reach the groundwater table, mix and start to disperse vertically and laterally. Only the lateral migration through the soil is taken into account in this model.

The model has one drawback. Mixing model results show an end pH of 1.37. The adsorbing Fe-hydroxide in the model is ferric hydroxide. Ferric iron is soluble at pH values below 3. Therefore the ferric hydroxide is expected to dissolve in the model upon contact with the tailings leachate. The pH is therefore set to 3, which

is still acid enough to keep metals in solution, but not acid enough to dissolve the ferric hydroxide thereby removing the adsorption capacity artificially. The effect of this is evaluated in the sensitivity analysis.

The model starts with an initial solution, which in this case is set to background groundwater. A water sample from shallow groundwater assumed to resemble uncontaminated water due to its low metal, alkaline pH and low SO_4 content, is used as the pristine groundwater in the model. The inlet solution, i.e. the solution that enters the shallow groundwater system, is set to a 1:10 mixture of tailings leachate and shallow groundwater. This is to take account of the soil solution being a mix between AMD from the tailings and the shallow groundwater.

X1t can incorporate simple 1-dimensional flow to model contaminant transport. The input required is the length of the aquifer, here substituted with depth, discharge, porosity and hydrodynamic dispersivity. Hydrodynamic dispersivity is an assumption and is set to 1% of the length of the domain by default (Bethke, 2008). The discharge is calculated using the soil permeabilities measured by Rösner et al. (2001) (Table 7-17) using the Darcy equation (Bethke, 2008):

$$\boldsymbol{q = \frac{k}{\mu}\left(\frac{\Delta \emptyset}{L}\right)} \qquad \textbf{Equation 93}$$

In Equation 93 q is discharge ($cm^3.cm^{-2}.s^{-1}$), *k* is the average permeability ($cm.s^{-1}$), μ is the viscosity (poise), $\Delta\Phi$ is the drop in hydraulic potential across the domain and *L* is the domain length. The drop in hydraulic potential can be calculated from the head drop by:

$$\Delta \emptyset = \boldsymbol{\rho g \Delta h} \qquad \textbf{Equation 94}$$

In Equation 94, ρ is the fluid density of 1 $g.cm^{-3}$, g the acceleration of gravity of 9.8 $m.s^{-2}$ and Δh is the head drop. Using Equation 93 and 94 a discharge of $5x10^{-4}$ $m.day^{-1}$ is calculated. The main uncertainty in the discharge value is the value of the length, as the migration is vertical. For the purposes of the study *L* is set to infinitesimally small. The results corresponds to the hydraulic conductivity values estimated by Africa Geo-Environmental Services (Pty) Ltd. (2006). A sensitivity analysis is done using different values to test the model sensitivity.

The average depth of the ERB soils is 1.7 m, varying between 1.0 and 2.3 m (σ = 0.50). The oxygen fugacity is fixed, as small amount of oxygen can ingress into the shallow soil. The UO^{2+}-U^{4+} redox pair is decoupled. These values and assumptions are evaluated in a sensitivity analysis. The model is run over 75 years, the time after tailings decommissioning.

7.4.1 Quantities of interest

The QOI in addition to those indicated in Section 7.2.1 are Co, Cu and Zn. These were not added to the pyrite oxidation models for computational reasons. Their concentrations are therefore unknown. However, unpublished tailings leachate results exist (Table 7-18) and the ratios shown to leach from the tailings samples in the leachate studies are comparable to the ratios of metals in solution in the pyrite oxidation model results. This can be used as another tool to evaluate the models.

Table 7-17 ERB soil geotechnical data (after Rösner et al. (2001))

Site	Total depth (m)	Soil classification	Clay (%)	Silt (%)	Sand (%)	Gravel (%)	pH	Dry density (kg/m^3)	SG	Void ratio (e - %)	Porocity (%)	Permeability (K - cm/s)
A	1.0	silty clayey sand with gravel	10.94	21.88	54.08	13.06	5.29	1706.80	2.75	0.62	0.38	$1.00x10^{-07}$
B	2.0	sandy clay with silt	40.23	27.36	31.20	1.21	5.21	1660.07	2.47	0.49	0.33	$1.00x10^{-08}$
C	2.3	clayey sand with silt	34.81	27.71	36.37	2.33	5.27	1640.51	2.60	0.59	0.37	$2.40x10^{-06}$
D	1.9	clayey sand with silt	33.23	26.65	38.81	1.27	5.07	1612.30	2.66	0.65	0.39	$6.44x10^{-07}$
E	1.5	sandy clay with silt	38.55	24.83	34.87	1.71	7.06	1582.75	2.65	0.69	0.41	$4.85x10^{-07}$
F	2.2	clayey sand with silt	30.37	25.62	41.63	2.32	4.98	1700.51	2.75	0.62	0.38	$3.30x10^{-07}$
G	1.2	silty sand with clay	22.54	26.33	44.38	6.63	5.47	1784.37	2.66	0.49	0.33	$2.97x10^{-07}$
Average	**1.7**	**clayey sand with silt**	**30.10**	**25.77**	**40.19**	**4.08**	**5.48**	**1669.62**	**2.65**	**0.59**	**0.37**	**$6.09x10^{-07}$**

Table 7-18 ICP-MS NH_4NO_3 leachate results from ERB tailings samples[22].

Sample	As	Ca	Co	Cr	Cu	Fe	Mg	Mn	Ni	Pb	S	U	Zn
	Units	*mg/kg*	*mg/kg*	*mg/kg*	*mg/kg*	*mg/kg*	*mg/kg*	*mg/kg*	*mg/kg*	*mg/kg*	*mg/kg*	*mg/kg*	*mg/kg*
1	0.00	1574.50	0.50	0.00	2.50	0.75	7.50	1.25	1.25	0.00	1257.50	0.00	0.25
2	0.00	660.00	1.00	0.00	2.50	2.50	72.50	2.50	2.50	0.00	697.50	0.00	1.50
3	0.00	202.50	0.00	0.00	0.00	0.50	17.50	0.50	0.00	0.00	60.00	0.00	0.25
4	0.00	860.00	0.00	0.00	0.25	0.00	10.00	0.50	0.00	0.00	650.00	0.00	
5	0.00	1082.50	10.00	1.75	12.52	50.00	460.00	15.00	32.50	0.00	3090.00	0.00	7.50
6	0.00	500.00	17.50	1.25	17.50	87.50	687.50	22.50	57.50	0.50	3712.00	0.00	10.00
7	0.25	1362.50	25.00	1.75	22.50	105.00	802.50	25.00	77.50	0.50	5097.00	0.00	12.50
8	0.00	1770.00	30.00	2.25	22.50	60.00	927.50	27.50	105.00	0.75	6132.50	0.00	15.00
9	0.00	1342.50	2.50	1.00	1.50	25.00	290.00	10.00	10.00	0.25	2510.00	0.00	10.00
10	0.00	2185.00	15.00	0.50	2.50	7.50	312.50	42.50	45.00	0.50	4837.50	0.00	80.00
11	0.00	2182.50	15.00	5.00	7.50	55.00	955.00	35.00	47.50	0.50	4820.00	0.00	40.00
12	0.00	1750.00	10.00	2.50	5.00	37.50	650.00	25.00	35.00	0.50	4827.50	0.00	27.50
13	0.00	3020.00	25.00	5.00	10.00	5.00	1487.00	45.00	80.00	0.75	11262.00	0.00	60.00
Average	***0.02***	***1422.46***	***11.65***	***1.62***	***8.21***	***33.56***	***513.81***	***19.40***	***37.98***	***0.33***	***3765.65***	***0.00***	***22.04***
Standard Deviation	***0.07***	***781.29***	***10.60***	***1.74***	***8.17***	***35.69***	***455.50***	***15.83***	***34.95***	***0.30***	***3001.91***	***0.00***	***25.52***
Maximum	***0.25***	***3020.00***	***30.00***	***5.00***	***22.50***	***105.00***	***1487.00***	***45.00***	***105.00***	***0.75***	***11262.00***	***0.00***	***80.00***
Minimum	***0.00***	***202.50***	***0.00***	***0.00***	***0.00***	***0.00***	***7.50***	***0.50***	***0.00***	***0.00***	***60.00***	***0.00***	***0.25***

[22] Council for Geoscience unpublished data – Strategic Water Management Project

The secondary minerals that form are also of interest, as they show the precipitation controls on the mobility of specific components.

7.4.2 Assumptions

7.4.2.1 Dispersivity

Hydrodynamic dispersion, or dispersivity, results from the mixing of groundwater due to chaotic flow through a porous and/or fractured medium. The dispersivity is a property of the medium through which flow occurs and the scale at which it is observed and hence there is no typical value for dispersivity. Therefore the dispersivity is assumed to be 1% of the domain length. For the ERB soil adsorption model, this equates to 2 cm. This is most probably a reasonable assumption, due to the slow water flow through the low conductivity ERB soils.

7.4.2.2 Fixed O_2 fugacity

The average concentration of dissolved oxygen in the ERB shallow groundwater is 3.49 mg/l (σ = 2.49), ranging between a minimum of 0.56 and a maximum of 10.40 mg/l. This equates to an average O_2 fugacity of 0.09 ranging from a minimum of 0.01 and a maximum of 0.25. The average O_2 fugacity is 43% of the atmospheric value of 0.21, ranging from a minimum of 5% to a maximum of 119% the atmospheric value. The upper value of 119% is unusually high compared to the rest of the ERB dissolved oxygen data of the shallow groundwater. Only 2 values out of 36 are above the O_2 equilibrium concentration value of 8.48. This indicates that the values may either be due to measurement error, or a process is active in the region of the specific borehole that produces oxygen. Both boreholes are located in the same industrial site.

The equilibrium O_2 concentration value is at pH of 7, but thermodynamic analysis of O_2 equilibrium concentrations from pH 7 to pH 1 shows a 0.4% difference, an insignificant difference on the concentration scale of the ERB adsorption model.

The O_2 concentration used and the fixed scenario is evaluated in the sensitivity analysis.

7.4.2.3 Redox disequilibrium

The redox state of the U system is unknown, but due to the extreme oxygenated environmental of the tailings and hence the generated leachate, the assumption is made that the U is in the U^{6+} state and occurs as the UO^{2+} specie. This has also been suggested by Coetzee et al. (2006) in their study of pollution sources in the Wonderfonteinspruit in the West Rand Basin and Tutu et al. (2009) in their study on radioactive disequilibrium in Witwatersrand gold tailings.

Oxygen fugacity diagrams (Figure 7-4 and Figure 7-5), constructed using the GWB program Act2®, show that UO_2^{2+} is stable at acidic (pH < 5) conditions, while UO_2OH^+ is stable at slightly acidic (pH 5) to alkaline conditions at the UO_2^{2+} activity determined from measure shallow groundwater U concentrations. At higher U activities ($8.00x10^{-7}$) the mineral Schoepite becomes stable between pH values of 6.21 and 6.32, a very narrow band. Above pH values of 6.32, the U-hydroxide complex $(UO_2)_3(OH)_7^-$ becomes stable. When SO_4 and HCO_3 are speciated over the U diagram, soluble U species remain dominant at high and low U activities (Figure 7-3).

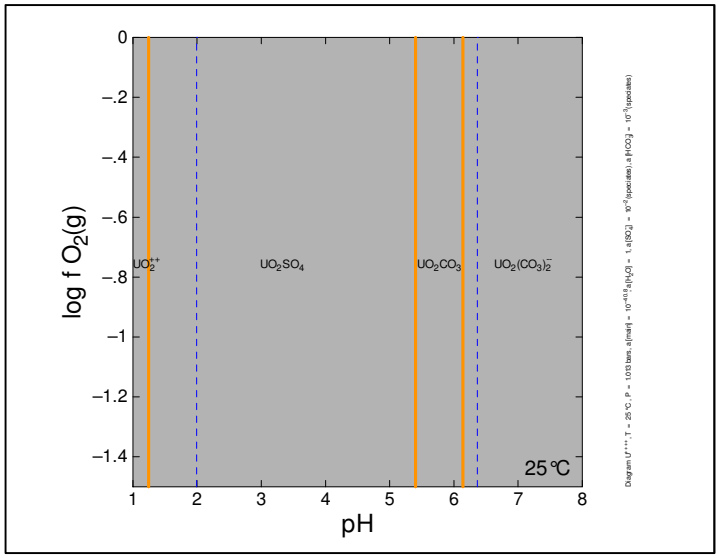

Figure 7-3 O2 fugacity - pH diagram of U species at low U activity ($1.589x10^{-41}$).

These calculations support the assumption that the dominant U species in ERB AMD, shallow groundwater and surface water is UO_2^{2+}.

To force the assumption the U^{4+}-UO^{2+} redox pair is decoupled in the model. The effect of this assumption on the model results is evaluated in a sensitivity analysis.

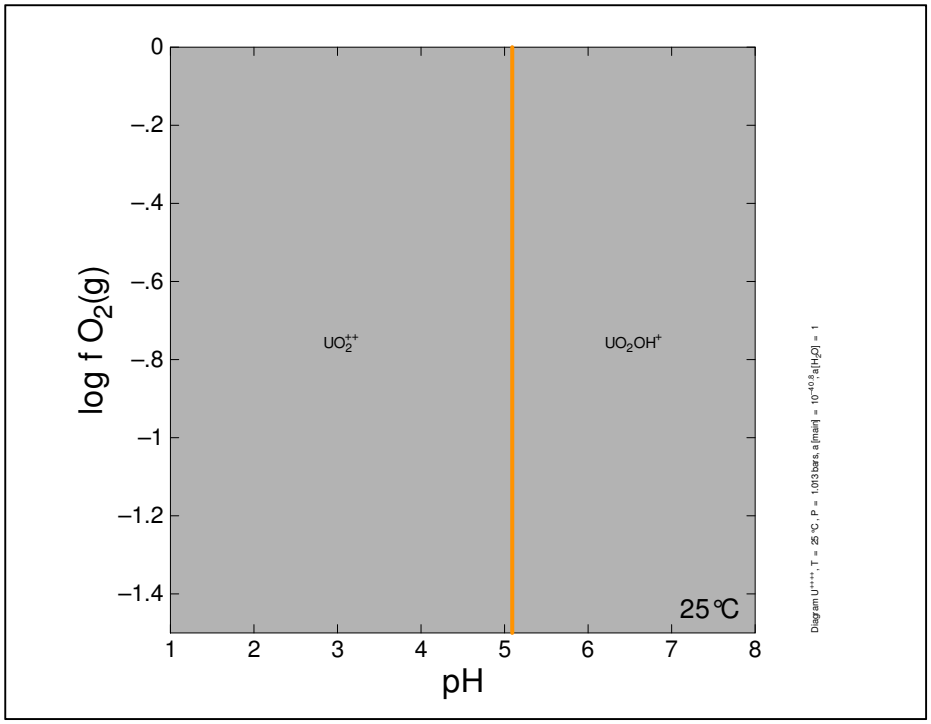

Figure 7-4 O_2 fugacity - pH diagram of U speciation at ERB shallow groundwater and surface conditions at low U activity ($1.589x10^{-41}$).

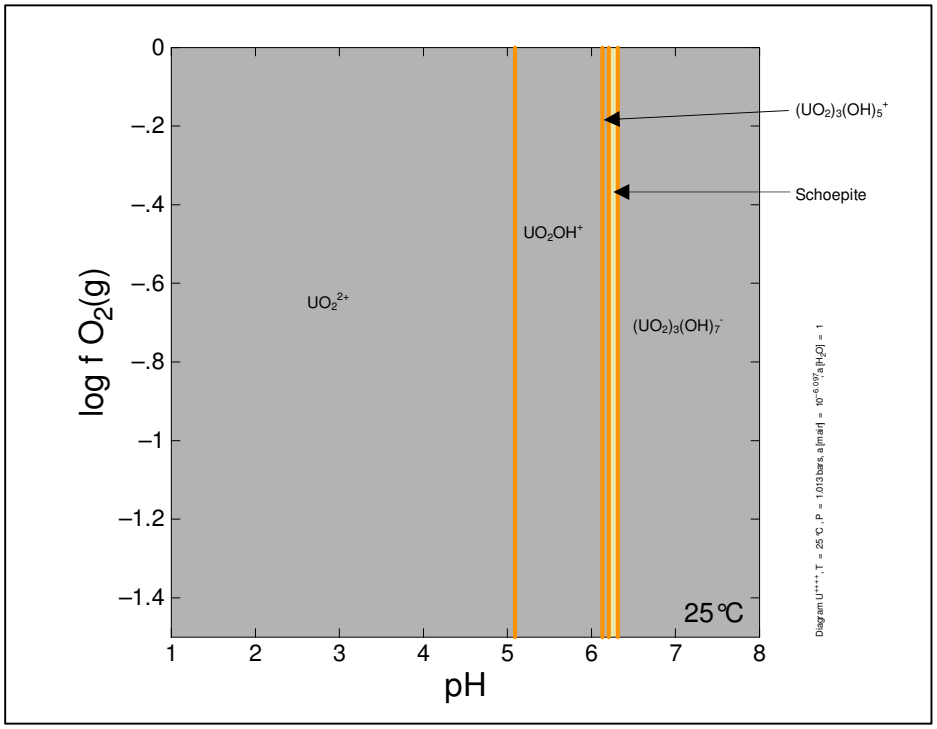

Figure 7-5 O_2 fugacity - pH diagram of U speciation at ERB shallow groundwater and surface water conditions at elevated U activity ($8.00x10^{-7}$)

7.4.2.4 Fe-hydroxide adsorption behaviour is equivalent to that of illite

This assumption is valid if the amount of Fe-hydroxide in the system equates to the average surface charge density of illite clays in general. This is indeed the case. An amount of 1.5 wt% Fe-hydroxide in the ERB soil adsorption model system has a surface charge density of 0.74 C.m^{-2}. This is calculated from the equation:

$$\omega = \frac{Fn_w}{A_{sf}} \sum_q z_q m_q \qquad \textbf{Equation 95}$$

In Equation 108 above, ω is the surface charge density (C.m^{-2}), F is the Faraday constant (96 485 C.mol^{-1}), n_w is the mass of solvent water (kg), A_{sf} is the sorbing surface area (m^2), z_q is the electrical charge on each complex of compound q and m_q is the molalities of the complexes of compound q.

The literature shows that generally the surface charge density of illite is between 0.5 and 0.8 C.m^{-2} (Srodon et al., 2006), but can be as high as 1.5 to 1.7 C.m^{-2} (Sinitsyn et al., 2000). As a more conservative approach is followed as part of the modelling philosophy, the amount of Fe-hydroxide is set to 1.5 wt%, with a surface charge density of 0.74 C.m^{-2}. A sensitivity analysis is done to determine the model sensitivity to changes to the amount of Fe-hydroxide in the system.

7.4.2.5 No minerals weather during the timeframe of the simulation

To simplify the model for the purposes of computational time and model convergence, no mineral weathering was taken into account. The main purpose of the adsorption model is to determine the time till the pollution plume migrates through the soil, i.e. the adsorptive capacity of the soil in terms of time. The results of the pyrite oxidation models, which do take weathering into account, show the metal concentrations in solution. Therefore a reasonable assumption on the conservative side is to assume that mineral weathering does not have an influence on the concentration of metals in solution and that the metals are only removed via adsorption and precipitation of minerals due to over saturation with respect to specific secondary minerals.

A weathering model is developed to compare predicted solutions resulting from the interaction of rain water with Witwatersrand and Karoo strata with actual samples from selected areas, assumed to represent pristine groundwater and to determine the cations and anions that are released during weathering. The results of the weathering model is compared to pyrite oxidation model results to determine the addition of cations and anions through weathering during the 75 years of simulated plume migration to determine whether weathering introduces a significant amount of specific ions to solution.

7.4.3 Uncertainties

The most important uncertainties is the spatial variation of geotechnical data (Table 7-19).

Table 7-19 Summary statistics of the ERB soil geotechnical data. The maximum uncertainty is shown.

Site	Total depth (m)	Clay (%)	Silt (%)	Sand (%)	Gravel (%)	Porosity	Permeability (K – cm.s^{-1})
Average	*1.7*	*30.10*	*25.77*	*40.19*	*4.08*	*0.37*	*6.09x10^{-7}*
Standard Deviation	*0.5*	*10.25*	*1.98*	*7.51*	*4.38*	*0.03*	*8.17x10^{-7}*
Coefficient of variation	*29%*	*34%*	*8%*	*19%*	*107%*	*8%*	*134%*
Maximum	*2.30*	*40.23*	*27.71*	*54.08*	*13.06*	*0.41*	*2.40x10^{-6}*
Minimum	*1.00*	*10.94*	*21.88*	*31.20*	*1.21*	*0.33*	*1.00x10^{-8}*
Uncertainty	*42%*	*64%*	*15%*	*35%*	*220%*	*10%*	*294%*

The results of the uncertainty analysis show that depth of the soil varies spatially by 42%, the clay content, which determines adsorption capacity, by 64% and the permeability by 294%. No temporal data was available at the time of this study, but is not expected to vary much, due to the physical nature of the measured results.

The uncertainty of dissolved components and species in the shallow groundwater has already been discussed in Section 7.2.4.

7.4.4 Sensitivity analysis

A sensitivity analyses are performed on some parameters that are expected to provide the most uncertainty in the soil adsorption model.

A sensitivity analysis on a contaminant transport model developed in X1t is different that developing a reaction model in React. The difference is in output. The X1t contaminant transport results can only be plotted and end results read from the graphs. Therefore QOI need to be evaluated separately. The end-concentrations are therefore of interest as well as the time it takes for the plume to reach the base of the soil layer. The time is assessed roughly by determining when the first metal concentration of >1 mg/l reaches the base of the soil and the time when the last metal reaches the input concentration, implying total saturation of the soil adsorptive capacity. Uranium is excluded from the assessment in terms of defining the timing of plume migration and breakthrough, due to the uncertainty surrounding U speciation. Changes in these parameters are used to evaluate the model sensitivity to the parameters mentioned below.

Conceptually the results reported in the sensitivity analysis tables represent a sample of the leachate at the bottom of the soil profile after the 75 years of simulation time.

7.4.4.1 Analysis of the effect of varying dispersivity

A sensitivity analysis is conducted to determine the effect of varying the hydrodynamic dispersion of the system by varying the dispersivity parameter in the model (Table 7-20).

Table 7-20 Results of a sensitivity analysis on dispersivity

	Base Case		Dispersivity (0.1)		Dispersivity (10)	
Time to first breakthrough (years)	50.2		51.2		46.8	
Time to last breakthrough (years)	69.6		70.8		67.8	
pH	3.99		3.99		3.99	
TDS (mg/kg)	19 500		19 500		19 510	
Eh (V)	0.98		0.98		0.98	
	Adsorbed (mg/kg)	**In solution (mg/kg)**	**Adsorbed (mg/kg)**	**In solution (mg/kg)**	**Adsorbed (mg/kg)**	**In solution (mg/kg)**
Fe^{2+}	n.a.	5 868	n.a.	5 868	n.a.	5 868
Fe^{3+}	n.a	0.00	n.a	0.00	n.a	0.00
SO_4	10 000	13 220	10 000	13 220	10 000	13 230
Mn	0.00	0.01	0.00	0.01	0.00	0.01
Co	0.01	3.91	0.12	1.91	0.01	3.92
Ni	0.13	10.76	0.13	10.76	0.13	10.76
Zn	0.00	0.00	0.00	0.00	0.00	0.00
Al	0.00	189.30	0.00	189	0.00	189
UO_2^{2+}	36.77	0.29	27.33	0.21	58.47	3.76

The results show that higher dispersivity values shorten the time till breakthrough of the pollution plume, but that the time difference is small (~4 years). Of all the QOI, U and Co show sensitivity to dispersivity and of these U is most significantly affected, but only at higher values of dispersivity. Therefore the model results are not significantly influenced by dispersivity.

7.4.4.2 Analysis of the effect of fixed vs. unfixed O_2 fugacity

A sensitivity analysis was conducted on the fixed O_2 fugacity to determine whether model results are significantly affected by a fixed or limited oxygen flux into the system (Table 7-21). The results show that almost none of the QOI are significantly affected by the fixing or unfixing of the O_2 fugacity. Manganese is affected as the solution concentration of Mn is controlled by pyrolusite [MnO_2], which is sensitive to the amount of O_2 in the system. Thus the model is insensitive to the fixing or unfixing of O_2 for all QOI, with the exception of Mn.

Table 7-21 Results of a sensitivity analysis on O_2 fugacity fixing

	Base Case		Unfixed O_2 Fugacity	
Time to first breakthrough (years)	50.2		50.2	
Time to last breakthrough (years)	69.6		69.6	
pH	3.99		3.99	
TDS (mg/kg)	19 500		19 500	
Eh (V)	0.98		0.94	
	Adsorbed (mg/kg)	**In solution (mg/kg)**	**Adsorbed (mg/kg)**	**In solution (mg/kg)**
Fe^{2+}	n.a.	5 868	n.a.	5 869
Fe^{3+}	n.a	0.00	n.a	0.00
SO_4	10 000	13 220	10 000	13 180
Mn	0.00	0.01	0.00	0.19
Co	0.01	3.91	0.01	3.92
Ni	0.13	10.76	0.13	10.79
Zn	0.00	0.00	0.00	0.00
Al	0.00	189	0.00	182
UO_2^{2+}	36.77	0.29	11.00	0.45

7.4.4.3 Analysis of the effect of varying the pH to below 3

The pH of the model is set to 3, as discussed in Section 7.4. A sensitivity analysis was conducted to determine the effect of lowering the pH below 3. In reality this change should not make a significant difference, as the clay mineral illite is stable in very acidic conditions, if the system contains sufficient quantities of Al (Reesman, 1974), which in the ERB AMD system is not an issue.

In the ERB soil adsorption model, however the model system is very sensitive to pH <3, but only in terms of the timing of breakthrough curves and the end solution concentration of ferric Fe, due to the dissolution of the ferric hydroxide adsorbate. The dissolution of adsorbate is not expected to be a significant issue in the real ERB soil system.

Table 7-22 Results of a sensitivity analysis on pH <3

	Base Case		Unfixed O_2 Fugacity	
Time to first breakthrough (years)	50.2		7.3	
Time to last breakthrough (years)	69.6		11.2	
pH	3.99		1.44	
TDS (mg/kg)	19 500		39 900	
Eh (V)	0.98		1.13	
	Adsorbed (mg/kg)	**In solution (mg/kg)**	**Adsorbed (mg/kg)**	**In solution (mg/kg)**
Fe^{2+}	n.a.	5 868	n.a.	5 798
Fe^{3+}	n.a	0.00	n.a	3 323
SO_4	10 000	13 220	10 310	26 830
Mn	0.00	0.01	0.00	6.77
Co	0.01	3.91	0.00	3.87
Ni	0.13	10.76	0.00	10.63
Zn	0.00	0.00	0.00	0.00
Al	0.00	189.30	0.00	217.40
UO_2^{2+}	36.77	0.29	0.01	4.83

7.4.4.4 Analysis of the effect of redox disequilibrium vs. equilibrium

The model sensitivity to the redox equilibrium and disequilibrium scenarios is evaluated. Two equilibrium scenarios are evaluated. The first in which the O_2 fugacity is fixed and a second in which the O_2 fugacity is unfixed.

The results show that 41% more U is in solution when the U^{4+} - UO_2^{2+} system is assumed to be in equilibrium and less U adsorbes when the O_2 fugacity is fixed and more when the O_2 fugacity is unfixed. This is because when the O_2 fugacity is unfixed, there is more U^{4+} in the system, which has a higher charge than UO_2^{2+} and can therefore adsorb more easily to the adsorbate.

Previous studies (Coetzee et al., 2006; Tutu et al., 2009) and calculations for the current study (Section 0) indicate that UO_2^{2+} is the dominant U specie in solution. Therefore disequilibrium is assumed and the model uncertainty due to uncertainty regarding the measure to which the U redox system is in equilibrium is ~41%.

Table 7-23 Results of sensitivity analysis on U redox equilibrium

	Base Case		Redox equilibrium (U^{4+} - UO_2^{2+}) - Fixed O_2 fugacity		Redox equilibrium (U^{4+} - UO_2^{2+}) - O_2 fugacity not fixed	
Time to first breakthrough (years)	50.2		50.2		50.2	
Time to last breakthrough (years)	69.6		69.6		69.6	
pH	3.99		3.99		3.99	
TDS (mg/kg)	19 500		19 500		19 500	
Eh (V)	0.98		0.98		0.94	
	Adsorbed (mg/kg)	**In solution (mg/kg)**	**Adsorbed (mg/kg)**	**In solution (mg/kg)**	**Adsorbed (mg/kg)**	**In solution (mg/kg)**
Fe^{2+}	n.a.	5 868	n.a.	5 869	n.a.	5 869
Fe^{3+}	n.a	0.00	n.a	0.00	n.a	0.00
SO_4	10 000	13 220	10 000	13 180	10 000	13 180
Mn	0.00	0.01	0.00	0.01	0.00	0.19
Co	0.01	3.91	0.01	3.92	0.01	3.92
Ni	0.13	10.76	0.13	10.79	0.13	10.79
Zn	0.00	0.00	0.00	0.00	0.00	0.00
Al	0.00	189	0.00	181	0.00	182
UO_2^{2+}	36.77	0.29	9.04	0.41	50.78	0.40

7.4.4.5 Analysis of the effect of varying the initial system Fe-hydroxide content

Model sensitivity is evaluated on varying amounts of ferric hydroxide in the soils system (Table 7-24). An additional QOI is used in this analysis, the surface charge density (σ) of the adsorbate species in the ERB soil adsorption system. The results show that the model is significantly sensitive to the amount of ferric hydroxide in the system, in terms of the timing of plume migration and the concentration of contaminants in solution. The concentrations at the base of the soil profile after the simulation time of 75 years is insignificant. This is because the plume migration through the soils is retarded by adsorption and the first breakthrough curves do not even reach the base of the soil after the simulation time has been reached. The sensitivity analysis results shows that the plume breaks through the base of the soil 30 years earlier with 0.5 wt% ferric hydroxide and more than 56 years later with 3 wt%. The surface charge density shows that the Base Case scenario is closest to published illite surface charge values (Srodon et al., 1986). Nonetheless, due to the system's sensitivity to the concentration of adsorbant in the system, the clay content and clay mineralogy will need to be studied in greater detail in follow-up studies to reduce uncertainty in the model. A detailed description of the clay mineralogy is beyond the scope of this study.

Table 7-24 Results of sensitivity analysis on the ferric hydroxide content

	Base Case		Fe-Hydroxide (0.5 free volume %		Fe-Hydroxide (3 free volume %)	
Time to first breakthrough (years)	50.2		18.3		> 75 years	
Time to last breakthrough (years)	69.6		32.4		Undetermined	
pH	3.99		3.12		7.30	
TDS (mg/kg)	19 500		19 160		18 540	
Eh (V)	0.98		1.03		0.78	
Surface charge ($C.m^{-2}$)	0.83		0.27		1.66	
	Adsorbed (mg/kg)	**In solution (mg/kg)**	**Adsorbed (mg/kg)**	**In solution (mg/kg)**	**Adsorbed (mg/kg)**	**In solution (mg/kg)**
Fe^{2+}	n.a.	5 868	n.a.	5 870	n.a.	5 885
Fe^{3+}	n.a	0.00	n.a	0.04	n.a	0.00
SO_4	10 000	13 220	3 335	12 780	8 727	12 350
Mn	0.00	0.01	0.00	0.76	0.00	0.00
Co	0.01	3.91	0.00	3.91	0.00	0.00
Ni	0.13	10.76	0.00	10.76	0.00	0.00
Zn	0.00	0.00	0.00	0.00	0.00	0.00
Al	0.00	189	0.00	232	0.00	0.00
UO_2^{2+}	36.77	0.29	4.05	4.89	0.00	0.00

7.4.4.6 Analysis of the effect of varying the soil discharge value

A sensitivity analysis is conducted to determine the effect of varying fluid discharge rates of the ERB soil (Table 7-25). The results show that the model is sensitive to changes in discharge rates. Varying discharge has comparable effects on the model results to varying ferric hydroxide content. Increasing the discharge rate by an order of magnitude decreases the plume breakthrough by 46 years of simulation. Increasing the discharge by 5 times, increases the breakthrough by more than 24 years, i.e. the plume never breaks through in the entire simulation time.

The results also show that at higher discharge rates reaction kinetics will need to be incorporated in the model, perhaps by simplifying the inlet solutions as the plume migrates through the system in ~ 4 years and then is flushed by background groundwater and the system reaches background values by the end of the simulation.

The discharge value used in the Base Case scenario is calculated from measured permeabilities and compares to the hydraulic conductivity values from previous studies (Africa Geo-Environmental Services (Pty) Ltd., 2006). The fact that the model is sensitive to discharge rates of the soil indicates that further

constraints on ERB soil discharge values are needed to reduce uncertainty in the model. A detailed study on the discharge of the ERB soils is beyond the scope of the study.

Table 7-25 results of sensitivity analysis on the ERB soil discharge rate

	Base Case		Discharge ($5x10^{-3}$ m/day)		Discharge ($1x10^{-5}$ m/day)	
Time to first breakthrough (years)	50.2		4.5		> 75 years	
Time to last breakthrough (years)	69.6		8.4		undetermined	
pH	3.99		3.12		7.88	
TDS (mg/kg)	19 500		20 120		487	
Eh (V)	0.98		1.03		0.75	
	Adsorbed (mg/kg)	**In solution (mg/kg)**	**Adsorbed (mg/kg)**	**In solution (mg/kg)**	**Adsorbed (mg/kg)**	**In solution (mg/kg)**
Fe^{2+}	n.a.	5 868	n.a.	5 865.00	n.a.	0.10
Fe^{3+}	n.a	0.00	n.a	0.04	n.a	0.00
SO_4	10 000	13 220	10 120	13 700	134	19.00
Mn	0.00	0.01	0.00	0.74	0.00	0.00
Co	0.01	3.91	0.00	3.91	0.00	0.00
Ni	0.13	10.76	0.00	10.75	0.00	0.00
Zn	0.00	0.00	0.00	0.00	0.00	0.00
Al	0.00	189	0.00	230.60	0.00	0.00
UO_2^{2+}	36.77	0.29	11.47	4.89	0.00	0.00

7.4.4.7 Analysis of the effect of varying the soil depth

A sensitivity analysis is conducted to determine the effect of varying soil depth on the model results. The results show that variations in soil depth have the same effect on model results as variations in ferric hydroxide content and variations in soil discharge values. Decreasing the soil depth to 0.5 m decreases the timing of plume break though by ~39 years of simulation. Increasing soil depth to 3 m increases the timing of break through by ~17 years of simulation. This implies that the depth beneath a tailings facility is an important consideration in determining the contaminant transport into the surrounding environment. Better constraint on the soil depth beneath specific tailings facilities can lead to the decrease in uncertainty of the model. A detailed consideration of the soil depth below each tailings facility is beyond the scope of this study.

Table 7-26 Results of sensitivity analysis on model soil depth

	Base Case		Lower limit (0.5 m)		Upper limit (3 m)	
Time to first breakthrough (years)	50.2		11.7		66.7	
Time to last breakthrough (years)	69.6		19.9		> 75 years	
pH	3.99		3.12		7.30	
TDS (mg/kg)	19 500		20 120		18 140	
Eh (V)	0.98		1.03		0.78	
	Adsorbed (mg/kg)	**In solution (mg/kg)**	**Adsorbed (mg/kg)**	**In solution (mg/kg)**	**Adsorbed (mg/kg)**	**In solution (mg/kg)**
Fe^{2+}	n.a.	5 868	n.a.	5 865	n.a.	5 925
Fe^{3+}	n.a	0.00	n.a	0.04	n.a	0.00
SO_4	10 000	13 220	10 110	13 700	4 340	11 900
Mn	0.00	0.01	0.00	0.74	0.00	0.00
Co	0.01	3.91	0.00	3.91	82.14	0.26
Ni	0.13	10.76	0.00	10.75	85.05	0.03
Zn	0.00	0.00	0.00	0.00	0.01	0.00
Al	0.00	189	0.00	231	0.00	0.00
UO_2^{2+}	36.77	0.29	11.46	4.89	0.00	0.00

7.4.5 Model results

The model results of the leachate at the base of the soil profile after the 75 years of simulation are shown in Table 7-27.

The results show that a solution with low pH (3.99) and elevated concentrations of Fe, Co, Ni, Zn, Al, U and SO_4 has migrated to the base of the soil profile. This indicates that the tailings leachate has migrated through the soil profile in the time of simulation. The time duration till the AMD plume breaks through the soil profile has been shown by the sensitivity analysis to be mostly dependent on soil thickness, adsorbate content and soil hydraulic conductivity. The age of the tailings facility is also expected to be of influence. Therefore results in the real system are expected to be varied, due to variations in these parameters. Uncertainty can therefore be significantly reduced for studies on individual tailings facilities by constraining these parameters. Nonetheless, the results from the current model highlight important processes and can be used in a generic sense.

The results in Table 7-27 show that SO_4 is predominantly adsorbed, followed by U > Zn > Ni. Charts of the breakthrough curves of Ni, Co and Zn (Figure 7-6, Figure 7-7 and Figure 7-8) show that these elements display similar behaviour in terms of adsorption as the plume migrates through the soil profile. The concentrations at year 0 are essentially zero. At 10 years the plume can be seen migrating through the soil profile. The tail end, however, is not reduced to 0, but is at a steady state equilibrium value.

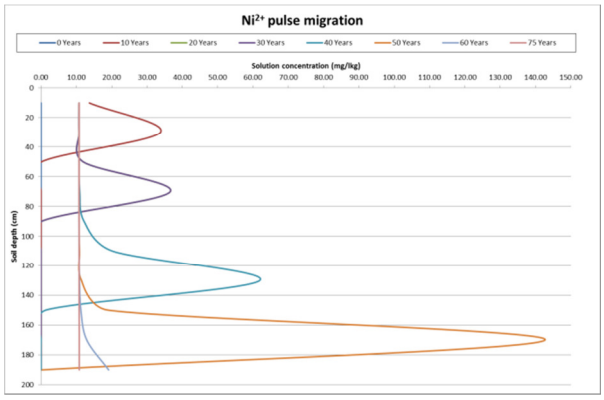

Figure 7-6 Ni breakthrough curves

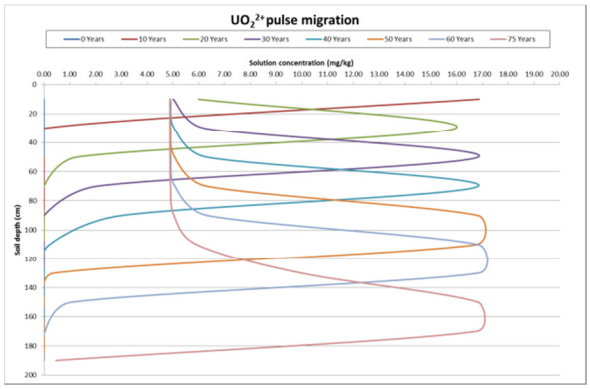

Figure 7-9 U breakthrough curves

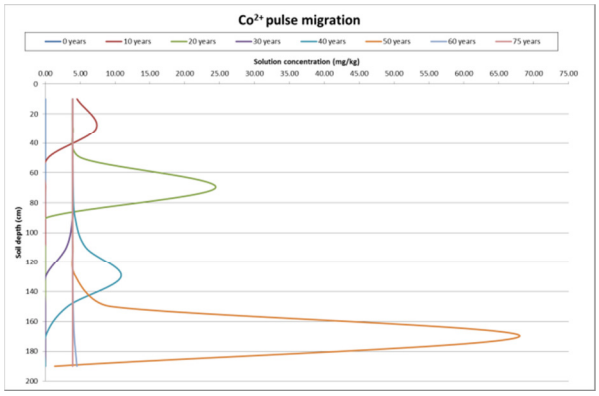

Figure 7-7 Co breakthrough curves

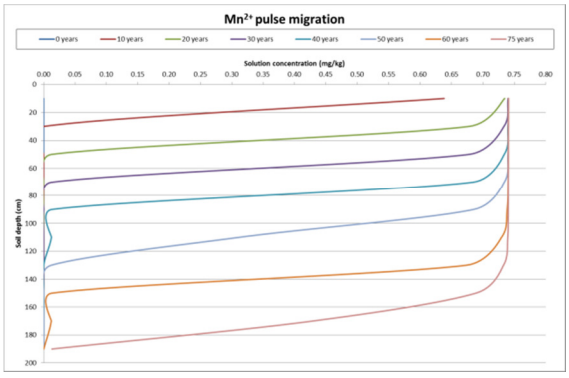

Figure 7-10 Mn breakthrough curves

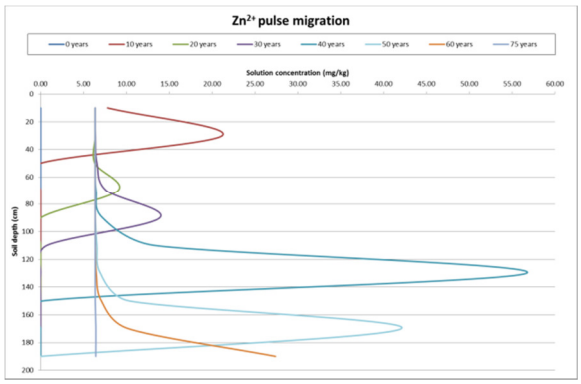

Figure 7-8 Zn breakthrough curves

Table 7-27 Results of soil adsorption model of leachate at the base of the soil profile after 75 years of simulation.

	Base Case	
Time to first breakthrough (years)	49.9	
Time to last breakthrough (years)	69.3	
pH	3.99	
TDS (mg/kg)	19 470	
Eh (V)	0.98	
	Adsorbed (mg/kg)	**In solution (mg/kg)**
Fe^{2+}	n.a.[23]	5 869
Fe^{3+}	n.a	0.00
SO_4	10 000	13 190
Mn	0.00	0.01
Co	0.01	3.92
Ni	0.13	10.79
Zn	0.24	6.42
Al	0.00	181
UO_2^{2+}	59.61	0.47

The breakthrough curves show that after the simulation period of 75 years, the pulse has migrated through the soil profile and metals leach from the soil at concentrations elevated in comparison to original background values. If a fresh pulse migrates through the system, the values will increase again. The model shows that mitigation by natural attenuation of the soil, even after removal of the tailings facility is unlikely, as the elevated concentrations persist for many years after the pulse migrated through the system.

The U breakthrough curves (Figure 7-9) show that U follows the same trend as Co, Ni and Zn. The effect of the pulse can be seen in the AMD solution after 10 years throughout the simulation as the pulse migrates through the soil profile. The tail end of the pulse reaches a new steady state equilibrium at higher U concentrations than background. The model shows that after 75 years the U pulse has not migrated entirely through the soil profile and values can be expected to increase with time, until a new steady state equilibrium is reached at ~5 mg/kg. The model indicates that a hydroxyl-sulphate of U [$UO_2SO_4.3H_2O$] precipitates and buffers the solution concentrations of U. This indicates that the U mobility is influenced by adsorption and precipitation processes. This is most probably the reason that the U pulse migrates slower than the Co, Ni and Zn pulse. The mobility of U in the ERB soils below tailings is therefore higher than for Co, Ni and Zn.

[23] Not applicable. The Fe^{2+}-Fe^{3+} redox pair is decoupled for the adsorption model and ferric hydroxide is used as the adsorbate.

The Mn breakthrough curves (Figure 7-10) show that Mn follows the same trend as U. An important difference is that the tail end of the U pulse reaches an equilibrium with the system at a maximum Mn concentration of ~0.75 mg/kg. The Mn pulse has not reached the base of the soil profile by year 75 of the simulation. The model indicates that pyrolusite [MnO_2] buffers the solution Mn concentration, thereby decreasing the mobility of Mn.

Breakthrough curves of pH (Figure 7-11) show that the pH starts off at alkaline conditions (7.85) and that by 60 years the solution at the base of the soil profile is 4.95 and by the end of the simulation time the pH is 3.99. This shows that the acid plume migrates through the soil profile by the end of the 75 year simulation time. This pH value correlates with the reclaimed tailings soil footprint data of Rösner et al. (2001).

The model also takes changes in porosity into account as precipitation and dissolution occurs throughout the simulation (Figure 7-12). The results show that the model starts with an average soil porosity of 0.37. Changes in this value can be seen after 10 years of simulation as precipitation of secondary minerals occur and the porosity decreases. This trend continues until the end of the simulation, with the porosity increasing at the tail of the breakthrough curves, due to partial mineral dissolution, although the porosity does not reach the original input value. The change in porosity is not great (maximum of 1%), but it does show how geochemical processes affect the physical parameters of the medium through which the plume migrates. These small changes may have significant implications the system, as has been shown from other studies on dynamical systems in other scientific fields (Gleick, 2011).

Permeability also changes with simulation time (Figure 7-13). The trend is identical to the porosity changes and show that the 2 parameters are linked. However, the maximum change is higher for the permeability (16%) than for porosity. The permeability can be seen to start recovering and after 75 years of simulation the permeability of the top of the soil profile has reached 95% of its original value. This equilibrium is expected to be maintained, until a new pulse migrates through the soil profile.

The minerals that precipitate from the solution throughout the simulation are goethite, gibbsite, alunite, pyrolusite, ferrous hydroxide, siderite and hydrous uranium sulphate. These minerals buffer solution concentrations of their respective components. The measure to which they buffer the components depend on the equilibrium solubility relationships of these minerals to the fluid from which they precipitate. In the ERB soil adsorption model precipitation and dissolution are proportionally much less important than the adsorption in controlling metal concentrations. This implies that the ERB soil, through the process of adsorption, plays an important role in retarding pollution plumes migrating to the shallow groundwater system.

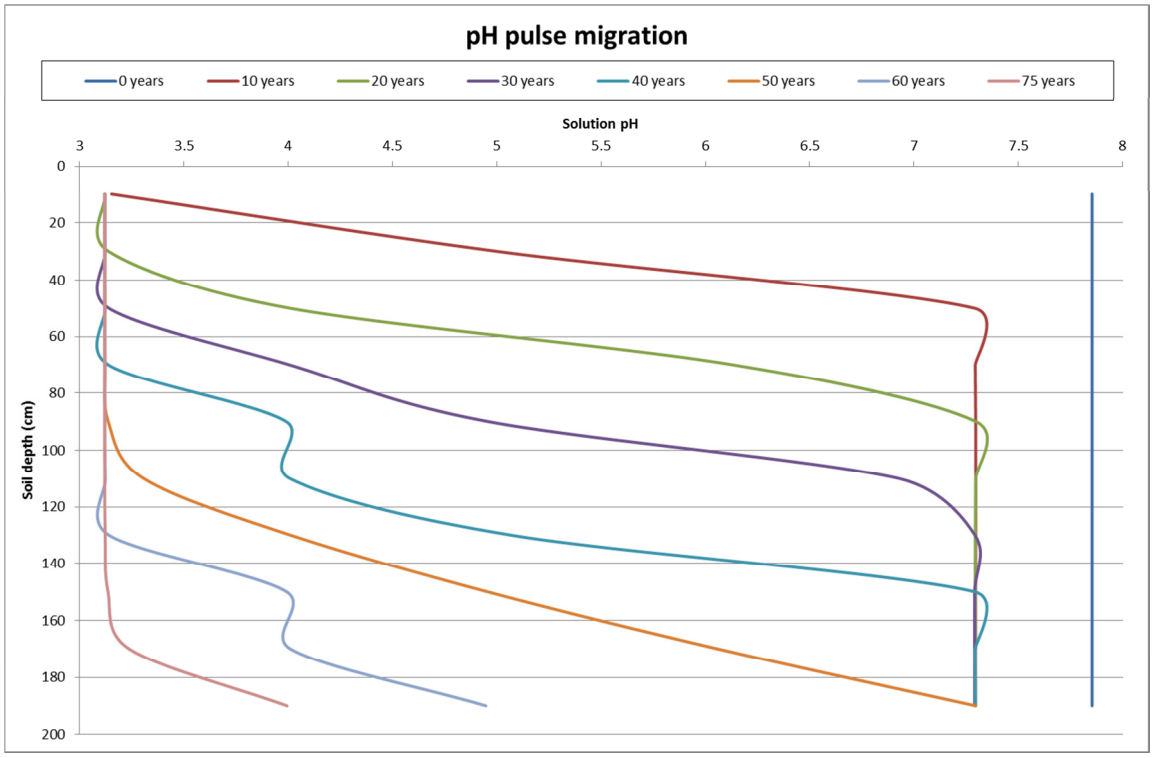

Figure 7-11 pH breakthrough curves

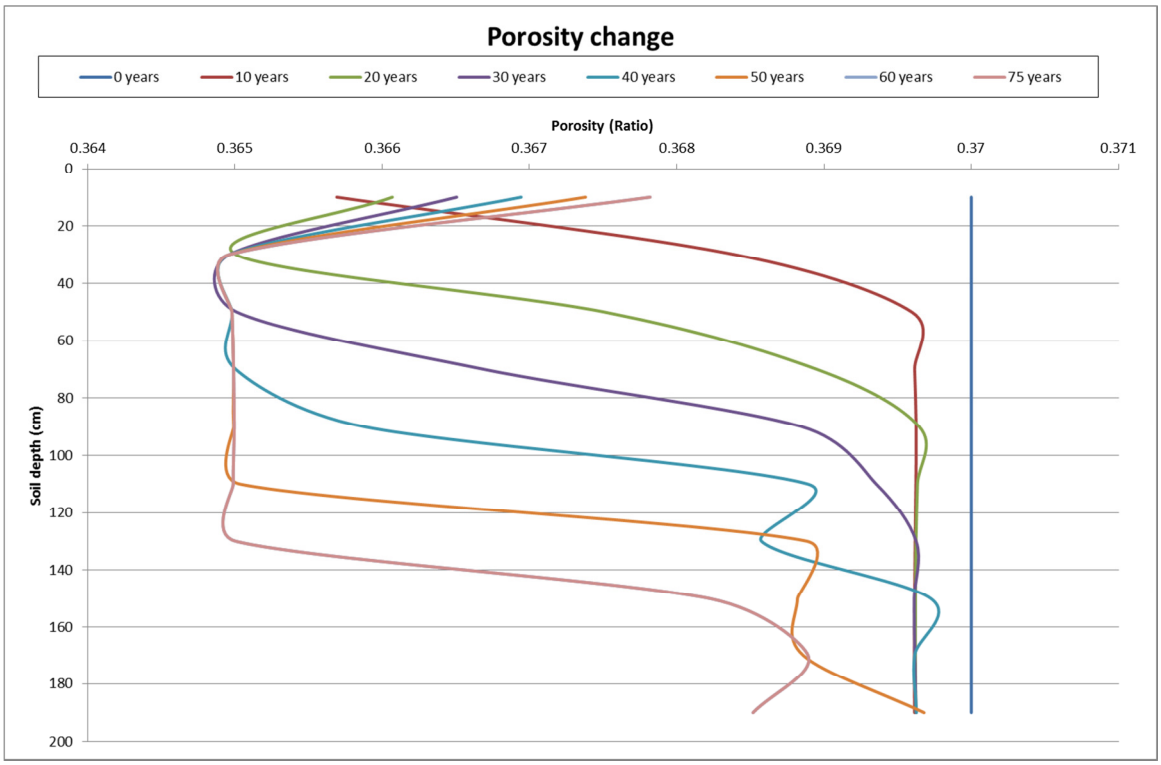

Figure 7-12 Porosity time over simulation time and distance

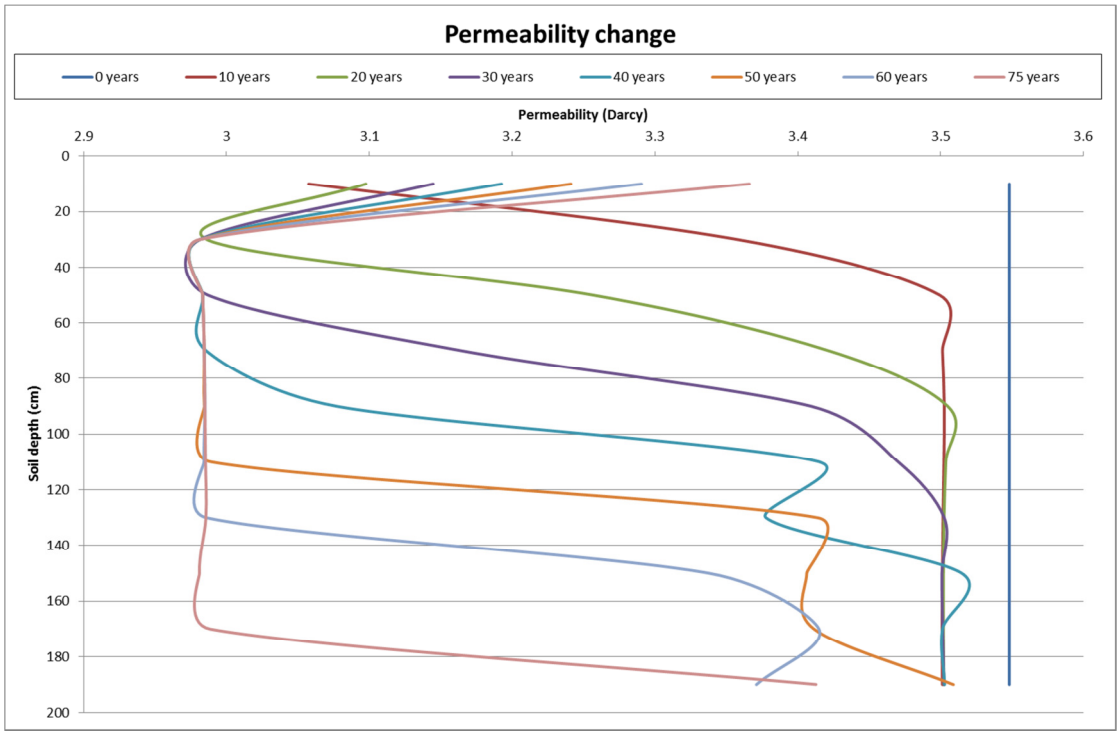

Figure 7-13 Permeability changes with simulation time

7.5 Tailings toe seepage model

Leachate does not just seep vertically through the tailings and the soil to the shallow groundwater system. Water also seeps from the base of the tailings due to the vertical hydraulic conductivity difference between the soil ($5x10^{-4}$ $m.day^{-1}$) (Africa Geo-Environmental Services (Pty) Ltd., 2006; Rösner et al., 2001) and the tailings (1 – 0.01 $m.day^{-1}$) (Bezuidenhout and Rousseau, 2005). This toe seepage interacts with the surface water environment. It can mix with various surface water sources as well as evaporate, to leave efflorescent salts behind, which can be dissolved upon the first rains in the rainy season, causing a pulse of acidic, metal laden water into the surface water systems (Alpers et al. 1994).

A total of 18% of tailings dams in the ERB representing 60% of the tailings facility surface area lie partially or totally on a dolomite substratum. This indicates that although the majority of tailings are not located on dolomite, the large ones in the ERB are.

The toe seepage from the facilities located on dolomite can be expected to interact with carbonate material, before it reaches the tributaries of streams, rivers and wetlands. There are thus 2 important processes influencing the geochemistry of toe seepage from tailings. The first is where toe seepage first encounters carbonate upon seepage from the tailings. The second is is dilution by the wetland surface water. Two models are develop to understand these two processes. Another scenario is where no carbonate is present and the toe seepage directly flows into the surface water system and is diluted.

Evaporation is also a potentially important factor, especially in the dry season. Therefore evaporation scenarios are run on each of the models. The leachate from the Post-Operational Phase is used to develop

these models. The leachate from the Post-operational phase is the worst quality and is expected therefore to have the most impact on ERB environmental component systems.

In this instance the mixing ratio between tailings toe seepage and surface water is unknown. Therefore existing results of the Blesbokspruit are used to determine this ratio.

7.5.1 Assumptions

7.5.1.1 Equilibrium with atmosphere

The O_2 fugacity is slid to negligible values in the pyrite oxidation models. The assumption is made that when leachate seeps from the base of the tailings facility, it reaches equilibrium with the atmosphere in terms of dissolved O_2 content. This is not expected to occur instantaneously. Therefore the O_2 fugacity is slid to the atmospheric value of 0.21. This is expected to be a reasonable assumption and is evaluated in the sensitivity analysis.

7.5.1.2 Amount of dolomite reacted

In essence, the amount of dolomite in the system available for reaction is infinite in relation to the toe seepage from the tailings. However, the model does not converge when very high amounts of dolomite are added to the system and carbonate minerals are forced to precipitate, which is unlikely in an acidic environment. Therefore, an amount of 500 g is added to the system and a sensitivity analysis conducted on varying amounts to determine the model sensitivity to the amount of dolomite in the model system.

7.5.1.3 Toe seepage

The assumption is made that the toe seepage flows directly to the surface water system and that the only interaction is with a carbonate sub-stratum. This is not necessarily the case, as toe seepage can seep into the soil and report to the shallow groundwater table. However, the surface water streams in the ERB do receive groundwater (Africa Geo-Environmental Services (Pty) Ltd., 2006). The soil adsorption model has shown that metals are removed from solution for a time, but that SO_4 and Fe remain elevated and the pH remains low. Therefore the assumption allows for a conservative assessment with and error probably lower than the uncertainties in the models.

7.5.2 Uncertainties

7.5.2.1 Calculated mixing ratio

The results of the Post-Operational phase pyrite oxidation model is used to determine the mixing ratio for interaction between the toe seepage leachate from tailings and wetland stream water. The sulphate concentration and pH is used to select a sample from the Blesbokspruit water chemical data to represent a pristine water sample. The leachate from the tailings is mixed with the water sample to determine the mixing ratio.

The uncertainty associated with the mixing ratio calculation is related to the spatial and temporal variation associated with the Blesbokspruit water chemical data as well as the spatial and temporal variation of tailings toe seepage volumes interacting with ERB surface water systems.

The purpose of calculating a mixing ratio is to get an idea of the ratio of volumes between surface water flow and toe seepage in the ERB. Secondly it is used as a standard to compare the effects of leachate interaction with carbonate, prior to mixing with surface water. For these purposes the calculated ratio can be used and the uncertainty associated with the ratio is acceptable, although the exact ratios can be calculated using tracer studies, but this is beyond the scope of the current study.

The calculated mixing ratio is of toe seepage volume to surface water volume is 3.5×10^{-4}.

7.5.3 Sensitivity analysis

The results of the mixing models are used to run the sensitivity analyses.

7.5.3.1 Equilibrium with the atmosphere

A sensitivity analysis was conducted on the carbonate and non-carbonate Blesbokspruit mixing models to evaluate model sensitivity to changes in oxygen fugacity (Table 7-28).

Table 7-28 Results of sensitivity analysis on oxygen fugacity.

		Carbonate Scenario		Non-Carbonate Scenario	
	Units	**Base Case**	**Ogygen fugacity lower (0.01)**	**Base Case**	**Ogygen fugacity lower (0.01)**
pH		6.56	6.56	5.53	5.53
TDS	*mg/kg*	570	559	673	663
Eh	*V*	0.85	0.83	0.91	0.89
Ca	*mg/kg*	35.15	35.15	34.21	34.21
Mg	*mg/kg*	11.20	11.20	10.50	10.50
K	*mg/kg*	12.71	12.71	13.24	13.24
Na	*mg/kg*	85.05	85.05	85.03	85.04
Mn	*mg/kg*	0.02	0.02	0.06	0.06
Ni	*mg/kg*	0.12	0.12	0.12	0.12
U	*mg/kg*	0.02	0.02	0.03	0.03
Fe	*mg/kg*	0.10	0.10	38.56	38.56
Al	*mg/kg*	0.00	0.00	1.40	1.40
SO_4	*mg/kg*	82.65	82.65	226	226
HCO_3	*mg/kg*	155	155	20.97	20.97

The results show that the models for both scenarios are insensitive to changes in oxygen fugacity.

7.5.3.2 Amount of dolomite reacted

A sensitivity analysis was conducted to evaluate the carbonate toe leachate model to changes in the amount of dolomite in the system (Table 7-29).

The results show that the model is sensitive to the amount of dolomite in the system. In the actual natural system, the amount of dolomite, if it forms a substratum to the tailings, is essentially a continuous unlimited source. However, the results of the sensitivity analysis show that when the dolomite amount is set to 2 500 g, too much carbonate remains dissolved in the resultant water and carbonate minerals become saturated and precipitate in large amounts. This is plausible if one is dissolved and others precipitate, but the model shows that dolomite precipitates, as the whole amount of dolomite input into the system is forced to dissolve. When the dolomite amount is set too low, the pH remains too low and no buffering takes place. Therefore the amount of 500 g is optimum to balance acid neutralisation effects and oversaturation of carbonate.

Table 7-29 Results of a sensitivity analysis on the carbonate toe seepage scenario.

		Carbonate Scenario		
	Units	**Base Case**	**Dolomite lower (100 g)**	**Dolomite higher (2 500 g)**
pH		5.01	1.21	8.88
TDS	*mg/kg*	131 673	249 338	599 853
Eh	*V*	0.92	1.15	0.69
Ca	*mg/kg*	1 672	382	207 600
Mg	*mg/kg*	2 538	11 240	0.16
K	*mg/kg*	10.51	9.16	469
Na	*mg/kg*	0.97	0.77	0.47
Mn	*mg/kg*	0.00	58.38	0.00
Ni	*mg/kg*	127	100	62.05
U	*mg/kg*	0.25	0.19	0.12
Fe	*mg/kg*	0.00	35 460	0.00
Al	*mg/kg*	0.06	1 972	0.07
SO_4	*mg/kg*	4 488	54 330	466
HCO_3	*mg/kg*	12 407	0.70	642 200

More detailed studies into the amount of dolomite that goes into solution would be beneficial, although this is beyond the scope of this study.

The sensitivity analysis also shows that the amount of dolomite in the system has a direct influence on the concentration of contaminants in solution, due to the buffering capacity in terms of pH control.

7.5.4 Model results

7.5.4.1 Dolomite scenario

The toe seepage model results (Table 7-30) show that reaction with the dolomite increase the pH significantly. Iron and Al concentrations are significantly lower compared to the pyrite oxidation model results, while Ni and SO_4 concentrations remain elevated. Bicarbonate concentrations are high, perhaps too high, due to the significant amount of dolomite dissolution.

The most important minerals in terms of mass that precipitate as a result of the interaction between the toe seepage and dolomite (Table 7-31) are gypsum, magnesite, goethite and alunite, with lesser amounts of gibbsite, pyrolusite and uranophane. Although alunite is shown by the model to fomr, it may not, as the alunite-jarosite series is stable at pH < 3. It is more likely that a range of Fe and Al hydrous sulphates will form.

Table 7-30 Toe seepage model results.

	Units	Base Case
pH		5.01
TDS	*mg/kg*	131 673
Eh	*V*	0.92
Ca	*mg/kg*	1 672
Mg	*mg/kg*	2 538
K	*mg/kg*	10.51
Na	*mg/kg*	0.97
Mn	*mg/kg*	0.00
Ni	*mg/kg*	127
U	*mg/kg*	0.25
Fe	*mg/kg*	0.00
Al	*mg/kg*	0.06
SO_4	*mg/kg*	4 488
HCO_3	*mg/kg*	12 408

Table 7-31 Mineralogical results of the toe seepage carbonate model. Three significant figures are shown to be able to report on the low concentration of pyrolusite and uranophane.

	Concentration (wt%)
Alunite	1.269
Gibbsite	0.195
Goethite	13.755
Gypsum	57.004
Magnesite	27.759
Pyrolusite	0.015
Uranophane	0.004

The mixing model results (Table 7-32) show that dilution causes the pH to rise to 6.56 and HCO_3 has a final concentration of 155 mg/kg, which occurs in the range of values for the Blesbokspruit surface water data. This implies that precipitation and dilution are important factors in controlling contaminant concentrations in the ERB surface water environment, corroborating the Roychoudgury and Starke (2006) results.

Table 7-32 Solution results of the carbonate mixing scenario.

	Units	Base Case
pH		6.70
TDS	*mg/kg*	544
Eh	*V*	0.84
Ca	*mg/kg*	34.82
Mg	*mg/kg*	10.68
K	*mg/kg*	12.71
Na	*mg/kg*	85.07
Mn	*mg/kg*	0.00
Ni	*mg/kg*	0.09
U	*mg/kg*	0.00
Fe	*mg/kg*	0.00
Al	*mg/kg*	0.00
SO_4	*mg/kg*	41.57
HCO_3	*mg/kg*	156.46

7.5.4.2 Silicate scenario

The solution results for the non-carbonate toe seepage mixing model (Table 7-33) shows that although the pH is increased in comparison to the pyrite oxidation model results, it is lower than for the carbonate scenario.

The contaminant concentrations decrease significantly. Small amounts (< 0.05 g) of goethite, pyrolusite, gibbsite and uranophane precipitate from solution.

The results of both the carbonate and non-carbonate mixing models show how, after 100 years of mining. Roychoudhury and Starke (2006) found that pollution of the Blesbokspruit is low to moderate from an eco-toxicological perspective. Dilution and precipitation, with dilution playing the most significant role, is buffering pollution concentration of inorganic contaminants in the surface water environment. This implies that the greatest risk from tailings seepage is soil and shallow and deep groundwater contamination.

Table 7-33 Results for the non-carbonate toe seepage mixing scenario.

	Units	Base Case
pH		5.88
TDS	*mg/kg*	553
Eh	*V*	0.88
Ca	*mg/kg*	34.22
Mg	*mg/kg*	10.24
K	*mg/kg*	13.05
Na	*mg/kg*	85.06
Mn	*mg/kg*	0.00
Ni	*mg/kg*	0.09
U	*mg/kg*	0.00
Fe	*mg/kg*	0.00
Al	*mg/kg*	0.00
SO_4	*mg/kg*	173
HCO_3	*mg/kg*	41.64

7.6 Evaporation model

Evaporation models of the Operational and Post-Operational Phase leachate were developed to determine the likely secondary salts to form and be re-dissolved upon the onset of the rainy season. This phenomenon has been termed a “fist-flush” event (Dold and Fontbote, 2001).

7.6.1 Assumptions

7.6.1.1 Evaporation is complete

The assumption is made that all the toe seepage evaporates. The assumption may hold in the peak dry season, but may not hold for most of the year. The purpose of the model is to determine the likely salts to form, so for this purpose the assumption is reasonable. The assumption is evaluated during a sensitivity analysis.

7.6.2 Uncertainty

7.6.2.1 Activity coefficients

The main uncertainty in the evaporation models is related to the activity coefficients for the evaporating solution. The thermodynamic database of Geochgemist's Workbench® employs the Debye-Hückel activity model, which becomes inaccurate at moderate ionic strengths (> 0.1 molal). The software has a database which uses virial methods, such as the Pitzer equations, but the data base has data for many fewer solution species, compared to the database employing the Debye-Hückel model. Therefore the Debye-Huckel model is used in the calculations due to the complexity of the ERB pyrite oxidation model. The ionic strength is however much larger than 0.1 molal for both the Operational Phase (0.45) and Post-Closure Phase (22 813) evaporated leachate solutions. The error is larger for the Post-Closure Phase solution. The error is expected to be small relative to the concentration of dissolved QOI and is therefore used in the evaporation model, as the purpose is to provide an estimate of the potential efflorescent salt to form from evaporating AMD and the results will not be used in any follow-up modelling.

7.6.3 Sensitivity analysis

7.6.3.1 Evaporation amount

The sensitivity of the model to the amount of water that evaporate is evaluated using the Post-Closure pyrite oxidation results (Table 7-34).

Table 7-34 Results of sensitivity analysis on the amount of seepage water evaporated.

	Units	Base Case	50% Evaporation
pH		-1.41	0.45
TDS	*mg/kg*	999 738	414 255
Eh	*V*	0.83	0.94
Ca	*mg/kg*	0.00	0.00
Mg	*mg/kg*	17.77	1 601.00
K	*mg/kg*	0.18	1 183.00
Na	*mg/kg*	2.97	1.20
Mn	*mg/kg*	226	91.20
Ni	*mg/kg*	21.27	157
U	*mg/kg*	0.64	17.73
Fe	*mg/kg*	210 900	84 760
Al	*mg/kg*	7 667	3 081
SO_4	*mg/kg*	776 813	321 750
HCO_3	*mg/kg*	0.00	0.00

The analysis shows that the model is sensitive to the amount of water that evaporates when the seepage flows from the toe of the tailings dam. When amounts < 99% of water evaporates, the concentration of dissolved components is higher, due to the lack of precipitation. This is illustrated in Figure 7-14, which shows that component concentrations decrease only after 99.98% of seepage water has been evaporated. This indicates that evaporation only increases the concentrations of dissolved components in seepage water. This illustrates why surface water salt loads are higher in the dry season, when evaporation exceeds precipitation. It is not only that water evaporates from surface water bodies, but also that they are receiving more concentrated seepage solutions.

7.6.4 Model results

7.6.4.1 Carbonate scenario

This scenario represents toe seepage that first comes into contact with carbonate and reacts, before it is evaporated. The solution results (Table 7-35) show that what remains after most of the water has evaporated, is a brine characterised by low pH and high salt loads. The concentrations of K, Mn, Fe, Al and SO4 are buffered by mineral precipitation (Table 7-36).

Uranium concentrations are excessive. This is due to the formation of a $UO_2(CO_3)_3^{4-}$ complex, which keeps the U in solution. This shows that although carbonate may decrease pH and the concentration of some contaminants, U concentrations may be increased to the U complexation with carbonate.

The mineralogical results (Table 7-36) show that a variety of sulphate and carbonate salts form. These salts are soluble, and can re-dissolve at the onset of the rainy season. This has been observed in studies on AMD (Dold and Fontbote, 2001; Moncur et al., 2009; Alpers et al., 1994).

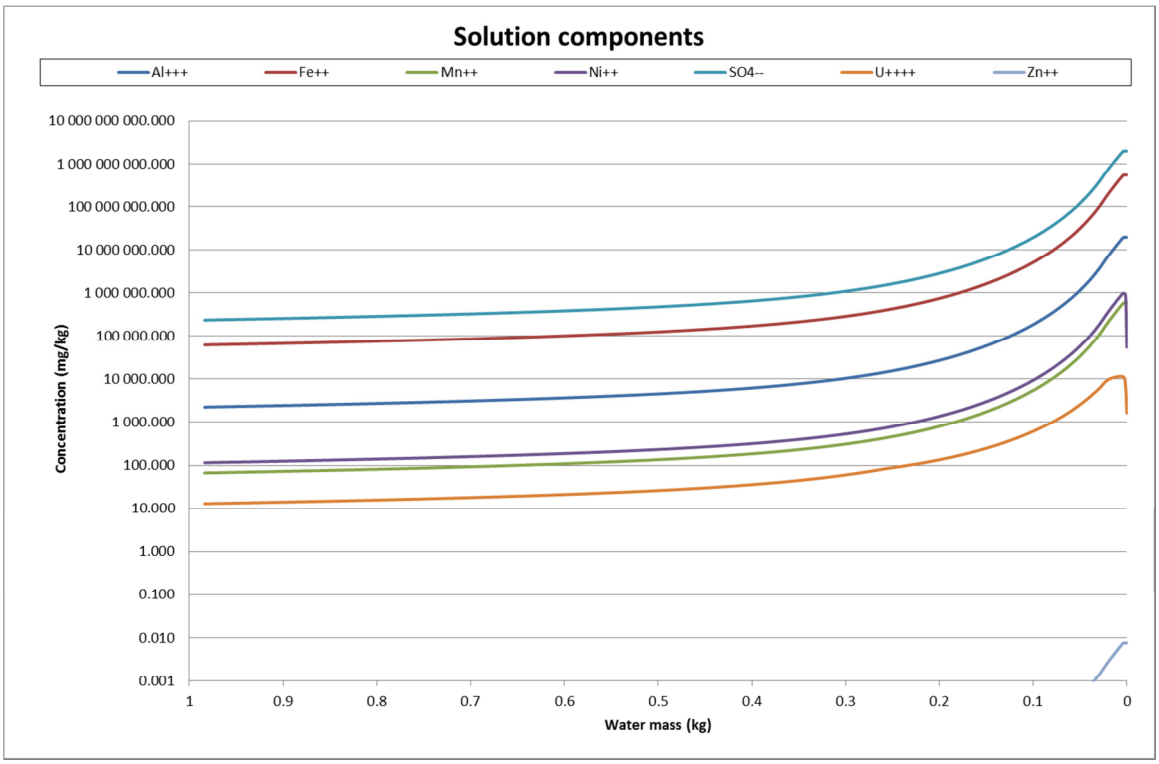

Figure 7-14 Graph showing increase in component concentration with decrease in water mass. The concentration of dissolved constituents dramatically increases after > 99% of the water has evaporated.

Table 7-35 Evaporation model results for the carbonate scenario.

	Units	Base Case
pH		3.34
TDS	*mg/kg*	999 899
Eh	*V*	1.10
Ca	*mg/kg*	496
Mg	*mg/kg*	4.44
K	*mg/kg*	0.08
Na	*mg/kg*	0.12
Mn	*mg/kg*	0.00
Ni	*mg/kg*	387
U	*mg/kg*	4 800
Fe	*mg/kg*	0.00
Al	*mg/kg*	0.01
SO_4	*mg/kg*	23.91
HCO_3	*mg/kg*	2 493

Table 7-36 Mineralogical results of the evaporation model carbonate scenario.

Minerals in system	Concentration (wt%)
Alunite	0.4
Dawsonite	0.1
Gypsum	35.6
Kalicinite	0.2
Magnesite	45.1
Hydrous nickel sulphate	1.9
Pyrolusite	0.0
Rutherfordine	4.3
Uranophane	12.6

7.6.4.2 Non-Carbonate scenario

The solution results of the non-carbonate scenario (Table 7-37) shows that what remains after most water has been evaporated is a brine with pH below 0 and excessive Mn, Fe, Al, Ni and SO4 concentrations. The mineralogical results (Table 7-38) show that although some sulphate salts precipitate, they are not sufficient to significantly lower the concentrations of most dissolved constituents. This indicates that in the carbonate scenario, metals and SO_4 are removed from solution upon the reaction of toe seepage with carbonate minerals and evaporation of the resultant seepage solution is a solution with significantly lower concentrations of metals and SO_4 than the solution could not react with carbonate. The exception is U, which has been shown to be much higher in carbonate solutions than non-carbonate solutions.

Table 7-37 Solution results of the non-carbonate evaporation model.

	Units	Base Case
pH		-1.41
TDS	*mg/kg*	999 739
Eh	*V*	0.83
Ca	*mg/kg*	0.00
Mg	*mg/kg*	17.76
K	*mg/kg*	0.18
Na	*mg/kg*	2.97
Mn	*mg/kg*	227
Ni	*mg/kg*	21.26
U	*mg/kg*	0.64
Fe	*mg/kg*	210 900
Al	*mg/kg*	7 667
SO_4	*mg/kg*	259 300
HCO_3	*mg/kg*	0.00

Table 7-38 Mineralogical results of the non-carbonate evaporation model

Minerals in system	Concentration (wt%)
Epsomite	77.0
Mercallite	19.6
Hydrous nickel sulphate	3.2
Hydrous uranium sulphate	0.2

7.7 Weathering model

A weathering model is developed to determine the characteristics of background groundwater to get an idea of pre-mining groundwater quality. The main aquifers with respect to ERB groundwater contamination are the shallow and deep groundwater aquifers. The shallow groundwater is located mostly in the rocks of the Karoo Supergroup and the deep aquifer mostly with the rocks of the Witwatersrand Supergroup. Therefore two scenarios are developed to reflect these two groundwater compositions.

7.7.1 Assumptions

7.7.1.1 Steady state

An assumption of system steady state is made. This assumption implies that no catastrophic or gradual changes occurred over the time of simulation which could cause the system to migrate towards a new equilibrium state and that the current system state can be traced back in time to at least 1 000 years. This assumption is deemed reasonable for the purpose of the model which is to get an idea of the background water that could form when in contact with the regional ERB geology during the Recent geological past (< 10 000 a).

7.7.1.2 Oxygen fugacity

The pre-mining groundwater oxygen fugacity is unknown. There is most probably a small amount of oxygen entering the groundwater system from recharge zones. A fugacity of 0.1 (~50% atmospheric levels) is assumed and evaluated during a sensitivity analysis.

7.7.2 Uncertainty

7.7.2.1 Dolomite

Uncertainty can be introduced in the model due to the fact that the rock of the Malmani dolomites is not taken into account. Small amounts of dolomite are added to both the Karoo and Witwatersrand models to account for influence from the dolomite groundwater. Dolomite introduces Ca, Mg and HCO_3 ions to solution

and has the ability to buffer acidic solutions. The effect of dolomite on the Karoo and Witwatersrand groundwater will be evaluated in a sensitivity analysis.

The uncertainty is expected to be limited, as previous work has shown that the dolomite aquifer is separated from at least the deep Witwatersrand aquifer (Africa Geo-Environmental Services (Pty) Ltd., 2006).

7.7.2.2 Water-rock ratio

The water-rock ratio is a source of uncertainty. The amount of water in contact with the rock mass is not known prior to mining. The effect of the water-rock ratio is evaluated in a sensitivity analysis.

7.7.2.3 Oxygen fugacity

The oxygen fugacity of especially the deep groundwater prior to mining is uncertain. Therefore a sensitivity analysis is conducted to determine the model sensitivity to the amount of oxygen in the system.

7.7.3 Sensitivity analysis

7.7.3.1 Amount of dolomite

The Witwatersrand weathering model is used to conduct the sensitivity analysis. The results (Table 7-39) show that the model is not significantly sensitive to changes in the amount of dolomite in the system. Calcium, Mg and HCO_3 concentrations change slightly.

Table 7-39 Results of a sensitivity analysis on the amount of dolomite in the system

	Units	Base Case	More Dolomite (1 wt%)	Less Dolomite (0.01 wt%)
pH		8.20	8.02	8.19
TDS	*mg/kg*	36.00	92.00	28.00
Eh	*V*	0.73	0.74	0.73
Ca	*mg/kg*	3.15	11.88	1.20
Mg	*mg/kg*	2.22	5.50	2.22
K	*mg/kg*	0.67	1.04	0.68
Na	*mg/kg*	0.00	0.00	0.00
U	*mg/kg*	0.00	0.00	0.00
Fe	*mg/kg*	0.00	0.00	0.00
Al	*mg/kg*	0.02	0.01	0.02
SO_4	*mg/kg*	8.84	8.84	8.84
HCO_3	*mg/kg*	10.06	52.86	4.25

7.7.3.2 Water-rock ratio

The sensitivity analysis on the water-rock ratio (Table 7-40) showed similar results as the dolomite analysis. The model is not significantly sensitive to changes in water-rock ratio and Ca, Mg and HCO_3 concentrations

vary slightly. The analysis showed that the lower ratio (1:100) produced slightly better results in that pH, TDS and HCO_3 concentrations are closer to underground samples with lower SO_4 content and could therefore be considered as closer to background. The ratio of 1:100 is therefore used in the model.

Table 7-40 Results of a sensitivity analysis on the water-rock ratio

	Units	Base Case	Higher ratio (1:100)	Lower ratio (1:1)
pH		8.20	7.75	8.51
TDS	*mg/kg*	36.00	191.00	18.00
Eh	*V*	0.73	0.76	0.71
Ca	*mg/kg*	3.15	16.94	1.04
Mg	*mg/kg*	2.22	21.63	0.49
K	*mg/kg*	0.67	1.97	0.32
Na	*mg/kg*	0.00	0.00	0.00
U	*mg/kg*	0.00	0.00	0.00
Fe	*mg/kg*	0.00	0.00	0.00
Al	*mg/kg*	0.02	0.01	0.03
SO_4	*mg/kg*	8.84	88.53	0.88
HCO_3	*mg/kg*	10.06	49.60	4.26

7.7.3.3 Oxygen fugacity

A sensitivity analysis is conducted to determine the effect of changes of oxygen fugacity on the model. The results (Table 7-41) show that the model is insensitive to changes in oxygen fugacity.

Table 7-41 Results of a sensitivity analysis on oxygen fugacity changes.

	Units	Base Case	Oxygen fugacity higher (0.21)	Oxygen fugacity lower (0.01)
pH		8.20	8.20	8.20
TDS	*mg/kg*	36.00	40.00	32.00
Eh	*V*	0.73	0.73	0.71
Ca	*mg/kg*	3.15	3.16	3.16
Mg	*mg/kg*	2.22	2.21	2.21
K	*mg/kg*	0.67	0.67	0.67
Na	*mg/kg*	0.00	0.00	0.00
U	*mg/kg*	0.00	0.00	0.00
Fe	*mg/kg*	0.00	0.00	0.00
Al	*mg/kg*	0.02	0.02	0.02
SO_4	*mg/kg*	8.84	8.84	8.84
HCO_3	*mg/kg*	10.06	10.06	10.06

7.7.4 Model results

7.7.4.1 Karoo

The Karoo modelling results covering a simulation time of 1 000 years are an alkaline solution with low dissolved solids and a Ca-HCO_3 water type (Table 7-42). The mineral that precipitates from solution is a clay mineral (Table 7-43). Specifically the solution has low SO_4 and low Al and Fe concentrations, showing that any increase of these values is due impact of a solution with elevated concentrations of these components. Nickel, Mn and Zn are not taken into account in the weathering models, as a background water sample could not be sourced. However, since these metals have been shown to be closely related to pyrite oxidation and AMD, it is expected that the concentration of these metals, like that of Fe, would be low.

Table 7-42 Solution results of Karoo weathering model.

	Units	Base Case
pH		8.84
TDS	*mg/kg*	26.00
Eh	*V*	0.69
Ca	*mg/kg*	3.05
Mg	*mg/kg*	0.10
K	*mg/kg*	1.36
Na	*mg/kg*	0.00
U	*mg/kg*	0.00
Fe	*mg/kg*	0.00
Al	*mg/kg*	0.07
SO_4	*mg/kg*	0.00
HCO_3	*mg/kg*	9.91

Table 7-43 Mineralogical results of the Karoo weathering model.

Mineral	Concentration (wt%)
Ca Saponite	100

7.7.4.2 Witwatersrand

Results of the Witwatersrand weathering model (Table 7-44) show similar results to the Karoo model, with a higher SO_4 concentration, due to the oxidation of sulphides. The results indicate that SO_4, Fe, Al and U concentrations are low, indicating that a significant increase in the concentrations of these constituents are due to secondary impacting activities.

The mineralogical results (Table 7-45) show that in addition to the smectite clay minerals, kaolinite and small amounts of uranophane precipitate.

Table 7-44 Solution results for the Witwatersrand weathering model.

	Units	Base Case
pH		8.24
TDS	*mg/kg*	25.00
Eh	*V*	0.73
Ca	*mg/kg*	1.19
Mg	*mg/kg*	1.78
K	*mg/kg*	0.61
Na	*mg/kg*	0.00
U	*mg/kg*	0.00
Fe	*mg/kg*	0.00
Al	*mg/kg*	0.02
SO_4	*mg/kg*	6.94
HCO_3	*mg/kg*	4.26

Table 7-45 Mineralogical results of the Witwatersrand weathering model.

Minerals	Concentration (wt%)
Kaolinite	51.6
Mg-Nontronite	26.5
Mg-Saponite	21.9
Uranophane	0.005

8 CHAPTER 8: A SYSTEMS GEOCHEMICAL MODEL OF THE EAST RAND BASIN

In this section the conceptual ERB systems model (Section 5) and numeric geochemical models of each component (Section 7) are integrated into a holistic numeric geochemical reaction process systems model incorporating uncertainty. The ERB numeric systems model is depicted graphically in Figure 8-1. The dynamic processes linking the components, which have been characterised in Sections 5 to 7 are numbered and will be discussed in this section.

8.1 Process 1

This process forms the link between the tailings facilities to the soils. AMD containing elevated concentrations of metals and SO_4, seeps from the tailings and into the soils. The soils are as much an interface between the shallow groundwater and AMD seepage from the tailings facilities as it is a medium itself being impacted on by the AMD solution. The soil contains illite, a clay mineral with adsorptive capacity. Therefore the ERB soils are capable of adsorbing contaminants from solution. However, the soils have a finite adsorptive capacity, implying temporal depletion of this capacity.

The soil adsorption model shows that after ~50 years the first breakthrough of the AMD pulse occurs. Final breakthrough occurs after ~69 years. The TDS of the final solution after 75 years of simulation is 19 470 mg/kg, which is a fraction (7.5%) of the input TDS of 258 038 mg/kg. This shows that after about 50 years the adsorption capacity of the soil starts to be depleted and the AMD pulse starts to migrate through the soil and starts impacting the shallow groundwater. These results correspond to those of Rösner et al. (2001) who showed firstly that significant amounts of contaminants leach from soils from reclaimed tailings sites and that groundwater beneath and in close proximity to these sites are contaminated. At the end of the simulated 75 years, the pH is 3.99, which also corresponds to the soils in the Rösner et al. (2001) study. The model indicates that the soil adsorption capacity was either completely depleted, or that the magnitude of depletion was sufficient that significant amounts of pollutants could migrate to the shallow groundwater. The main pollutants are Fe^{2+}, SO_4, Co, Ni, Zn, Al and U. The model showed that although significant amounts of SO_4 (10 000 mg/kg) are adsorbed by the soil, still larger amounts migrate in the solution through the soil (13 190 mg/kg). In general SO_4 is sometimes seen as a conservative ion (Bethke, 2008). However, for the ERB system, the elevated SO_4 concentrations in especially groundwater seem to be more a function of its abundance than of geochemical processes, such as adsorption and precipitation. Studies of SO_4 concentrations in solutions in the ERB should therefore not be assumed to be conservative, as the soil has been shown to be a significant source of SO_4, due to adsorption and precipitation in secondary sulpho-salts, even after tailings facilities have been reclaimed. The total SO_4 budget of the ERB is therefore not only in the AMD, groundwater and surface water solutions.

Uncertainty analysis showed that the model is sensitive to:

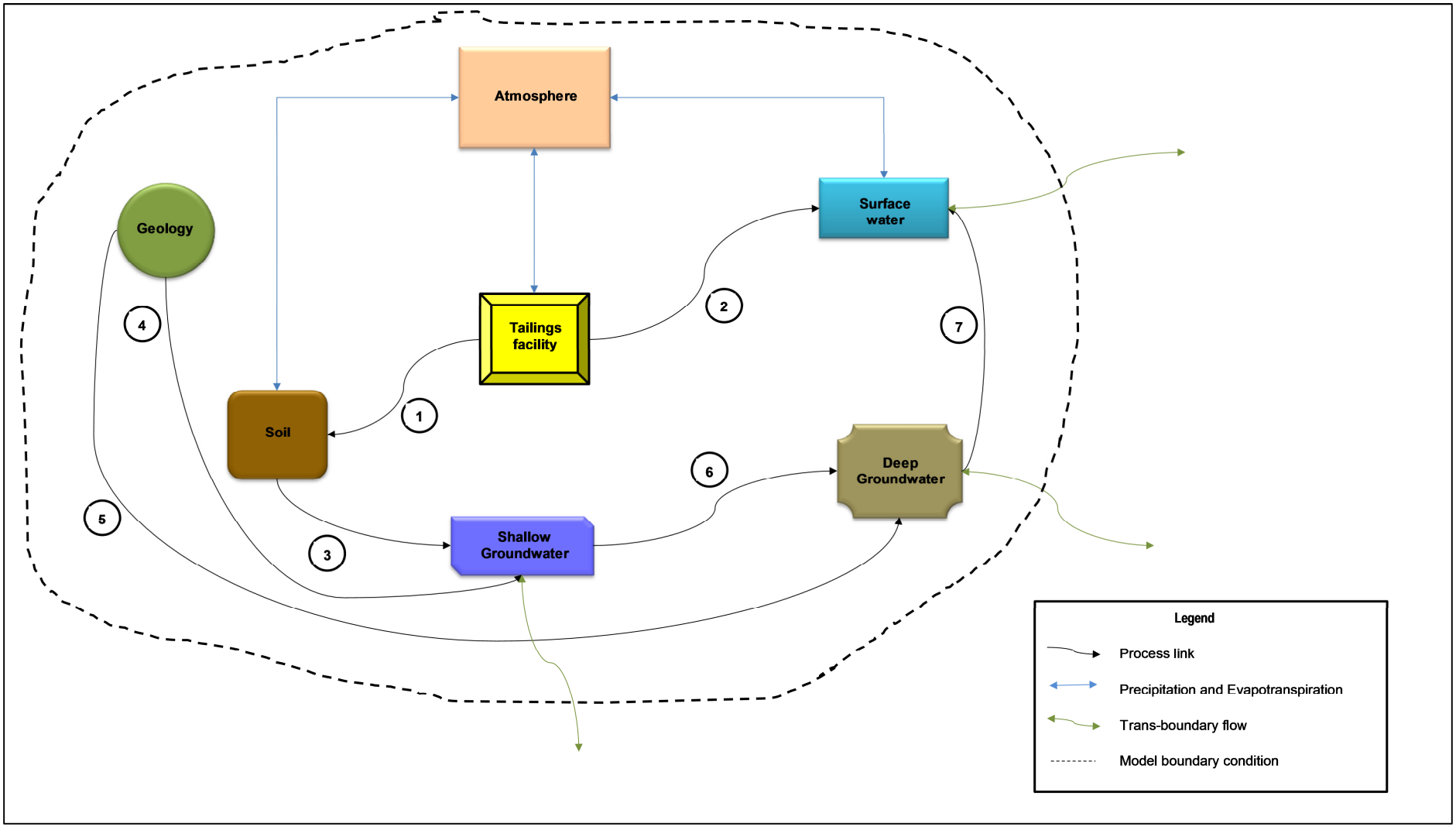

Figure 8-1 ERB systems model showing the system components and the process flows linking them. The various processes are discussed in the text.

- Soil depth
- Soil discharge values
- The clay content of the soil
- O_2 fugacity – only in terms of end solution U concentration

These parameters need to be constrained to reduce uncertainty to the soil adsorption model.

Although spatial geochemical data for the ERB soils are limited, geotechnical data varies from a minimum data variation of 12% for the soil porosity and a maximum of 294% for soil permeability with an average variability of 97%. This implies that the results can be expected to vary by 97% on average. Impact on the ERB soil is by introducing higher concentrations of pollutants into the soil than was previously present. The error in variation is therefore expected to be on the higher values.

8.2 Process 2

This process links the tailings facility with the surface water. This can occur in two ways: Firstly by the seepage of water from the toe of the tailings and secondly by the erosion of material from tailings facilities adjacent to stream drainage channels. The concentration of contaminants in the toe seepage is dependent on the measure of pyrite oxidation in the tailings and on the nature of the geologic substratum to the tailings. If the substratum is dolomitic, it has the capacity to buffer acidity and contaminant concentrations seeping from the tailings facilities. The dissolved mass of toe seepage in contact with dolomite prior to discharge into a surface water stream is 131 673 mg/kg compared to the Post-Closure seepage concentration of 258 038, which is twice that of the leachate in contact with carbonate. This implies significant dissolution of the carbonate minerals within the dolomitic rock[24]. In addition, the SO_4 content of the leachate in contact with dolomite prior to discharge into surface streams is 3.4% of the dissolved mass compared to 77.6% in a scenario where no dolomite is present. Dissolved HCO_3 and CO_2 makes up the bulk of the dissolved salt load in the scenario where dolomite is present, thereby adding to the buffer capacity of stream water, such as the Blesbokspruit.

Although the AMD solution in both the Operational and Post-Closure scenarios contain elevated concentrations of Fe, SO_4, Mn, Ni, Al and U, the surface water streams, especially the Blesbokspruit has sufficient water flow volumes to dilute the concentrations of these contaminants. These results correlate with those of Roychoudhury & Starke (2006), which showed the level of pollution of the Blesbokspruit to be low to moderate. Additional mixing models between toe seepage from tailings for carbonate and non-carbonate scenarios and Blesbokspruit stream water indicates that the mixing ratio between Blesbokspruit water and tailings seepage is ~3 000:1. A previous study (Vivier, 2012) has shown the Blesbokspruit flow volume to be 163.4 Mℓ/d. However, this study used a Grootvlei pumping volume of 85Mℓ/d. When the latest pumping rate of 108 Mℓ/d is used (Expert team to the inter-ministerial commission, 2010; Council for Geoscience

[24] These minerals are mostly dolomite [$CaMg(CO_3)_2$] and calcite [$CaCO_3$]

unpublished data[25]), a flow volume of 223 Mℓ/d is calculated. Using this volume a tailings seepage volume of 0.07 Mℓ/d (70 m^3/d) can be calculated analytically.

Analysis of uncertainty has shown that the numeric pyrite oxidation model is sensitive to:

- Reaction rates
- Mineral surface areas
- Water-rock ratios
- Measure of redox equilibrium of Fe redox pair
- Initial pyrite content of the tailings facility.

Analysis of spatial and temporal variation of existing surface water data has shown that the uncertainty for the QOI range from a minimum of 28% (pH) to a maximum of 2 485% (Ni) with an average of 318%. This implies that on average the model results for dissolved constituents can be expected to vary on average by 300% with pH varying in the order of 28%. Trends in analysed data (Section 5) show that a data distribution with elevated dissolved contaminants is influencing the background concentrations. Therefore the variation can be expected to be higher, rather than lower.

8.3 Process 3

This process links the soil with the shallow groundwater. The results of the numeric soil adsorption geochemical model are applicable to this process as well. The pre-mining condition is that water infiltrating through the soil is rain water, which recharges the shallow groundwater aquifer. As soon as a tailings facility is constructed with the soil as substrate and as soon as the AMD solution has percolated through the tailings and reaches the soil the soil adsorption processes begin to become active. Contaminants such as SO_4, Mn, U, Co, Ni, Zn, Al and Fe^{2+} are contained in the AMD seepage from the tailings facilities. These contaminants migrate through the soil, which contains adsorption capacity due to the presence of clay minerals, such as illite. When the adsorption capacity is depleted contaminates are dissolved into the shallow groundwater and forms a contamination plume. The adsorption model shows that SO_4 and Fe^{2+} concentrations remain elevated in the percolating AMD pulse and contaminates the shallow groundwater early in the simulation (< 10 years). Although significant concentrations of SO_4 are adsorbed by the soil particles, the concentrations in the AMD solution remain high (13 190 mg/kg). Therefore SO_4 is the first contaminate to impact on the shallow groundwater.

The geochemistry of U and Mn is complex. The mobility of both these metals is controlled by adsorption and precipitation reactions, of which adsorption is most probably the dominant process.

The uncertainty associated with this process is expected to the similar to Process 1, as the results are dependent on the same input data and uncertainties.

[25] Council for Geoscience, Strategic water management project

8.4 Process 4

This process links the geology with the shallow groundwater and is defined by the weathering reactions of the Karoo Supergroup rocks and its influence on the shallow groundwater dissolved mass. Weathering of the Karoo Supergroup geology produces a low TDS, alkaline solution with Ca and K as the main cations and HCO_3 as the dominant anion. The Al concentration is 0.07 mg/kg. The alkaline pH is due to the release of hydroxide from the weathering of K-feldspar. Although kaolinite could participate in dissolution reactions, it is more likely a secondary mineral resulting from the weathering of primary mineral, such as K-feldspar (Wilson, 2004). The end solution hydroxide concentration is 0.12 mg/kg. Sulphate and Fe have concentrations which would be below detection using the ICP-MS analytical method. This indicates that any detectable concentrations of Fe and SO_4 and a decrease in pH to below 7 would be the result of an incremental impact on the background groundwater solution. An AMD solution would be a prime candidate.

Influence of the dolomite was taken into account in the model by adding small amounts of dolomite to the mineralogy. The model was shown to be sensitive to changes in the amount of dolomite only in terms of Ca, Mg and HCO_3 concentrations. Smectite clay minerals are shown to precipitate from solution as secondary minerals.

8.5 Process 5

This process links the geology to the deep groundwater aquifer. Weathering of the rocks from the Witwatersrand Supergroup rocks produce an alkaline solution with low TDS (25 mg/kg). The major cations are Ca and Mg. The main anions are SO_4 (6.94 mg/kg) and HCO_3. Although SO_4 is in solution due to the presence of pyrite in the system, the concentration is low and Fe and U remain in concentrations below detection by ICP-MS. This indicates that a decrease in pH and increase in SO_4, Fe and U would imply an impacting solution such as AMD. Smectite clay minerals, kaolinite and small amounts of uranophane are shown to precipitate from solution as secondary minerals.

8.6 Process 6

This process links the geology to the surface water and is similar to the influence of geology with the shallow groundwater. The Vryheid formation of the Karoo Supergroup forms the largest portion (70%) of the surface geological outcrop in the ERB. The drainage channel of the Blesbokspruit is located on the Malmani dolomites. The dolomites are expected to introduce Ca, Mg and HCO_3 to the surface water with the HCO_3 providing buffer capacity to the surface water of the Blesbokspruit.

8.7 Process 7

Process 7 links the deep groundwater with the surface water. This link is formed by the dewatering of the Grootvlei mine operations, the treatment of the raw effluent and the discharge of treated effluent into the Blesbokspruit drainage channel. Analysis of water quality data of treated effluent shows that although the water is treated, SO_4, Fe, Mn and Zn are still introduced into the wetland system. Water volumes pumped in 2006 were and average of 108 Mℓ/day.

9 CHAPTER 9: IMPLICATIONS FOR SUSTAINABLE DEVELOPMENT

The ERB systems model, with identified components and processes can now be used to place the model in a sustainable development context by answering the question posed in Section 1.2.

9.1 What are the main pollution issues?

The main issues have been shown to result from pyrite oxidation and associated metal leaching in an acidic solution. This solution contaminates surface water, soil and groundwater with SO_4 and heavy metals (Mn, Ni, U, Co, Zn and Al).

9.2 What do the models show in terms of clean-up priorities?

The geochemical models have shown that the mine tailings facilities are the most important source of contamination of surface water, shallow, and perhaps deep, groundwater and soil in the ERB. The main contaminants of concern are Fe^{2+}, SO_4, Mn, Ni, U, Co, Zn and Al, including acidity. The soil adsorption model has shown that Fe, Co, Ni, Zn, U and SO_4 could leach through the relatively thin (~2 m) soil beneath the tailings facilities and contaminate shallow groundwater. Existing shallow groundwater monitoring results have shown that this has already occurred.

9.3 Where should mitigation/remediation be focussed

The models show that the mine tailings facilities can account for the majority of inorganic water and soil pollution in the ERB. These facilities should therefore be targeted in any remediation strategies. The soil adsorption model showed that the soil adsorption capacity becomes saturated in the duration of the existence of the tailings facility. Therefore should tailings facilities be removed, the soil beneath these facilities will also need to be removed and remediated. This correlates with a previous study on the soil from reclaimed tailings facilities (Rösner et al., 2001).

9.4 How long can we expect the environmental issues to continue?

The dynamic geochemical reaction models showed that ~57% of the pyrite oxidises in 100 years of tailings existence, implying that the pyrite oxidation can be expected to continue for at least another 100 years before cessation. This estimate is expected to be the lower limit, as oxidation rates generally decrease with time due to secondary mineral coatings of pyrite grains and the slower O_2 diffusion rates with depth in the tailings facilities. It could also be expected that leaching could occur years after the cessation of pyrite oxidation due to the dissolution of secondary mineral phases and desorption of adsorbed phases. Therefore the tailings facilities need to be viewed as continuous sources of contamination.

9.5 What are the cost implications of operational mitigation versus post-closure remediation?

This question cannot be answered from a geochemical perspective alone. Economics needs to be considered, especially in the light of the fact that mines are now forced to set aside capital to fund mitigation and post-closure remediation measures.

The costs associated with remediation of modern mine sites are not well documented in the public record of published literature (United States Environmental Protection Agency, 1997). The United States Environmental Protection Agency (1997) provides several reasons for this:

- Remedial measures may be designed and implemented in response to compliance and enforcement actions, chemical spill events, state license requirements, etc. However, while specific remedial actions taken must be reported by regulatory agencies, costs typically are not.
- Some actions may involve limited, short-term actions (i.e. cleaning up of minor spills); however, others may require more complex, long-term solutions that are often completed in multiple phases. Cumulative cost data are unlikely to be readily available for such long-term actions.
- Costs are often considered proprietary to the mine operator.

In the South African context the lack of knowledge of remediation of especially large-scale problems, such as the Witwatersrand AMD issue is shown in headlines such as ***TCTA to approach Treasury for more AMD funding*** (Mining Weekly, 10/10/2011), ***TCTA again warns of funding shortfall for acid water projects*** (Mining Weekly, 19/01/2012) and ***TCTA signs R 319m AMD agreement with group five*** (Mining Weekly, 10/12/2012). The TCTA is the Trans-Caledon Tunnel Authority which is a state-owned entity which was brought into existence by the promulgation of the national water act of 1988[26]. The TCTA is tasked with implementing short-term solutions and developing medium to long-term solutions for the Witwatersrand AMD issue (DWA, 2012b).

Such medium- and long-term solutions have yet to be found and implemented.

This section is not an exhaustive economic analysis as defined by the United States Environmental Protection Agency (2010), but is rather a basic cost benefit assessment of the cost of mitigation as opposed to post-closure remediation in context of the East Rand Basin AMD issue. Company profits as reflected in their annual reports are used as a benchmark to evaluate the two options, i.e. operational mitigation and post-closure remediation. The main focus of the assessment is on the tailings facilities and the associated mitigation of water and soil contamination.

9.5.1 Basic cost benefit analysis

The purpose of the basic cost benefit analysis is to determine the economic implications of two scenarios:

1. Implementation of pollution mitigation measures in the operational phase of a mine in the ERB.
2. Post-closure pollution remediation without operational mitigation.

[26] National Water Act (NWA); Act 36 of 1998

A theoretical mine site was conceptualised based on the East Rand Basin Grootvlei mine. This approach was followed due to lack of mine specific information and Grootvlei was the only mine to pump and treat during operation (Roychoudhury and Starke, 2006; Expert team of the inter-ministerial commission; 2010). The mine is no longer in operation following a liquidation suit (Creamer, 2011). The conceptual mine layout is shown in Figure 9-1.

To determine the shallow groundwater clean-up volumes, sulphate data from existing boreholes were contoured to determine the plume extents[27]. A cut-off concentration of 400 mg/ℓ was used to delineate the plumes[28]. Three plumes could be delineated (Figure 9-2). Of these the northeastern most plume corresponded to the most shallow groundwater monitoring points. Therefore this plume, which corresponds to a mining area, was used for the calculations. The plume surface area calculated using this method is 4 674 341 m^2. The average estimated shallow groundwater depth of 40 m (Africa Geo-Environmental Services (Pty) Ltd, 2006) was used to estimate shallow groundwater clean-up volumes. The input values used to calculate mitigation and remediation costing is shown in Table 9-1.

[27] Council for Geoscience unpublished data; Strategic Water Management Project

[28] 400 mg/l is the South African National Standards drinking water quality guideline value (SANS, 2011)

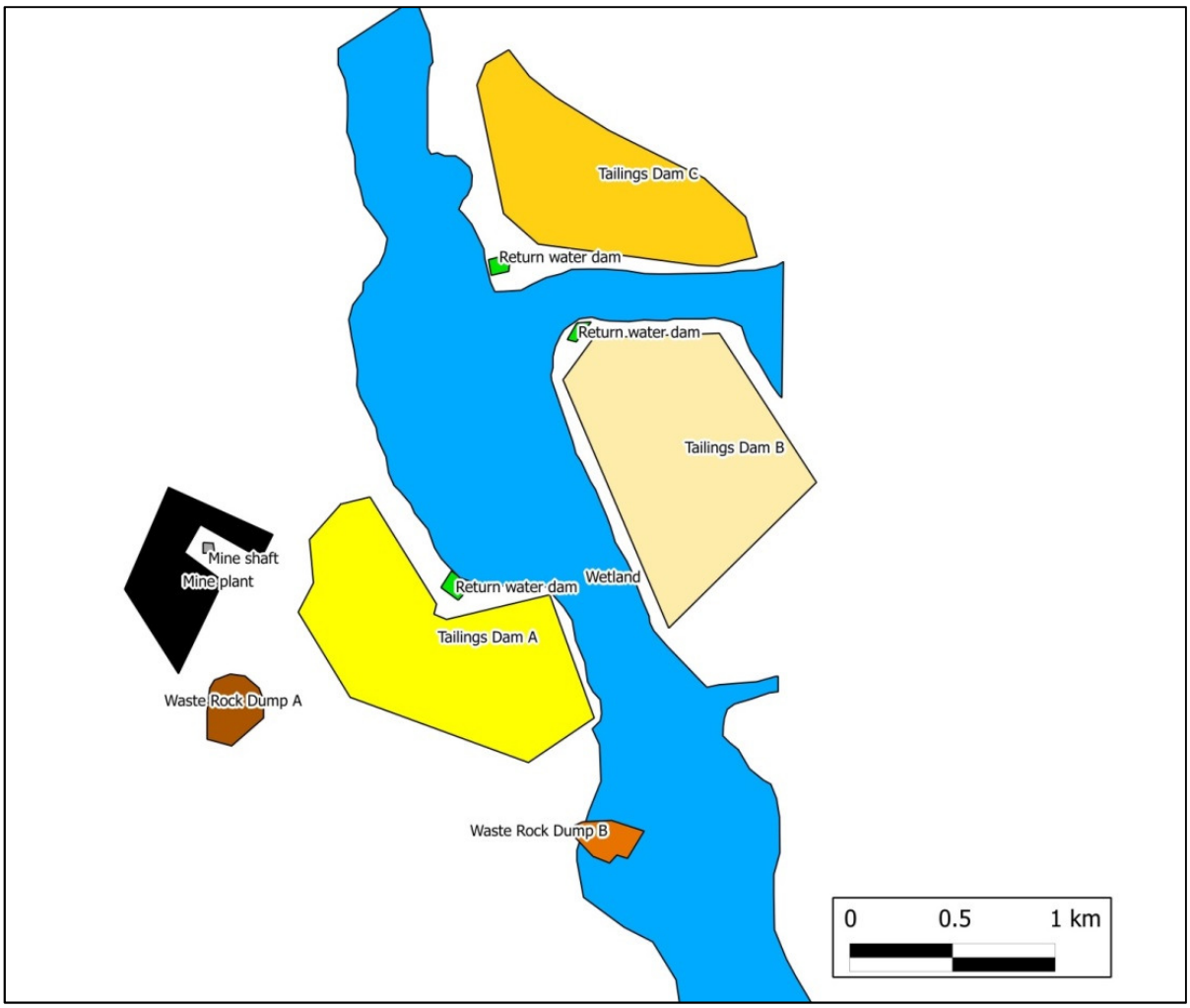

Figure 9-1 Conceptual mine infrastructure.

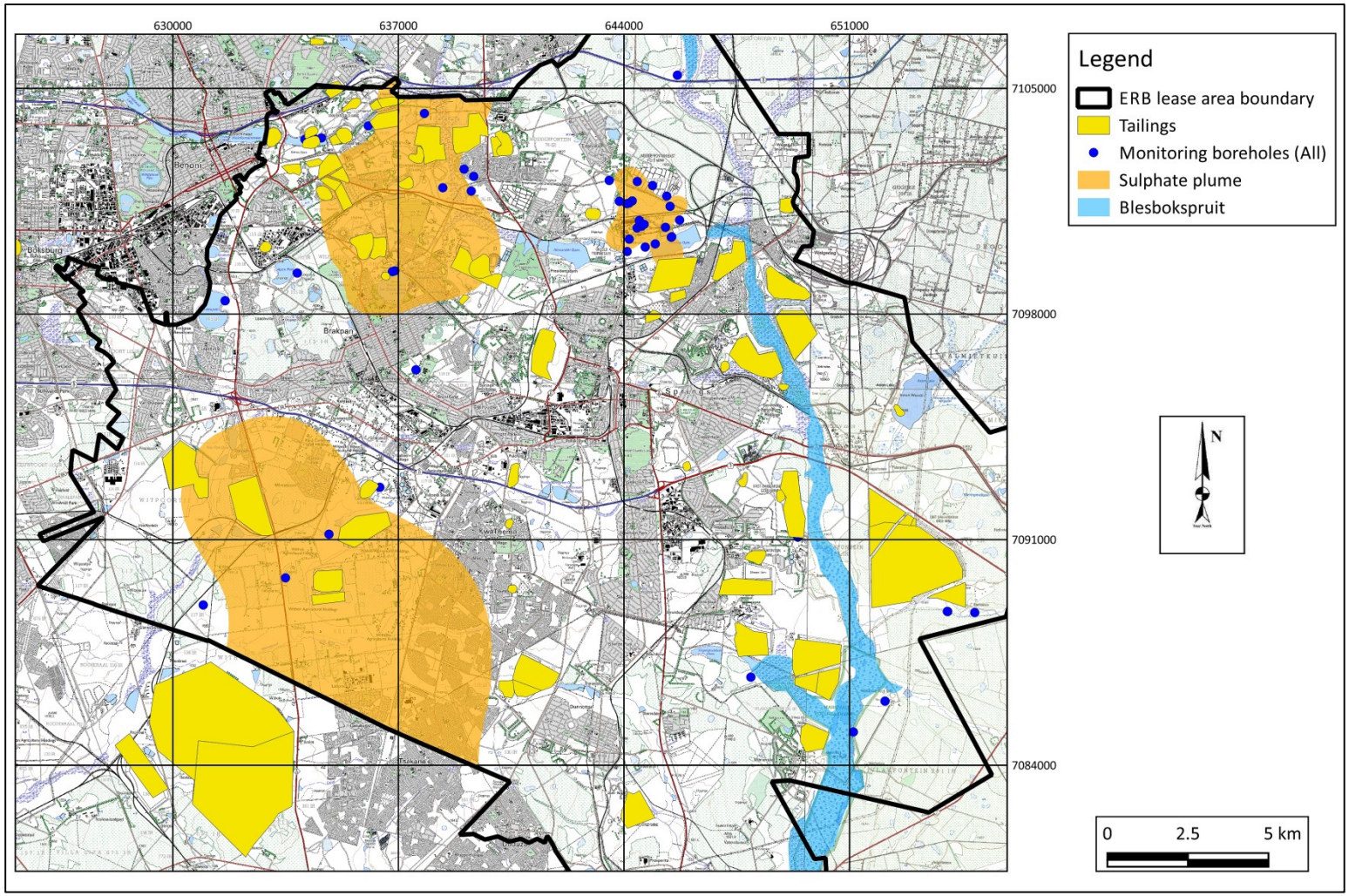

Figure 9-2 ERB sulphate plume. Existing shallow groundwater borehole sulphate data was contoured. The sulphate plume in the northeastern part of the map corresponds to the most data points and is therefore conceivably the most accurate. The surface area of this plume is 4 647 341 m^2.

Table 9-1 Cost benefit analysis input data.

	Unit	Comments	Number	Thickness	Area	Volume	Mass
				m	m^2	m^3	*t*
Tailings	Tailings A			4 756	1 193 007	71 580 420	101 644 196
	Tailings B			4 370	1 162 207	69 732 420	99 020 036
	Tailings C			3 929	817 706	49 062 360	69 668 551
	Total Tailings			***13 055***	***3 172 920***	***190 375 200***	***270 332 784***
Waste rock dump	Waste rock dump A			995	73 442	734 420	1 982 934
	Waste rock dump B			870	50 290	502 900	1 357 830
	Total WRD			***1 865***	***123 732***	***1 237 320***	***3 340 764***
General	Pump and treat - underground - Operational	Daily pumping volume calculated from Grootvlei pumping data from 13 June 1996 to 31 October 2004				82 910	
	Pump and treat - underground - Operational (Total volume)	Average daily pump[ing volume used to calculate total volume pumped from 13 June 1996 to 31 January 2013				741 178 814	
	Tailings and WRD contamination plume - shallow groundwater cleanup	Average shallow groundwater aquifer thickness used together with eliptical plume dimensions as derived from the sulphate contours to calculate total contaminated shallow groundwater.		40	4 647 341	185 893 640	
	Deep groundwater clean-up	This is the total deep groundwater pump-and-treat volume required for an assumed 10 years after 31 January 2013 till a new solution is found.				302 950 000	
	Soil beneath tailings and WRD - washing	Calculated total volume of soil beneath tailings dams and waste rock dumps which require clean-up		2	3 296 652	6 593 304	
	Cladding (Tailings)	Caldding is assumed for opeartional and post-operational scenarios, as it is expected to take time to re-process the tailings and dust will need to be kept to a minimum.		0.3	3 172 920		
	Monitoring	Monitoring is calculated from Ages monitoring project costing data for drilling (average of R911/ m) and sampling and anlysis (average R3 183.51 per sample). Bi-annual monitoring is assumed for 6 tailings (3 upstream and 3 downstream) and 4 waste-rock dump (2 upstream and 2 downstream) boreholes as well as 6 surface water samples (3 upstream and 3 downstream). 1 Underground monitoring point is assumed and 1 effluent discharge monitoring point. This totals 18 samples per year for 100 years of mining operation.	72				
	Drilling (monitoring)	10 Monitoring boreholes at 60 m deep	600				
	Erosions ditches and berms	Average width of erosion trenches surrounding the tailings dams are used to calculate total surface area of erosion ditches surrounding the tailings dams. An assumed depthf of 0.5 m is assumed to claculate the potential volume of soil moved				228 338	

9.6 Basic cost-benefit analysis results

The results of the mitigation and post-closure remediation costing are shown in Table 9-3 and Table 9-4. To calculate the costs as a percentage of turn-over and as a percentage of profit the data in Table 9-2 was used.

Table 9-2 Cost benefit analysis financial input data.

Parameter	Value
Average grade (g/t)	5.86
Gold price (R/oz)	14 577
Average profit margins	20%
Amount gold produced (g)	1 582 798 450
Total income	R 813 866 426 500.17

The average profit margin was calculated using data from the following company annual reports and is simply the difference between income and expenditure (DRD Ltd, 2003, 2012; Anglogold, 1998, 2012, Harmony Gold, 2000, 2012). The detail of the expenditures, i.e. mining costs, was not considered individually, as they are reflected in the expenditures of the company annual reports used. The main purpose was to determine the most cost effective environmental remediation strategy. For this purpose the average profit margin is simply a benchmark to evaluate the potential economic implications of the two proposed scenarios. The average values were used, as profits are expected to be higher in the past, due to higher gold grades and nearer-to-surface mines as well as lack of necessity of implementing environmental mitigation measures.

The results show that mitigation over the 100 years of operation for the theoretical mine would be an estimated total cost of R 31 billion. This value is 4% of the total estimated turnover of R 814 billion and an estimated 19% of the total profit of R 163 billion.

In contrast, the estimated post-closure remediation, assuming no mitigation measures were employed during operation, would be an estimated R 66 billion. This is 8% of turnover and 41% of estimated profits.

These figures are based on a basic cost-benefit analysis and do not take factors such as loss in property value due to polluted water and potential degradation of the local economy and society of a post-closure mining community into account. These numbers could therefore be regarded as conservative from an economic perspective and it is unlikely that these values overestimate mitigation and remediation costs. In addition delays in finding a solution to the ERB AMD issue is expected to increase remediation costs with time. This is in part due to rising inflation, but also due to increase in volumes of polluted surface water and groundwater.

The results show that from an economic point of view from the mining operation perspective, it makes sense for a mine to remediate during operation, rather than trying to clean-up post-closure. This basic cost-benefit analysis indicates that concurrent remediation may make sense as opposed to post-closure remediation. This result correlates with existing guidelines and studies (Chamber of mines of South Africa, 2007; International Council of Mining and Metals, 2008; WWF, 2012).

Therefore from a sustainable development point of view, it also makes sense to remediate during operation, rather than post closure. The result is a lower cost to society post-closure. The geochemical modelling has shown that the tailings facilities would not cease to produce AMD and to contaminate the surrounding environment with heavy metals and sulphate. Companies now operating in the ERB are marginal as companies have to mine at greater depths for ore with lower grades. It is therefore unlikely that they will be able to cover the costs of remediation. Thus the South African society may be paying for the gold mining legacy for generations to come.

Table 9-3 Total mitigation costs over 100 years of operation.

Mitigation measure	Facility	Unit cost	Unit	Cost (R)
Cladding	Tailings	2 914	R/m^2	9 246 682 110.00
Liner	Tailings; Waste rock dump	2 838	R/m^2	9 004 175 834.40
Treatment of mine discharge	Mine	4.44	R/m^3	3 290 833 934.16
Monitoring	Tailings and waste rock	3 183.51	R/sample	22 921 272.00
Monitoring boreholes	Tailings; Waste rock dump	911.00	R/m	R 546 600.00
Erosion trenches and berms	Tailings	879	R/m^3	200 810 252.60
Lining of Return water dams	Tailings and waste rock	2 838	R/m^2	9 004 188 832.57
Total				**30 770 158 835.73**
Percentage of turnover				**4%**
Percentage of profit				**19%**

Table 9-4 Post-closure remediation costs.

Remediation measure	Facility	Unit cost	Unit	Cost (R)
Cladding	Tailings	2 914.25	R/m^2	9 246 690 405.34
Shallow groundwater pump and treat	Mine	4.44	R/m^3	1 254 907 086.01
Deep groundwater pump and treat	Mine	4.44	R/m^3	1 345 098 000.00
Soil clean-up (washing)	Tailings; Waste rock dump	8 334.55	R/m^3	54 952 220 668.70
Total				**66 369 098 137.40**
Percentage of turnover				**8%**
Percentage of profit				**41%**

10 CHAPTER 10: CONCLUSIONS

Acid mine drainage has been recognised as a major environmental concern in the Witwatersrand gold mining basins, including the ERB. This study has shown that the tailings dams are major contributors to the issue and can account for all the salt loads in the ERB subsystems, such as the soil, shallow groundwater and surface water in terms of SO_4, Fe, U, Mn, Ni, Zn, Co and acidity. Analysis of existing data shows that surface and shallow groundwater is also contaminated with NO_3, Na and Cl. This study shows that it is unlikely that the latter contaminants are ensuing from mine tailings dams.

A systems theory approach was followed to develop a model for the ERB in terms of geochemical processes thereby identifying contamination source terms as well as fate and transport. To develop the systems model, several subsystems, or components, were identified as well as possible links, or processes, between them. This dictated that the development of one all-encompassing geochemical reaction model would be insufficient to reach an understanding of the regional ERB AMD processes. Therefore 5 main geochemical reaction models, representing the main geochemical components of the ERB system, were developed to study processes linking these components.

Uncertainty analysis formed an integral part of the modelling process. Uncertainty was found to be of two main types: 1. Uncertainty related to spatial and temporal variation of the values of the quantities of interest (QOI); 2. Uncertainty related to assumptions made. The only viable method of determining the model sensitivity to specific key input parameters is through a sensitivity analysis. The results of the sensitivity analysis identify those input parameters for which the model is sensitive and therefore identifies specific parameters for which more data is required, so that the model uncertainty can be decreased.

The uncertainty analysis showed that it is not possible to quantify uncertainty in the true sense of the word. Uncertainty qualification would be a better term. However, the power of the uncertainty analysis is that it provides information on the likely uncertainty in a specific parameter due to spatial and temporal variability and it identifies the specific parameters for which more data is required, thereby eliminating the costly trial and error data collection exercise, which often focusses on the wrong areas and does not reduce uncertainty. This can lead to the phenomenon of “analysis paralysis” due to unguided scientific studies.

The models showed that the tailings facilities are significant contamination point sources in the ERB. The specific contaminants are acidity, SO_4, Fe, Mn, Ni, Co, Zn, Al and U. When the AMD solution enters the soil beneath the tailings, Fe^{2+} and SO_4 concentrations in the solution remain elevated, while Mn, U, Ni, Co, U and perhaps other metals are adsorbed. After ~50 years the pollution plume starts to break through the base of the soil profile and the concentration of the adsorbed metals increase in the discharging solution as the adsorption capacity of the soil becomes saturated. The pollution pulse then starts to migrate to the shallow groundwater where contamination of this resource occurs.

Toe seepage from the tailings either first reacts with carbonate, where acidity is neutralised to a degree and some metals precipitated from solution, where after it reaches the surface water drainage, such as the Blesbokspruit, where it is diluted to about 3 000 times. This dilution factor is qualitative only as it was derived

by comparison between the mixing model results and existing Blesboksrpuit surface water quality data. Another scenario is where the toe seepage does not come into contact with dolomite and therefore reaches the surface drainage as raw seepage. Some evaporation can occur, but evaporation only leads to concentration of acidity and dissolved constituents, thereby effectively worsening the AMD solution quality. The mixing models have shown that the dilution factor is sufficient to mitigate much of the AMD, although seasonal variability in precipitation and evapotranspiration is expected to have some influence on the mixing ratio and some variability in the initial solution will also be reflected in variation in surface water quality. The results did correlate with previous assessments on surface water and stream sediment studies.

Geochemical reaction models of the Karoo and Witwatersrand geology showed that the weathering of both these geological packages produce alkaline solutions with low dissolved salt loads. Any significant increase in SO_4, Fe and other metals is therefore due to anthropogenic influence. In the ERB that influence is mining. The results of the models correlate with existing surface water and groundwater quality data which indicates multiple distributions in the data sets. These data sets are generally polymodal, skewed towards higher concentrations of dissolved Fe, SO_4 and metals and lower pH. Much controversy surrounds the notion of rising AMD in the Witwatersrand gold mines. The controversy is not on whether it is occurring, but rather centres on its origins. The commonly accepted notion is that the rising AMD forms by the oxidation of sulphides in the mine voids. Although this is most certainly possible due to increased O_2 flux through shafts and mine ventilation infrastructure, influences from ingress of contaminated shallow groundwater and seepage from tailings could also significantly contribute to the rising AMD.

This study has shown that the ERB AMD geochemistry can only really be understood from a systems perspective. It shows that the detailed analysis of data distributions prior to model development is important for preliminary conceptual ideas on the system, which can be evaluated in the numerical models. It also shows that a sensitivity analysis is a powerful tool in identifying parameters for which more data is required and that uncertainty analysis should be an integral part of the modelling process. This allows for the model results to be placed in the correct context so that the model can be used for management decisions and evaluation of future scenarios and effects of proposed mitigation measures.

From a sustainability perspective, a basic cost benefit analysis shows that the costs for the operating mine and society in general is lower when mitigation measures are employed during operation. For a theoretical mine in the ERB with an operating life of 100 years, the cost of operational mitigation measures is 4% of turnover and 19% of profits over the time period. Post closure remediation costs form 8% of turnover and 41% of profit over the time period. Although the initial capital investment in mitigation measures may be substantial some measures will be implemented during operation, implying that not all remediation capital will be spent upon start of operations. Operational mitigation measures form a smaller percentage of profits than eventual post-closure mitigation. This is especially important considering that much of the post-closure clean-up costs have now become a burden on the South African tax payer.

11 REFERENCES

Acero, P., Ayora, C., Carrera, J., Saaltink, M.W. and Olivella, S. (2009) Multiphase flow and reactive transport model in vadose tailings. *Applied Geochemistry* **24**, 1238-1250

Africa Geo-Environmental Services (Pty) Ltd (2005) Groundwater flow model of the Far East Rand Basin – Grootvlei sub-catchment Phase II: Calbrated for the canal area. *Technical Report* **AS/R/05/04/01**, p 40

Africa Geo-Environmental Services (Pty) Ltd. (2006) Regional groundwater flow management model for the Far East Rand Basin. *Technical Report* **AS/R/06/01/30**, p 60

Al, T.A. and Blowes, D.W. (1999) The hydrogeology of a tailings impoundment formed by central discharge of thickened tailings: implications for tailings management. *Journal of Contaminant Hydrology* **38**, 489-505

Allison, J., Brown, D. and Novo-Gradac, K. (1991) MINTEQA2/PODEFA2, A geochemical assessment model for environmental systems: Version 3.0 user's manual. *United States Environmental Protection Agency Technical Report* **EPA/600/3-91/21**, p 107

Alpers, C.N., Blowes, D.W, Nordstrom, D.K. and Jambor, J.L. (1994) Secondary minerals and acid mine-water chemistry. *In* Blowes D.W. and Jambor, J.L. (*Eds.*) The environmental geochemistry of sulphide mine-wastes, *Mineralogical Association of Canada short course handbook* **22**, 247-270

An, L. (2012) Modeling human decisions in coupled human and natural systems: Review of agent-based models. *Ecological Modelling* **229**, 25-36

Anglogold (1998) Report to shareholders 1998. Available at www.anglogold.co.za [Accessed April 17 2013.

Anglogold (2012) Report for the quarter and year ended of 31 December 2012. Available at www.anglogold.co.za [Accessed April 17 2013]

Anon, Inflation rate and CPI. *Available at: http://www.rateinflation.com/* [Accessed April 17, 2013]

Balistrieri, L.S., Seal, R.R., Piatak, N.M. and Paul, B. (2007) Assessing the concentration, speciation and toxicity of dissolved metals during mixing of acid-mine drainage and ambient river water downstream of the Elizabeth Copper Mine, Vermont, USA. *Applied Geochemistry* **22**, 930-952

Ball, J.W. and Nordstrom, D.K. (1991) User's manual for WATEQ4, with revised thermodynamic data base and test cases for calculating speciation of major, trace and redox elements in natural waters. *United States Geological Survey Open-File Report* **91-183**, p 195

Baron, D. and Palmer, C.D. (1996) Solubility of jarosite at 4 – 35°C. *Geochimica et Cosmochimica Acta* **60**, 185-195

Barthel, R., Janisch, J., Schwartz, N., Trifkovic, A., Nickel, D., Schultz, C. and Mauser, W. (2008) An integrated modelling framework for simulating regional-scale actor responses to global change in the water domain. *Environmental Modelling & Software* **23**, 1095-1121

Ben-Haim, Y. (2004) Uncertainty, probability and information-gaps. *Reliability Engineering and System Safety* **85**, 249-266

Bethke, C.M. and Brady, P.V. (2000) How the Kd approach undermines ground water cleanup. *Ground Water* **38**, 435-443

Bethke, C.M. (2008) Geochemical and biogeochemical reaction modelling, 2nd Edition. *Cambridge Univeristy Press*, p 543

Bezuidenhout, N. and Rousseau, P.D.S. (2005) An investigation into the depth and rate of weathering on gold tailings dam surfaces as key information for long-term AMD risk assessments. *Water Research Commission Technical Report* **1347/1/05**

Blanc, P., Lassin, A. and Piantone, P. (2007) THERMODDEM A database devoted to waste minerals, BRGM (Orléans, France). Available at http://thremoddem.brgm.en [Accessed 30 June 2010)

Blanchard, M., Poitrasson, F., Méheut, M., Lazzeri, M., Mauri, F. and Balan, E. (2009) Iron isotope fractionation between pyrite (FeS_2), hematite (Fe_2O_3) and siderite ($FeCO_3$): A first-principles density function theory study. *Geochimica et Cosmochimica Acta* **73**, 6565-6578

Body, K. and Lomberg, K. (2008) Elsburg tailings dam complex independent competent persons report. *RSG Global technical report* **JCGR01**, p 72

Boon, M., Brasser, H.J., Hansford, G.S. and Heijen, J.J. (1999) Comparison of the oxidation kinetics of different pyrites in the presence of *Thiobacillus ferrooxidans* or *Leptospirilum ferrooxidans. Hydrometallurgy* **53**, 57-72

Bosch, P.J.A. (2010) The geological architecture of the East Rand Basin. *Council for Geoscience unpublished report*

Brantley, S.L. (2008) Kinetics of mineral dissolution. *In* Bratley, S., Kubicki, J. and White A. (*Eds.*) Kinetics of water-rock interactions. *Springer*, 151-210

Bühmann, C. (1992) Smectite-to-illite conversion in a geothermally and lithologically complex permian sedimentary sequency. *Clays and Clay Minerals* **40**, 53-64

Butler, T.W. (2007) Isotope geochemistry of drainage from an acid mine impaired watershed, Oakland, California. *Applied Geochemistry* **22**, 1416-1426

Byrne, R.H. and Luo, Y-R. (2000) Direct observations of nonintegral hydrous ferrix oxide solubility products: $K^{*}_{SO} = [Fe^{3+}][H^{+}]^{-2.86}$. *Geochimica et Cosmochimica Acta* **64**, 1873-1877

Cabrera, D., Colosi, L. and Lobdell, C. (2008) Systems thinking. *Evaluation and Program Planning.* **31**, 299-310

Caldeira, C.L., Ciminelli, V.S.T. and Osseo-Asare, K. (2010) The role of carbonate ions in pyrite oxidation in aqueous systems. *Geochemica et Cosmochimica Acta,* **74**, 1777-1789

Chamber of Mines South Africa and Coaltech Research Association (2007) Guidelines for the rehabilitation of mined lands.

Chandra, A.P. and Gerson, A.R. (2010) The mechanisms of pyrite oxidation and leaching: A fundamental perspective. *Durface Science Reports* **65**, 293-315

Chapman, E.C., Capo, R.C., Stewart, B.W., Hedin, R.S., Weaver, T.J. and Edenborn, H.M. (2013) Strontium isotope qualification of siderite, brine and acid mine drainage contributions to abandoned gas well discharges in the Appalachian Plateau. *Applied Geochemistry* **31**, 109-118

Coetzee, H., Venter, J. and Ntsume, G. (2006) Contamination of wetlands by Witwatersrand gold mine processes and economic potential of gold in wetlands. *Council for Geoscience Technical Report* **2005-0106**, p 106

Coetzee, H., Winde, F. and Wade, P.W. (2006) An assessment of sources, pathways, mechanisms and risks of current and potential future pollution of water and sediments in gold-mining areas of the Wonderfonteinspruit catchment. *Water Research Commission Technical Report* **1214/1/06**, p 91

Coggon, M., Becerra, C.A., Nüsslein, K., Miller, K., Yuretich, R. and Ergas, S.J. (2012) Bioavailability of jarosite for stimulating acid mine drainage attenuation. *Geochimica et Cosmochimica Acta* **78**, 65-76

Côte, C.M., Moran, C.J., Hedemann, C.J. and Koch, C. (2010) Systems modelling for effective mine water management. *Environmental Modelling & Software* **25**, 1664-1671

Cowie, B.R., Slater, G.F., Bernier, L. and Warren, L.A. (2009) Carbon isotope fractionation in phospholipid fatty acid biomarkers of bacteria and fungi native to an acid mine drainage lake. *Organic Chemistry* **40**, 956-962

Creamer, M. (2011) New liquidators oust Aurora from troubled Grootvlei, Orkey gold mines. *Mining Weekly* **27 May 2011**, available at http://www.miningweekly.com/article/new-liquidators-oust-aurora-from-troubled-grootvlei-orkney-gold-mines-2011-05-27 [Accessed 21 July 2014]

Criscenti, L.J., Eliassi, M., Cygan, R.T. and Cólón, C.F.J. (2006) Modelling adsorption processes: Issues in uncertainty, scaling and prediction. *United States Nuclear Regulatory Commission Office of Nuclear Regulatory Research, Washington DC, Technical Report* **20555-0001**

Cukrowska, E.M., Govender, K. and Viljoen, M. (2004) Ion mobility based on column leaching of South African gold tailings dam with chemometric evaluation. *Chemosphere* **56**, 39-50

Department of Water Affairs (2012a) Feasibility study for a long-term solution to address the acid mine drainage associated with East, Central and West Rand underground mining basins – Assessment of the quality and quantity of the Witwatersrand mine voids. *Technical Report* **P RSA 000/00/16512/2**, p 201

Department of Water Affairs (2012b) Feasibility study for a long-term solution to address the acid mine drainage associated with East, Central and West Rand underground mining basins – Inception report. *Technical Report* **P RSA 000/00/16112**, p 127

Department of Water Affairs (2013) Options for the sustainable management and use of residue products from the treatment of AMD. *Department of Water Affairs Study Report no.* **5.5 P RSA 000/00/16512/5**, p 154

Davis, B.M. (2009) Buidling engineered wetlands to reduce costs. *Pollution Engineering* **August 2009**, 12-16

Dickinson, E.J.F., Limon-Petersen, J.G. and Compton, R.G. (2011) The electroneutrality approximation in electrochemistry. *Journal of Solid State Electrochemistry* **15**, 1335-1345

Dold, B. and Fontboté, L. (2001) Element cycling and secondary mineralogy in porphyry copper tailings as a function of climate, primary mineralogy and mineral processing. *Journal of Geochemical Exploration* **74**, 3-55

DRDGold Ltd. (2012) Annual financial statements 2012. Available at www.drd.co.za [Accessed April 17 2013]

Drouet, C., Pass, K.L., Baron, D., Draucker, S. and Navrotsky, A. (2004) Thermochemistry of jarosite-alunite and natrojarosite-natroalunite solid solutions. *Geochimica et Cosmochimica Acta* **68**, 2197-2205

Duane M.J., Pigozzi, G. and Harris, C. (1997) Geochemistry of some deep gold mine waters from the western portion of the Witwatersrand Basin, South Africa. *Journal of African Earth Sciences*, **24**, 105-123

Durand, J.F. (2012) The impact of gold mining on the Witwatersrand on the rivers and karst system of Gauteng and North West Province, South Africa. *Journal of African Earth Sciences* **68**, 24-43

Dzombak, D.A. and Morel, F.M.M. (1990) Surface complexation modelling. *Wiley-Interscience*, p 416

Edraki, M., Golding, S.D., Baublys, K.A. and Lawrence, M.G. (2005) Hydrochemistry, mineralogy and sulphur isotope geochemistry of acid mine drainage at Mt. Morgan mine environment, Queensland, Australia. *Applied Geochemistry* **20**, 789-805

English Partnerships (2008) Best Practice Note 27 (revised February 2008) Contamination and dereliction remediation costs. *Reference* **ENG0085**, p 32

Equeenuddin, Sk. Md., Tripathy, S., Sahoo, P.K. and Panigrahi, M.K. (2010) Hydrogeochemical characteristics of acid mine drainage and water pollution at Makum Coalfield, India. *Journal of Geochemical Exploration* **105**, 75-82

Erickson, P.G., Alterman, W. and Hartzer, F.J. (2006) The Transvaal Supergroup and its precursors. *In* Johnson, M.R., Anhaeusser, C.R. and Thomas, R.J. (*Eds*.) *The Geology of South Africa*. Geological Society of South Africa, Johannesburg/Council for Geoscience, Pretoria, 237-260.

España, J.S., Pamo, E.L. abd Pastor, E.S. (2007) The oxidation of ferrous iron in acidic mine effluents from the Iberian Pyrite Belt (Odiel Basin, Huelva, Spain): Field and laboratory rates. *Journal of Geochemical Exploration* **92**, 120-132

Ewel, J.J. (1999) Natural systems as models for the design of sustainable systems of land use. *Agroforestry Systems* **45**, 1-21

Expert Team of the Inter-Ministerial Committee under the coordination of the Council for Geoscience (2010) Mine water management in the Witwatersrand Gold Fields with special emphasis on acid mine drainage. *Report to the Inter-Ministerial committee on acid mine drainage, p 146*

Fernandez, A. and Borrok, D.M. (2009) Fractionation of Cu, Fe, and Zn isotopes during the oxidative weathering of sulphide-rich rocks. *Chemical Geology* **264**, 1-12

Gammons, C.H., Duaime, T.E., Parker, S.R., Poulson, S.R. and Kennelly, P. (2010) Geochemistry and stable isotope investigation of acid mine drainage associated with abandoned coal mines in central Montana, USA. *Chemical Geology* **269**, 100-112

Gleick, J. (2011) Chaos, the making of a new science. *Open Road Media*, p 333

Gleisner, M. and Herbert, R.B. (2002) Sulfide mineral oxidation in freshly processed tailings: batch experiments. *Journal of Geochemical Exploration* **76**, 139-153

Gleisner, M., Herbert, R.B. and Kockum, P.C.F. (2006) Pyrite oxidation by *Acidithiobacillus ferrooxidans* at various concentrations of dissolved oxygen. *Chemical Geology* **225**, 16-29

Goldstein, M. and Ritterling, J. (2001) A practical guide to estimating cleanup costs. *Remediation Journal* **11**, 103-121

Groebner, D.F., Shannon, P.W. and Fry, P.C. (2013) Business statistics, 9th edition. *Pearson publishing*, p 912

Guangqing, X. (2005) Rethinking systems thinking: from a perspective of Chinese philosophy and sustainable development. *6th European Conference on Systems Science, Abstract*

Gunsinger, M.R., Ptacek, C.J., Blowes, D.W., Jambor, J.L. and Moncur, M.C. (2006) Mechanisms controlling acid mine neutralization and metal mobility within a Ni-rich tailings impoundment. *Applied Geochemistry* **21**, 1301-1321

Haggis, T. (2008) 'Knowledge must be contextual': Some possible implications of complexity and dynamic systems theories for educational research. *Educational Philosophy and Theory* **40**, 158-176

Hallbauer, D.K. (1986) The mineralogy and geochemistry of Witwatersrand pyrite, gold, uranium and carbonaceous matter. *In* Annheausser, C.R. and Maske, S. (*Eds.*) *Mineral Deposits of Southern Africa* **I**, 731-752

Hamel, B.L., Stewart, B.W. and Kim, A.G. (2010) Tracing the interaction of acid mine drainage with coal utilization byproducts in a grouted mine: Strontium isotope study of the inactive Omega Coal Mine, West Virginia (USA). *Applied Geochemistry* **25**, 212-223

Hammarstrom, J.M., Seal, R.R., Meier, A.L. and Kornfeld, J.M. (2005) Secondary sulphate minerals associated with acid mine drainage in the eastern US: recycling of metals and acidity in surficial environments. *Chemical Geology* **215**, 407-431

Hansen, Y., Broadhurst, J.L. and Petrie, J.G. (2008) Modelling leachate generation and mobility from copper sulphide tailings – An integrated approach to impact assessment. *Minerals Engineering* **21**, 288-301

Harmony Gold (2000) Annual report 2000. Available at www.harmony.co.za [Accessed April 17 2013]

Harmony Gold (2012) Harmony integrated annual report 2012. Available at www.harmony.co.za [Accessed April 17 2013]

Hatfield, A.J. and Hipel, K.W. (2002) Risk and systems theory. *Risk Analysis* **22**, 1043-1057

Hayes, S.M., White, S.A., Thompson, T.L., Maier, R.M. and Chorover, J. (2009) Changes in lead and zinc lability during weathering-induced acidification of desert mine tailings: Coupling chemical and micro-scale analyses. *Applied Geochemistry* **24**, 2234-2245

Heidel, C. and Tichomirowa, M. (2010) The role of dissolved molecular oxygen in abiotic pyrite oxidation under acid pH conditions – Experiments with ^{18}O-enriched molecular oxygen. *Applied Geochemistry* **25**, 166-1675

Hem, J.D. (1985) Study and interpretation of the chemical characteristics of natural water. *United States Geological Survey Water-Supply Paper* **2254**, p 281

Hipsey, M.R., Salmon, S.U. and Mosley, L.M. (2014) A three-dimensional hydro-geochemical model to assess lake acidification risk. *Environmental Modelling & Software* **http://dx.doi.org/10.1016/j.envsoft.2014.02.007**, 1-25

Homes, P.R. and Crundwell, F.K. (2000) The kinetics of the oxidation of pyrite by ferric ions and dissolved oxygen: An electrochemical study. *Geochimica et Cosmochimica Acta* **64**, 263-274

Hubard, C.G., Black, S. and Coleman, M.L. (2009) Aqueous geochemistry and oxygen isotope compositions of acid mine drainage from the Rio Tinto, SW Spain, highlight inconsistencies in current models. *Chemical Geology* **265**, 321-334

International Council on Mining & Metals (2008) Planning for integrated mine closure: Toolkit. *ICMM, ISBN* **978-0-3591-8-7**, p 86

Jackson, M.C. (2001) Critical systems thinking and practice. *European Journal of Operational Research* **128**, 233-244

Jerz, J.K. and Rimstidt, J.D. (2004) Pyrite oxidation in moist air. *Geochimica et Cosmochimica Acta* **68**, 701-714

Johnson, M.R., Van Vuuren, C.J., Visser, J.N.J., Cole, D.I., De V. Wickens, H., Christie, A.D.M., Roberts, D.L. and Brandl, G. (2006) The sedimentary rocks of the Karoo Supergroup. *In* Johnson, M.R., Anhaeusser, C.R. and Thomas, R.J. (*Eds.*) *The Geology of South Africa*. Geological Society of South Africa, Johannesburg/Council for Geoscience, Pretoria, 237-260.

Jönsson, J., Jönsson, J. and Lövgren, L. (2006) Precipitation of secondary Fe(III) minerals from acid mine drainage. *Applied Geochemistry* **21**, 437-445

Jung, H-B., Yun, S-T., Kwon, J-S. and Zheng, Y. (2012) Role of iron colloids in copper speciation deuring neutralization in a coastal acid mine drainage, South Korea: Insight from voltammetric analyses and surface complexation modelling. *Journal of Geochemical Exploration* **112**, 244-251

Kimball, B.E., Mathur, R., Dohnalkova, A.C., Wall, A.J., Runkel, R.L. and Brantley, S.L. (2009) Copper isotope fractionation in acid mine drainage. *Geochimica et Cosmochimica Acta* **73**, 1247-1263

Klein, C. and Hurlbut, C.S. (1993) Manual of mineralogy. *John Wiley & Sons, Inc.,* p 681

Laszlo, A. and Krippner, S. (1998) Systems theories: Their origins, foundations and development. *In* Jordan, J. (*Ed.*) Systems theories and a priori aspects of perception. *North Holland*, p 366

Law, A.M. and Kelton, W.D. (1991) Simulation modelling & analysis, 2nd edition. *McGraw-Hill College,* p 544

Lee, J.S. and Chon, H.T. (2006) Hydrogeochemical characteristics of acid mine drainage in the vicinity of an abandoned mine, Daduk Creek, Korea. *Journal of Geochemical Exploration* **88**, 37-40

Lefticariu, L., Pratt, L.A., LaVerne, J.A. and Schimmelmann, A. (2010) Anoxic pyrite oxidation by water radiolysius products – A potential source of biosustaining energy. *Earth and Planetary Science Letters* **292**, 57-67

Lenong, S. and Hansen, R.N. (2009) Preliminary determination of the ECL in the East Rand Basin. *Council for Geoscience Technical Report* **2009-0275**, p 17

Lippman, J., Stute, M., Togersen, T., Moser, D.P., Hall, A., Lin, L., Borcsik, M., Bellamy, R.E.S. and Onstott, T.C. (2003) Dating ultra-deep mine waters with noble gases and ^{36}Cl, Witwatersrand Basin, South Africa. *Geochimica et Cosmochimica Acta* **67**, 4597-4619

Jin-yan, L., Xiu-xiang, T. and Pei, C. (2009) Study of formation of jarosite mediated by thiobacillus ferrooxidans in 9K medium. *Procedia Earth and Planetary Science* **1**, 706-712

Lizama, K., Fletcher, T.D. and Sun, G. (2011) Removal processes for arsenic in constructed wetlands. *Chemosphere* **84**, 1032-1043

Madzivire, G., Gitari, W.M., Vadapalli, V.R.K., Ojumu, T.V. and Petrik, L.F. (2011) Fate of sulphate removed during the treatment of circumneutral mine water and acid mine drainage with coal fly ash: Modelling and experimental approach. *Mineral Engineering* **24**, 1467-1477

McCarthy, T.S., Arnold, V., Venter, J. and Ellery, W.N. (2007) The collapse of Johannesburg's Klip River wetland. *South African Journal of Science* **103**, 391-409

McCarthy, T.S. and Venter, J.S. (2006) Increasing pollution levels on the Witwatersrand recorded in the peat deposits of the Klip River wetland. *South African Journal of Science* **102**, 27-34

McCluskey, J.J. and Rausser, G.C. (2003) Hazardous waste sites and housing appreciation rates. *Journal of Environmental Economics and Management* **45**, 166-176

McMahon, T. (2013) Inflation data. Available at: https://inflationdata.com [Accessed April 17, 2013]

Meima, J.A., Graupner, T. and Rammlmair, D. (2012) Modeling the effect of stratification on cemented layer formation in sulphide-bearing mine tailings. *Applied Geochemistry* **27**, 124-137

Midgley, G. (2008) Systems thinking, complexity and the philosophy of science. *E:CO* **10**, 55-73

Migaszewski, Z.M., Galuszka, A., Halas, S., Dolegowska, S., Dabek, J. and Starnawska, E. (2008) Geochemistry and stable sulfur and oxygen isotope ratios of the Podwisniowka pit pond water generated by acid mine drainage (Holy Cross Mountains, south-central Poland. *Applied Geochemistry* **23**, 3620-3634

Mirecki, J.E. (2006) Geochemical models of water-quality changes during aquifer storage recovery (ASR) cycle tests, Phase I: Geochemical models using existing data. *United States Army Corps of Engineers Technical Report* **ERDC/EL TR-06-8ERDC/EL TR-06-8**, p 76

Molson, J.W., Fala, O., Aubertin, M. and Bussière, B. (2005) Numerical simulations of pyrite oxidation and acid mine drainage in unsaturated waste rock piles. *Journal of Contaminant Hydrology* **78**, 343-371

Moncur, M.C., Jambor, J.L., Ptacek, C.J. and Blowes, D.W. (2009) Mine drainage from the weathering of sulphide minerals and magnetite. *Applied Geochemistry* **24**, 2362-2373

Moreno, L. and Neretnieks, I. (2006) Long-term environmental impact of tailings deposits. *Hydrometallurgy* **83**, 176-183

Naicker, K., Cukrowska, E. and McCarthy, T.S. (2003) Acid mine drainage arising from gold mining activity in Johannesburg, South Africa and environs. *Environmental Pollution* **122**, 29-40

Néel, C., Bril, H., Courtin-Nomade, A. and Dutreuil, J-P. (2003) Factors affecting natural development of soil on 35-year-old sulphide-rich mine tailings. *Geoderma* **111**, 1-20

Nengovhela, A.C., Yibas, B. and Ogola, J.S. (2007) An investigation into the availability and role of oxygen gas in gold tailings dams of the Witwatersrand basin with reference to their acid mine drainage potential. *Water SA* **33**, 271-274

Nicholson, R.V., Elberling, B. and Williams, G. (1995) A new oxygen consumption technique to provide rapid assessment of tailings reactivity in the field and the laboratory.

Nicholson, R.V., Erberling, B. and Williams, G. (1995) A new oxygen consumption technique to provide rapid assessment of tailings reactivity in the field and the laboratory. *95th Conference on Mining and the Environment Abstracts*, 999 – 1006

Nordstrom, D.K. (2009) Acid rock drainage and climate change. *Journal of Geochemical Exploration* **100**, 97-104

Nordstrom, D.K. (2012) Models, validation and applied geochemistry: Issues in science, communication and philosophy. *Applied Geochemistry* **27**, 1899-1919

Norlund, K.L.I., Baron, C. and Warren, L.A. (2010) Jarosite formation by an AMD sulphide-oxidizing environmental enrichment: Implications for biomarkers on Mars. *Chemical Geology* **275**, 235-242

OANDA, Forex trading and exchange services. Available at http://www.oanda.com [Accessed April 17, 2013]

Office of National Statistics – UK. Available at http://www.ons.gov.uk/ons/index.html [Accessed Aptil 17, 2013]

Pabalan, R.T. (2004) Software validation report for Geochemist's Workbench, version 4.0.2. *Center for Nuclear Waste Regulatory Analyses San Antonio, Texas Technical Report* **ML050240172**, p 47

Pabalan, R.T. (2005) Software validation report for Geochemist's Workbench, version 5.0. *Center for Nuclear Waste Regulatory Analyses San Antonio, Texas Technical Report* **ML062430517**, p 30

Pabalan, R.T. and Sabido, L.M. (2007) Software validation report for Geochemist's Workbench, version 6.0. *Center for Nuclear Waste Regulatory Analyses San Antonio, Texas Technical Report* **ML080430497**, p 33

Pakzadeh, B. and Batista, J.R. (2011) Surface complexation modelling of the removal of arsenic from ion-exchange waste brines with ferric chloride. *Journal of Hazardous Materials* **188**, 399-407

Papassiopi, N., Zaharia, C., Xendis, A., Adam, K/. Liakopoulos, A. and Romaidis, I. (2014) Assessment of contaminants transport in a watershed affected by acid mine drainage, by coupling hydrological and geochemical modelling tools. *Minerals Engineering* **64**, 78-91

Palisades Corporation (2010) Guide to using @Risk: Risk analysis and simulation add-in form Microsoft Excel, version 5.7. *Palisades Corporation*, p 693

Papassiopi, N., Zaharia, C., Xendis, A., Adam, K., Liakopoulos, A. and Romaidis, I. (2014) Assessment of contaminants transport in a watershed affected by acid mine drainage, by coupling hydrological and geochemical modelling tools. *Minerals Engineering* **64**, 78-91

Parkhurst, D.L. and Appelo, C.A.J. (1999) User's guide to PHREEQC (version 2) – A computer program for speciation, batch-reaction, one-dimensional transport and inverse geochemical calculations. *United States Geological Survey Water Resources Investigations Report* **99-4259**, p 326

Peretyazkho, T., Zachara, J.M., Boily, J-F., Xia, Y., Gassman, P.L., Arey, B.W. and Burgos, W.D. (2009) Mineralogical transformations controlling acid mine drainage chemistry. *Chemical Geology* **262**, 169-178

Petrunic, B.M., Al, T.A., Weaver, L. and Douglas, H. (2009) Identification and characterization of secondary minerals formed in tungsten mine tailings using transmission electron microscopy. *Applied Geochemistry* **24**, 2222-2233

Pretorius, D.A. (1974) The nature of the Witwatersrand gold-uranium deposits. *University of the Witwatersrand Economic Geology Research Unit Information Circular* **86**, p 50

Reesman, A.L. (1974) Aqueous dissolution studies for illite under ambient conditions. *Clay and Clay Minerals* **22**, 443-454

Rimstidt, J.D. and Vaughan, D.J. (2003) Pyrite oxidation: A state-of-the-art assessment of the reaction mechanisms. *Geochimica et Cosmochimica Acta* **67**, 873-880

Ritchie, A.I.M. (1994) Sulphide oxidation mechanisms: Controls on rates on oxygen transport. *In* Blowes D.W. and Jambor, J.L. (*Eds.*) The environmental geochemistry of sulphide mine-wastes, *Mineralogical Association of Canada short course handbook* **22**, 201-246

Robb, L.J. and Robb, V.M. (1998) Gold in the Witwatersrand Basin. *In* Wilson, M.G.C. and Annhaeusser, C.R. (*Eds.*) *The mineral resources of South Africa. Council for Geoscience*, 294-298

Robertson, W.D. (1994) The physical hydrology of mill-tailings impoundments. *In* Blowes D.W. and Jambor, J.L. (*Eds.*) The environmental geochemistry of sulphide mine-wastes, *Mineralogical Association of Canada short course handbook* **22**, 1-18

Rösner, T., Boer, R., Reynecke, R., Aucamp, P. and Vermaak, J. (2001) A preliminary assessment of pollution contained in the unsaturated zone beneath reclaimed gold-mine residue deposits. *Water Research Commission Report* **797/1/01**, p 210

Rossouw, A.S., Annegarn, H.J., Weiersbye, I.M. and Furniss, D.G. (2010) Evaluating the functional status of a rehabilitated gold tailings storage facility – A case study in the Witwatersrand. *South African Journal of Botany* **76**, 402

Roychoudhury, A.N. and Starke, M.F. (2006) Partitioning and mobility of trace metals in the Blesbokspruit: Impact assessment of dewatering of mine waters in the East Rand, South Africa. *Applied Geochemistry* **21**, 1044-1063

Salmon, S.U. and Malmström, M.E. (2006) Quantification of mineral dissolution rates and applicability of rate laws: Laboratory studies of mill tailings. *Applied Geochemistry* **21**, 269-288

Salmon, S.U. and Malmström, M.E. (2004) Geochemical processes in mill tailings deposits: modelling of groundwater composition. *Applied Geochemistry* **19**, 1-17

Sanders, D., Vernon, D. and Langdon, D. (2009) Cost model land remediation. *Building Magazine* **27.11.2009**, 55-59

SANS (2011) Drinking water Part 1: Microbiiological, physical, aesthetic, and chemical determinants. **SANS 241-1:2011**, p 17

Schoeman, J.J. and Steyn, A. (2001) Investigation into alternative water treatment technologies for the treatment of underground mine water discharged by Grootvlei Popriety Mines Ltd. into the Blesbokspruit in South Africa. *Desalination* **133**, 13-30

Schrenk, M.O., Edwards, K.J., Goodman, R.M., Hamers, R.J. and Banfield, J.F. (1998) Distribution of Thiobacillus ferrooxidans and Leptospirilum ferrooxidans: Implications for generation of acid mine drainage. *Science* **279**, 1519-1522

Scott, R. (1995) Flooding of central and east rand gold mines: An investigation into controls over the inflow rate, water quality and predicted impacts of flooded mines. *Water Research Commission Report* **486/1/95**, p 275

Sheoran, A.S. and Sheoran, V. (2006) Heavy metal removal mechanism of acid mine drainage in wetlands: A critical review. *Minerals Engineering* **19**, 105-116

Sidenko, N.V., Khozhina, E.I. and Sherriff, B.L. (2007) The cycling of Ni, Zn, Cu in system “mine tailings-ground water-plants”: A case study. *Applied Geochemistry* **22**, 30-52

Simón, M., Martín, F., Bouza, G.P., Dorronsoro, C. and Aguilar, J. (2005) Interaction of limestone grains and acidic solutions from the oxidation of pyrite tailings. *Environmental Pollution* **135**, 65-72

Singer, P.C. and Stumm, W. (1970) Acidic mine drainage: The rate-determining step. *Science* **167**, 1121-1123

Sinitsyn, V.A., Aja, S.U., Kulik, D.A. and Wood, S.A. (Acid-base surface chemistry and sorption of some lanthanides on K^+-saturated Marblehead illite: I. Results of an experimental investigation. *Geochimica et Cosmochimica Acta* **64**, 185-194

Smith, K.S. (1999) Metal sorption on mineral surfaces: An overview with examples relating to mineral deposits. *In* Plumlee, G.S., Logsdon, M.J. and Flipek, L.F. (*Eds.*) The environmental geochemistry of mineral deposits Part A: Processes, techniques and health issues. *Reviews in Economic Geology* **6**, 161-182

Smith, K.S. and Huyck, H.L.O. (1999) An overview of the abundance, relative mobility, bioavailability and human toxicity of metals. *In* Plumlee, G.S., Logsdon, M.J. and Flipek, L.F. (*Eds.*) The environmental geochemistry of mineral deposits Part A: Processes, techniques and health issues. *Reviews in Economic Geology* **6**, 161-182

Smith, A.M.L., Hudson-Edwards, K.A., Dubbin, W.E. and Wright, K. Dissolution of jarosite [$KFe_3(SO_4)_2(OH)_6$] at pH 2 and 8: Insights from batch experiments and computational modelling. *Geochimica et Cosmoichimica Acta* **70**, 608-621

Søndergaard, J., Elberling, B. and Asmund, G. (2008) Metal speciation and bioavailability in acid mine drainage from a high Arctic coal mine waste rock pile: Temporal variations assessed through high-resolution water sampling, geochemical modeling and DGT. *Cold Regions Science and Technology* **54**, 89-96

Sorwebplus (2006) Soil remediation costs. Available at http://www.sorwebplus.com [Accessed April 17, 2013)

Sracek, O., Choquette, M., Gélinas, P., Lefebvre, R. and Nicholson, R.V. (2004) Geochemical characterisation of acid mine drainage from a waste rock pile, Mine Doyon, Québec, Canada. *Journal of Contaminant Hydrology* **69**, 45-71

SRK Consulting (2005) Estimate of water quantities entering the underground workings of the East Rand Basin at selected areas. *Technical Report* **348207/1**, p 161

Srodon, J., Morgan, D.J., Eslinger, E.V., Eberl, D.D. and Karlinger, M.R. (1986) Chemistry of illite/smectite and end-member illite. *Clay and Clay Minerals* **34**, 368-378

Statistics South Africa. Available at http://www.statssa.gov.za [Accessed April 17, 2013]

Stumm, W. and Lee, G.F. (1961) Oxygenation of ferrous iron. *Industrial and Engineering Chemistry* **53**, 143-146

Summersgill, M. (2005) Remediation technologiy costs in the UK & Europe; drivers and changes from 2001 to 2005. Available at http://www.cordis.lu [Accessed April 17, 2013]

Swartz, C., Du Plessis, J.A., Burger, A.J. and Offringa, G. (2006) A desalination guide for South African municipal engineers. *Water SA* **32**, 641-647

Taleb, N.N. (2001) Fooled by randomness: The hidden role of chance in life and in the markets. *Norton, Inc.,* p 220

Tichomirowa, M. and Junghans, M. (2009) Oxygen isotopic evidence for sorption of molecular oxygen to pyrite surface sites and incorporation into sulphate in oxidation experiments. *Applied Geochemistry* **24**, 2072-2092

Tooth, S. and McCarthy, T.S. (2007) Wetlands in drylands: geomorphological and sedimentological characteristics, with emphasis on examples from southern Africa. *Progress in Physical Geography* **31**, 3-41

Tutu, H., McCarthy, T.S. and Cukrowska, E.M. (2008) The chemical characteristics of acid mine drainage with particular reference to sources, distribution and remediation: The Witwatersrand Basin, South Africa as a case study. *Applied Geochemistry* **23**, 3666-3684

Tutu, H., Cukrowska, E.M., McCarthy, T.S., Hart, R. and Chimuka, L. (2009) Radioactive disequilibrium and geochemical modelling as evidence of uranium leaching from gold tailings dumps in the Witwatersrand Basin. *International Journal of Envrionmental and Analytical Chemistry* **89**, 687-703

Ulrich, K-U., Ilton, E.S., Veeramani, H., Sharp, J.O., Bernier-Latmani, R., Schofield, E.J., Bargar, J.R. and Giammar, D.E. (2009) Comparative dissolution kinetics of biogenic and chemogenic uraninite under oxidizing conditions in the presence of carbonate. *Geochimica et Cosmochimica Acta* **73**, 6065-6083

United States Environmental Protection Agency (1994) Acid mine drainage prediction. *Technical Document* **EPA530-R-94-036**, p 52

United States Environmental Protection Agency (1997) Cost of remediation at mine sites. *Techical Report* **January 2007**, p 65

United States Environmental Protection Agency (1997) Guiding principles for Monte Carlo analysis. *Technical Report* **EPA/630/R-97/001**, p 35

United States Environmental Protection Agency (1998) Guide to documenting and managing costs and performance information for remediation projects. *Technical Report* **EPA542-B-98-007**, p 77

United States Environmental Protection Agency (2009) Guidance on the development, evaluation and application of environmental models. *Technical Report* **EPA/100/K-09/003**

United States Environmental Protection Agency (2010) Guidelines for preparing economic analyses. *Technical Report* **December 2010**, p 272

Vivier, J.J.P. (2011) Development of an assured systems management model for environmental decision-making. *Unpublished PhD thesis, North-West University*, p 295

Von Bertalanffy, L. (1950) An outline of general systems theory. *The British Journal for the Philosophy of Science* **I(2)**, 134-165

Walpole, R.E., Myers, R.H., Myers, S.L. and Ye, K.E. (2011) Probability statistics for engineers and scientists, 9th edition. *Pearson*, p 816

Werhane, P.H. (2008) Mental models, moral imagination and systems thinking in the age of globalization. *Journal of Business Ethics* **78**, 463-474

White, A.F. and Brantley, S.L. (2003) The effect of time on the weathering of silicate mienrals: why do weathering rates differ in the laboratory and field. *Chemical Geology* **202**, 479-506

Williamson, M.A. and Rimstidt, J.D. (1994) The kinetics and electrochemical rate-determining step of aqueous pyrite oxidation. *Geochimica et Cosmochimica Acta* **58**, 5443-5454

Wilson, M.J. (2004) Weathering of primary rock-forming minerals: processes, products and rates. *Clay Minerals* **39**, 233-266

Winde, F. (2010) Uranium pollution of the Wonderfonteinspruit, 1997-2008 Part 1: Uranium toxicity, regional background and mining-related sources of uranium pollution. *Water SA* **36**, 239-256

Wood, A. (2003) Remediation control strategies and cost data for an economic analysis of a mercury total maximum daily load in California. *United States Geological Survey Open-File Report* **03-284**, 58

World Wildlife Fund South Africa (2012) Financial provisions for rehabilitation and closure in South African Mining: Discussion document on challenges and recommended improvements (Summary). *Report*, p 12

Water Reasearch Commission (2005) Water Resources of South Africa 2005. *Water Research Commission Report* **K5/1491**

Zhu, C. (2003) A case against K_d-based transport models: natural attenuation at a mill tailings site. *Computers & Geosciences* **29**, 351-359

Zhu, C. and Anderson, G. (2002) Environmental applications of geochemical modelling. *Cambridge University Press,* p 300